72-14,951

MUSCARA, Joseph, 1942-
A METALLURGICAL STUDY OF HIGH STRESS ABRASION.

The University of Michigan, Ph.D., 1971
Engineering, metallurgy

University Microfilms, A XEROX Company, Ann Arbor, Michigan

A METALLURGICAL STUDY

OF HIGH STRESS ABRASION

by
Joseph Muscara

A dissertation submitted in partial fulfillment
of the requirements for the degree of
Doctor of Philosophy
(Metallurgical Engineering)
in The University of Michigan
1971

Doctoral Committee:

Professor Maurice J. Sinnott, Chairman
Professor Richard A. Flinn
Professor Edward E. Hucke
Associate Professor Kenneth C. Ludema
Professor Clarence A. Siebert
Mr. Douglas V. Doane, Climax Molybdenum Company

PLEASE NOTE:

Some pages have indistinct
print. Filmed as received.

University Microfilms, A Xerox Education Company

TO CAROL AND MARIA

ACKNOWLEDGEMENTS

The author wishes to express his appreciation to the many people who have been instrumental in his advancement as a graduate student and who have aided in the course of this investigation, and particularly to the following:

Professors Maurice J. Sinnott, Clarence A. Siebert, and J. D. Hanawalt for providing financial support and for their continued interest in the author's professional development; Professor Maurice J. Sinnott, Chairman of the Doctoral Committee, for advice, guidance and encouragement throughout the course of this investigation; Professors Richard A. Flinn, Edward E. Hucke, Kenneth C. Ludema and Clarence A. Siebert, members of the Doctoral Committee, for their advice and suggestions; Mr. D. V. Doane of the Climax Molybdenum Company and member of the Doctoral Committee for his advice and helpful discussions.

This research was partially performed in and supported by the Research Laboratory of the Climax Molybdenum Company. The author wishes to express his gratitude to the laboratory staff and especially to Mr. V. Biss, Mrs. A. Tudor, Mrs. H. G. Denning, Mr. C. W. Johnson, Mr. K. E. Kienholz, Mr. F. Maass, Mr. R. W. McKenzie, and Mr. W. Stockdale for helpful suggestions and assistance on different phases of this research.

Finally, I wish to express my sincere appreciation to my wife, Carol, for performing the density measurements,

microprobe and other calculations, editing and proofreading of the text, but especially for her understanding and encouragement in the many times of stress during my tenure as a student and for constantly providing care and love.

TABLE OF CONTENTS

	Page
ACKNOWLEDGEMENTS	iii
LIST OF FIGURES.	ix
LIST OF TABLES	xiv
LIST OF APPENDICES.	xvii
ABSTRACT	xviii
INTRODUCTION.	1
LITERATURE SURVEY	5
Mechanics of Abrasive Wear	5
Effect of Load on Abrasive Wear	6
Effect of Abrasion Path Length	7
Effect of Speed of Abrasion on Abrasive Wear.	8
Effect of Abrasive Particle Hardness on Abrasive Wear	8
Effect of Abrasive Grit Size on Abrasive Wear	9
Effect of Specimen Diameter on Abrasive Wear.	11
Assessment of Abrasive Wear Resistance - The Wear Ratio	12
Metallurgical Studies of Abrasive Wear in White Cast Irons.	12
ABRASIVE WEAR TESTING.	19
Design and Construction of the Abrasion Testing Apparatus	20
Motions of the Abrasive and of the Specimen	21
Loading	23
Other Features.	26
Experimental Procedure.	27
Description of Specimens	27

Page

Abrasive Cloths 28

Test Conditions 29

Testing Procedure. 29

Results and Discussion. 32

Statistical Description. 32

Study of Different Abrasives 36

Study of the Effects of Load and Grit Size . . . 42

METALLURGICAL STUDIES OF HIGH STRESS ABRASIVE WEAR OF Fe-C-Cr ALLOYS 50

Experimental Procedures 50

Specimen Materials 50

Alloy Design. 50

Melting Materials 52

Melting Procedure 52

Specimen Preparation 54

Chemical Analysis 56

Abrasion Testing 57

Density Determinations 58

Hardness Testing 59

Electron Microprobe Analysis 60

Alloys for Calibration Curves 60

Microprobe Parameters and Data Collection for Calibration Curve Studies 63

The "Probe Ratio" 64

Microprobe Data Collection for the Alloys Tested in Abrasion 65

Quantitative Metallography. 66

Scanning Electron Microscopy 67

Page

Electron Microscopy 68

Light Metallography 68

Experimental Results 69

Chemical Analysis of alloys Used for High Stress Abrasion Testing 69

Density 70

High-Stress Abrasion Test Results 71

Hardness. 72

Electron Microprobe Results 73

Calibration Curves. 73

Phase Compositions of Alloys Tested in High-Stress Abrasion. 76

Light Metallography 77

Quantitative Metallography. 78

Results of Point Counting 78

Quantimet Results 79

Electron Microscopy 79

Scanning-Electron Microscopy Results 80

Regression Analysis 80

DISCUSSION 82

Phase Structures and Properties. 82

Matrix Phase 82

Carbide Phase 85

High Stress Abrasion Resistance. 89

Regression Analysis. 93

Mechanistic Discussion of High Stress Abrasion. . . 97

CONCLUSIONS 101

Page

Abrasive Wear. 101

Metallurgical Studies of High Stress Abrasive Wear . 102

REFERENCES 105

FIGURES 109

TABLES. 175

APPENDICES 202

LIST OF FIGURES

Figure		Page
1.	Photograph of the Abrasion Wear-Testing Apparatus	110
2.	Schematic Drawing of the Abrasion Wear-Testing Apparatus	111
3.	Schematic Diagram of the External Wiring of the Abrasion Wear-Testing Apparatus.	112
4.	Positions of Specimens Trepanned from the 5-Inch Balls	113
5.	Microstructure of Alloy AA, Martensitic High Chromium Cr-Mo White Iron.	114
6.	Microstructure of Alloy BB, Cr-Mo Steel	114
7.	Microstructure of Alloy CC, 2Si-1Mo Steel	115
8.	Microstructure of Alloy FF, Ni-Cr White Iron	115
9.	Microstructure of Alloy GG, Pearlitic Cr-Mo Steel	116
10.	Microstructure of Alloy II, Austenitic Manganese Steel	116
11.	Weight Loss as a Function of Type of Abrasive and Alloy Tested Under 7 lb Loading on 105μ Particle Size Abrasive.	117
12.	Wear Ratio using BB as a Standard as a Function of the Type of Abrasive and the Alloy Tested under 7 lb Loading on 105μ Particle Size Abrasive.	118
13.	Wear Ratio using II as a Standard as a Function of the Type of Abrasive and the Type of Alloy Tested under 7 lb Loading on 105μ Particle Size Abrasive	119
14.	Wear Ratio using AA as a Standard as a Function of the Type of Abrasive and the Type of Alloy Tested under 7 lb Loading on 105μ Particle Size Abrasive	120
15.	Weight Loss as a Function of Load for the Alloys Tested on 80μ Alumina	121
16.	Weight Loss as a Function of Load for the Alloys Tested on 130μ Alumina.	122

Figure		Page
17.	Weight Loss as a Function of Load for the Alloys Tested on 200μ Alumina.	123
18.	Weight Loss as a Function of Abrasive Particle Size for the Alloys Tested on Alumina Abrasive under 3.5 and 15 lb.	124
19.	Weight Loss as a Function of Abrasive Particle Size for the Alloys Tested on Alumina Abrasive under 7 lb.	125
20.	Weight Loss as a Function of Load and Alumina Abrasive Particle Size for Alloy AA	126
21.	Weight Loss as a Function of Load and Alumina Abrasive Particle Size for Alloy FF	127
22.	Weight Loss as a Function of Load and Alumina Abrasive Particle Size for Alloy BB	128
23.	Weight Loss as a Function of Load and Alumina Abrasive Particle Size for Alloy II	129
24.	Weight Loss as a Function of Load and Alumina Abrasive Particle Size for Alloy CC	130
25.	Wear Ratio as a Function of Load and Alumina Abrasive Particle Size for Alloy BB using as Standards Alloys AA and CC	131
26.	Relation Among the Chromium Content, the Amount of Carbon, and the Microstructure	132
27.	Effect of Chromium and Carbon Content on the Type and Morphology of Carbide	133
28.	Liquidus Surface of the Fe-C-Cr System	134
29.	Specimen Positions	135
30.	Alloy Density as a Function of Composition in Alloys with a Cr:C of 6.64	136
31.	Vickers Hardness Determined under 10 kg Loading as a Function of Composition in the Non-Abraded Alloys with a Cr:C of 6.64	137
32.	Vickers Hardness Determined under 10 kg Loading as a Function of Composition in the Abraded Alloys with a Cr:C of 6.64	138

Figure		Page
33.	Microprobe Calibration Curves for Fe-Cr Solid Solution Phases and for $(Cr,Fe)_7C_3$.	139
34.	Microprobe Calibration Curve for Cr in Fe-Cr-Mo Alloys with up to 5 Weight Percent Mo.	140
35.	Microprobe Calibration Curve for Mo in Fe-Cr-Mo Alloys with Less than 4 Weight Percent Cr . . .	141
36.	Microprobe Calibration Curve for Mo in Fe-Cr-Mo Alloys with 13 Weight Percent Cr	142
37.	Microprobe Calibration Curve for Mo in Fe-Cr-Mo Alloys with 17.5 Weight Percent Cr.	143
38.	Microprobe Calibration Curve for Mo in Fe-Cr-Mo Alloys with 25 Weight Percent Cr	144
39.	Chromium Content of the Matrix as a Function of Total Chromium in Alloys with a Cr:C of 6.64 . .	145
40.	Chromium Content of the Carbides as a Function of Total Chromium in Alloys with a Cr:C of 6.64 .	146
41.	Carbide Morphologies (a and b) Lamellar Eutectic Carbides in Specimens KV and I Respectively, (c and d) Radiating Eutectic Carbides in Specimens I and IV Respectively	147
42.	Carbide Morphologies and Structures in Molybdenum-Containing Alloys (a and c) Radiating and Transverse Cross Section Eutectic Carbides, and Mo_2C Eutectic Carbides in Specimen I2V, (b) Radiating, Lamellar, and Mo_2C Eutectic Carbides in Specimen I2V	149
43.	Mixed Carbide Morphologies	150
44.	Surface Replica of Specimen K1	152
45.	Surface Replica of Specimen N	152
46.	Surface Replica showing Slip Lines in Specimen C-	153
47.	Surface Replica showing the Mo_2C Eutectic in Specimen F2	153
48.	Particle Extracted from the Surface of Specimen K2, and its Diffraction Pattern.	154

Figure		Page
49.	Scanning Electron Images of the Abraded Surface of Specimen B-	155
50.	Scanning Electron Images of the Abraded Surface of Specimen E-	156
51.	Scanning Electron Images of the Abraded Surface of Specimen GV-	157
52.	Scanning Electron Images of the Abraded Surface of Specimen IV-	158
53.	Scanning Electron Images of the Abraded Surface of Specimen KV-	159
54.	Scanning Electron Images of the Abraded Surface of Specimen N-	160
55.	Scanning Electron Images of the Abraded Surface of Specimen P-	161
56.	Scanning Electron Image of the Abraded Surface of Specimen H2- after Light Removal of the Matrix	162
57.	Scanning Electron Images of the Abraded Surface of Specimen FV- after Light Removal of the Matrix.	163
58.	Scanning Electron Images of the Abraded Surface of Specimen J- after Light Removal of the Matrix .	164
59.	Scanning Electron Images of the Abraded Surface of Specimen M- after Light Removal of the Matrix .	165
60.	Scanning Electron Images of the Abraded Surface of Specimen N- after Light Removal of the Matrix .	166
61.	Scanning Electron Images of Carbide Morphology in Specimen F-	168
62.	Scanning Electron Images of Carbide Morphology in Specimen H-	169
63.	Scanning Electron Images of Carbide Morphology (a) and (b) Specimen KV- X160 and X800 Respectively, (c) Specimen BV- X1600	170
64.	Scanning Electron Images of Carbide Morphology in Specimen O-	171

Figure Page

65. Carbide Volume as a Function of Total Chromium in Alloys with Cr:C of 6.64 172

66. Abrasion Resistance as a Function of Total Cr Content in Alloys with Cr:C of 6.64 173

67. Abrasion Resistance as a Function of Volume Percent Carbide 174

LIST OF TABLES

Table		Page
1.	Alloys Used to Evaluate the Abrasion Testing Apparatus	176
2.	Densities of the Alloys Used to Evaluate the Abrasion Testing Apparatus	177
3.	Statistical Results for the Alloys Tested on Different Abrasives of 105μ Particle Size under 7 lb Load	178
4.	Statistical Results for the Alloys Tested on 80μ Particle Size Alumina under the Given Loads	179
5.	Statistical Results for the Alloys Tested on 104μ Particle Size Alumina under the Given Loads	180
6.	Statistical Results for the Alloys Tested on 130μ Particle Size Alumina under the Given Loads	181
7.	Statistical Results for the Alloys Tested on 200μ Particle Size Alumina under the Given Loads	182
8.	Mean Weight Losses and Ranking of Alloys Tested on Alumina Abrasive and in the Ball Mill	183
9.	Composition (Cr and C) and Heat-Treating Temperature of "Commercial-Type" Alloys used in Microprobe Calibration Studies	184
10.	Compositions in Weight Percent of the Alloys Tested in High Stress Abrasion	185
11.	Densities in g/cc of the Alloys Tested in High Stress Abrasion	186
12.	High Stress Abrasion Test Results	187
13.	Vickers Hardness Numbers of Alloys Tested in High Stress Abrasion	189
14.	Vickers Microhardness, 20-g Load, of Micro-constituents in the Alloys Tested in High Stress Abrasion	190
15.	Alloy Compositions for Microprobe Calibration Curve of the Fe-Cr System.	191

Table		Page
16.	Alloys Utilized for the Study of the Effect of Mo on the Microprobe Calibration for Cr in the Fe-Cr Base System	192
17.	Alloys Utilized for the Study of the Effect of Cr on the Microprobe Calibration for Mo in the Fe-Cr Base System	193
18.	Microprobe Background Counts of Alloys Based on 100 Seconds Counting Time, 1.25×10^7 Amperes Beam Current, and 20 kv Excitation Voltage.	194
19.	Average Composition of the Matrix and Carbide Phase of the Alloys Tested in High Stress Abrasion	195
20.	Quantitative Metallography Results of Carbide Morphology.	196
21.	Quantitative Metallography Results Obtained from the Quantimet Analysis and from Point Counting	197
22.	Interplanar Spacings from the Electron Diffraction Patterns of Particles within the Minor Phase Present in the Molybdenum-Containing Alloys	199
23.	Variables Used in the Regression Analysis	200
24.	Regression Analysis Equations	201

Appendices

A-1	Weight Losses for the Alloys Tested on 105 Micron Particle Size Alumina Abrasive under 7 lb Loading	204
A-2	Weight Losses for the Alloys Tested on 105 Micron Particle Size Silicon Carbide Abrasive under 7 lb Loading	205
A-3	Weight Losses for the Alloys Tested on 105 Micron Particle Size Garnet Abrasive under 7 lb Loading	206
A-4	Statistical Analysis for the Data of the Alloys Tested on 105 Micron Particle Size Alumina Abrasive under 7 lb Loading	207

Table		Page
A-5	Statistical Analysis for the Data of the Alloys Tested on 105 Micron Particle Size Silicon Carbide Abrasive under 7 lb Loading	208
A-6	Statistical Analysis for the Data of the Alloys Tested on 105 Micron Particle Size Garnet Abrasive under 7 lb Loading	209
B-1	Weight Losses for the Alloys Tested on 80 Micron Particle Size Alumina under the Given Loading . .	211
B-2	Weight Losses for the Alloys Tested on 105 Micron Particle Size Alumina under the Given Loading . .	212
B-3	Weight Losses for the Alloys Tested on 130 Micron Particle Size Alumina under the Given Loading . .	213
B-4	Weight Losses for the Alloys Tested on 200 Micron Particle Size Alumina under the Given Loading . .	214
B-5	Statistical Analysis for the Data of the Alloys Tested on 80 Micron Particle Size Alumina under the Given Loading	215
B-6	Statistical Analysis for the Data of the Alloys Tested on 105 Micron Particle Size Alumina under the Given Loading	216
B-7	Statistical Analysis for the Data of the Alloys Tested on 130 Micron Particle Size Alumina under the Given Loading	217
B-8	Statistical Analysis for the Data of the Alloys Tested on 200 Micron Particle Size Alumina under the Given Loading	218
C-1	High Stress Abrasion Test Results	220
D-1	Composition of Alloys Utilized in Microprobe Calibration Studies.	225
D-2	Microprobe Ratios, K's and Compositions in Weight Percent of Phases in the High-Stress Abrasion Tested Alloys.	226

LIST OF APPENDICES

	Page
APPENDIX A - DATA AND STATISTICAL RESULTS ON THE EFFECTS OF DIFFERENT ABRASIVES	203
APPENDIX B - DATA AND STATISTICAL RESULTS ON THE EFFECTS OF LOAD AND GRIT SIZE.	210
APPENDIX C - DATA AND STATISTICAL RESULTS OF THE Fe-C-Cr AND Fe-C-Cr-Mo ALLOYS TESTED IN HIGH STRESS ABRASION.	219
APPENDIX D - MICROPROBE DATA AND RESULTS	224
APPENDIX E - QUANTITATIVE METALLOGRAPHY PARAMETERS . .	228

ABSTRACT

A METALLURGICAL STUDY
OF HIGH STRESS ABRASION

by
Joseph Muscara

Chairman: Maurice J. Sinnott

Little research has been performed in an organized and quantitative manner to define the effects of varying metallurgical parameters on abrasive wear. It was the intent of this study to contribute to the scientific knowledge of high stress abrasion from the metallurgical point of view of relating structure to properties. A series of 27 Fe-C-Cr and Fe-C-Cr-Mo alloys with constant Cr:C ratios of 6.64 ranging from 1.40% C and 9.44% Cr to 5.07% C and 33.56% Cr with 0, 1.5, or 3 percent Mo in some of the hypoeutectic alloys were prepared. The alloys were designed to determine the effects of volume fraction, morphology and composition of $(Cr, Fe)_7C_3$ carbides on high stress abrasion resistance. This was accomplished by increasing the Cr and C contents to vary the above carbide parameters while the matrix structure in all the alloys was austenitic and its properties were approximately constant.

To study small changes in the carbide properties required a test which yields precise data and discriminates between materials. Since no such test was available, one was devised and evaluated. In the test developed, the

specimen is abraded by sliding contact with bonded abrasives. To evaluate the abrasive wear response of the apparatus, six ferrous alloys were tested under varying abrasion conditions of abrasive type (alumina, silicon carbide, and garnet), load (3.5 to 29.2 pounds for a ¼-inch diameter pin), and abrasive particle size (80 to 200 microns). It was found that alumina is most suited for studies of ferrous alloys containing carbides of different microstructural properties. The abrasive test conditions of 15-pound loading for a ¼-inch diameter pin specimen on 80-micron particle size alumina abrasive yielded the most precise and reproducible data. Under these conditions the test discriminated between the alloys tested and rated them similarly to the ranking of the field tests in an ore grinding ball mill. The 95 percent confidence limits on the mean weight loss reported as a percentage of the mean ranged from ±0.353 percent to ±0.931 percent for the alloys tested.

The Fe-C-Cr and Fe-C-Cr-Mo alloys were tested using the above abrasion parameters which simulate severe high stress abrasion. The high stress abrasion resistance of the hypoeutectic alloys did not increase with an increase in eutectic carbide volume fraction. A small decrease in abrasion resistance corresponding to one percent per ten percent increase in eutectic carbide volume was found. The different eutectic carbide morphologies had very little effect on high stress abrasion resistance. A two-fold increase in the carbide shape parameter (area/perimeter)

improved the high stress abrasion resistance by approximately 5 percent. The abrasion resistance of the hypoeutectic alloys is increased by 2 percent per percent of Mo addition. The greatest effect in increasing high stress abrasion resistance was an increase in the primary carbide volume fraction of the hypereutectic alloys. The morphology of these massive primary carbides is considerably different than the eutectic carbide morphologies. The increase in primary carbide volume fraction increased the high stress abrasion resistance by one percent per percent primary carbide to an optimum at 20 volume percent. Based on the results of the present research, on scanning electron microscopy of the abraded surfaces and on results of field experience, a mechanism of high-stress abrasion for the alloys studied was proposed.

INTRODUCTION

Wear plays an important role in many engineering and non-technical applications, yet wear phenomena have not been thoroughly investigated and are not well understood. Many reference books do not consider problems of wear in detail and most physical metallurgy books entirely neglect the subject. Wear information is generally not comprehensive and is scattered among many different fields. For example, while wear in general could be considered a metallurgical problem, it has been studied very little by the metallurgist; problems of friction and wear are normally studied by the mechanical engineer and physicist, and problems of lubrication by the chemist.

The performance of industrial and domestic machinery is limited by wear between contacting moving parts. Wear is an important factor in the performance of piston and jet engines; and in the metallurgical field wear occurs in mining, metalworking and metal cutting operations. In modern computer operations, wear by punched card stock occurs in card handling systems. It is interesting, since wear encompasses many disciplines, that an interdisciplinary approach to the study, understanding, and description of wear phenomena is, in general, lacking.

Several types of wear are recognized; these are surface fatigue wear, corrosive wear, adhesive wear, and abrasive wear.

Probably the least understood form is abrasive wear. This is emphasized by the need of a technical society to form a group promoting study in the field of abrasive wear. Their first short report[1]* presents the limited information available and points out the lack of knowledge in this area. Bowden and Tabor[2] in their two classic volumes on friction and wear comprising approximately 1000 pages were able to review the topic of abrasive wear in just six pages.

Abrasive wear is caused by the dynamic interaction of abrasive particles with a wear surface. This interaction results in surface removal of material and affects the remaining surface layer. Abrasive wear is generally classified into three types based on observations of field applications[3]: (1) Gouging Abrasion - This type of abrasive wear results in the removal of large metal particles from the wearing surface by well supported abrasive particles, often under impact, which penetrate and cut the surface. Typical examples from the mining field are the wear on shovel dippers digging into rock and the wear on hammers in impact pulverizers. (2) High Stress or Grinding Abrasion - This type of abrasive wear occurs when two wearing surfaces with abrasive particles between them rub together with sufficient force to crush the abrasive particles. A typical example is the grinding of ore in a ball mill. (3) Low Stress Scratching Abrasion or Erosion - This abrasive wear results in the

---

*Superscript numbers refer to the list of references at end of the text.

scratching of a wearing surface by abrasive particles which are under stresses insufficient either to penetrate the surface deeply or to be crushed. Pumps conveying sand slurries are examples of this type of abrasion.

While the influence of metallurgical variables on abrasive wear behavior of alloys is recognized, there exists no comprehensive study, especially of high stress abrasion, in an organized and quantitative fashion. In the past, abrasive wear has been studied mainly from a mechanical point of view and there is a need to contribute to abrasive wear knowledge from the metallurgical viewpoint of relating structure to properties. Since white cast irons can make an important contribution to the resistance to high stress abrasion, the microstructural factors affecting the resistance of these irons need to be examined. For these reasons, the present research was carried out to study the effect of composition, volume fraction, and morphology of the carbide phase and composition of the matrix phase on the high stress abrasion resistance of Fe-C-Cr alloys. It is the intent of this research to contribute to high stress abrasion technology in terms of new scientific data and understanding of the high stress abrasion phenomenon in these multiphase alloys. These new data and understanding can set guidelines for the design of better abrasion resistant alloys. The accompanying economic benefit to industry is evident, but more importantly conservation of our natural resources could be realized.

Because no testing apparatus was available for the present studies, suitable equipment was designed and evaluated as described in detail in a following section. Test parameters were standardized to simulate high stress abrasion conditions; however, accelerated tests on the laboratory equipment resulted in wear rates approximately ten to one hundred times faster than those in typical field applications[4].

LITERATURE SURVEY

Mechanics of Abrasive Wear

Literature exists wherein the effects of applied abrasion parameters and theoretical aspects of abrasive wear are reported. Due to several restrictions of these studies, the results are of limited use. A principal limitation is an almost complete disregard for the characteristic properties of the test material; usually only pure metals (and sometimes single phase alloys) were studied. These pure metals are seldom, if ever, used for their abrasion resistance in industrial applications. Further, in the theoretical treatments for predictive equations of wear in multiphase systems (alloys), simplifying assumptions are made about the behavior of these systems under abrasion which are not correct for the real materials used. Finally, the test conditions often do not represent observed industrial applications of abrasive wear.

Scientific studies of abrasive wear do, however, have a short history. If this field is to advance to the point where alloys can be designed to provide abrasion resistance for a given application, then more scientific studies are necessary. This will facilitate elimination of the limitations and assumptions now existing and promote development of a general theory that will apply to useful materials and real conditions. Mechanistic studies, available in the current literature, were of value in the design

and evaluation of the test apparatus (described in a following section).

Basic research on abrasive wear is carried out on apparatus in which the test specimen and the abrasive conform to one of two configurations: (1) two-body abrasion and (2) three-body abrasion. In the two-body abrasion configuration, a fixed abrasive is in contact with the test specimen as occurs when testing on bonded abrasives. In the three-body configuration, free abrasive particles are introduced between two sliding surfaces. Most research has been performed on equipment which conforms to the two-body abrasion configuration and, unless otherwise stated, this literature survey pertains to that type of testing.

Effect of Load on Abrasive Wear

It is often assumed that the relationship of load on the wear rate is one of direct proportionality as reported by Kruschov and Babichev[5] who tested 2 mm diameter specimens on 80 micron alumina abrasive under loads of up to 1 kg. Nathan and Jones[6] find a linear relationship of load (up to 6 kg) with wear for 5 mm diameter specimens tested on silicon carbide of particle sizes 710, 420 and 250 micron but not for smaller particle sizes of 70 and 125 micron. However, they find that at lower loads (not exceeding 2 kg) a linear relationship does exist. A greater deviation in linearity and decreasing wear is reported as the load is increased. The specimen materials used by these authors

were "brass" and Swedish iron. Richardson[7] tested 0.100 in. diameter specimens of Armco iron on 80 micron aluminum oxide and on 80 micron silicon carbide at two load levels of 218 and 500 g. He found that the wear per unit load decreased by about 8% as the load was increased on both the aluminum oxide and silicon carbide. Larsen-Badse[8] also found that the relationship of load and wear rate is not one of direct proportionality and is influenced by the grit size and the sample diameter. He used copper specimens of 2.2 to 7.7 mm diameter abraded on silicon carbide of 20 to 200 microns under loads of 100 to 900 grams. Within the limits of his experiments, he represents the relationship as: $R = R_1 p^n$, where R is the wear rate, p is the average pressure on the specimen surface and R_1 and n are constants which depend on the grit size and specimen diameter.

Effect of Abrasion Path Length

The effect of abrasion path length was studied by Nathan and Jones[6] using 5 mm diameter specimens of brass and Swedish iron tested on silicon carbide abrasive of 200 micron particle size under a load of 2 kg. They found a linear relationship between volume of abrasive wear and abrasion path length. Rabinowicz et al[9] (three-body conditions) found that the specimens increased in weight at short increments after starting a test. This was attributed to abrasive particles becoming embedded on the specimen surface. A finite time was required before the specimen reached an equilibrium state of particle pick-up, after which the

authors report a constant wear rate. Larsen-Badse[10] in testing hardened and tempered steels found that less than one meter of abrasion path was required before the specimen surface reached an equilibrium hardness (work-hardening) and contained an equilibrium amount of imbedded abrasive particles. Beyond this point, they found a constant wear per unit distance.

The above studies point out the necessity for a "run-in" test under the conditions to be studied before wear data are collected.

Effect of Speed of Abrasion on Abrasive Wear

Nathan and Jones[6] determined the volume of abrasive wear of aluminum, brass, and Swedish iron using silicon carbide of 70 and 300 micron particle size under a load of 2 kg for the velocity range of 0.032 to 2.50 m/sec. They found wear to be independent of velocity at the lower velocities, and concluded wear to be independent of velocity if heating of the specimen is avoided. As reported in the paper by Nathan and Jones, Kruschov and Babichev also found wear to be independent of velocity in the range 0.023 to 2.74 m/sec.

Effect of Abrasive Particle Hardness on Abrasive Wear

It is generally accepted[6,11] that the effect of abrasive hardness on metal wear is negligible if the hardness of the abrasive is higher than that of the test specimen. From the studies of several investigations,

Richardson[7,12,13] has recognized two levels of abrasive wear. He has shown[12] that what he terms soft abrasive wear begins when the hardness (maximum work-hardened hardness) of the test material exceeds a value of 0.80 times the hardness of the abrasive particles. When the hardness of the test material is lower than 0.80 times the hardness of the abrasive particles, wear is termed hard abrasive wear. Richardson[12] found that the abrasive wear resistance increased markedly when testing under conditions of soft abrasive wear as compared to hard abrasive wear and that the increase was more rapid as the hardness of the abrasive decreased.

Effect of Abrasive Grit Size on Abrasive Wear

The existence of a critical abrasive particle diameter has been reported. The volume of abrasive wear increases linearly and steeply with increasing particle size for small sizes, but larger particle sizes have little effect on the volume of abrasive wear. When the abrasive particles are larger than the critical grit size, the wear of materials is reported independent of grit size[6,8,9,14-17], slowly increasing with grit size[6,9], or decreasing with grit size[8]. The critical grit diameter has been reported between 40 and 100 microns. Nathan and Jones[6] found that the behavior of abrasive wear with larger particle sizes depended on the applied load. They ran tests on 5 mm diameter samples of Swedish iron at loads between 0.5 and 6 kg. The volume of abrasive wear above the critical grit size was independent of grit size and 1/2 and 1 kg load, but

increased with grit size at 2, 4 and 6 kg (and at an increasing rate with load). Larsen-Badse[8] found that the value of the critical grit diameter depended on the diameter of the specimen tested. For copper specimens of 2 to 9.5 mm diameter abraded on silicon carbide, the critical grit diameter increased linearly up to 70 microns with specimen diameter

Several explanations have been offered for the effect of the abrasive particle size on volume of wear, and the critical grit diameter. Avient et al[14] considered the effect due to clogging of finer grit abrasive paper by worn metal chips. Clogging decreases the number of abrasive grains which can contact and abrade the metal surface decreasing the wear rate. Mulhearn and Samuels[16] studied samples of silicon carbide papers and concluded that the fine grits have a large number of cracks which would result in fracture of the particles under abrasion and reduce their ability to remove material. Larsen-Badse[18] studied the size and number of grooves formed on copper samples as a function of silicon carbide grit size and load. They concluded that some of the abrasive grains were in contact with the metal surface elastically and did not contribute to metal removal. The effect was strongly dependent on grit size, pronounced on fine grits and non-existent at grit sizes above the critical grit diameters. Rabinowicz and Mutis[17] and Rabinowicz[19] studying three-body abrasion, concluded that adhesive wear fragments interfere with the

cutting process. Based on surface energy considerations, the adhesive wear fragments were expected to be larger than the fine abrasive grits and prevent these grits from cutting the specimen.

Effect of Specimen Diameter on Abrasive Wear

Richardson[7] tested a variety of materials, including wrought and annealed plain carbon and alloyed steels, pure metals and non-ferrous alloys, cast irons and hardfacing alloys, as 0.100 inch diameter pins under 500 g loading on varying abrasives and grit sizes. He found that burrs were visible on the trailing edge of the softer material specimens even when tested on the finer grit (80 micron) abrasives. The burr was larger after testing on coarser abrasives. In some cases it extended around most of the circumference. In Richardson's tests, the specimen was rubbed unidirectionally on a rotating disc. It was concluded that some of the wear resulted from a secondary wear mechanism in which metal was removed from the extension and fragmentation of a burr. This effect can be reduced by testing samples of larger surface area so that the volume of metal lost through this mechanism is small compared to that lost from the wear surface. As described earlier, Larsen-Badse[8] reported an equation for the abrasive wear rate of a specimen as $R = R_1 p^n$ where n is a constant dependent on the specimen diameter (for abrasion of copper). He found that the exponent n increased from approximately 0.78 to 0.92 with an increase in sample diameter from 2 to 5 mm. For diameters

above 6 mm, n remained approximately constant.

Assessment of Abrasive Wear Resistance - The Wear Ratio

Kruschov[11] devised the concept of the relative wear resistance of metals. Changes in applied and environmental test conditions can significantly influence the results of different tests. If the change in length of a specimen made from a standard material, $\Delta\ell_M$, and of the material under study, $\Delta\ell_S$, are measured under the same conditions, the ratio of these quantities:

$$\varepsilon = \frac{\Delta\ell_S}{\Delta\ell_M} \quad ,$$

was defined by Kruschov[11] as the relative wear resistance of the sample material under study. The ratio is claimed to be independent of the experimental peculiarities. This approach of evaluating relative abrasion resistance of materials is widely used, although sometimes the ratio is calculated from the volume loss. Richardson[7,12,13] has found a considerable difference between the relative abrasion resistance of the same alloys tested under conditions of soft abrasive wear and hard abrasive wear.

Metallurgical Studies of Abrasive Wear in White Cast Irons

Literature discussing well designed, and executed experiments studying effects of metallurgical parameters on abrasion resistance is, in general, lacking. Further, it is difficult to relate findings of different investigators since standard equipment for testing abrasion resistance does not exist and most investigators use basically different tests. In this country very little work is reported

either on the mechanics or on metallurgical studies of abrasion. Those industries in which abrasion wear is of importance have done some work in this area. However, most of the work is performed on the alloys as commercially used. Because the range of alloys encompasses many complex structures and varying properties, it is difficult to determine each effect of various metallurgical parameters on abrasion resistance. Much of the information available is based on field experience and has been of some use in alloy design. Two authors, Norman[4,20-23] and Avery[3,24-26] have contributed to the literature on abrasion resistance of industrial alloys. Because these authors are using the same approach, many of their results are similar. Further little new information is reported in the several reviews covering a time span from the later 1940's to present. It should be realized then, that the older approaches are no longer so effective and a new scientific approach to the metallurgical study of abrasion is necessary to improve and advance our knowledge of abrasion processes.

Literature from well organized research studying effects of metallurgical variables on high stress abrasion behavior of white cast irons was not found. Some Russian work is reported on metallurgical studies of low stress abrasion. In the following reviews, the low stress abrasion testing was performed by rotating the test specimens in a sand slurry. Garber et al.[27] studied white cast irons in various heat treated conditions commonly used by industry.

The microstructures, microhardness of constituents and wear resistance of these irons were reported. A wide range, indicating large scatter, for the wear resistance of each determination was given. They reported that white cast irons are more abrasion resistant than steels of the same hardness, and alloyed white cast irons more resistant than unalloyed white cast irons of the same hardness. Their conclusion was based on the presence of free carbides in the white cast irons containing carbides of higher hardness than the sand abrasive, and the absence of carbides of high hardness in the less abrasion resistant materials. However, neither the matrix structures nor carbide type, morphology and size of those alloys were comparable, and their conclusions as to the effect of carbide hardness may not be entirely correct. Richardson[12,13] had reported considerable scale effects (carbide particle size relative to the abrasive size) in testing under conditions of soft, low stress abrasion. Garber et al.[27] also concluded that wear resistance of cast irons increases with the carbide hardness. The comparison was made between irons with different types of carbides and different matrices. The more resistant cast iron did contain a higher hardness carbide (M_7C_3) but it was dispersed in a tempered martensite matrix of much higher microhardness. The other iron (of lower abrasion resistance) contained M_3C carbides as the continuous matrix phase and dispersed within it was martensite and retained austenite. The carbides in these irons thus differed greatly in morphology, size and type. The

difference in abrasion resistance of these irons cannot be attributed solely to the difference in their carbide hardness. A further conclusion of this work[27] was that the abrasion resistance of white cast irons increases with their volume percent carbide. The two irons used for comparison were of similar composition except for a higher carbon level and the presence of 1.5 percent Mo in the iron of higher abrasion resistance. The two irons contained a reported 18-20 and 25-30 volume percents carbide. The material with higher volume of carbide was reported 50% more wear resistant. Heat treatments for the two irons were not the same and the matrix structures were reported as martensite for the lower volume carbide iron and martensite plus spot carbides for the other iron. The 50 percent increase in wear resistance cannot be attributed entirely to an increase in carbide volume. The authors[27] finally concluded that if the hard phase is not properly supported by a hard matrix the abrasion resistance of the hard phase may not be realized. Although this may be true, they[27] compared an iron which had an alloyed M_3C carbide with austenite and martensite dispersed in it to an unalloyed iron with a pearlitic structure. The iron with the higher abrasion resistance was that which contained alloyed M_3C; further, the carbides in these irons are continuous and not held by the other phase which is dispersed within them.

Ruznak[28] studied the low stress abrasion resistance of a 6% Cr 1.12% C steel, and a series of hypoeutectic 12,

15, and 27% Cr white cast irons of varying carbon contents between approximately 2.50 to 3.50%. Some of the alloys contained 0.60 or 1.90% Mo. The alloys were tested in the as cast and heat treated conditions. Ruznak[28] found that austenitic irons of 12 and 15% Cr had abrasion resistance comparable to that of the 6% Cr steel whose structure contained retained austenite. He concluded that increasing volumes of M_7C_3 carbides in these austenitic irons did not contribute to the low stress abrasion resistance. Martensitic irons containing 12, 15 and 27% Cr showed a higher abrasion resistance than the martensitic steel and austenitic irons. It was concluded[28] that the carbide in these irons played an important role in the abrasion resistance. However, although the resistance of the martensitic irons was higher, there did not seem to be an improvement with increasing carbide content. Ruznak[28] and Garber et al.[29] found that aside from the effect on the hardenability, no other effect of Mo in the martensitic irons could be identified.

Garber et al.[30] studied the effect of volume, size and microhardness of the carbides and of microhardness of the metallic base on low stress abrasion resistance of white cast irons. Their cast irons were alloyed with up to 29.3% Cr and up to 1.8% Mo with 1.53 to 4.2% C.

They[30] concluded that the wear resistance of white cast iron increases with the hardness of the carbide. That conclusion was based on wear resistance of alloys with

approximately constant volume fractions of M_7C_3 plus M_3C carbides embedded in matrices of approximately constant microhardness. The irons with increasing volume fraction of the M_7C_3 (which is harder than M_3C) were more abrasion resistant. Important factors not considered were (1) the change in size and morphology of the two types of carbides and (2) the adhesion of the different types of carbide to the remainder of the structure.

They also concluded that the abrasion resistance of the hypoeutectic irons increases linearly with the volume fraction of carbide; but increasing the carbon content above the eutectic did not increase the abrasion because hypereutectic carbides were formed. The fact that abrasion resistance did not change should not be attributed to the fact that hypereutectic carbides do not, in general, contribute to wear resistance, because the hypereutectic carbides in this instance were the M_3C type (which for various reasons may not be as abrasion resistant as M_7C_3) while the eutectic carbides were the M_7C_3 type which the authors had concluded were more resistant than the M_3C.

The authors[30] found that the abrasion resistance decreases with increasing carbide size. Although their data showed this to be true, they obtained different carbide sizes by varying drastically solidification rates of several castings of the same alloy. Different carbide sizes in the various castings were also accompanied by different matrix and carbide compositions, since the castings solidified

under different degrees of non-equilibrium. The authors do not state whether the above castings cooled at different rates were heat treated to produce similar matrix structures. If the samples were tested in the as-cast condition, the alloys with smaller carbide size would also contain martensite, or martensite plus austenite matrices, while slower cooling rates would result in high temperature decomposition products of the austenite for the matrices of the alloys with coarser carbides. The alloys with martensite and martensite plus austenite matrices which also contained finer carbides would be more abrasion resistant due to the matrix structure.

The authors[30] also reported that the wear resistance of white cast irons increases linearly with the hardness of the metallic base and the highest wear resistance was obtained with a martensitic matrix.

ABRASIVE WEAR TESTING

To study small changes of metallurgical variables on abrasive wear required a test which yields precise data and discriminates between materials. Since no such test was available, one was devised. Tests in which the specimen is in sliding contact with bonded abrasives in a two-body abrasion configuration have been widely used by investigators conducting basic wear studies[5-8,10-16,18], but most authors do not state the precision of their data. Larsen-Badse[10] has shown that a test of this type was useful in a study of the effect of carbide volume on abrasive wear of quenched and tempered steels. He reports reproducibility of ±3%, which is the best published result, but he failed to define his criteria for reproducibility.

To obtain accurate tests of the high-stress abrasion of alloys and to discriminate between them, particularly the white cast irons, a laboratory testing apparatus was designed, constructed, and evaluated. It incorporates the use of bonded abrasives in two-body contact with the test specimen. To achieve high reproducibility, the apparatus was constructed so that all the parameters which effect wear could be controlled and their values precisely measured. Observations of specimens tested in unidirectional abrasion have shown that some of the wear scars were abnormally large. It was believed that loose abrasive particles preferentially followed an existing scratch, thus widening the wear scar. For this reason unidirectional abrasion was

avoided, and the apparatus was designed to rotate the specimen.

A vertical milling machine with a massive base and of stiff construction was converted to an abrasion wear testing machine. This section describes the machine that was developed, the testing procedure adopted, and the precision of the data obtained.

Design and Construction of the Abrasion Testing Apparatus

A Bridgeport vertical milling machine was converted to an apparatus for testing two-body abrasion by bonded abrasives. With this apparatus one can vary and control parameters, within specified limits, which are important in the wear process. These are as follows:

1. Load: variable, up to 100 lb. (restricted only by the load cell capacity).
2. Length of abrasion path: variable, up to 18 in. per pass, with the number of passes depending on the specimen diameter. A maximum width of 9 in. may be covered. For example, using a specimen diameter of 0.250 in., 30 passes could easily be obtained for a total of 540 in. of fresh abrasive path.
3. Type of abrasive: those types which are commercially available in bonded form are most easily adaptable; however, special types of abrasive cloth could be made. The easily avail-

able bonded abrasives are silicon carbide, alumina, garnet, emery, and silica.

4. Abrasive grit size: variable between a few microns to 900 microns for the commercially available bonded abrasives.
5. Specimen diameter: variable, up to 1/2-inch.
6. Speed of abrasive surface: variable, up to 100 inches per minute.
7. Specimen rotation: variable up to 1750 rpm.
8. Lubrication: wet or dry conditions as desired; water, most alcohols, and solvents may be used with many of the commercially available bonded abrasives.

Motions of the Abrasive and of the Specimen

Figure 1 is a photograph of the abrasion wear testing apparatus and Figure 2, a schematic drawing on which the various components are identified. Three one-horsepower d-c motors in conjunction with three variable speed controllers, which rectify and control the amount of current supplied to the motors, move the table and rotate the specimen. As the machine table A moves in the X-direction and comes to either end of its predetermined travel (by positioning the limit switches), a tripping plate B affixed to the moving portion of the machine table depresses a lever which simultaneously activates two limiting switches C. One of these limit switches activates the timer D which in turn

activates the indexing motor controller E. The controller E rectifies the a-c input and the d-c output drives the indexing motor F, thereby indexing the machine table in the Y-direction. Dependent upon the time setting on the timer and the speed setting on the variable speed motor controller, different widths of indexing are obtainable. At the end of the time interval, the power output from the timer to the motor controller is cut off and the indexing motor is stopped. The other limit switch sends a signal to the table cycling motor-controller G for the X-direction table movement. This signal turns off the table-cycling motor H for approximately 1.2 seconds (during this interval the table is indexing in the Y-direction). Then the polarity of the motor is reversed and the table is driven in the opposite X-direction.

The specimen rotation is accomplished through the variable speed motor-controller I which supplies power to the motor J to drive the spindle K through a set of pulleys. The specimen L is placed in a tapered collet of suitable size and affixed to the spindle K by tightening the drawbar M which pulls the tapered collet up against the spindle housing and thereby tightens the specimen in the collet to the spindle and the drawbar. The specimen is thus attached to the spindle in the same manner that a cutting tool is held in a milling operation and thus rotates with the spindle.

The table and the specimen movements can be operated

through the variable speed motor controllers either manually or automatically. The automatic mode is controlled through the subtracting electrical impulse counter N. When the controllers are set on the automatic mode and a given number of cycles dialed on the counter, all the power to the machine is turned on and the table and spindle functions are repeated for the given number of cycles. At the end of each cycle the number on the counter is automatically subtracted by one. When this number reaches zero, all the power supply to the machine is turned off and all the machine functions stop simultaneously. The subtracting counter N opens or closes a relay switch when it reads zero or when a given number is dialed on it, and thereby cuts off or supplies the main power to the machine. A schematic diagram of the external electrical wiring for the machine instrumentation is shown in Figure 3.

Loading

Loading is accomplished through the combined weight of the spindle, the quill, and the frame assembly. On the quill O is attached a collar P and a frame assembly Q which transmits the combined weight of K, L, M, O, P, and Q to the load cell R through the spring S. For simplicity, the combination of K, L, M, O, P, Q, and S will be called the "ram"; the ram then comprises all of the weight which hangs from the load cell. A linear bearing is incorporated inside the quill housing T along which bearing the quill O can slide vertically in a nearly frictionless manner. All of the

parts in the construction of the ram assembly, including the quill housing and the load cell frames and platforms, hereafter called the machine head assembly, were accurately machined so that the center line of the load cell and the center line of the specimen correspond. All components of the machine head assembly are symmetric about the center line which is perpendicular to the abrasive-carrying platform U. On the quill housing T are affixed two circular bearings V, 180 degrees apart, so that the quill O can move without friction in the vertical direction, but restrict any tendency for the ram to move radially about the linear bearing between the quill and the quill housing. Thus, any torque transmission to the load cell is avoided. Because of the symmetry of the machine head assembly, the frictionless vertical movement of the ram, and the non-transmittal of torque, the load cell registers a force due to gravity registers a force due to gravity corresponding to the ram assembly weight of 29.2 lbs.

The force sensed by the load cell is measured and recorded on a single channel recorder W. A compressive load between the specimen and the abrasive is generated and recorded in the following manner:

1. With the machine table lowered, the entire ram weight hangs from the load cell R and extends the spring S 0.022 in./lb.
2. The recorder W is calibrated with known weights and the ram weight of 29.2 lb. is balanced on

the recorder so that the ram weight, acting on the load cell, registers zero lb. at this time.

3. When the machine table is raised so that the abrasive makes contact with the specimen, there is zero compressive load between the abrasive and specimen up to initial contact; then as the table is moved up, a compressive force develops with its intensity in proportion to the amount that the table is raised and the extended spring thereby is shortened in length. As the ram is moved up frictionlessly along the linear bearing in the quill housing, every 0.022 inches of upward movement lessens the weight hanging from the load cell by one lb., which is the one-lb. force exerted upward by the table. The load cell then effectively "sees" 28.2 lb., but because the recorder was balanced to zero under the tensile load of the ram weight of 29.2 lb., each 0.022 inches of upward movement of the ram against the load cell registers one lb. in compression on the recorder, which is the actual compressive load between the specimen and the abrasive. In this manner a force of 29.2 lb. can be exerted between the specimen and the abrasive when the spring is fully closed. Upon further upward movement against the load cell, higher loads may be obtained but with much less

resiliency since now the spring is fully closed. However, the ram weight may be increased by symmetrically placing weights on the ram frame Q, thereby extending the spring further and thus increasing the loading that can be applied under the resilient conditions of the spring. With the present load cell capacity, up to 100 lb. in compression can be applied.

Alternately, loading may be accomplished without the use of the load cell, the spring, or the recorder. This can be done by removing the load cell R from its platform, attaching on the platform a bearing pulley, and affixing a cord to the frame Q where the spring is presently placed. By running the cord over the pulley, and by hanging weights from the cord, the weight of the ram can be counterbalanced, and different degrees of compressive force can thus be applied between the abrasive and specimen. Loading through the spring as previously described is preferred since in that manner the sample can more dynamically follow the surface irregularities of the abrasive.

Other Features

The abrasive cloth roll X is dispensed from the roller, and after cutting to length, it is applied on the platform U by means of the pressure-sensitive adhesive backing available on the abrasive cloth roll. If abrasive rolls are not available with adhesive backing, then a separate sheet of double coated pressure-sensitive tape is

applied to the platform U and the abrasive sheet adheres to the platform by means of this tape.

The weight Y is used to counterbalance the weight of the motor H which hangs from the machine table section moving in the X-direction. The smaller weights Z are used to counterbalance the weight of the abrasive roll X; as the abrasive roll diminishes, some of the weights at Z are removed. These counterbalancing weights are primarily used so that at either end of the table cycle in the X-direction when indexing in the Y-direction is performed, there is approximately equal torque on the table ways. Therefore, the indexing motor F is under similar loading, and uniform indexing widths at either end of the table are obtained.

Experimental Procedure

Description of Specimens

The test specimens used to evaluate the present apparatus were obtained from several ferrous materials which were field-tested as 5-inch diameter balls in a commercial grinding mill operation as described by Norman and Loeb[20]. The 5-inch balls were sectioned along a chordal plane approximately 1½ inches from the ball surface and three pin specimens were trepanned, using electrical discharge machining, from each ball section (Figure 4) so that the axis of the pin specimen was perpendicular to a tangent on the ball surface. In this manner, the end surface of the pin, which is the testing surface on the present apparatus, corresponded most closely to the field-tested surface on the ball.

The pin specimens, trepanned to approximately 0.280 inch in diameter, were centerless ground to 0.250 inch diameter ±0.001 inch. After being centerless ground, each specimen was placed in a V-block and the end surface which was to be tested was surface ground to approximately 0.030 inch below the surface to obtain a flat testing surface perpendicular to the specimen axis.

The alloys had been sand cast as 5-inch diameter balls. Table 1 lists the composition, the heat treatment, the Rockwell C hardness of the worn ball surface after grinding mill tests, and the ball-mill wear ratio for each material calculated as the volume loss of the given material divided by the volume loss of the standard material BB.

Abrasive Cloths

The coated abrasives used have a cloth backing with resin over resin bonds which anchor and lock the mineral to the backing. The cloth backing of the alumina and silicon carbide abrasives are coated with a pressure-sensitive adhesive for application of the abrasive cloth to the abrasive-carrying platform. Since the garnet cloth roll is not supplied with an adhesive backing, a separate double coated pressure-sensitive tape is applied to the abrasive-carrying platform and the abrasive cloth adheres to the platform by means of this tape. The cloth rolls are supplied in 50-yard lengths of the desired width (8 or 9 inches) and are cut to the proper lengths for testing.

Test Conditions

The abrasive wear response to varying test parameters of alloy material, load, abrasive particle size, and type of abrasive was investigated. The alloys investigated are listed in Table 1. The loads for testing alumina ranged from 3.5 lb. to 29.2 lb. The abrasive particle sizes varied from a nominal particle size of 80 microns to 200 microns; the abrasives, silicon carbide, alumina, and garnet, of 105 micron particle size were used to test the various alloys at a loading of 7 lb.

The parameters kept constant throughout the testing program were the specimen diameter at 0.250 inch, the speed of the abrasive surface at 100 inches/minute, the speed of indexing at 17 inches/minute, the specimen rotation at 20 rpm, and the abrasion path at 488.25 inches made up of 28 passes each 17-7/16 inches long. The ambient conditions of temperature and humidity were approximately constant throughout the testing program, because the tests were performed in an air-conditioned laboratory.

Testing Procedure

1. A clean and weighed specimen is placed in the machine by inserting it in a collet, placing the collet inside the spindle, and tightening the drawbar as already described.
2. The single channel recorder is balanced and calibrated so that it reads zero load with the ram hanging from the load cell and extending the spring. An upward movement of the ram would register a compressive load.

3. The abrasive cloth is rolled out over the abrasive-carrying platform, cut, and affixed to the platform.
4. The machine table is raised so that the abrasive surface pushes against the specimen until the desired load is indicated on the recorder. The machine table is locked in that position so that upward or downward movement of the table is not possible. The ram can still follow the contour of the abrasive surface by moving vertically along the linear bearing in the quill.
5. The variable speed motor controllers are set on the automatic mode of control and are switched on.
6. The desired number of passes is dialed on the counter, and simultaneously the table begins to cycle in the X-direction, the spindle begins to rotate the specimen, the recorder begins to record the load (which is recorded throughout the test), and power is supplied to the other instruments.
7. At the end of each pass, indexing is performed and the counter subtracts one pass from the remaining total.
8. When the counter reaches zero, the test run is complete and all instrumentation is turned off automatically, thereby ending all the machine functions simultaneously. The duration for a run of 28 passes is 5 minutes, and including setting-up time, a run can be completed every 10 to 15 minutes.
9. After each test, the specimen is demagnetized and then cleaned. The specimen is washed in acetone and rubbed

with cotton. (To prevent fingerprints from being left on the specimen, the person handling it wears polyethylene gloves.) The specimen is then placed in clean acetone and ultrasonically cleaned for no less than 5 minutes, after which it is rinsed and rubbed in clean acetone (a new pair of gloves must be worn by the handler). Finally it is dried under a blast of warm air. After being washed and dried, the specimen is placed in a clean glass vial which has been ultrasonically cleaned in acetone.

10. After the specimen has been standing in the stoppered glass vial for no less than 15 minutes, it is handled with forceps and weighed to 0.00001 g on a Mettler analytical balance. After each test the weight is recorded and is used to calculate weight-loss or volume-loss data.

11. Before a new set of abrasive test parameters is applied, each specimen is given a full run-in under the conditions to be studied. The weight losses are recorded but not used for wear data. The purpose of the running-in is to equilibrate the surface characteristics of the specimen (scratches, strain-hardening, etc.) to the new set of abrasive test parameters (load, grit size, grit type, etc.).

Results and Discussion

Statistical Description

To represent quantitative and meaningful parameters indicating the reproducibility of the testing apparatus and the precision of the measurements obtained from the given number of tests, it was necessary to subject the data to statistical analysis. The two parameters chosen were the 95% confidence limits for the population mean weight loss and the number of repetitive tests, calculated *a priori* from the existing data, that would be required to obtain a given precision. As the interval of the confidence limits becomes smaller, the precision or the reproducibility is higher. For less reproducible data, the number of tests required to obtain a given precision becomes larger. A description of the statistics required to arrive at the parameters of reproducibility and precision follows.

If X_1, X_2, X_3, ..., X_n are n determinations of the weight loss for n abrasive wear tests, then the sample mean

$$\overline{X} = \frac{\Sigma X}{n} \tag{1}$$

The standard deviation

$$S(x) = \frac{\Sigma (X-\overline{X})^2}{n-1} \tag{2}$$

S(x) represents the best estimate of the population standard deviation from the sample X_1, X_2, X_3, ..., X_n. The occurrence of n-1 (instead of n) in the denominator of Eq. (2) is to counteract the bias introduced in calculating

the deviations of X from the sample mean, $\bar{X}$, rather than from the true population mean.[31,32,33] The estimated standard deviation of the mean

$$S(\bar{x}) = \frac{S(x)}{\sqrt{n}} \tag{3}$$

The measure of reproducibility or precision of the test to be used here is the 95% confidence limits for the mean of the population, m, as estimated from small sample statistics using the student-t distribution. The t distribution for the present application can be defined[31,32] as the difference between the mean of a sample, $\bar{X}$, and the true mean of the population, m, from which the sample is drawn, divided by the estimated standard deviation of the mean, $S(\bar{x})$:

$$t = \frac{\bar{X}-m}{S(\bar{x})} \tag{4}$$

The t distribution is not a normal distribution. The t function depends on the number of measurements, n, involved in the calculation of $S(\bar{x})$ and has a different distribution for each value of n, approaching the normal distribution as n becomes infinitely large. The number of measurements, n, enters into Eq. (4) as the degrees of freedom, equal to (n-1) for the present calculations. Values of t for different degrees of freedom and at the level of confidence desired are tabulated in many statistics references.[31,32]

To calculate the confidence limits for the mean of the population from the observed sample mean, from the

sample size, and at the level of confidence desired, Eq. (4) can be used in the form

$$m = \bar{X} \pm t[S(\bar{x})] \quad . \tag{5}$$

In n = 4 measurements, the degrees of freedom = 3; at the 95% confidence level, t = 3.182, and therefore, the 95% confidence limits for the mean of the population would be $m = \bar{X} \pm 3.182\ S(\bar{x})$. In contrast with this result, using normal distribution statistics for the 95% confidence limits would yield $m = \bar{X} \pm 1.96\ S(\bar{x})$. Using the student-t statistics to evaluate the reproducibility and precision of data for the wear testing apparatus results in a "tougher", but nevertheless more correct analysis than would normal distribution methods.

Another measure of the reproducibility or the precision of the data obtained under different abrasive testing conditions is the calculated number of repetitive tests, n, needed to locate the true population mean, m, within the predetermined interval $\bar{X} \pm 0.01\ \bar{X}$ when $\bar{X}$ is calculated from the sample of n tests. In the above manner, the standard error (or deviation) of the mean is specified. The statistical hypothesis is that by running n tests, one can locate the true population mean within the specified precision, $m = \bar{X} \pm 0.01\ \bar{X}$.

Since the above hypothesis is based on observed sample statistics computed on n observations, the result is subjected to possible errors or risks.[31,34,35] If the true

population mean is really within ±0.01 $\bar{X}$ of the computed $\bar{X}$, but the sample of n tests shows that it is not, a Type I error is committed. The probability of the occurrence of a Type I error is designated as α. If the true population mean does not fall within 0.01 $\bar{X}$ of the computed $\bar{X}$, but the sample of n tests shows that it does, a Type II error is committed and its probability is designated β. Therefore, α and β are the risks that the n samples will not conform to the predicted hypothesis, and to obtain meaningful results both α and β should be small. The α risk can be set arbitrarily but judiciously. In the present analysis it is essentially the confidence level of the mean (for the t-test). The risk β is affected by several quantities: the difference between the sample mean and its limit desired, the value of α, and the value of the estimated standard deviation.[31] The larger the limit on the mean, the smaller is the risk β; other quantities being fixed, the larger the value of α, the smaller is the value of β. Further, β is dependent on the estimated standard deviation of the mean; as it becomes smaller, β also decreases. The standard deviation of the mean decreases as n increases; thus the risk β is decreased by increasing the sample size. Because α, β, and n are interdependent, the sample size would have to be calculated by a trial and error. However, tables[31] and graphs[34] in the statistical literature give the number of tests needed in a student-t distribution for the significance of a mean in order to control the probabilities of

errors of Types I and II at α and β, respectively, as a function of the maximum deviation between the sample mean and the true population mean desired divided by the estimated standard deviation: $\frac{|\bar{X}-m|}{S(\bar{x})}$; in the present case, $\frac{|0.01\ \bar{X}|}{S(\bar{x})}$.

The index to be used here for the evaluation of reproducibility and precision of the data is to find the number of tests n that would be required to locate the true population mean within $\pm 0.01\ \bar{X}$ of the calculated sample mean $\bar{X}$ with risks of 0.05 for α and 0.05 for β.

Study of Different Abrasives

Table 1 gives the composition, heat treatment, and other pertinent data of the ferrous alloys used in the entire study. Photomicrographs of these alloys are included in Figures 5-10.

The measure for abrasive wear adopted here is the weight loss for the test. Because the samples are of the same size and of similar densities, it was not necessary to use the more rigorous measure of volume loss for the test. Three density determinations obtained for the alloys on three samples for each alloy are reported in Table 2.

To study the abrasive wear response on the three different types of abrasives, alumina, garnet, and silicon carbide, the ferrous alloys listed in Table 1, were tested as ¼-inch diameter pins on 105 micron (120 grit) abrasive under 7 lb. loading. Three samples of each alloy were

were tested; each sample was tested for four runs on garnet and three runs on alumina and silicon carbide. Accordingly, a total of twelve determinations were available for each material tested on garnet and nine determinations on alumina and silicon carbide.

Tables A-1 through A-3 (Appendix A) contain a compilation of the weight loss data for the three types of abrasives including the mean, the range, and the range expressed as a percentage of the mean. The range and percentage range are not statistically so rigorous in describing the precision of the data as the other parameters. Nevertheless, because they are simple concepts and give some indication of the reproducibility and precision of the data, they are included in Tables A-1 through A-3.

Tables A-4 through A-6 give the statistical analysis of the data for the three types of abrasives studied. Table 3 gives the statistical data in condensed form with the mean weight loss, the 95% confidence limits of the mean expressed as a percentage of the mean, and the number of tests n, that would be required to locate the population mean weight loss within one percent of the sample mean weight loss with 95% confidence. These parameters were calculated from the tests for a given material (i.e., the data for all three samples from each material was utilized). It is seen from Tables 3 and A-4 through A-6, that at 7 lb. loading on 105 micron abrasive, the highest precision and reproducibility in the data are available by using alumina; silicon carbide does

not give as good precision as alumina, and garnet gives by far the poorest precision and reproducibility. The above conclusion is based on the magnitude of the interval for the 95% confidence limits, which is progressively larger for alumina, silicon carbide, and garnet for each of the materials tested. Also the number of tests which would be required to give the same desired precision for the three abrasives increases in the order of alumina, silicon carbide, and garnet. Figure 11 is a bar graph showing the mean weight losses for the different materials tested on the three abrasives. Figure 11 shows that under the test conditions studied for all three abrasives the test can adequately discriminate between the materials tested. Abrading with garnet gives the greatest discrimination between the steels and the white cast irons. This is due to the fact that garnet, because it is soft relative to the carbide phase, does not very effectively abrade the carbides, which in the white cast irons tested are present in large volumes and cause small weight losses for the white cast irons. On the other hand, garnet can abrade the steels with nearly as much aggressiveness as alumina or silicon carbide. The result is a wider range of weight losses with garnet than with the other abrasives since alumina and silicon carbide can abrade the carbides in the white cast irons to a higher degree than the garnet.

Figure 12 is a bar graph showing the wear ratios, R, for each material tested on the three different types of

abrasives and also includes the ball mill ratios. The wear ratio is the value of the weight loss for a given material divided by the weight loss of a standard material, taken as material BB for Figure 12 which is also the standard material for reporting data from the field tests.

Figures 11 and 12 demonstrate conclusively that the wear ratio of a given alloy cannot be used directly to compare its relative wear resistance when even one abrasion parameter is varied, although the same materials was used as the standard. If one were to compare the wear ratios in Figure 12 directly, one might conclude that material CC is more resistant to abrasion by silicon carbide than by garnet. Material CC, as were all other materials tested, is less resistant to abrasion by silicon carbide than by garnet as is seen from the weight loss data of Figure 11.

By using the wear ratios, one can compare only the relative wear resistance of the different materials under the same conditions of testing, i.e., Figure 12 truly portrays that when abraded by garnet, material AA is more resistant than FF which is more resistant than BB. The reason that one cannot compare wear ratios for the same material tested under similar conditions with one parameter varied (for example, the type of abrasive) is that the wear ratio is not a true measure of the wear resistance. A true measure of the wear resistance of materials is the volume loss, or in this case, the weight loss, under given conditions of loading, length of abrasion path, and other

testing parameters. Because the wear ratio depends on the wear characteristics of the standard material, it does not usually represent the weight loss data for a given material tested under conditions of a varying parameter, as, for example, different abrasives, since the standard material usually wears mechanistically and quantitatively differently on the different abrasives.

When material BB is taken as standard as in Figure 12, then the wear ratio is set to 100 for material BB when it is tested under garnet, alumina, or silicon carbide, other testing parameters being the same. When comparisons are attempted for the resistance of a given material to abrasion by garnet, alumina, or silicon carbide, one is essentially saying that the weight losses for material BB under the three different abrasive conditions were the same (R = 100) when in reality the weight losses differed. If for some reason the weight losses cannot be used for comparisons, and a wear ratio has to be used, the ideal material that can be chosen for the standard is one that does not change its wear resistance under the changing conditions (i.e., in the present analysis, one that has the same weight loss for all the abrasives). Such a material would directly represent the weight loss data even for changing abrasive conditions, and comparisons could be made either for the resistance of several materials tested under the same abrasive or for the resistance of the same material tested under several abrasives. The poorest choice for a

standard would be a material that varies greatly in weight loss under varying types of abrasive. Figure 11 shows that for the materials tested under the three abrasives, material II would be the best choice, even though not an ideal choice, since the weight losses were the same under garnet and alumina but the weight loss was higher under silicon carbide; the poorest choice for a standard would be material AA since the weight losses under garnet, alumina, and silicon carbide differed greatly. Figures 13 and 14 are included to illustrate the result of using II and AA as standards. Notice that in Figure 14, if one directly compared the same material for the different abrasives, the conclusion would be wrong; for example, one would erroneously conclude that material CC is about 3.65 times more abrasion resistant when tested on silicon carbide than when tested on garnet. The proper conclusion from Figure 14 is that when compared to material AA, material CC wears 4.84 times faster than AA on garnet and only 1.33 times faster than AA on silicon carbide. From Figure 11 material CC wears very little more when tested on silicon carbide than on garnet (not that it wears 3.65 more on garnet than on silicon carbide as might be concluded from Figure 14).

From the preceding discussions, it is seen that the wear ratio is not an intrinsic property of the material and cannot be used to evaluate the abrasion resistance of a given material under different abrasives, as might have been concluded from the work of Kruschov[11] and from a review by

Finkin.[36] The wear ratio depends on the abrasion resistance of the standard material, such property usually changing with changing abrasive conditions but not necessarily changing similarly to the other materials tested. Earlier work by Richardson[7,12] had shown that the wear ratios differed when the materials were tested by soft abrasives or hard abrasives.

Study of the Effects of Load and Grit Size

From the study of the wear resistance on the three abrasives, alumina was chosen for further study of the effects of load and grit size on the abrasive wear phenomenon. This choice was based on the fact that at the parameters of load and grit size (7 lb., 105 micron) previously studied, alumina gave the most reproducible and precise weight loss data. Also from the previous study, it was realized that garnet did not abrade the cast irons to a great degree. It was concluded that garnet was not abrading the carbides which in the white cast irons tested were of the M_7C_3 type, occurring as the second phase for material AA and of the M_3C type occurring as the matrix phase in material FF. Because the present testing apparatus will be used for a study of the effects of carbide morphology, constitution, hardness, and volume on the abrasive wear of Fe-C-Cr white irons, garnet, then, would not be a good choice except for a study of the effects of changing carbide volume. On the other hand, it was felt that silicon carbide

was too hard compared to the carbide phase in the Fe-C-Cr alloys and would not distinguish changes in the parameters to be studied since it would abrade the carbides with equal aggressiveness. Another reason for choosing alumina as the abrasive for further study is its relative hardness compared to that of the carbides. The hardness of the alumina is higher than that of the carbides, but not so high that it could not discriminate between small changes in carbide properties. Furthermore, the alumina seems to rank the materials tested more closely to the ball mill field test than the other abrasives. Therefore, it is anticipated that future work using alumina as the abrasive will more closely relate to field conditions of high stress abrasion.

Tables B-1 through B-4 give a compilation of the weight loss data, the range, and the range expressed as a percentage of the mean for the alloys tested on alumina at varying loads and grit sizes. Alloy GG was eliminated from testing because of the difficulty in obtaining accurate weight loss data after it was tested. Tables B-5 to B-8 give the statistical analysis of the data for varying loads and grit sizes. The statistical data in condensed form, in which the mean weight loss, the 95% confidence limits of the mean expressed as a percentage of the mean, and the required number of tests n to achieve the stated precision on the mean, are given in Tables 4 to 7. It is seen from Tables 4 to 7 and Tables B-5 to B-8 that the testing parameters of 15 lb. loading on 80 micron alumina abrasive give the most

precise and reproducible data for all the alloys tested. The ferrous alloys tested encompassed steels and white cast irons with a wide range of microstructures and compositions, four of which were commercially cast and contained porosities and inclusions in greater proportion than would laboratory alloys. Under similar conditions, future tests of ferrous alloys on the apparatus described would most probably result in data of precision no worse, and most probably better, than the poorest data obtained in the present tests. It is seen from Tables 4 and B-5 that at 15 lb. loading on 80 micron alumina abrasive, the 95% confidence limits for the mean weight loss in 4 tests are ±0.931% of the mean at worst and ±0.353% at best for the alloys tested.

The effect of load on the weight loss for the alloys tested is reported in Figures 15, 16, and 17 for 80 micron, 130 micron, and 200 micron particle size of alumina respectively. It is noted from Figures 15, 16, and 17 that the relationship of weight loss versus load is nearly linear. It can be seen that the relationship becomes more linear as the wear resistance of the alloys decreases; for example, the relationship is more linear for the steels than for the white cast irons.

The effect of grit size on abrasive wear resistance of alloys has been widely reported.[6,8,9,15-17] As the grit size is increased, the wear resistance of the alloy decreases rapidly. At larger grit sizes, the wear resistance is only slightly affected. Above the critical grit size,

increasing, decreasing, or no dependence of wear on grit size is reported.

Figures 18 and 19 show the same general phenomenon. Although the present work lacks sufficient data at small grit sizes, it can be seen that the critical grit size is dependent on the type of alloy tested, and on the load applied, the critical grit size increasing with increasing applied load. Wear beyond the critical grit size is dependent on the type of alloy tested and on the load applied. The wear may be independent, increasing or decreasing with increasing grit size, depending on the alloy and on the test conditions.

It is noticed from Figures 18 and 19, and Tables B-1 to B-4 that the relative wear resistance of the two white cast irons AA and FF depends on the applied conditions of load and grit size. Under certain conditions, material AA is more wear resistant than FF, while under other conditions the opposite is true. Material AA (high Cr white iron) is more abrasion resistant than FF (Ni-Cr white iron) under conditions of small grit size, but the grit size at which FF becomes more wear resistant depends on the applied load. At the lower loads, a larger grit size is required before FF becomes more wear resistant than AA. Because of the dependence of the abrasion resistance of materials AA and FF to varying load and grit size, conditions of testing may be chosen so that the ranking of these two materials under laboratory testing can be the same as the ball mill test ranking.

The same results in conjunction with Figures 5 and 8 strongly suggest the dependence of abrasion resistance to the type of wear process, and on the matrix microstructure, the type, size, shape, and distribution of carbides in multiphase alloys and the carbide size relative to the size of the abrasive particles. This conclusion is based on the fact that in material AA the carbide phase of the M_7C_3 type is discontinuous, while material FF consists of the M_3C type, a continuous network carbide. In material AA, the carbide forms part of the eutectic, while in material FF, the carbide is the primary phase; thus they vary greatly in morphology. Richardson[12,13] has also reported a marked effect on the abrasion resistance of the grit size relative to the carbide size in carbide containing alloys.

The combined effect of load and grit size on the abrasive wear of the alloys tested is shown in Figures 20 through 24. From Figures 20 and 21, it is seen that for the highly abrasion resistant white cast irons, grit size (in the range tested) has a specific effect on the wear resistance of the alloy, the wear resistance decreasing with increasing abrasive particle size. However, the steels (Figures 22 through 24) have a lower abrasion resistance than the cast irons. As these steels become less resistant to abrasion, there is a difference in abrasion resistance on the finest and coarsest particle size abrasive; but there is very little or no difference in abrasion between the larger particle sizes of abrasive. Figures 20 through 24 show also

that the relationship of weight loss versus load is more linear for the larger grit sizes for all the alloys tested. It can be seen again that the relationship of weight loss versus load becomes more linear as the weight losses increase or the wear resistance decreases, whether this is brought about by increasing grit size for the same alloy or by comparing alloys with lower wear resistance.

The wear ratio, R, cannot be used to compare the abrasive wear resistance of a given alloy under changing conditions of load and grit size. This was also true under changing conditions of abrasive type. Figure 25 is included to illustrate the consequences of using the wear ratio for the comparison of the relative wear resistance of a given alloy under changing conditions of the test. For example, if one were to compare the wear resistance of material BB when tested under 7 lb. loading on 200 micron alumina abrasive or on 80 micron abrasive using material AA as a standard, one might conclude that material BB is 1.351 times more resistant when tested on 200 micron abrasive than when tested on 80 micron abrasive. This conclusion is erroneous. From the weight loss data (Table B-1) material BB is 1.085 times more abrasion resistant when tested on 80 micron than on 200 micron alumina abrasive. When material CC is used as a standard, the erroneous conclusion is that material BB is 1.021 times more resistant when abraded on 200 micron than on 80 micron abrasive. It should be noted that both standards can give erroneous conclusions and that the

apparent difference in relative wear resistance changes with the standard. The arguments relating to and explaining the failure of the wear ratio in indicating comparative wear resistances of a given alloy under changing conditions have been given in an earlier section in connection with the discussion of abrasive wear under different types of abrasives. Basically the wear ratio R, is not an intrinsic property of a given alloy, but varies under changing conditions depending on the standard used. The wear ratio can be used only to compare different alloys under constant conditions of abrasive type, abrasive particle size, applied load, and any other applied conditions which effect the wear characteristics of alloys.

The abrasive test conditions of 15 lb. on 80 micron particle size alumina abrasive give the best precision in weight loss data, as already discussed; in addition, these conditions rank the white cast irons AA and FF in the same order as they were ranked by the ball mill test in the field; and finally, these conditions definitely discriminate between all materials tested, and especially between AA and FF. Such was not the case under conditions of 7 lb. and 105 micron alumina (chosen earlier for study of different abrasives) as shown in Figure 11. Table 8 lists the weight losses and ranking of the alloys for testing on alumina abrasive of 105 micron particle size under 7 lb. loading and on 80 micron particle size under 15 lb. loading. Included

also are the weight losses and ranking of the alloys field tested as grinding balls in a ball mill.

METALLURGICAL STUDIES OF HIGH STRESS ABRASIVE WEAR OF Fe-C-Cr ALLOYS

Experimental Procedures

Specimen Materials

Alloy Design. Fe-C-Cr alloys were designed in order to study the effect of volume fraction, morphology, composition, and other microstructural aspects of the carbide phase on high-stress abrasion resistance. Several carbide morphologies in alloyed white cast irons may be obtained by varying solidification rates.[22] Alternatively, various carbide morphologies may be obtained by controlling alloy composition and keeping solidification conditions constant. The composition control method was utilized in the present study.

Maratray[37] has studied the interrelationships of chemical composition, the amount of carbides, and the matrix structure obtained for a given solidification and cooling rate in alloyed white cast irons containing 12 to 25% chromium, 2.2 to 4.3% carbon, and 0, 1.5, or 3.0% molybdenum. Maratray has categorized the morphologies of the primary and eutectic carbides (as attained in various compositions and at the solidification and cooling rate resulting from sand-casting 25 mm diameter bars) into four classes: (1) carbide network plus radiating eutectic, (2) carbide network plus lamellar eutectic, (3) lamellar eutectic, and (4) primary hexagonal carbides plus lamellar eutectic. Figure 26 is a

plot relating the occurrence of the four different morphologies as a function of chromium and carbon contents.[37] Although Figure 26 shows the regions of different carbide morphologies, the plot does not distinguish between the different types of carbides (i.e., M_3C, M_7C_3, $M_{23}C_6$). Figure 27 is a replot of Figure 26, incorporating additional data. The area (Figure 27) bound by the solid lines a-a' shows the chromium-carbon compositions resulting in the M_7C_3 type carbide. In Figure 27, the lines a and a' are boundaries enclosing the $\alpha + M_7C_3$ field as given in an isothermal section at 850 C of the Fe-C-Cr diagram.[38] Since it was desired to study the M_7C_3 type of carbide occurring in several morphologies, the compositions proposed for study are restricted to the area bound by the lines a-a' in Figure 27. Further, a constant matrix composition is expected[39] in alloys of constant Cr:C ratio. Therefore a set of alloys was designed with a constant Cr:C ratio at 6.7 shown as line b in Figure 27. Thus it can be seen that compositions along line b (Figure 27) of increasing Cr and C contents result in alloys of increasing volume fractions of M_7C_3-type carbides within each of several morphology fields, with constant matrix compositions. An austenitic matrix structure for all the alloys can be obtained by cooling the alloys in air from a high temperature after solidification.

The Fe-C-Cr alloys whose compositions fall within the morphology type 2 field were chosen for the study of the effect of molybdenum on high-stress abrasion resistance; two

levels of molybdenum of the aim composition 1.5 and 3.0 percent were added to each Fe-C-Cr alloy in the type 2 field. This particular group was chosen because it encompasses alloys of compositions presently used commercially in high-stress abrasion applications.

Melting Materials. The cast alloys used for specimen materials were made by the addition of commercial ferroalloys and of graphite to Armco iron. The composition in weight percent of the charge materials follows:

Material	C	Cr	Mn	Mo	Ni	P	Si	Fe
Graphite	100	--	--	--	--	--	--	--
Armco Iron	0.019	<0.10	0.08	<0.08	<0.10	0.003	<0.05	Balance
Ferro-chromium	0.038	69.93	0.43	--	--	--	0.20	Balance
Ferro-manganese	0.098	--	85.19	--	--	0.097	0.97	Balance
Ferro-silicon	0.050	0.20	0.99	--	0.16	0.015	46.2	Balance
Ferro-molybdenum	0.050	--	--	61.0	--	--	0.60	Balance

The Armco iron was added as ½-inch rods of one to two inches in length and the other materials as granules of approximately 1/8-inch size.

Melting Procedure. A series of 27 Fe-C-Cr and Fe-C-Cr-Mo alloys were induction air-melted in 26,000 gram batches. Fifteen Fe-C-Cr alloys of increasing C and Cr composition were melted in fifteen separate heating campaigns, while twelve Fe-C-Cr-Mo alloys were obtained from six heating campaigns,

each heat split to obtain an aim composition of 1.5% Mo for the first split and of 3% Mo for the second split. All of the alloys also contained 0.40% Mn and 0.55% Si (aim composition).

The charge materials consisting of the iron, graphite, ferrochromium, and one-half of the total amount of ferrosilicon were packed in alternating layers into alumina crucibles and melted. One minute after the attainment of a melt, the remainder of the ferrosilicon was added and the temperature of the melt was equilibrated to 200 F above the liquidus for the particular alloy. After holding for one minute at the aforementioned temperature, the ferromanganese was added, the melt stirred, and the temperature increased an additional 50 F. Upon reaching a total of 250 F super-heat, the melt was again stirred, a sample for chemical analysis was withdrawn from the melt by suction, and the melt was poured (1) into a "tectip" (essentially a baked sand cup with a thermocouple in the middle of the cup and thermocouple connections outside the cup) and (2) into baked sand molds as ½-inch Y-blocks (ASTM* Specification for Austenitic Ductile Iron Castings -A571). The casting was held in the sand mold for 6 minutes and subsequently shaken out and cooled in air. In the case of the molybdenum-containing alloys, the ferromolybdenum for the first split was included in the charge materials. The additional ferro-

*The Y-block utilized in this study differs from the ASTM standard block in the dimension E which is 8 inches for the present design and 6 inches for the ASTM standard.

molybdenum required for the second split was added to the melt (after the first split was poured) along with small amounts of ferrochromium and graphite to make up for losses due to the longer heating period. The melt was again equilibrated to the pouring temperature and the second split was poured two minutes after the additions were made. The duration of a melting campaign was 60 to 75 minutes, dependent on the alloy (pouring temperature) and on whether the crucible was charged hot or cold.

All of the alloys were poured at approximately a constant superheat of 250 F which was determined by utilizing the liquidus surface of the Fe-C-Cr system as reported by Griffing and coworkers[40] (Figure 28). Pouring the alloys at a constant superheat as opposed to a constant pouring temperature was preferable since with a constant superheat the driving forces for solidification in all the alloys would be similar.

The castings were shaken out of the sand and air-cooled to insure that the austenitic matrix would not undergo high temperature decomposition. The 6-minute wait was based on a preliminary experiment where temperatures in a ½-inch Y-block casting of a similar alloy were monitored at four different positions; for all the alloys cast, waiting six minutes insures solidification of the casting and temperatures of approximately 1800 to 2000 F.

Specimen Preparation. The pin specimens utilized for abrasion testing were trepanned from the Y-block

castings using electrical discharge machining with a graphite electrode. The trepanned specimens approximately one inch in length and 0.280 inches in diameter were centerless ground to a diameter of 0.2500 to +0.0005 -0.0000 inches. Specimens were subsequently placed on a "V-block" and the end-face of the cylindrical specimen was surface ground to remove 0.030 inches of material. This last step produced a testing surface perpendicular to the specimen axis. To avoid heating of the specimen, surface grinding was carried out with a coolant and specimen material was removed at the rate of 0.00025 inches per pass. The specimens were machined from their castings at positions as shown in Figure 29. For the hypoeutectic alloys, two specimens were machined with their axis parallel to the axis of the "Y" and two specimens with their axis perpendicular to the axis of the "Y"; the resulting specimens had test surfaces perpendicular and parallel, respectively, to the heat flow during solidification of the casting. For the hypereutectic alloys, two specimens per alloy were machined with their axis perpendicular to the axis of the "Y".

Specimens were identified by marking the non-testing surface on the end of the pin with a letter for the alloy designation and with a "V" for the specimens machined parallel to the axis of the "Y" in the casting. The duplicate samples for each direction were separated by notching on the end surface one set of specimens, and leaving the other set of duplicate specimens unnotched. The identification of the

alloys abrasion tested is as follows:

Hypoeutectic Alloys	Hypereutictic Alloys	Mo-containing Alloys	
A, A-*	K, K-	F1, F1-	F2, F2-
AV, AV-	KV, KV-	F1V, F1V-	F2V, F2V-
B, B-	L, L-	G1, G1-	G2, G2-
BV, BV-	M, M-	G1V, G1V-	G2V, G2V-
C, C-	N, N-	H1, H1-	H2, H2-
CV, CV-	O, O-	H1V, H1V-	H2V, H2V-
D, D-	P, P-	I1, I1-	I2, I2-
DV, DV-		I1V, I1V-	I2V, I2V-
E, E-		J1, J1-	J2, J2-
EV, EV-		J1V, J1V-	J2V, J2V-
F, F-		K1, K1-	K2, K2-
FV, FV-		K1V, K1V-	K2V, K2V-
G, G-			
GV, GV-			
H, H-			
HV, HV-			
I, I-			
IV, IV-			
J, J-			
JV, JV-			

Chemical Analysis. Two samples for each alloy composition were obtained by suction into an 8 mm pyrex tubing with a Leco sampling gun just prior to pouring the melt and were utilized for chemical analysis. Carbon analyses were obtained by a combustion technique utilizing the Leco 70-sec Automatic Analyzer. Chromium, silicon, and manganese analyses were conducted by wet chemistry.

*The minus sign designates a notched specimen.

Abrasion Testing

Abrasion testing procedures and techniques utilized for this portion of the study were described in the previous section. The abrasion path was 528.75 inches (as opposed to 488.25 inches for that described in the previous section), made up of 30 passes, each 17.625 inches long. The 0.2500 inch diameter specimens were tested under 15 pounds loading on 80 micron particle size alumina. During the test, specimens were rotated at 20 rpm, the abrasive surface was moved at 100 inches per minute, and indexing speed was 17 inches per minute. Each specimen was run-in once under the above conditions and then tested in four consecutive runs. After abrasion testing, the tested specimens were used for most of the metallurgical studies. Not all specimens were used in each study. A flow sheet indicating the specimens used in the sequence of studies follows:

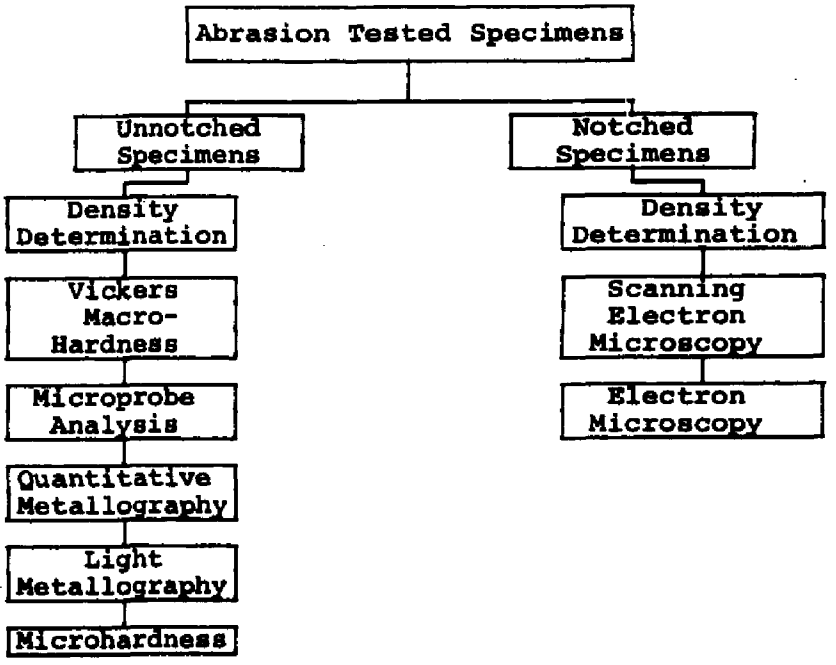

Density Determinations

The density of all the samples tested in high-stress abrasion was determined at the completion of abrasion testing. At this stage, the samples were clean and had been weighed in air to 0.00001 gram. The method applied is based on Archimedes' principle.

To facilitate the complete wetting of the sample by water and the exclusion of air bubbles from the sample surface, 0.2 ml of a wetting agent was added to 500 ml of distilled water. A double hook frame was prepared from 0.010-inch tungsten wire to support the sample for weighing. The clean sample was handled with forceps and transferred to the support frame which was immersed in the distilled water and suspended from the hook on the beam of a keyboard beam balance capable of weighing to 0.0001 gram. In this manner, the frame and sample were weighed while immersed in water. The sample was then lifted with forceps from the support frame and allowed to rest on the bottom of the beaker so that the level of the water in the beaker was unchanged. The frame (without the sample) was then weighed while immersed in water. The temperature of the water was measured and recorded to the closest 0.05 C. The above procedure was repeated for each sample, and from these data the density was determined from the following formula:

$$d = \frac{W_a \, d_w}{W_a - [(W_w + W_f) - W_f]}$$

Where W_a = weight of the sample in air,

W_w = weight of the sample in water,

W_f = weight of the frame in water, and

d_w = density of the water at the temperature measurements were made.

The values for the density of water were obtained from the Handbook of Chemistry[41].

Hardness Testing

Vickers hardness numbers were determined for all the alloys in the as-cast non-abraded condition and on the abraded surfaces of the tested specimens. The hardness tests were performed by using a square-based pyramidal diamond indenter having included face angles of 136 degrees under a load of 10 kg. The hardness of the non-abraded alloys was determined on mounted and polished specimens obtained from material adjacent to the pin specimens. For each specimen tested, four hardness identations were made, and therefore eight determinations per alloy were available for the non-abraded specimens. The abraded surfaces of the unnotched specimens were hardness-tested and five hardness indentations were made on each specimen. Thus, ten determinations were performed on the hypoeutectic and molybdenum-containing alloys and five on hypereutectic alloys.

Microhardness testing utilizing the microhardness-test attachment for the Vickers projection metallograph was performed on the micro-constituents of the polished and etched surfaces of the tested pins. This particular testing

method utilizes the square-based Vickers pyramidal diamond mounted directly on the objective lens. Microhardness testing was performed under 20-gram loading. Each microconstituent phase (austenite, eutectic carbide, and primary carbide) was indented 10 to 20 times for each alloy and the diagonals for all the indentations were measured. However, since the larger indentations for the carbides and the smallest identations for the austenite in each alloy were neglected, only 5 to 10 indentations per microconstituent per alloy were averaged for the final microhardness determinations.

Electron Microprobe Analysis

The electron microprobe was utilized to study alloy partitioning (Fe, Cr, Mo) between the austenite and carbide phases of the experimental Fe-C-Cr and Fe-C-Cr-Mo alloys. Because of the significant effect of Fe in fluorescing Cr and of Cr in absorbing Fe when an alloy containing Fe and Cr is irradiated, the microprobe data must be corrected to obtain a true Cr and Fe analyses. Calibration curves determined experimentally were used to correct such data.

Alloys for Calibration Curves. Coupons from a series of alloys which had been previously prepared for other investigations were available. These alloys simulated commercial compositions and contained varying amounts of C and other minor alloying elements, and were usually not single phase. In order to obtain samples with a single homogeneous phase suitable for microprobe analysis and for

comparison with chemical analysis by standard methods, specimens from the available coupons were heat-treated. Heat treatment temperatures were obtained from constant Cr sections of the Fe-C-Cr diagram[38,42] so that at the level of C present in the alloy, only one phase exists at equilibrium (usually austenite, except in a few cases where carbon was approximately zero and the phase is alpha). The specimen alloy compositions, as were determined by chemical analysis, with their respective heat-treating temperatures, are shown in Table 9. All the specimens in this particular series were heat-treated 25 hours in a tube furnace under argon atmosphere and subsequently water-quenched. The temperature control in the furnace zone utilized was ±5 C.

Another series of pure Fe-Cr alloys ranging from approximately 4 to 81 weight percent Cr were prepared to determine whether C and other minor elements had any effect on the calibration curve. Powders of 99.99 weight percent Cr and Fe were pelletized in the desired proportions and melted in a resistance-heated furnace under vacuum in zirconia crucibles. To obtain good homogeneity, the alloys were cycled 5 times between temperatures of approximately 50 C below the solidus and 50 C above the liquidus and were subsequently cooled to 1400 C, held for 25 hours, and rapidly cooled to room temperature. The entire procedure (as described above) of melting, cycling, and homogenization was carried out without interruption and under vacuum. The cycling portion of the procedure required approximately 90

minutes since heating and cooling in this region was carried out at a rate of 10 C per minute. The ingots obtained from melting were approximately 1/2 inch in diameter by 3/4 inch long. To achieve further homogenization, the ingots were hot-worked at 1400 C by pressing (with an extrusion press) the 3/4 inch-tall ingot to a disc of approximately 1/8 inch thick, which was subsequently oil-quenched. Two adjacent samples were obtained from each disc at a position approximately 1/3 of the radius from the circumference to the center; one specimen was used for microprobe analysis, the other for analysis by wet chemistry.

Three M_7C_3-type carbides of varying Cr and Fe compositions were prepared to generate a calibration curve suitable for microprobe analysis of these types of carbides and to determine whether the calibration for Cr and Fe in the carbide differs from that of the binary. A 40-gram button of each carbide was melted in a furnace using a nonconsumable, thoriated-tungsten electrode and a protective argon atmosphere. Each composition was melted in a water-cooled copper block in approximately 30 seconds. These carbide buttons were subsequently pulverized to obtain -100 mesh powders and the powders repellitized. The new carbide pellets were remelted in a vacuum furnace, held for 10 minutes, cooled to 1350 C, and held for 24 hours. Samples from these heats were used for chemical analysis and for microprobe analysis.

Pure elements Fe, Cr, and Mo were required for

microprobe analysis. Iron of 99.999% Fe, chromium of 99.9999% Cr, and molybdenum of 99.995% Mo were used in the investigation. All the samples were prepared for microprobe analysis by mounting in Bakelite and polishing through laps of one micron diamond paste and finally finished on a vibratory polisher with 0.05 micron alumina powder.

Microprobe Parameters and Data Collection for Calibration Curve Studies. The alloy structures were detected on the microprobe screen from their unetched specimens by using the sample current for detection. Phases of different atomic numbers absorb electrons to different degrees (the higher the atomic numbers, the more absorption); since the emerging electrons are used to form a sample-current picture, phases may be differentiated by this mode of detection from a polished, unetched specimen. The alloys used for calibration were single phase; nevertheless, the structures were viewed with a sample current picture to insure that the specimen was well focussed with the electron beam, and that the beam was probing at a "clean" point (not on inclusions, cracks, etc.).

Microprobe data were collected by using point count mode (i.e., probing at a point rather than on a line or an area scan) with 20 kv excitation voltage while the beam current (as opposed to sample current) was monitored and controlled at 1.25×10^{-7} amperes. Point counting was performed at five different locations for each specimen; at each point two consecutive 50-sec counts were determined for

a total of 100 sec of counting per point. In this manner, the intensities of the Cr $K\alpha_{1,2}$, Fe $K\alpha_{1,2}$ and Mo $L\alpha_1$ lines were recorded in the form of a count. Cr and Fe intensities were obtained simultaneously at each point, since the microprobe is equipped with three spectrometers, two of which are suitable for heavy element detection. The intensity counts were also recorded for the pure elements (Fe, Cr, Mo) at the beginning and the end of each period of counting for the alloys. Background counts for the pure elements and several of the alloys were obtained by setting the spectrometer angle for each line (Fe $K\alpha_{1,2}$, Cr $K\alpha_{1,2}$, Mo $L\alpha_1$) on either side of the peak for the given line, the average of these two counts making up the background count.

The "Probe Ratio". Calibration curves were generated by plotting the probe-ratio K for a given element in the alloy versus the chemical composition of that element in the alloy in weight percent. The probe ratio K is a ratio of the corrected intensity count for the element of interest in the alloy divided by the corrected intensity count for the pure element of interest multiplied by 100. The corrected intensity count is the intensity count minus the background count. For example, K_{Cr} is equal to the corrected intensity for Cr in the alloy divided by the corrected intensity for pure Cr multiplied by 100. The five counts for each element were averaged, and the average count (based on 100 seconds) was corrected and utilized in the determination of K.

Microprobe Data Collection for the Alloys Tested in Abrasion. The austenite and carbide phases (primary and eutectic) were analyzed by microprobe point counting. After abrasion, each specimen was prepared by lightly removing the abraded surface on 400 and 600 grit silicon carbide discs, then polished on diamond laps and finished on a vibratory polisher with 0.05 micron alumina. The samples were "probed" unetched. The structures were detected with a sample current picture. Irradiation of the samples was performed by using 20-kv excitation voltage, and monitoring and controlling the beam current at 1.25×10^{-7} amperes. For each specimen analyzed with the microprobe, two consecutive 50-second counts for the austenite, eutectic carbide, and also for primary carbides in the hypereutectic alloys, were obtained at each of five positions in the pin specimens; at the center of the specimen and on the circumference 0.030 inch toward the center from the outer circumference of the pin at 12, 3, 6, and 9 o'clock positions. Data for Fe and Cr were obtained simultaneously at each point for all the alloys probed. The molybdenum-containing alloys were probed a second time and Mo and Cr counts were recorded; thus for this series of alloys, twice as many Cr determinations were available. Counts for the pure elements were obtained at the beginning and the end of each day for which the alloys were probed. The Cr and Fe analyses of the phases in the alloys were determined by converting the probe data to K ratios and utilizing the calibration curves.

Quantitative Metallography

A Quantimet 720 Microscope Image Analyzing Computer was utilized to obtain quantitative metallography data for the entire series of abrasion-tested alloys. A television camera scans the microscope image with a series of parallel line scans and the image is displayed on a monitor screen. Electrical impulses detected from the line scans and based on the degree of contrast (gray level) of the microstructural features are channeled to a computer whose logic circuits enable it to perform counting, sizing, measuring, and other quantitative operations.

The same abrasion-tested specimens used for the microprobe analysis, were utilized for the Quantimet study. They were lightly repolished on a vibratory polisher with 0.05 micron alumina. Contrast between the carbides and the austenite was developed by stain etching of the carbides in a solution of 4% NaOH saturated with $KMnO_4$ for 10 to 15 seconds.

The Quantimet analysis was performed at a magnification of 520. Fifty fields per specimen, uniformly spaced throughout the end area of the pin, were analyzed. The structure was projected on a screen of approximately 293 by 234 mm with 500,000 picture points per field utilized in the detection. The parameters recorded in picture-points for the detected carbide particles were the total area of the particles, the intercept, and the end count for each of the fifty fields. The intercept measurement was the total pro-

jected length (90° to the direction of line scans) of the particles. The end count was the number of downward projecting carbide particle segments. The calibration of the Quantimet counting system at the magnification utilized (520X) was such that 0.200 mm was equal to 786 picture points; the calibration was obtained by using a stage measuring micrometer scale.

To quantitatively determine the carbide morphologies in the alloys, specimens were analyzed by point counting of the several carbide morphologies available in each specimen. Point counts were obtained on the microstructure projected on the ground glass screen of the metallograph. A grid was placed on the screen which contained 176 points, one cm apart in a 16 by 11-point array. Ten areas were counted at 400X for each determination except for some of the hypereutectic alloys which has a coarser structure and were counted at 300X.

Scanning Electron Microscopy

The abraded surfaces of some of the notched specimens were examined by scanning electron microscopy using the secondary electron image with an exictation voltage of 25 kv. The actual abraded pin specimen was used without further preparation.

To study damage of the carbide phase, specimens were examined under the same conditions as above, but a thin layer of the matrix phase was removed by electrolytically etching the abraded surface. A 10% solution of HCl in

methanol with the specimen as anode under a current density of 0.09 amperes/cm^2 was utilized. Specimens were etched between 30 and 45 seconds, depending on the alloy. Carbide morphology was examined similarly except that the matrix was removed to greater depth by electrolytically etching 1 to 2 minutes.

Electron Microscopy

Specimens were examined by electron microscopy to study structural changes induced by the abrasion. A longitudinal cross section (at a depth of approximately 1/3 of the radius) of the specimen leading to the abraded edge was mounted. Surface replicas from the mounted, polished, and etched specimens were prepared, employing the two-stage plastic-carbon technique. The preparation of the specimen surfaces for replication consisted of mechanical polishing followed by vibratory polishing (in the final stage) and electrolytic etching in 50 percent aqueous HNO_3 solution using the specimen as cathode.

Light Metallography

The microstructures of all the unnotched specimens were examined after abrasion-testing by means of light microscopy. The specimens, which had been previously prepared for Quantimet analysis, were repolished on 6, 3, and 1 micron diamond paste laps and finally polished by using an "attack-polish" technique. This technique was carried out by polishing on a cloth wheel utilizing alumina powder of

0.05 micron size suspended in saturated picric acid. The microstructures were revealed by etching the specimens for 10 seconds in a solution of

2.5 g	Ferric chloride,
5.0 g	Picric acid,
2.0 ml	HCl (s.g. 1.19), and
90 ml	Ethyl alcohol.

Experimental Results

Chemical Analysis of Alloys Used for High Stress Abrasion Testing

The chemical analyses of the alloys utilized for high stress abrasion are given in Table 10; included also in this table is the value for the Cr to C ratio for each alloy. The manganese, silicon, and molybdenum analyses are correct to within ±0.01 percentage point. The carbon up to 2% was correct to ±0.01 percentage point, up to 3.25% correct to ±0.02 percentage point, and above 3.25% correct to ±0.03 percentage point. The Cr up to 25% was correct to ±0.1 percentage point, and above 25% was correct to ±0.15 percentage point. The Cr to C ratio for the Fe-C-Cr alloys had a mean value of 6.64 + 0.10 - 0.11 with six alloys above and eight alloys below the mean value. The composition for alloy J was designed to produce a fully eutectic structure and of necessity deviated from the constant Cr to C ratio; its ratio was 7.37. The Fe-C-Cr-Mo alloys whose compositions were aimed to contain the Cr and carbon contents of alloys F through K in the Fe-C-Cr series and with 1.5 and 3.0 per-

cent molybdenum had a slightly higher mean Cr to C ratio of 6.91 + 0.08, -0.13 (excluding alloy J1 and J2) with five alloys above and five below the mean value.

The Fe-C-Cr alloys were designated by using alphabetical letters; as the Cr and C of the alloy was increased, a "higher" letter was used for designation. The molybdenum-containing alloys were given the same letter for the given Cr and C aim composition of the Fe-C-Cr series, and a number designating the level of aim molybdenum present: 1 and 2 for 1.5 and 3.0 percent Mo, respectively. For example, alloy F belongs to the Fe-C-Cr series and F1 and F2 have the same aim Cr and C as F, and in addition, an aim composition of 1.5 and 3.0 percent molybdenum, respectively.

In the following studies, wherever a result is compared or correlated with the total composition of the alloys, the chromium content was chosen. However, since the carbon content of the alloys is directly proportional (constant Cr:C) to the chromium content, similar functional relationships exist for the C as for the Cr.

Density

The results on the density of the specimens are reported in Table 11 and Figure 30. The average of the specimen densities for a given alloy is reported as the alloy density. In a few cases, the density of a given specimen was not utilized in the average since its measured density deviated from the other specimens of the same alloy. The alloy densities were subsequently utilized in the con-

version of the weight loss data to volume loss for the alloys tested in high-stress abrasion.

High-Stress Abrasion Test Results

It was noticed in a preliminary study of the alloy microstructures that the eutectic carbide morphology for a given alloy varied on different cross sections of the same casting. Specimens in two directions for each of the hypo-eutectic alloys with their test surfaces either parallel or perpendicular to heat flow during solidification were abrasion tested. It is recalled that the specimens with their test surfaces perpendicular to the heat flow were marked with a "V".

The results of abrasion testing are reported in Table 12. Included in this table are the mean weight losses for the alloys tested in either of one or two directions, the 95% confidence limits of the mean weight loss (calculated using the "Student-t" statistic), the mean volume loss, and the abrasion resistance, AR, defined for the purpose of this study as the reciprocal of the volume loss. Appendix Table C-1 gives more detailed data on the abrasion testing and included are the weight losses for each of the respective tests, the mean weight loss, the standard deviation and the standard error of the mean.

From these data the remarkably high reproducibility of the abrasion testing is evident. One exception was for alloy P, which contains a large amount of massive primary carbide held within a relatively small amount of austenite.

The hypoeutectic alloys do not show a marked change in abrasion resistance with increasing carbon and chromium content, and indeed, a general decrease in abrasion resistance is evident. There is a small difference in abrasion resistance of the same alloy tested in different directions; in general the "V" specimens had lower wear resistance. A very marked effect in abrasion resistance is realized in the hypereutectic alloys and an increase in the carbon and chromium content (therefore, the volume fraction of primary carbide) results in increased high-stress abrasion resistance. The molybdenum-containing alloys show a small increase in abrasion resistance compared to the base Fe-C-Cr alloys.

Hardness

The Vickers hardness for the alloys in the non-abraded and abraded conditions are reported in Table 13 and plotted in Figures 31 and 32. As the C and Cr of the alloys are increased (therefore, the volume fraction carbide), the hardness is increased. The abraded specimens have higher hardness than the non-abraded specimens and therefore work-hardening must have accompanied the high-stress abrasion. Furthermore, even the alloys with substantial amounts of carbide show an increase in hardness after abrasion testing. Thus the carbide phase must undergo work-hardening. No appreciable differences are noticed in the hardness values of the molybdenum containing alloys.

The microhardness of the austenite and of the

carbides in the alloy is reported in Table 14; also included is the number of filar units for the average length of the indentation diagonals at 800X (the maximum magnification obtainable for the measuring of the diagonals). Since the austenite and carbide indentations are affected by underlying carbide and austenite, respectively, and because of difficulty in correctly reading the diagonals of small indentations; the differences shown in Table 14 are not significant and the microhardness of constituents in all the alloys are considered approximately constant.

Electron Microprobe Results

Calibration Curves. The composition of all the alloys for the major elements utilized in the calibration studies are included in Appendix Table D-1; the weight percent Fe was obtained by difference. The alloy compositions and probe ratios, K, for the specimens used in the calibration for Fe and Cr in solid solution phases of Fe-Cr (with carbon and other minor elements in solid solution), and in the M_7C_3 type carbide are reported in Table 15. Figure 33 is the K vs composition in weight percent calibration curve generated for determination of Fe and Cr from microprobe data. From Figure 33, the Fe calibration for the carbides falls on the Fe calibration for the binary, while the Cr in the carbide was fluoresced to a lesser degree than the Cr in the binary. Also the Cr was fluoresced and the iron was absorbed; as shown by the calibration curve, since Cr and Fe lie above and below, respectively, the 1 to 1

ratio (45° line) of K versus composition in Figure 33. It is seen from Figure 33 that the points for the "pure" Fe-Cr alloys and for the commercial type alloys fall on the same curve, and therefore, the calibration is not affected by the presence of minor elements (C, Mn, Si, etc.).

The alloys utilized for the study of the effect of Mo on the Cr calibration are grouped into four series of approximately 1, 2, 3.5, and 5 percent (by weight) Mo, respectively, with the Cr ranging from approximately zero to 20 percent as shown in Table 16. Figure 34 is a plot of K_{Cr} versus percent by weight of Cr for the above alloys. The actual data points at the different levels of Mo are plotted, and the curve drawn through the points is the same curve as Figure 33 for the pure Fe-Cr calibration up to 20 percent Cr. It is seen that Mo up to approximately 5 weight percent had no effect on the calibration curve for Cr in the Fe-Cr base alloys up to approximately 20 percent Cr. It is assumed that Mo will have no effect on the Cr calibration for Cr composition of the M_7C_3 carbide (40-50% Cr) and that the Cr analysis for a carbide containing Mo can be obtained from the carbide calibration (without Mo) curve of Figure 33.

Data for the calibration of Mo up to approximately 5 percent Mo in Fe-Cr alloys was grouped into four series of alloys at various levels of Cr, as shown in Table 17. The data are plotted in Figures 35 through 38; it is seen that the plots are straight lines and furthermore all the slopes are approximately the same. Therefore, Cr up to approx-

imately 25 percent has no effect on the Mo calibration in iron base chromium molybdenum alloys (up to 5% Mo). As seen from Figures 35-38, some of the X-rays from the molybdenum irradiation in the iron-chrome base alloys were absorbed (Fe must have absorbed Mo radiation since Cr had no effect) and from the average of the approximately constant slopes of Figures 35-38, K_{Mo} = (0.81) (weight percent Mo). A regression analysis on K_{Mo} with percent Mo and percent Cr as the independent variables showed the same result: Cr did not significantly contribute to the regression equation and a regression coefficient on percent Mo of 0.806 and a correlation coefficient of 0.999 was given without the inclusion of % Cr in the equation. Because the regression could not be forced to zero with the available program, a negligible intercept of -0.0018 was also given. To analyze for Mo from the microprobe data, the equation as given above (K_{Mo} = 0.81% Mo) was utilized for the molybdenum-containing abrasion tested alloys.

Table 18 shows the background counts obtained on several of the alloy compositions and on the three carbides. The background counts subtracted to correct for the element intensity for the calculation of K was a constant number for the element in a particular phase of each alloy. This was justified since the background count was independent or only a mild function of alloy composition, and more importantly, the background count is a very small number compared to the pure element count and for the count in the alloy (which is

divided by the pure element count to obtain K) of the compositions of interest. For example, the intensity counts per 100 seconds for pure Fe and Cr are approximately 680,000 and 820,000 counts, respectively. For an Fe-Cr alloy containing approximately 10 weight percent Cr, the intensity count per 100 sec is approximately 110,000 and 600,000 counts for Cr and Fe, respectively. It is noted that the fluctuations in the relatively small background counts (Table 18) would result in negligible changes in the corrected intensities, and even smaller changes in the calculation of K. The background counts per 100 seconds utilized in the present studies for the Fe-Cr single phase alloys and for the pure standards were 1450 and 2250 counts for Cr and Fe, respectively; for the carbides, 1400 and 2000 counts for Cr and Fe, respectively; and for the molybdenum-containing alloys, 720 counts for Mo in either the austenite or carbide phase, and 1820 counts for the pure Mo standard.

Phase Compositions of Alloys Tested in High-Stress Abrasion. The alloy phase compositions, as determined from the microprobe data and calibration curves, are reported in Table 19 and Appendix Table D-2. In Table 19, the compositions are averages of all the determinations per alloy per phase. For the hypoeutectic alloys, specimens of the alloy were tested in two different directions. Appendix Table D-2 lists the K's and compositions of the alloys for each determination. Figure 39 is a plot of the chromium in the matrix as a function of total Cr of the alloy. Although

the alloys were of constant Cr to C ratio, the chromium in the matrix was not constant as predicted by Maratray[39]. The Cr in the matrix increases with total Cr for the hypo-eutectic alloys, and decreases in the hypereutectic alloys. Figure 40 is a plot of the eutectic and primary carbide compositions as a function of total Cr in the alloy. In general, the Cr in the carbides increases as the total Cr of the alloys is increased. From Table 19, the Mo content of the matrix seems to be constant at each level of total Mo in the alloys. For the carbides, the Mo is not uniformly distributed (Appendix Table D-2), but as an approximation, it could be considered constant. Tables 19 and D-2 and Figures 39 and 40 show that Mo in the matrix (austenite) and carbide phases substitutes for iron since the Cr compositions of the phases in the Mo-containing alloys do not differ from the Cr composition of the Fe-C-Cr alloys.

Light Metallography

Representative microstructures of the alloys tested in high-stress abrasion are included in Figures 41-43. The matrix structures of all the alloys were austenitic. Carbide morphologies of several types were present in the alloys. Contrary to the results reported by Maratray[37], the carbide morphology was not solely a function of composition, but several carbide morphologies were present in each alloy composition. Also, the carbide morphology differed in specimens sectioned in different directions from the "Y"-block castings (that is the relative amounts of the

different morphologies in specimens of the same alloy reviewed in different cross sections differed). It was necessary to classify an additional type morphology (additional to the types described in the previous section) which was found in the present alloys and is shown in Figure 4le and f. For the purpose of these studies, this type of morphology is called the "carbide rod in transverse cross section" morphology.

The molybdenum-containing alloys were similar to the Fe-C-Cr alloys. However, the Mo alloys contained smaller volume fraction of carbides and different relative amounts of the carbide morphology types. An additional minor microconstituent (approximately 1% in the 3% Mo alloys, and less than 1% in the 1.5% Mo alloys) was present in the molybdenum-containing alloys; this was an eutectic-like phase containing a very fine dispersion of Mo_2C carbide. This phase appeared at austenite grain boundaries and was resolved at a magnification of 1000X.

Quantitative Metallography

Results of Point Counting. The results of point counting the different types of carbide morphologies, lamellar eutectic carbide, radiating eutectic carbide, and eutectic carbide rod in transverse cross section, are reported as a percentage of each type and as an absolute percent of the alloy microstructure for the primary carbide in Table 20.

Quantimet Results. The mean value in picture points (50 fields) for the intercept, the end counts and the area of the carbide phase for each specimen as obtained from the quantimet are reported in Table 21; included also are the calculated standard deviations for these values as obtained from the 50 fields. Table 21 also reports results calculated from the quantimet data. A brief description of the parameters calculated from the quantimet data is given in Appendix E. These are the area fraction of carbide, the average particle size (area/end count), the average radius of curvature of the carbide particles, a shape parameter (area/intercept ≃ area/perimeter, since perimeter = intercept $\pi/2$), another shape parameter $\left(\frac{I}{A} \times \text{area fraction}\right)$, and a number representative of the average austenite grain size (500,000/I = total no. of picture points in the field/intercept). The point counting data on the percentage of each type of morphology in a given alloy, in conjunction with the total area fraction of the carbide phase obtained from the quantimet data was utilized to calculate the specific area fraction of carbide of each type morphology. These values are also reported in Table 21.

Electron Microscopy

Results of the surface replicas are shown as electron micrographs in Figures 44 to 48. Figures 44 and 45 show austenitic matrices with eutectic carbides, and eutectic plus primary carbides, respectively. Figure 46 shows slip lines in austenite adjacent to the abraded

surface, but no transformation of the austenite to martensite due to the abrasion is evident. Figure 47 shows the minor eutectic-like phase in the molybdenum-containing alloys. A particle which was extracted from this phase and its diffraction pattern is included in Figure 48. Table 22 gives the d-spacings calculated from the diffraction patterns of three such particles which are identified as Mo_2C by comparison with published[43] d-spacings.

Scanning-Electron Microscopy Results

Results of scanning electron microscopy are included in Figures 49 to 64. Figures 49 to 55 show the abraded surfaces. Figures 56 to 60 show abraded surfaces after light removal of the matrix. Carbide morphologies are shown in Figures 61 to 64 (and 56-60). The lamellar carbide normally thought to consist of "wavy" plates is a complex structure made up of imperfect bundles of rods which are often hollow. Figures 62c and d show how the hollow rods may be infiltrated with austenite during solidification.

Regression Analysis

A stepwise regression analysis program which selects independent variables in the order in which they account for variation in a dependent variable was used to analyze the wear data. Variables in the regression are entered in the order in which they cause the greatest reduction in the sum of squares per step.

Table 23 shows the variables that were analyzed for correlation, using 40 observations per variable in the

analysis. Included in Table 23 are the values of the correlation coefficients for the highly correlated variables. Because of the systematic design of the alloys, many of the variables showed a high correlation and were thus not truly independent. The variables used in the regression analysis did not have a high correlation to each other. Three data matrices were used for regression analysis: (1) the data for hypoeutectic Fe-C-Cr alloys, (2) the data for all the hypoeutectic alloys, i.e., including molybdenum containing alloys and (3) all the data from hypoeutectic and hypereutectic Fe-C-Cr and Mo containing alloys. Interaction parameters for the regressions of the above data matrices did not improve the correlations. The dependent variable for the analyses was the abrasion resistance, AR, previously defined as the reciprocal of the volume loss for the given alloy tested in high stress abrasion. The independent variables 3, 5, 6, 7, 21, 23, 24 and 25 were used in the regression analysis of data matrix (1), the variables 3, 5, 6, 7, 14 and 21 for data matrix (2), and variables 2, 3, 5, 6, 7, 14, 21, 22, 23, 24, and 25 for data matrix (3). The regression equations obtained for each of the three sets of data are reported in Table 24.

DISCUSSION

Phase Structures and Properties

Matrix Phase

It was the intent of this research to study the effects of varying carbide characteristics on the high stress abrasion resistance of Fe-C-Cr alloys. As outlined in a previous section, based on the knowledge of Fe-C-Cr alloys at the inception of this research, the alloys investigated were designed to contain constant matrix properties with varying volume fractions and morphologies of M_7C_3 carbides.

The matrix structures of the alloys were austenitic, typical structures are shown in Figures 41-43. Electron microscopy of surface replicas, Figures 44 and 45, also showed the matrix to be single phase. The two "pools" of austenite completely surrounded by and within the primary carbide in Figure 45, indicate that the carbides are not always solid and are infiltrated with matrix.

The matrix microhardness of the alloys reported in Table 14 are of approximately constant hardness at 380 (kg/mm^2) VHN. Although the (matrix) values in Table 14 seem to increase slowly with increase in Cr and C contents, the hardness indentation is affected by increasing volumes of underlying carbide.

The matrix Cr and Mo contents of the alloys were

analyzed using the electron microprobe. The microprobe data for Cr were corrected using the calibration curve of Figure 33. The Mo data were corrected using the equation K_{Mo} = (0.81)(weight percent Mo), where K_{Mo} is the probe ratio. The equation was derived from the calibration curves for Mo of Figures 35 to 38, and a regression analysis on K_{Mo} with percent Mo and percent Cr as the independent variables as discussed earlier.

The relationship of matrix Cr composition as a function of total chromium, in alloys with a constant Cr:C ratio of 6.64, is shown in Figure 39. It is seen that the matrix Cr is not constant, as reported by Maratray[39], for constant Cr:C compositions, but varies with the total Cr of the alloy. Figure 39 shows that the chromium in the matrix for the hypoeutectic alloys increases from approximately 7.8 to 12.8 percent with increasing total Cr of the alloys. At low Cr contents in the alloy, there is not enough Cr to satisfy the maximum solubility of Cr in the austenite and as the total Cr is increased more is available for the matrix. Thus the matrix Cr increases with increasing total Cr up to the eutectic composition. In the hypereutectic alloys, primary carbide forms first during solidification and since it is higher in Cr than the eutectic carbide (Figure 40), and tends toward the stoichimetric Cr_7C_3 composition, the remaining liquid is impoverished in Cr and less Cr is available for solution in the matrix. As the Cr content of the alloys is increased above the eutectic,

more primary carbides of increasing Cr composition are formed (Figure 40), and thus the matrix Cr decreases. When enough total Cr is present to satisfy the primary carbide Cr composition, the matrix Cr composition begins to rise with increasing total Cr.

Table 20 shows that the molybdenum in the matrix remained approximately constant at 0.73 and 1.30 weight percent for the 1.5 and 3% molybdenum containing alloys, respectively. Figure 39 shows that the Cr content of the matrix for the molybdenum alloys did not vary from the Cr content of the Fe-C-Cr base alloys and therefore Mo substituted for some of the iron in the matrix. Table 14 shows that molybdenum had no appreciable effect on the microhardness of the matrix.

Electron microscopy showed that the austenitic matrix of the alloys did not undergo a martensitic transformation under high stress abrasion. Alloys most likely to transform would have been those of lowest matrix Cr content. Several specimen surfaces were studied with low Cr in the matrix and Figure 46 is typical of these studies. The area shown in Figure 46 is adjacent to the abraded surface; slip lines and fractured carbides due to the high stress abrasion are evident, but no martensitic transformation was found.

The above studies show that the matrix characteristics of all the alloys were kept constant except for the matrix Cr composition. However, the hardness of the matrix

was not affected by the variation of its Cr content. It will be shown that the variation in matrix Cr probably had no effect in the work-hardening characteristics of the matrix during high stress abrasion.

Carbide Phase

Light microscopy micrographs showing the carbide morphologies are reported in Figures 41 to 43. A morphology type additional to those described in an earlier section under "Alloy Design", was found in the present alloys and is described as the "carbide rod in transverse cross section" morphology. It was important to classify this type of carbide morphology for the present studies, since the carbide rod is aligned approximately normal to the abrasion surface. It would remain in the structure for a longer time during abrasion and when finally pulled out of the structure only a small volume of carbide would be lost. If the carbide rod is aligned parallel to the surface such as in the lamellar eutectic carbide morphology, after a short time under abrasion the rod may be pulled out resulting in a larger volume of carbide lost. It is realized that the three eutectic carbide morphologies shown in Figure 41 may not indeed be distinct forms of carbides in their three-dimensional aspects; however, since abrasion is a surface phenomenon it is justifiable to classify the morphologies as has been described. Contrary to the results reported by Maratray[37], the carbide morphology was not solely a function of composition but several morphologies

were present in each alloy (Figure 43 and Tables 20 and 21). Further, the relative amounts of each type of eutectic carbide morphology differed in specimens of the same alloy taken in mutually perpendicular directions as shown in Tables 20 and 21. Carbide morphologies as studied by scanning electron microscopy are shown in Figures 61 to 64. Figures 61, 62 and 63(a) and (b) show that the lamellar eutectic carbide is not made up of plates as is often assumed. It is seen that the lamellar eutectic is made up of bundles of imperfect carbide rods, which are often hollow, surrounded by austenite in the present alloys. Many of these carbides are only half formed and resemble sugar cane split longitudinally, Figures 62(c) and (d) and 63(a) and (b). Figure 64 shows primary carbides which are massive and imperfectly formed. These carbides contain many fissures which became infiltrated with matrix (as is seen in Figures 43 and 45). Figure 64(a) shows that the eutectic carbides in certain instances grow from the primary carbides.

The microhardness of the carbides reported in Table 14 are considered approximately constant, although the hardness number shows considerable variation. The length of the microhardness indentations (Table 14) does not vary significantly, and further, it is difficult to correctly measure the diagonals of small indentations. More importantly, the carbide morphology (hollow rods) is such that on the polished surface the carbide appears "solid", but in fact is probably very thin and filled with austenite just

beneath the surface; the low microhardness determinations in Table 14 are thus suspect, and the carbide microhardness is probably constant at 1735 kg/mm^2 (VHN 0.02). Maratray[39] has reported Vickers microhardness (VHN 0.05) in carbides of alloys similar to those studied in the present work at 950 and 1444 for carbides indented on a transverse cross section and longitudinal cross section, respectively. The carbides are probably not anisotropic enough to show such a large difference in Vickers microhardness under an applied load of 50 gram. The difference in hardness is probably due to the morphology of the carbide rod filled with matrix.

The volume fraction of carbide increased with increasing Cr and C contents of the alloys as shown in Figure 65 and Table 21. The carbide volume of the hypoeutectic and the hypereutectic alloys increased linearly with increasing Cr content, but a discontinuity (Figure 65) occurs in the transition between the hypoeutectic and hypereutectic alloys. The volume fraction of carbide in the hypereutectic alloys is 7 to 10 volume percent lower than would be obtained by extrapolation of the curve from the hypoeutectic alloys. As would be expected, the volume fraction carbide versus percent Cr curve of Figure 65 is similar to the density versus percent Cr plot of Figure 30.

The chromium composition of the eutectic and primary carbides as a function of total alloy chromium is reported in Figure 40. It is seen that Cr in the eutectic carbides increases (with a discontinuity at the eutectic composition)

with total Cr of the alloy and reaches a maximum at 30% total Cr. Further increase in total Cr results in a drop in eutectic carbide Cr. The Cr compositions of the eutectic carbides in the alloys studied, ranges from a low of approximately 44 weight percent Cr at a total alloy Cr content of 10 percent to approximately 55 weight percent eutectic carbide Cr at an alloy Cr content of 30 percent (for constant Cr:C of 6.64). In general, the Cr content of the primary carbides increases with total alloy Cr, although there are some fluctuations as shown in Figure 40. The primary carbide Cr ranges from approximately 56 to 62% Cr at 22 and 30 weight percent total Cr of the alloy, respectively. Figure 40 shows that in all the hypereutectic alloys the Cr composition of the primary carbides is higher than that of the eutectic carbides.

The carbide type in the alloys is M_7C_3 , as discussed earlier (in the alloy design section), based on the 850 C isothermal section of the Fe-C-Cr phase diagram[38], the alloy compositions fall entirely within the γ + M_7C_3 field as shown in Figure 27. Two other possibilities, but not likely in these alloys, are the M_3C and $M_{23}C_6$ carbides. Kuo[46] reports a maximum solubility of Cr in the M_3C carbide of 18 weight percent; the carbides in the present alloys cannot be of the M_3C type since Cr in these carbides ranged from approximately 44 to 62 weight percent as shown in Figure 40 and Table 19. Carbides of the $M_{23}C_6$ type contain approximately 5.4 weight percent C and the M_7C_3 approximately 8.7% C. If the total Cr and Fe composition of the carbide in the alloys

studied (Table 19) are subtracted from 100, an approximate number for the carbon composition is obtained. In this manner the calculated carbon contents range from approximately 7 to 9 weight percent. The carbides in the alloys studied are therefore not $M_{23}C_6$. Further, X-ray diffraction of carbides extracted from two alloys of compositions, 20.44 chromium and 2.72 carbon and 25.74 chromium and 3.61 carbon, with higher Cr:C ratios than the alloys studied (i.e., these alloys fell closer to the $\gamma + M_7C_3 + M_{23}C_6$ field) showed those carbides to be M_7C_3.

As an approximation, molybdenum in the carbides can be considered constant at 2 and 4 weight percent for the 1.5 and 3% Mo alloys, respectively. Table 14 shows that molybdenum had no appreciable effect in altering the carbide microhardness. Molybdenum had no appreciable effect in altering the Cr composition of the carbides as shown in Figure 40 and Table 19. The volume fraction of carbides in the molybdenum containing alloys decreased by 2 to 8 volume percent at the same Cr level as shown in Figure 65 and Table 21.

The above discussion shows that carbide volume fractions, morphologies, and carbide chromium contents were varied while the carbide type and hardness were kept constant in the alloys studied.

High Stress Abrasion Resistance

As the Cr in the matrix increases (Figure 39) for most of the hypoeutectic alloys, the abrasion resistance

decreases (Figure 66). The increase in hardness (Figure 32) of the abraded surface, over the non-abraded surface hardness (Figure 31), was small and approximately constant in these alloys (of increasing total Cr up to 17.5%) with approximately 7.8 to 12% Cr in the matrix. Although a small amount of hardening of the matrix or eutectic carbide occurred, the abrasion resistance decreased and the effect must have been due to an increase in eutectic carbide volume. The Cr in the matrix remained approximately constant at 12 ± 1 percent in the alloys of higher Cr and C contents, while the total fraction of matrix decreased. The substantial increase in the abraded surface hardness of those alloys above 18% total Cr (at Cr:C of 6.64) cannot be attributed to work-hardening of the matrix. The increase in hardness of the abraded surface must be due to work-hardening of the carbide phase. A comparison of Figures 32 and 40 shows that the degree of work-hardening may be related to the Cr content of the carbides. Figure 66 and Table 12 show that the abrasion resistance of the hypereutectic alloys increases by approximately 22% for alloys up to 28.6% Cr (with Cr:C of 6.64) containing up to 53 volume percent of total carbides with up to 20 percent primary carbides (Figure 65 and Table 21). These alloys show a higher hardness for the abraded surfaces (Figures 31 and 32). However, the hypereutectic alloys with up to 26 percent Cr containing up to 17.5% volume fraction of primary carbides (Table 21) and up to 48 percent total carbides (Figure 65)

show an approximately constant abraded surface hardness (Figure 32) while their abrasion resistance increased by approximately 17.5% (Figure 66). The increase in abrasion resistance of the hypereutectic alloys must be due to an increase in the volume fraction of the massive primary carbides.

The abraded surface hardness decreased from its maximum value at 28.6% Cr, Figure 32 (20% primary carbide), and reached the hardness of the non-abraded surface in the 33.6% Cr alloy (35% primary carbide). The abrasion resistance (Figure 66) followed the same pattern and dropped from its maximum value in the 20 percent primary carbide alloy to a value similar to that for a few percent primary carbide (or to the high range for the hypoeutectic alloys) in the 35 volume percent primary carbide alloy. The decrease in the abraded surface hardness in the above alloys is probably due to spalling of the primary carbides under the applied high stress abrasion preventing deformation and work-hardening of the carbide. The spalling also caused greater volume losses during abrasion. The larger scatter in the weight loss data (Table C-1) for specimen P (33% Cr, 36% primary carbide) gives the same evidence for spalling. It was also virtually impossible to polish specimen P without spalling of the primary carbide.

It is seen that although work-hardening occurs in the carbide phase and that it may be related to its Cr content, the abrasion resistance of the alloys must be more

fundamentally related to the presence of varying volumes of eutectic and primary carbides. The abrasion resistance as a function of volume fraction carbide reported in Figure 67 is similar to Figure 66, not because Cr content per se affects abrasion resistance, but because the carbide volume in these alloys of constant Cr:C ratio is directly related to the Cr content of the alloy (Figure 65). Figure 67 shows that the abrasion resistance decreases in the hypoeutectic alloys with increasing carbide volume. The abrasion resistance in the hypereutectic alloys is markedly improved and increases with volume fraction of primary carbide up to a maximum of approximately 20 percent (with a total carbide volume of 53%). Since the metallurgical and compositional factors of the alloys were kept constant or had no effect on abrasion resistance and eutectic carbides had a negative effect, the increase in abrasion resistance within the hypereutectic alloys is due to the large change in morphology of the primary carbides (compared to eutectic carbides) and to their increasing volume fractions. Figure 67 shows that the abrasion resistance is improved by approximately 1 percent for each percent increase in primary carbide volume. The abrasion resistance decreases at about the same rate in alloys with primary carbide volumes greater than 20 percent. The decrease in abrasion resistance is probably due to spalling and to the inability of the relatively small amounts of austenite to effectively hold even the very massive carbides during high stress abrasion.

Regression Analysis

The effects on abrasion resistance of most of the variables listed in Table 23 were minimal and obscured by the relatively greater effects of the primary carbide volume and of the molybdenum content. In an attempt to describe the relative importance of these other variables, the data set was subdivided into three matrices.

The regression equation obtained for the hypo-eutectic Fe-C-Cr alloys reported in Table 24 shows that the effects of even the more important variables are small as is reflected by the small coefficients. The end count was the most important parameter and by itself it could account for 74% of the variability in the data. The minus sign for the coefficient indicates that increasing the end count is detrimental to abrasion. This is expected since an increase in the end count in the hypoeutectic alloys would reflect an increase in the eutectic carbide volume fraction which was found to decrease the high stress abrasion resistance. The next variable is the fraction of eutectic carbide rod in transverse cross section and the regression coefficient indicates a small increase in abrasion resistance with an increase in carbide of this morphology. These two factors together accounted for 74% of the variability in the data. An increase in the value of the shape parameter was shown to be beneficial since it results in increased abrasion resistance. As the shape parameter (related to the area/perimeter) increases in value, the shape of the carbide

particles becomes less elongated and broader, so that carbide morphologies such as the rod in transverse cross section which is broad in the plane of abrasion are preferred for abrasion resistance. The fraction of lamellar eutectic carbide entered the regression equation with a small negative coefficient; this morphology is detrimental. The above four factors (Table 24) accounted for 81% of the variability in the data. The regression equation for the hypoeutectic alloys and including the molybdenum containing alloys is reported in Table 24 and shows that molybdenum is the most important factor (in these hypoeutectic alloys) in increasing wear resistance and it accounted for 75% of the variability in the data. The range of values for the abrasion resistance and the magnitude of the regression coefficient for Mo indicate that molybdenum increases the abrasion resistance by two percent for each percent Mo in the alloy. One way in which Mo acts to increase the high stress abrasion resistance is by its effect in decreasing the carbide volume fraction. A comparison of the abrasion resistance values in Table 12 for the Fe-C-Cr and the Mo containing alloys shows that the latter are 3 to 7.6% more abrasion resistant. The other two variables which appear in the regression equation are the volume fraction of eutectic carbide and the end count whose increasing values are detrimental to high stress abrasion. The regression coefficient indicates that a 10 percent increase in the volume fraction of eutectic carbides decrease the abrasion

resistance by one percent.

The data set for all the alloys studied except for alloys O and P gives the following regression equation which is also listed in Table 24:

$$AR(cm^{-3}) = 132.17 + 1.30\ (\text{Volume \% Primary Carbide}) + 2.88\ (\text{\% Mo in the alloy}) + 7.53 \times 10^{-1}\ (\text{Shape, pp})^{*} - 2.88 \times 10^{-1}\ (\text{Volume \% Eutectic Carbide Rod in Transverse Cross Section}).$$

The equation applies to those alloys of increasing Cr and C content (at Cr:C of 6.64) containing from 7.5 to 53 volume percent of total carbide with 0 to 20 volume percent of primary carbides. The two alloys of increasing volume fraction of primary carbide above 20 percent which caused a drop in abrasion resistance were not included. It is seen that the most important factor in increasing the abrasion resistance of these alloys is the volume fraction of primary carbide (up to 20% primary carbide). This factor alone accounts for 85% of the variability in the data. The volume percent primary carbides is seen to contribute to the high stress abrasion resistance (from the regression coefficient) by approximately one percent per percent increase in the volume fraction up to 20 percent. The next factor of importance is the Mo content (only studied in some of the hypoeutectic alloys) of the alloy and it contributes to abrasion resistance by two percent per percent increase in

---

*pp = Dimension expressed in quantimet picture points, 786 pp = 0.200 mm.

Mo. The weight percent Mo per se probably does not increase the abrasion resistance since it did not effect most of the properties measured (hardness of the phases, hardness of the alloy, Cr contents of the matrix and carbides, etc.), but it is beneficial since it decreases the volume fraction of eutectic carbides. Also, the minor Mo_2C eutectic phase (Figure 42) present in the Mo containing alloys may be beneficial, and Mo might alter the adhesion between the matrix and carbides. These points need further study. The two factors, volume of primary carbides and Mo content, account for 90 percent of the variability in the data. The third factor in order of importance was the shape parameter (≃ area of carbide/perimeter). Table 21 shows that the value for the shape parameter of the carbide particles varied from 10 to 20 quantimet picture points (786 picture points = 0.200 mm); the larger values are representative of the massive primary carbides. An increase in the shape parameter by a factor of two (10 to 20 pp) results in an increase in the high stress abrasion resistance of about five percent (from the regression coefficient). A change in the carbide shape (area/perimeter) by a factor of two results in a considerable change in the morphology. The result is similar to the transition from a rectangular shaped particle of dimensions 1 by 16 units to one of 4 by 4 units. The last term reported in the regression equation is a small negative coefficient for the fraction of eutectic carbide rod in transverse cross section. The above four

parameters account for 94% in the variability of the abrasion resistance data.

Mechanistic Discussion of High Stress Abrasion

Figures 49 to 55 show scanning electron images of the abraded surfaces of alloys of increasing carbide volumes. The lower magnification photographs show that abrasion occurs on planes at several depths. As the carbide volume of the alloys is increased, abrasion takes place on fewer planes and closer to the surface. Also increasing carbide volumes results in increased surface damage and disruption. For example, in Specimen B (Figure 49) which has very little carbide, the scratches are relatively deep, smooth and continuous. While in Specimen I (Figure 52) which contains a larger volume of eutectic carbides, the scratches are not as deep, are discontinuous and stopped in many areas. They were accompanied by surface disruption at the leading edge. The interactions at the leading edge of the scratches is shown in the higher magnification surface images of Figures 50b, 52c and d, 53c and 54c. The particles shown in these figures are probably carbides, but could also be abrasive particles. Figures 49 to 52 show that material is removed in a series of steps whereby the surface is sectioned and isolated. When a small thin layer is left on the surface it is torn or abraded. Figures 49d and 51c and d illustrate this point; Figure 51d shows a previously existing scratch partially covered with a thin layer of smeared material which will probably be removed on the next encounter with an

abrasive particle. Figures 50d and 51b show that a "fin" of material can be generated by an abrasive particle with several cutting edges. A "fin" of this type is subsequently easily removed.

Electron scanning images showing the abraded carbides after light removal of the austenite are reported in Figures 56 to 60. The lower magnification image of Figure 56 shows that the carbides can be aggressively abraded. These figures show that under high stress abrasion the carbides can be scratched, broken, and deformed. Figure 58 shows lamellar eutectic carbides, some of which have been plowed, deformed, and broken. Figure 60 shows that the primary carbides can be abraded; further, the deformation due to plowing shown in Figure 60c is an indication that the primary carbides have high toughness and undergo strain hardening. Figure 60 shows the result of a collision between an abrasive particle and a primary carbide cross sectioned transversely; the damage is minimal compared to the spalling in the primary carbides cross sectioned longitudinally (Figures 59d and 60d and e).

Based on the above observations, on the abrasion resistance behavior of the alloys studied, and on the morphological aspects of the carbides, a mechanism of high stress abrasion for these multiphase alloys can be derived. The abrasion is dependent on (1) the ability of the abrasive to penetrate and remove materials from a surface which is related to the indentation hardness, and

(2) on the interaction between the abrasive particles and the microstructural components of multiphase alloys. If the material is single phase the abrasion behavior is directly related to its hardness. If the alloy is multiphase and the microstructural components can keep their overall integrity within the structure, then the abrasion resistance is related to the volume fraction and hardness of each component. The Fe-C-Cr alloys studied under severe conditions of high stress abrasion consist of carbides embedded in austenite. The adhesion of the relatively small and shallow eutectic carbides to the austenite was not great enough under the abrasion conditions to keep the carbides within the structure. The eutectic carbides were uprooted by the action of the abrasive resulting in undue volume loss. Further, as the eutectic carbides were uprooted, the matrix surrounding and above the carbides (or within the eutectic colony) was torn and lifted above the specimen surface resulting in accelerated removal of this surrounding matrix. As the volume fraction of eutectic carbide is increased, the interaction between carbide and abrasive particles is increased which results in decreased wear resistance. In the alloys containing primary carbides, the surface area of carbide in contact with the matrix generates enough adhesion to keep these carbides from being uprooted. Since the primary carbides are harder than the matrix and are able to remain within the matrix during abrasion, the resistance of alloys should increase with increasing primary carbide con-

tent. High stress abrasion resistance can be increased to an optimum by increasing the volume of primary carbide until their volume is such that they are embedded in very little matrix and are easily removed; or until morphology or composition changes cause large scale spalling.

CONCLUSIONS

Abrasive Wear

The studies performed to evaluate the response of the wear testing apparatus to the abrasive wear of ferrous alloys under varying applied conditions, lead to the following conclusions:

1. Alumina is the abrasive material most suited for use in the test apparatus designed for high stress abrasive wear. A particle size of 80 micron with 15 lb loading on a ¼-inch diameter pin specimen is optimal for testing high stress abrasion resistance of alloys. Under these conditions one obtains the highest precision in the wear data, good discrimination between the alloys tested, and a ranking which matches commercial ball mill data.

2. The wear ratio, R, a commonly used measure of wear, is unsuitable for comparisons of the wear resistance of a given material under varying test conditions. The wear ratio should only be used to compare different materials when abrasive parameters are invariant.

3. The test material is as important a variable as the applied test conditions.

Metallurgical Studies of High Stress Abrasive Wear

The following conclusions are based on studies of Fe-C-Cr (and some Fe-C-Cr-Mo) alloys with constant Cr:C ratios of 6.64 ranging from 1.40% C and 9.44% Cr to 5.07% C and 33.56% Cr. They consist of eutectic and eutectic plus

primary M_7C_3 carbides embedded in austenitic matrices. The alloys were tested under severe conditions of high stress abrasion.

1. High stress abrasion resistance is markedly improved in the hypereutectic alloys which contain massive carbides; it increases one percent per percent increase in primary carbide up to an optimum abrasion resistance at 20% primary carbide. Increased primary carbide volume above 20% decreases the high stress abrasion resistance; the probable cause, based on visual observation of polished specimens, is spalling of the carbides.

2. High stress abrasion resistance of the hypoeutectic alloys does not increase with increasing eutectic carbide volume fraction. A decrease in abrasion resistance corresponding to one percent per ten percent increase in eutectic carbide volume is found.

3. An increase in the value of the shape parameter, proportional to the area/perimeter of the carbides, results in increased abrasion resistance. This is an indication that large, massive carbides aid high stress abrasion resistance.

4. The chromium content of the matrix is not constant in alloys of constant Cr:C ratio, but is a function of total chromium content of the alloy.

5. The microhardness of the matrix of all the alloys was constant and independent of its chromium content.

6. The austenitic matrix in the alloys studied

does not undergo martensitic transformation during high stress abrasion.

7. Molybdenum additions of 1.5 and 3 weight percent had no significant effect on the microhardness or the chromium content of the matrix.

8. Carbide morphologies are not dependent only on composition; several may be present in a given alloy composition. The observed morphologies are a function of the geometry of sectioning.

9. The lamellar eutectic frequently consists of imperfectly formed bundles of hollow carbide rods (tubes) infiltrated and surrounded by austenite. The carbides in the lamellar eutectic are not wavy plates as is often inferred from the observation of metallographic specimens.

10. The chromium content of the carbides increases with increasing chromium content of the alloy. The chromium content of the primary carbide is higher than the eutectic carbide of the same alloy.

11. The carbide phase in these alloys can be plastically deformed during high stress abrasion.

12. Molybdenum additions of 1.5 and 3 percent had no effect on the microhardness or the Cr content of the carbides. Molybdenum had an effect in decreasing the carbide volume fraction (by 2 to 8%) in alloys of the same Cr content.

13. The high stress abrasion resistance of the hypoeutectic molybdenum containing alloys is increased by two

percent per percent Mo.

14. The different eutectic carbide morphologies do not have a marked effect on the high stress abrasion resistance.

REFERENCES

1. Committee on Abrasive Wear of Ferrous Materials, SAE-ISTC Div. 18, "Abrasive Wear" Information Report, J1965, Society of Automotive Engineers, Aug. 1966.

2. F. P. Bowden and T. Tabor, The Friction and Lubrication of Solids, Oxford University Press, Oxford, Vol. II, pp. 359-364.

3. H. S. Avery, "The Measurement of Wear Resistance," Wear, Vol. 4, No. 6, Nov./Dec., 1961, p. 427.

4. T. E. Norman, "Abrasive Wear of Metals," Ch. 13, pp. 277-314, C. Lipson and L. V. Colwell (eds.), Handbook of Mechanical Wear, University of Michigan Press, Ann Arbor, Michigan, 1961.

5. M. M. Khruschov and M. A. Babichev, Method of Testing Abrasive Wear on Machine KH4-B, NEL Translation, No. 889, 1962.

6. G. K. Nathan and W. J. D. Jones, "The Empirical Relationship Between Abrasive Wear and the Applied Conditions," Wear, Vol. 9, 1966, pp. 300-309.

7. R. C. D. Richardson, "The Wear of Metals by Hard Abrasives," Wear, Vol. 10, 1967, pp. 291-309.

8. J. Larsen-Badse, "Influence of Grit Diameter and Specimen Size on Wear During Sliding Abrasion," Wear, Vol. 12, 1968, pp. 35-53.

9. E. Rabinowicz, L. A. Dunn, and P. G. Russell, "A Study of Abrasive Wear Under Three Body Conditions," Wear, Vol. 4, 1961, pp. 345-355.

10. J. Larsen-Badse, "The Abrasion Resistance of some Hardened and Tempered Carbon Steels, " Trans. Met. Soc. AIME, Vol. 236, October 1966, pp. 1461-1466.

11. M. M. Khruschov, "Resistance of Metals to Wear by Abrasion, as Related to Hardness," Inst. Mech. Eng., Proc. Conf. on Lubrication and Wear, London, 1st-3rd October, 1957.

12. R. C. D. Richardson, "The Wear of Metals by Relatively Soft Abrasives," Wear, Vol. 11, 1968, pp. 248-275.

13. R. C. D. Richardson, "The Wear of Metallic Materials by Soil - Practical Phenomena," J. Agri. Eng. Res., Vol. 12(1), 1967, pp. 22-39.

14. B. W. E. Avient, J. Goddard, and H. Wilman, "An Experimental Study of Friction and Wear During Abrasion of Metals," Royal Soc. Proc., Series A, Vol. 258, October-November, 1960, pp. 159-180.

15. J. Goddard and H. Wilman, "A Theory of Friction and Wear During the Abrasion of Metals," Wear, Vol. 5, 1962, pp. 114-135.

16. T. O. Mulhearn and L. E. Samuels, "The Abrasion of Metals: A Model of the Process," Wear, Vol. 5, 1962, pp. 478-498.

17. E. Rabinowicz and A. Mutis, "Effect of Abrasive Particle Size on Wear," Wear, Vol. 8, 1965, pp. 381-390.

18. J. Larsen-Badse, "Influence of Grit Size on the Groove Formation During Sliding Abrasion," Wear, Vol. 11, 1968, pp. 213-222.

19. E. Rabinowicz, "Practical Uses of the Surface Energy Criterion," Wear, Vol. 7, 1964, pp. 9-22.

20. T. E. Norman and C. M. Loeb, Jr., "Wear Tests on Grinding Balls," Trans. AIME, Vol. 176, 1948, pp. 490-520.

21. T. E. Norman, "Factors Influencing the Resistance of Steel Castings to High Stress Abrasion," A.F.S. Trans., Vol. 66, 1958, pp. 187-196.

22. T. E. Norman, A. Solomon, and D. V. Doane, "Martensitic White Irons for Abrasion-Resistant Castings," A.F.S. Trans., Vol. 67, 1959, p. 242-256.

23. T. E. Norman and E. R. Hall, "Abrasive Wear of Ferrous Materials in Climax Operations," ASTM STP 446, American Society for Testing and Materials, 1969, pp. 91-114.

24. H. S. Avery, "Hard Facing for Impact," Welding J., Vol. 31(2), 1952, pp. 116-143.

25. H. S. Avery, "Selecting Materials for Wear Resistance," Ch. 3, Surface Protection Against Wear and Corrosion, ASM, Metals Park, Ohio, 1954.

26. H. S. Avery, "Wear Resistance," Ch. 14, Handbook of Mechanical Wear, C. Lipson and L. V. Colwell (ed.), University of Michigan Press, Ann Arbor, Michigan, 1961.

27. M. E. Garber, I. D. Zeilikman and I. I. Tsypin, "An Investigation of the Properties of White Cast Iron," Russian Castings Production, August, 1965.

28. Zdenek Ruznak, "The Effect of Structure of Cast Materials on the Resistance to Slurry-Type Abrasion," Slevarenstvi (Foundry), Vol. 16, No. 12, 1968, pp. 468-486.

29. M. E. Garber, E. V. Rozhkova, and I. I. Tsypin, "Effect of Carbon, Chromium, Silicon, and Molybdenum on the Hardenability and Wear Resistance of White Irons," Metallovedenie I Termicheskaya Obrabotka Metallov, No. 5, 1969, pp. 11-14.

30. M. E. Garber, L. I. Levi, E. V. Rozhkova, and I. I. Tsypin, "Effect of Microstructure on the Wear Resistance of White Cast Iron," Metallovedenie I Termicheskaya Obrabotka Metallov, No. 11, November 1968, pp. 48-52.

31. William Volk, Applied Statistics for Engineers, McGraw-Hill Book Company, Inc., New York, Toronto, London, 1958.

32. Henry L. Alder and Edward B. Roessler, Introduction to Probability and Statistics, Second Edition, W. H. Freeman and Company, San Francisco and London, 1962.

33. Nathan H. Cook and Ernest Rabinowicz, Physical Measurement and Analysis, Addison-Wesley Publishing Company, Inc., Reading, Massachusetts, Palo Alto, London, 1963.

34. Acheson J. Duncan, Quality Control and Industrial Statistics, Richard D. Irwin, Inc., Homewood, Illinois, Third Edition, 1965.

35. Charles R. Hicks, Fundamental Concepts in the Design of Experiments, Holt, Rinehard and Winston, New York, Chicago, San Francisco, Toronto, London, 1964.

36. E. F. Finkin, "Abrasive Wear," Evaluation of Wear Testing, ASTM STP 446, Amer. Soc. for Testing and Materials, 1969, pp. 55-90.

37. F. Maratray, "Investigation of High-Chromium White Irons," Progress Report; July 10, 1966, Climax Molybdenum Company Internal Report.

38. K. Bungardt, E. Kunze, and E. Horn, "Investigations on the Structure of the System Iron-Chromium-Carbon," Arch. Eisenhüttenwesen, Vol. 29, No. 3, 1958, pp. 193-203.

39. F. Maratray and R. Usseglio-Nanot, "Factors Affecting the Structrue of Chromium and Chromium-Molybdenum White Irons," Climax Molybdenum S.A. 61, Avenue Victor Hugo-

75 Paris 16e, France and private communications with F. Maratray.

40. N. R. Griffing, W. D. Forgeng, and G. W. Healy, "C-Cr-Fe Liquidus Surface," Trans. Met. Soc. AIME, Vol. 224, February 1962, pp. 148-159.

41. N. A. Lange, Handbook of Chemistry, Seventh Edition, Handbook Publishers, Inc., Sandusky, Ohio, 1949, p. 1387.

42. M. L. Bernshtein and A. G. Rakhshtadt, eds., Physical Metallurgy and Heat Treatment of Steel (A handbook, Vol. 1), Metallyrgizdat, 1961, pp. 544-550. (In Russian)

43. K. W. Andrews, D. J. Dyson, and S. R. Keown, Interpretation of Electron Diffraction Patterns, Hilger and Watts Ltd., London, 1967, p. 173.

44. C. S. Smith, and L. Guttman, "Measurement of Internal Boundaries in Three-Dimensional Structures by Random Sectioning," Trans. Met. Soc. AIME, Vol. 197, 1953, pp. 81-87.

45. R. T. DeHoff and F. N. Rhines, Quantitative Microscopy, McGraw-Hill Book Company, New York, 1968, pp. 302-305.

46. K. Kuo, "Carbides in Chromium, Molybdenum, and Tungsten Steels," JISI, Vol. 173, 1953, pp. 363-375.

FIGURES

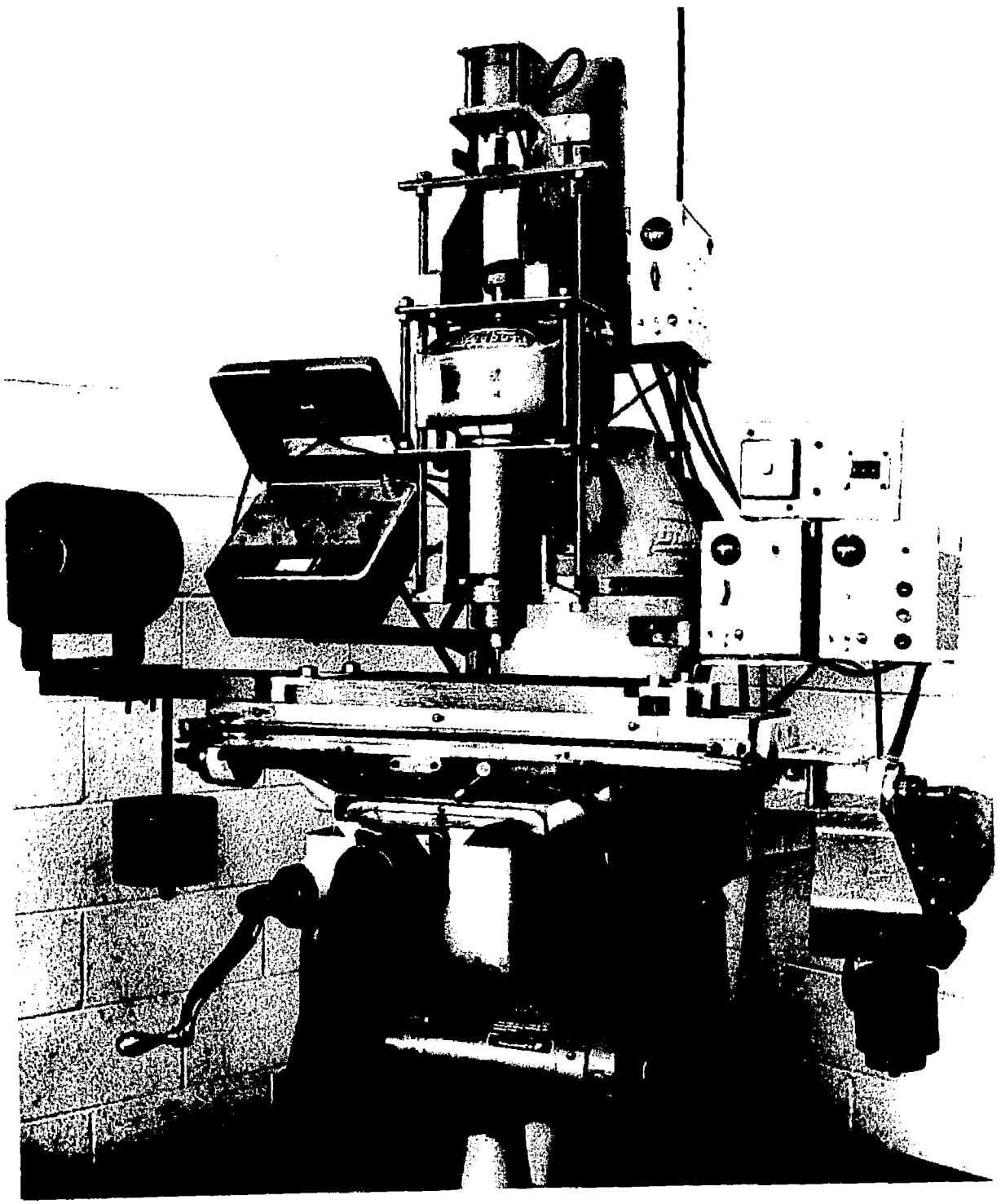

Figure 1 Photograph of the Abrasion Wear-Testing Apparatus

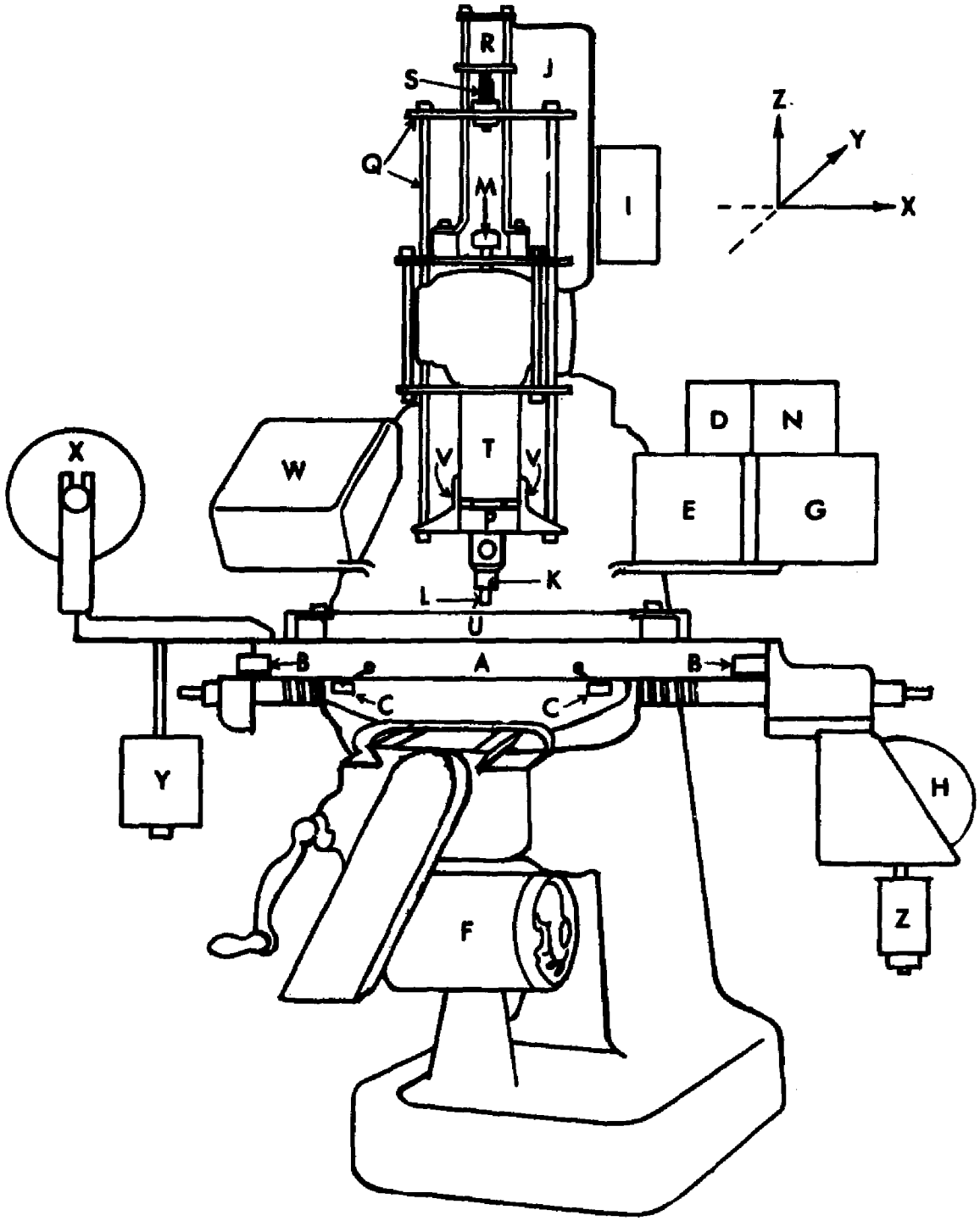

Figure 2 Schematic Drawing of the Abrasion Wear-Testing Apparatus

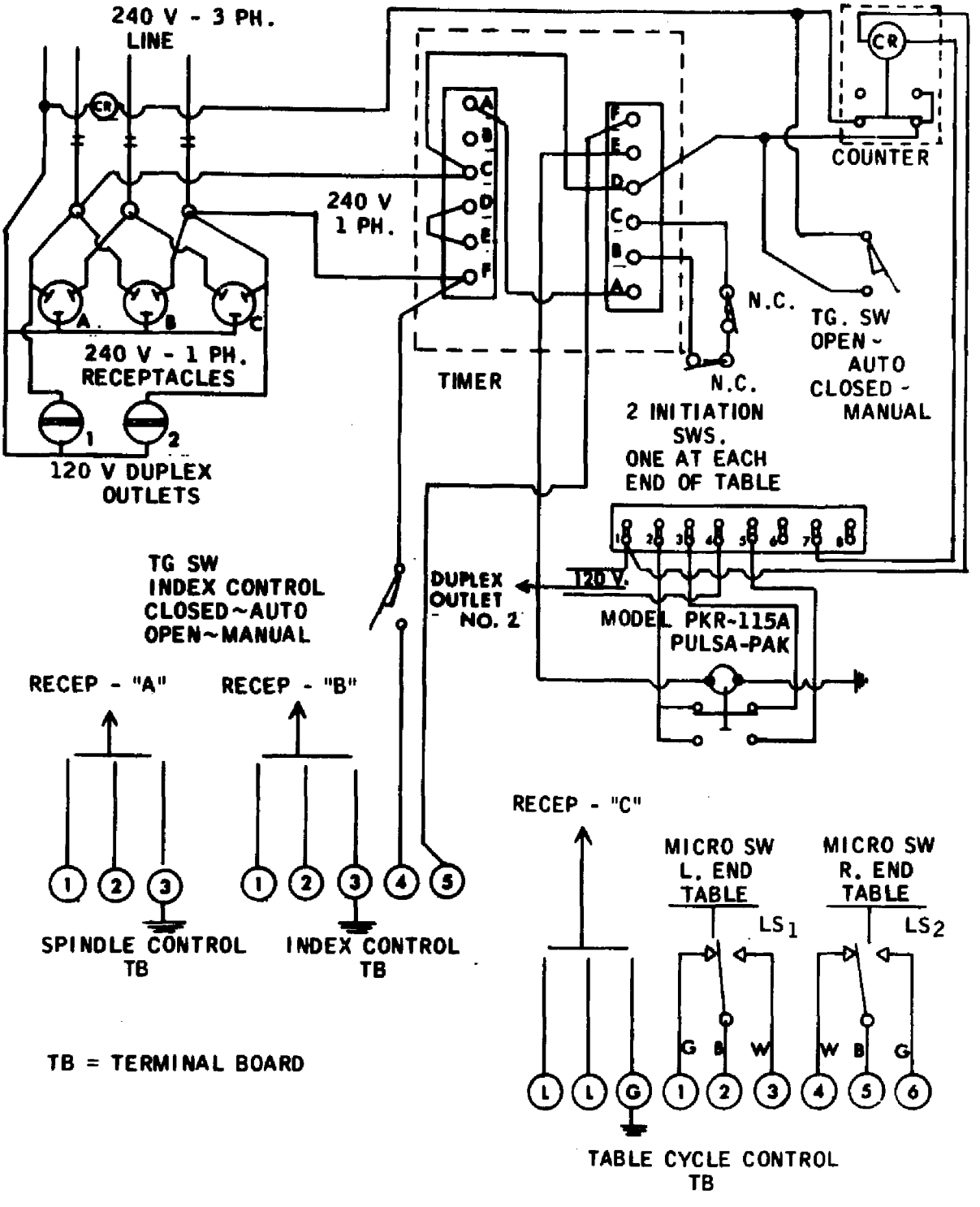

Figure 3 Schematic Diagram of the External Wiring of the Abrasion Wear-Testing Apparatus

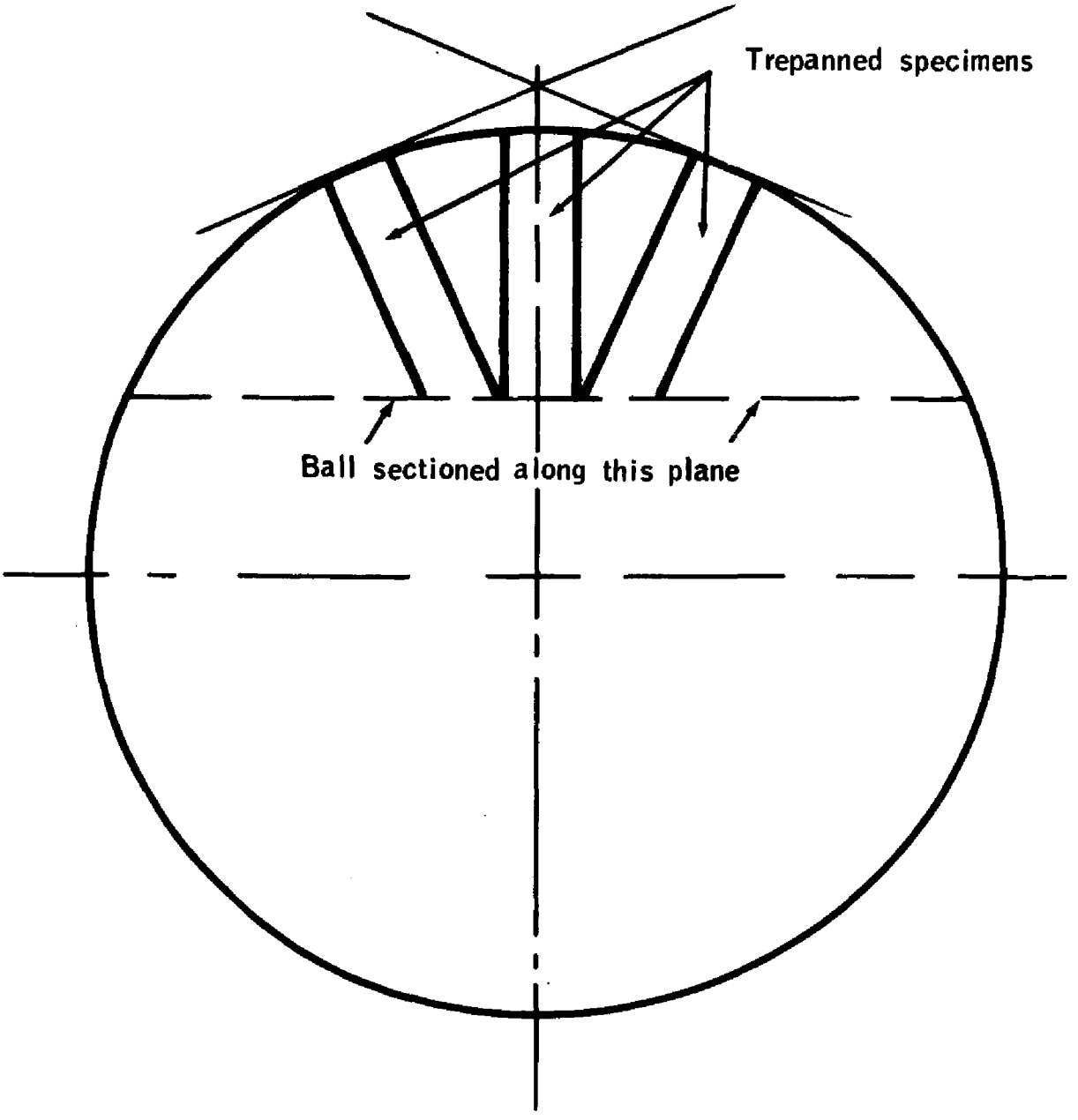

Figure 4 Positions of Specimens Trepanned from the 5-Inch Balls

Martensitic Etch X500

Figure 5 Microstructure of Alloy AA, Martensitic High Chromium Cr-Mo White Iron

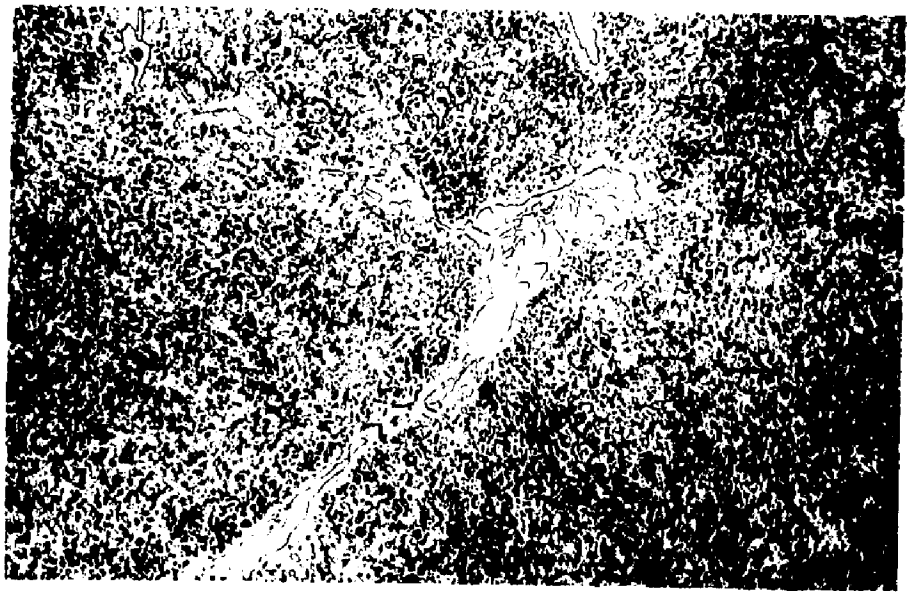

Martensitic Etch X500

Figure 6 Microstructure of Alloy BB, Cr-Mo Steel

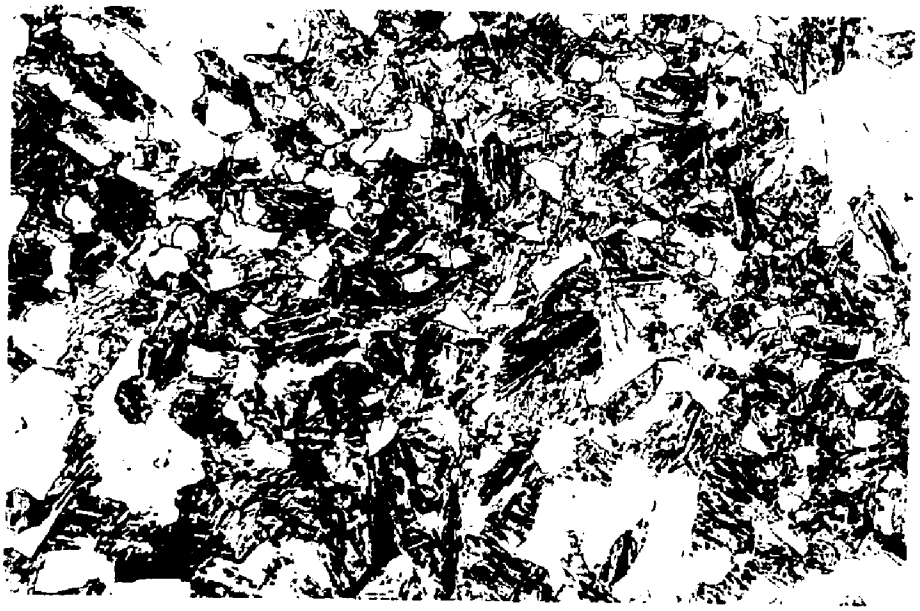

2% Nital X500

Figure 7 Microstructure of Alloy CC, 2Si-1Mo Steel

Martensitic Etch X500

Figure 8 Microstructure of Alloy FF, Ni-Cr White Iron

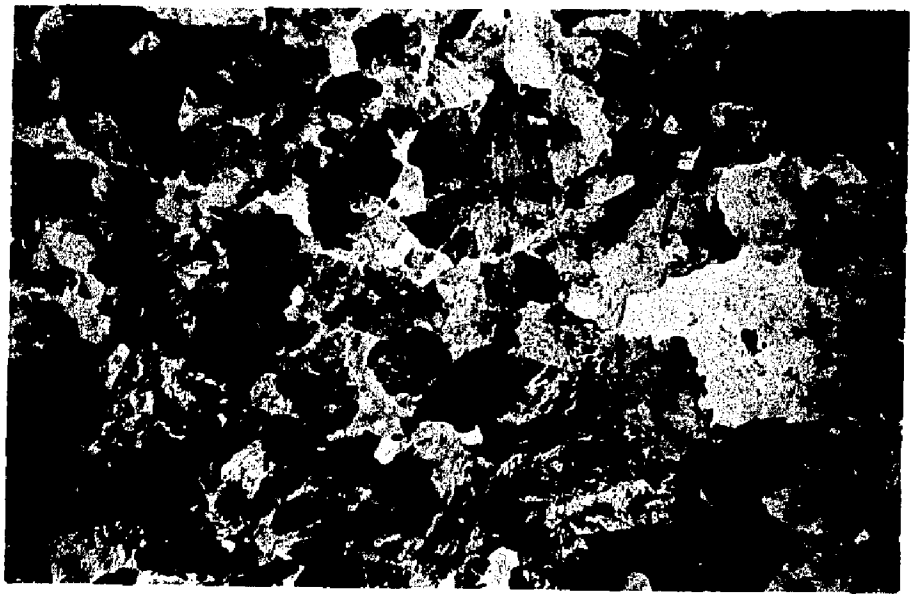

4% Picral X500

Figure 9 Microstructure of Alloy GG, Pearlitic Cr-Mo Steel

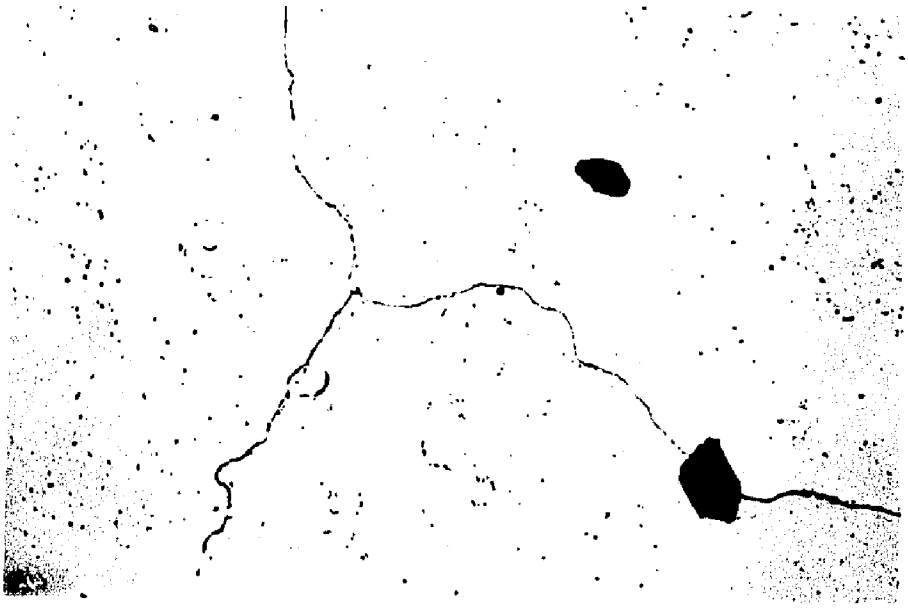

2% Nital X500

Figure 10 Microstructure of Alloy II, Austenitic Manganese Steel

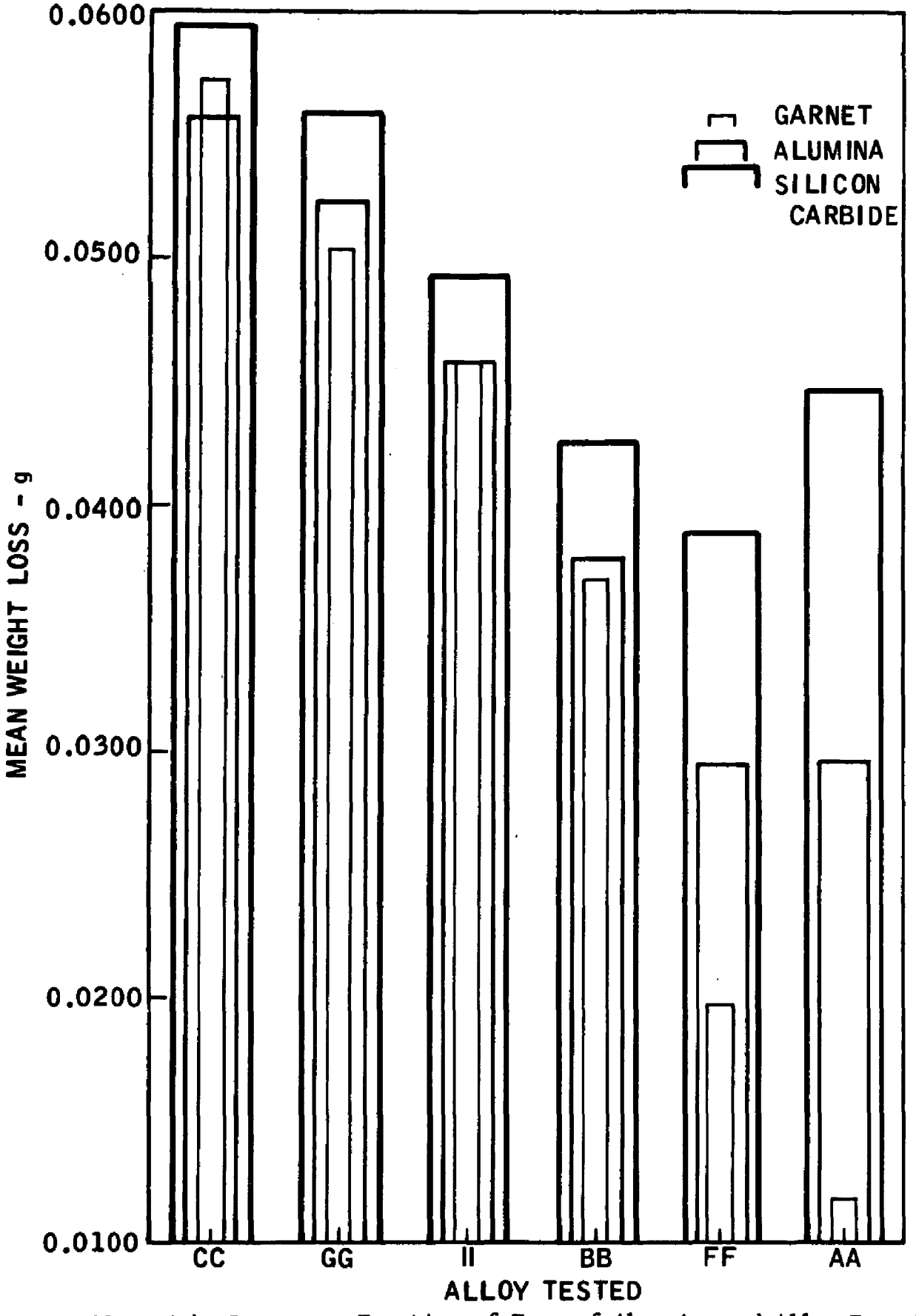

Figure 11 Weight Loss as a Function of Type of Abrasive and Alloy Tested under 7 lb Loading on 105μ Particle Size Abrasive

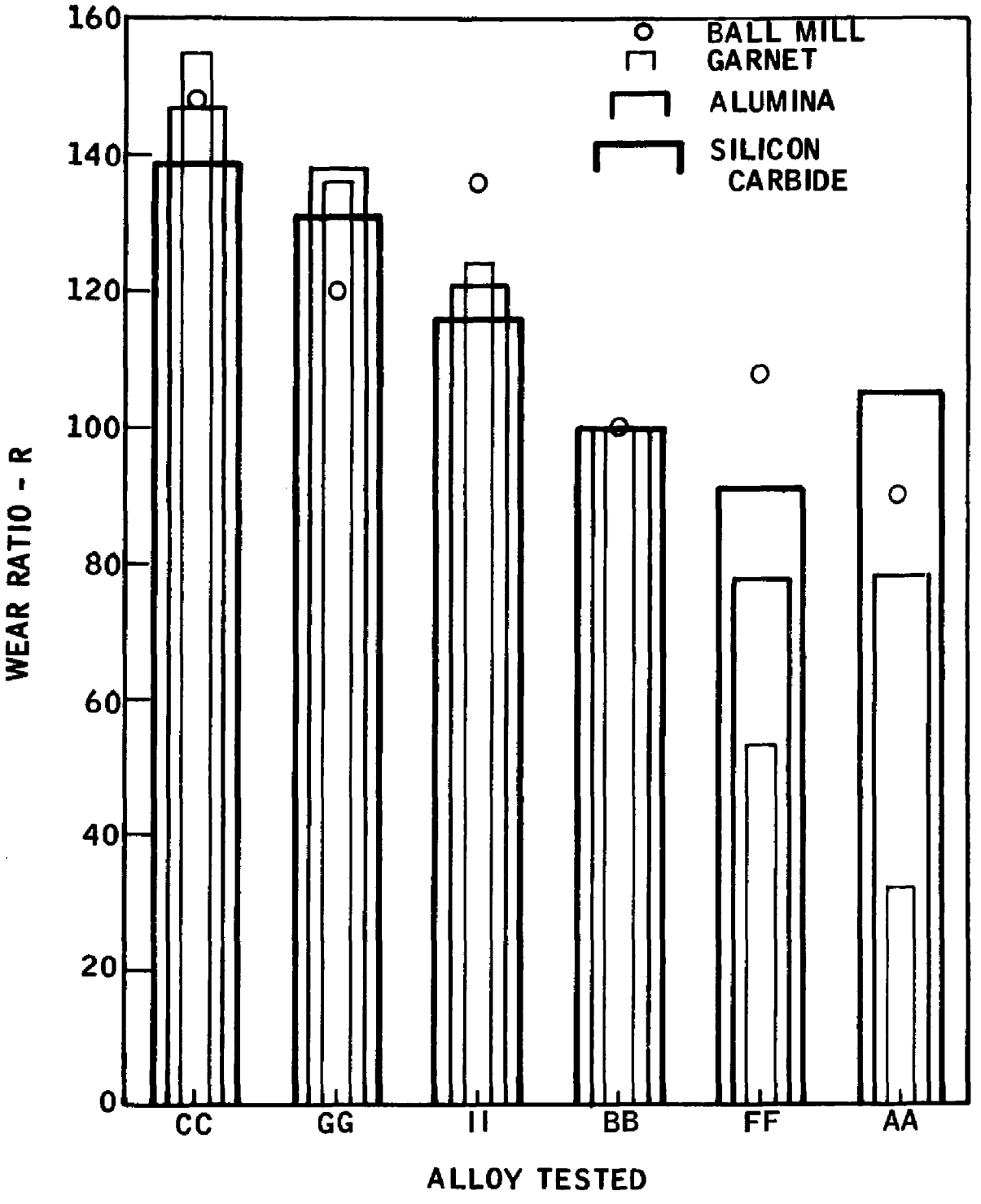

Figure 12 Wear Ratio using BB as a Standard as a Function of the Type of Abrasive and the Alloy Tested under 7 lb Loading on 105μ Particle Size Abrasive

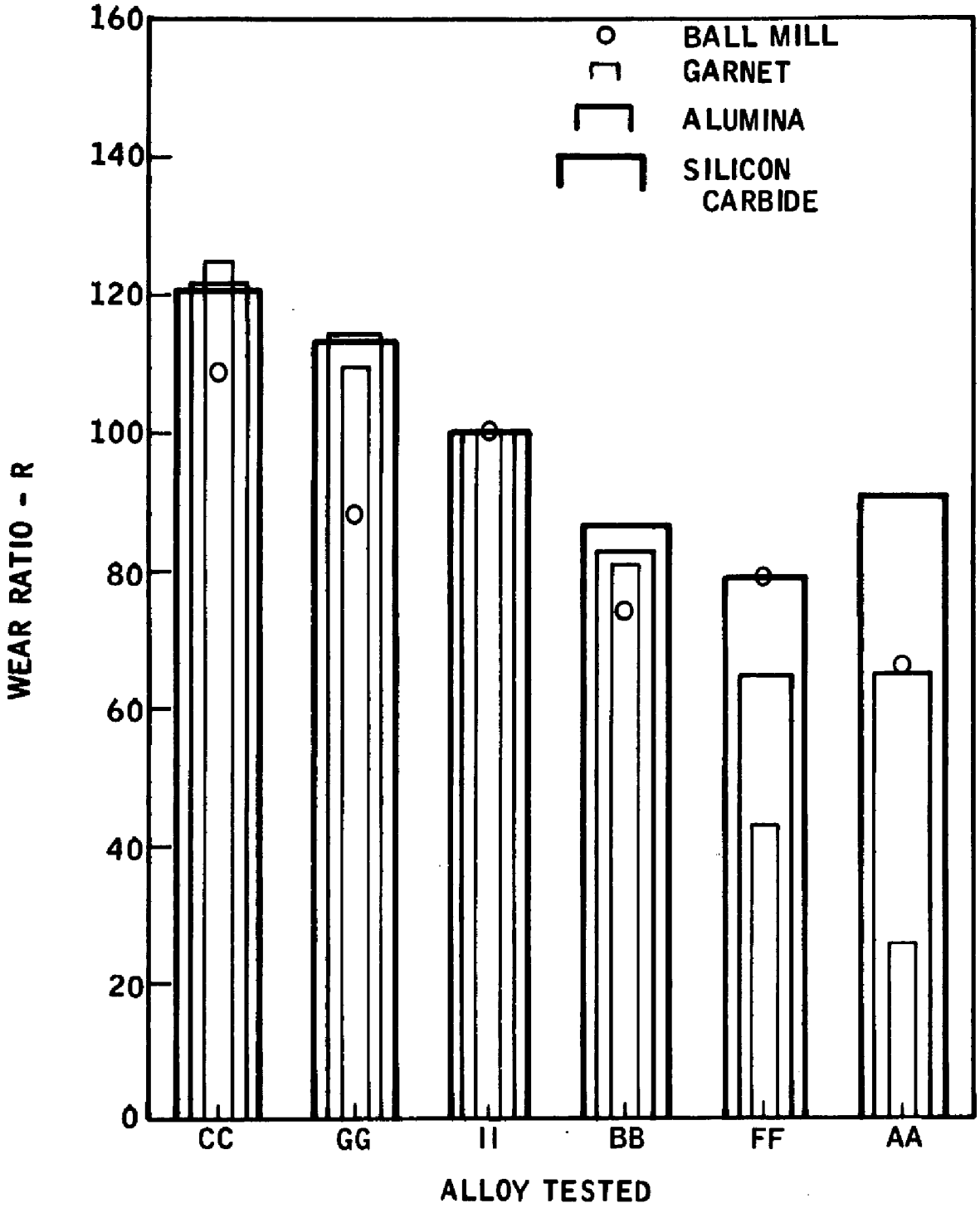

Figure 13 Wear Ratio using II as a Standard as a Function of the Type of Abrasive and the Type of Alloy Tested under 7 lb Loading on 105μ Particle Size Abrasive

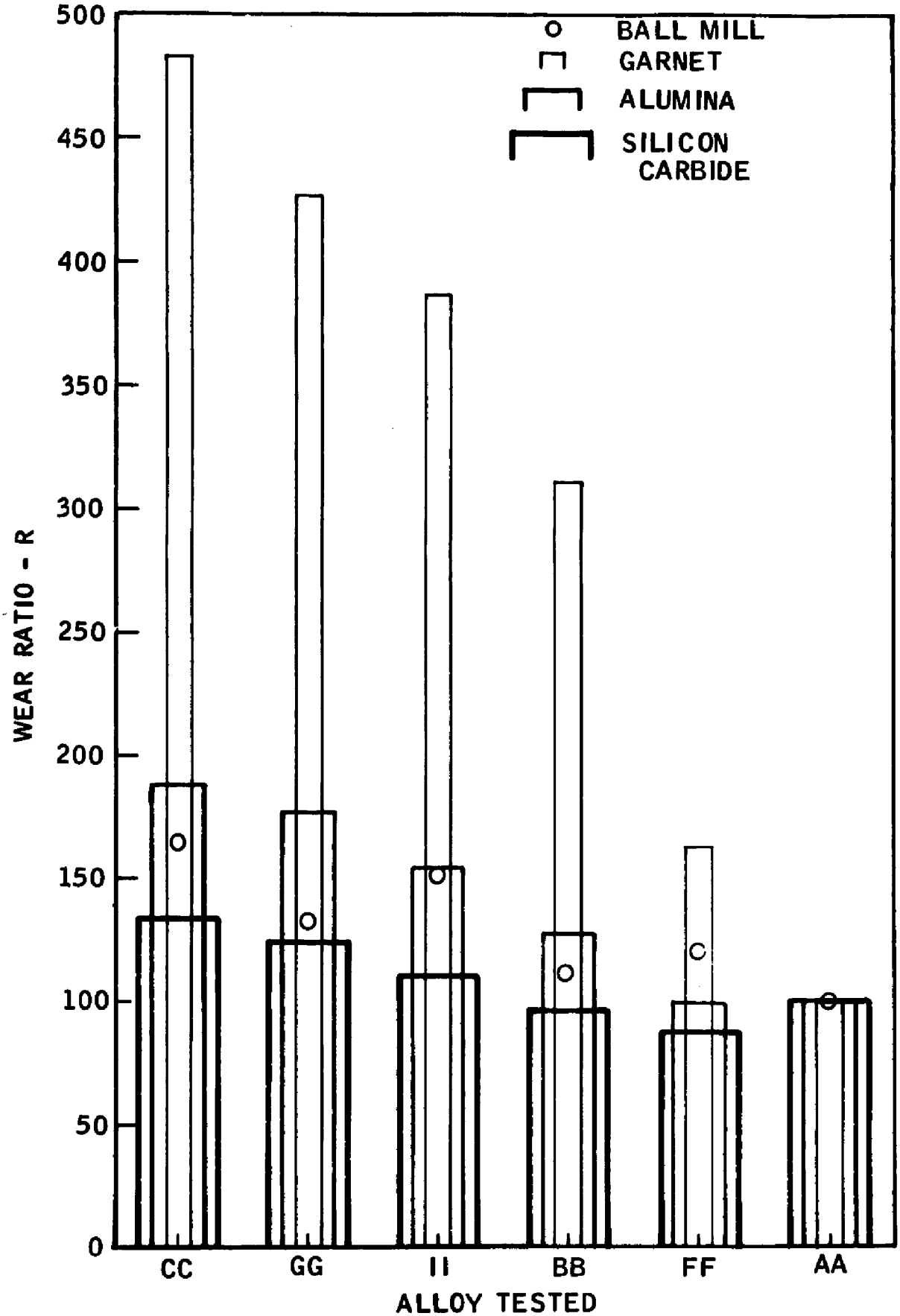

Figure 14 Wear Ratio using AA as a Standard as a Function of the Type of Abrasive and the Type of Alloy Tested under 7 lb Loading on 105μ Particle Size Abrasive

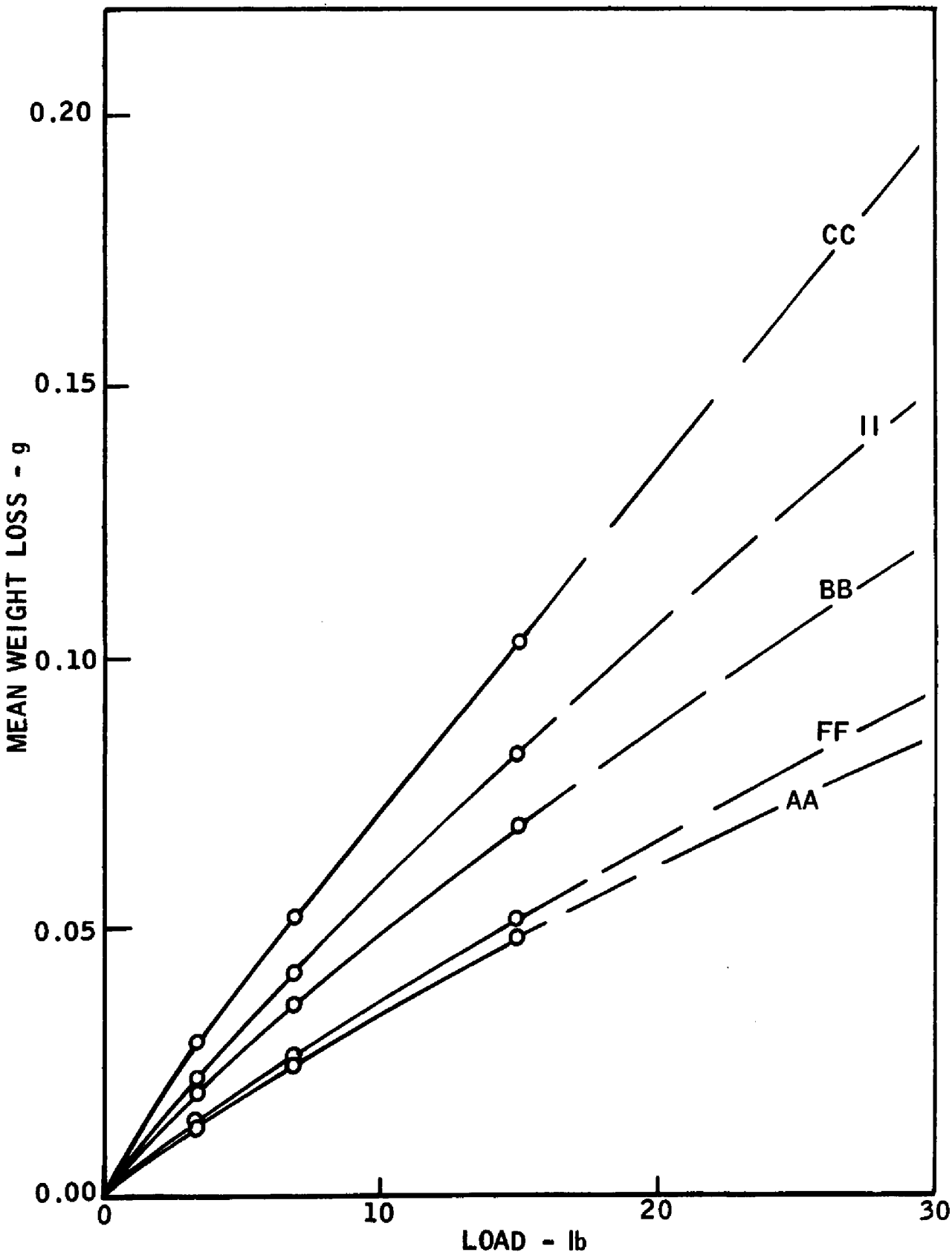

Figure 15 Weight Loss as a Function of Load for the Alloys Tested on 80μ Alumina

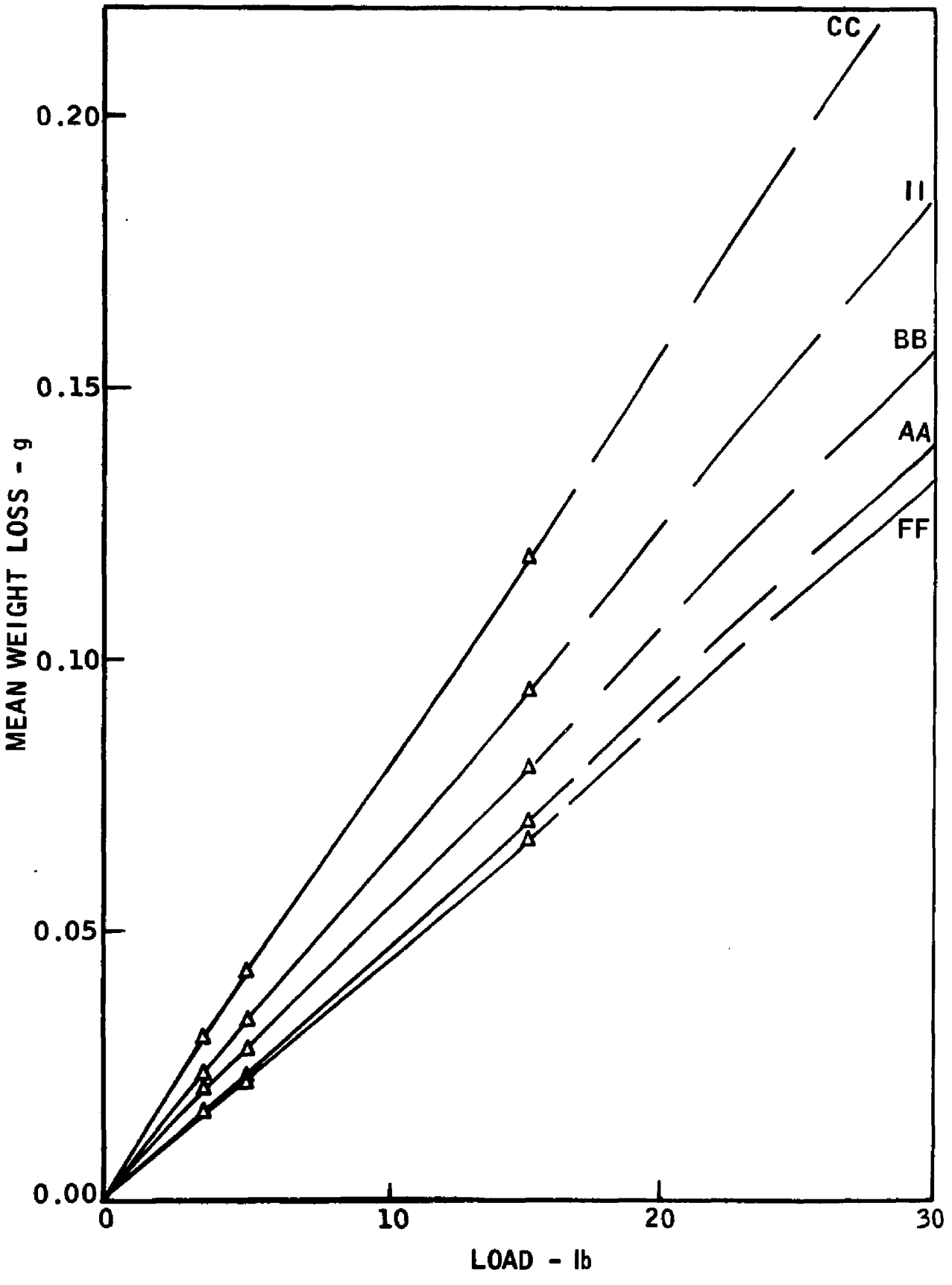

Figure 16 Weight Loss as a Function of Load for the Alloys Tested on 130μ Alumina

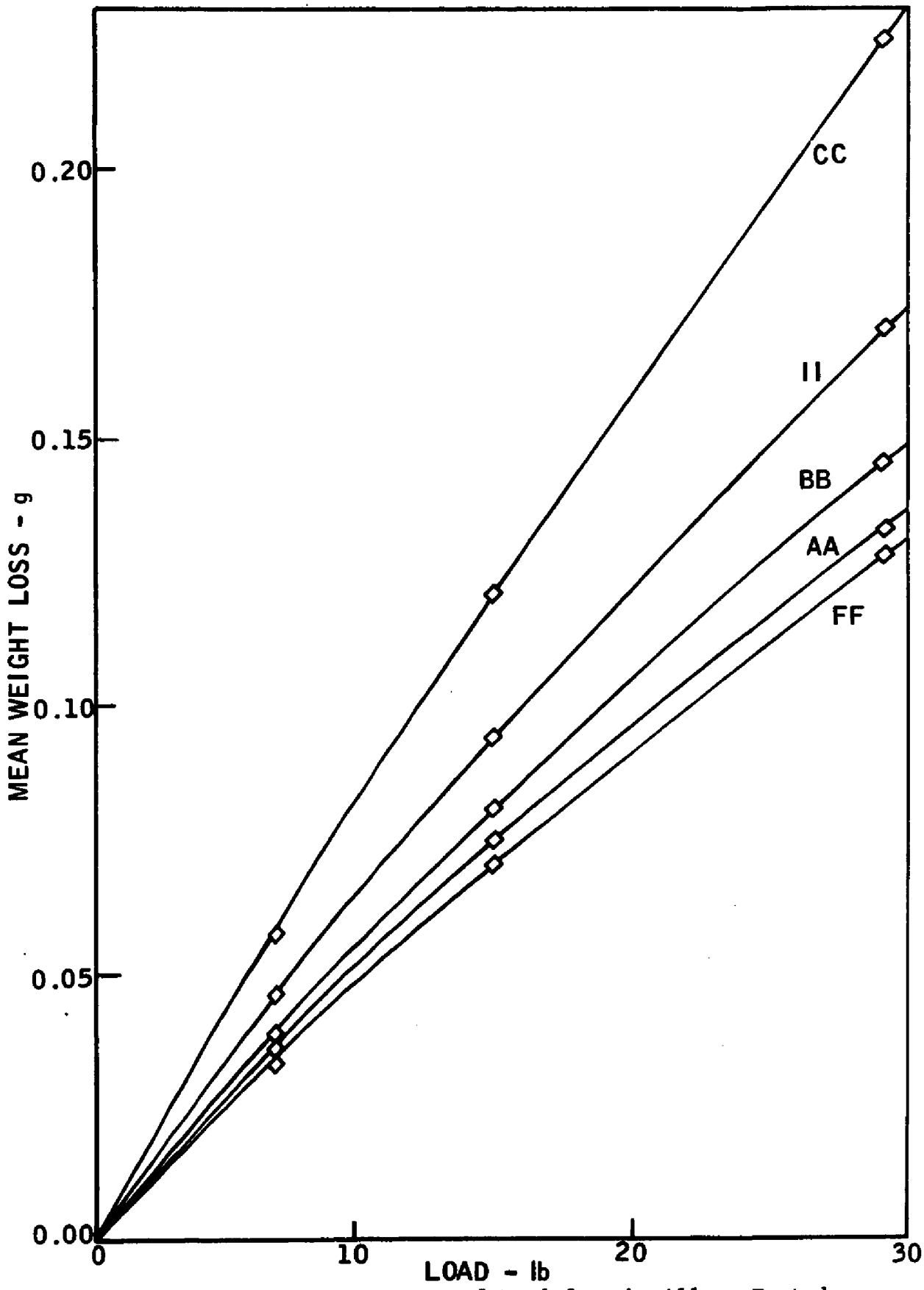

Figure 17 Weight Loss as a Function of Load for the Alloys Tested on 200μ Alumina

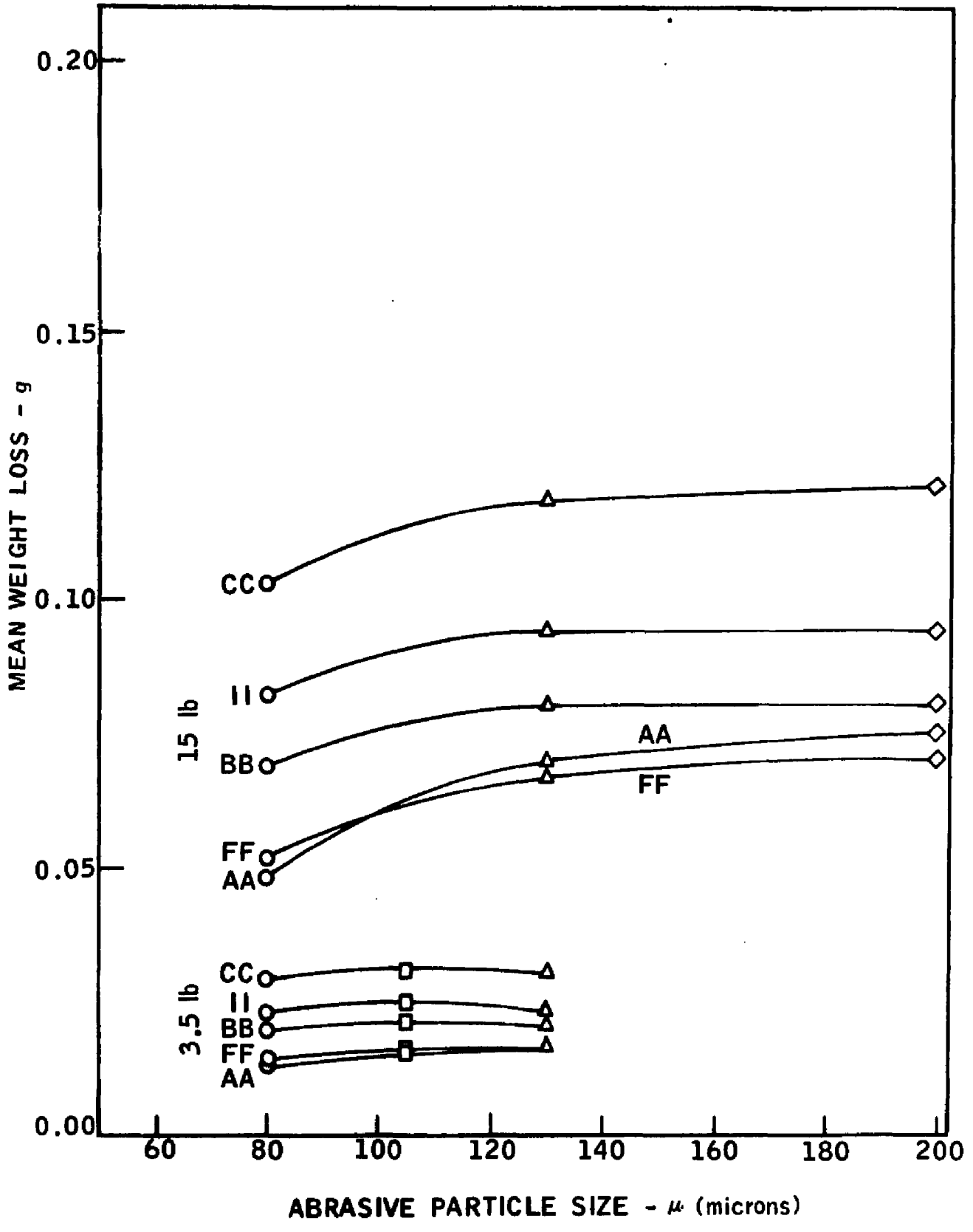

Figure 18 Weight Loss as a Function of Abrasive Particle Size for the Alloys Tested on Alumina Abrasive under 3.5 and 15 lb

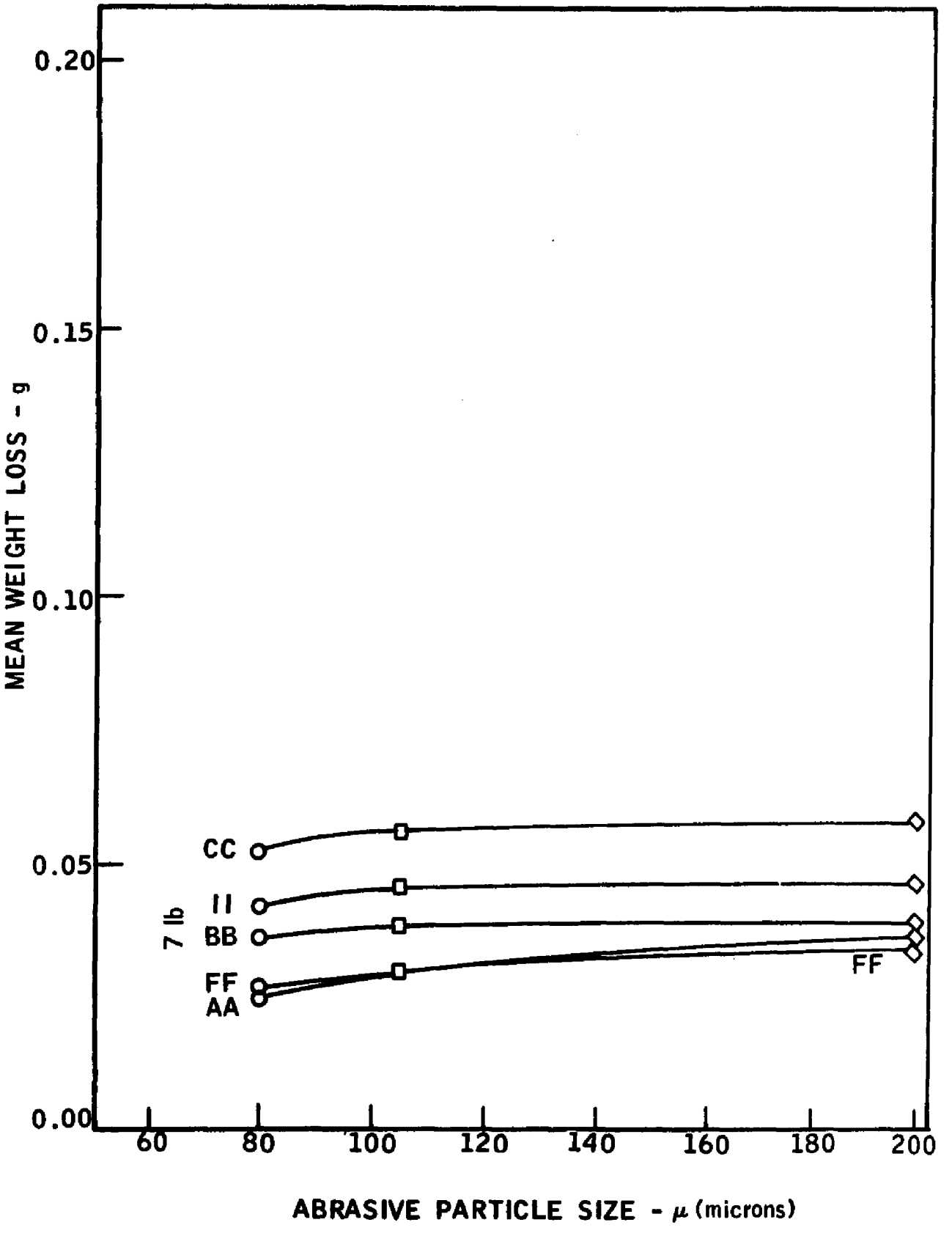

Figure 19 Weight Loss as a Function of Abrasive Particle Size for the Alloys Tested on Alumina Abrasive under 7 lb

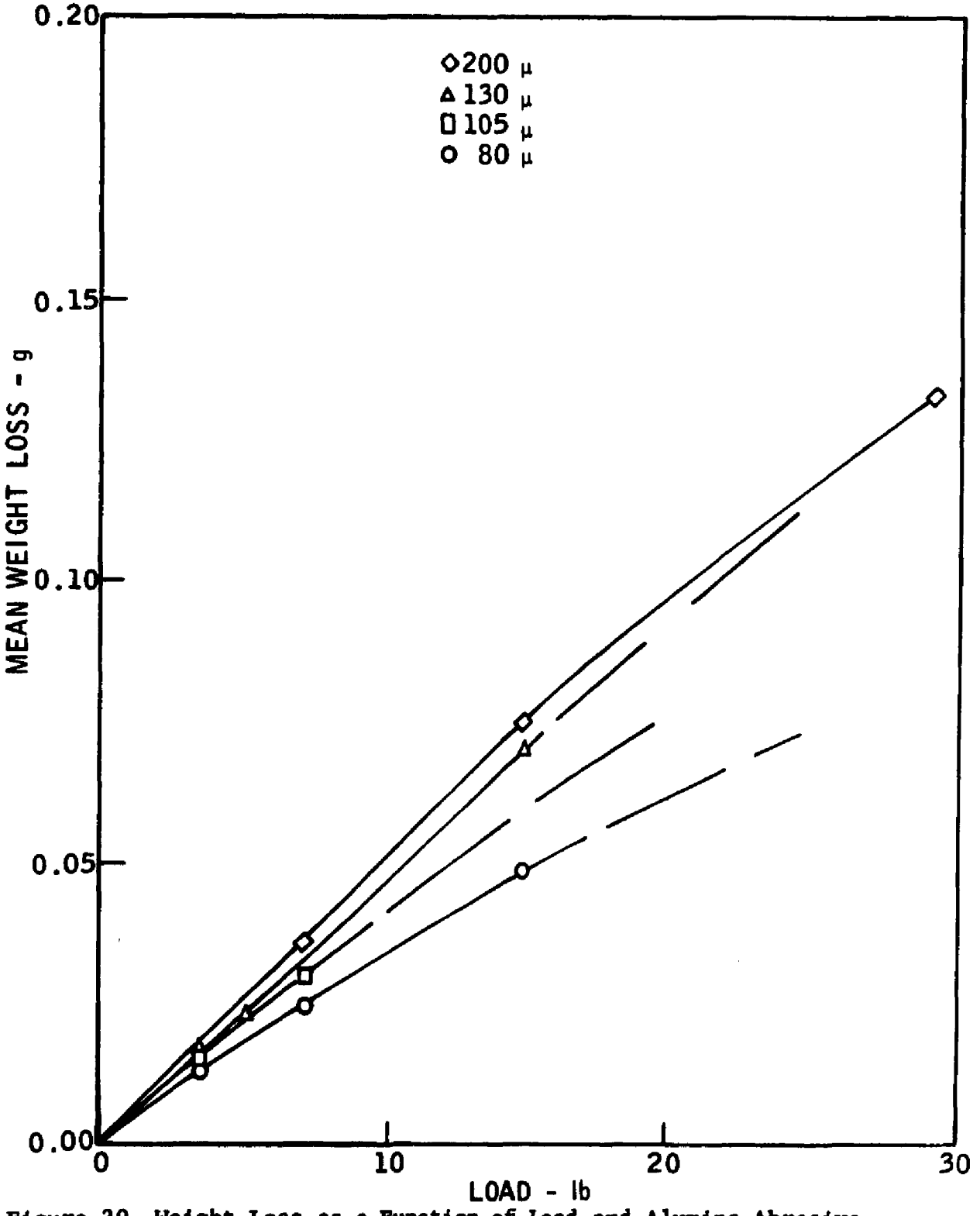

Figure 20 Weight Loss as a Function of Load and Alumina Abrasive Particle Size for Alloy AA

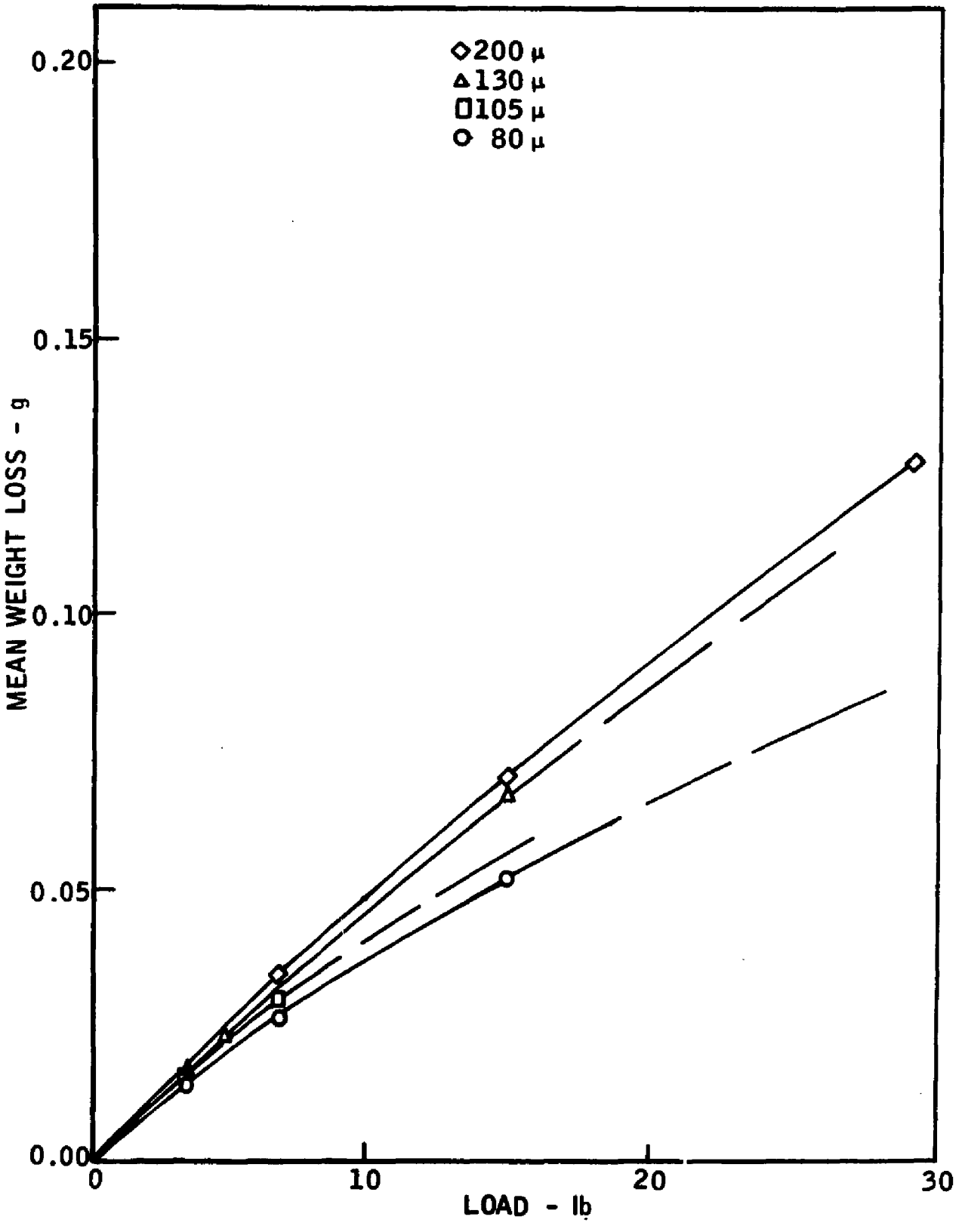

Figure 21 Weight Loss as a Function of Load and Alumina Abrasive Particle Size for Alloy FF

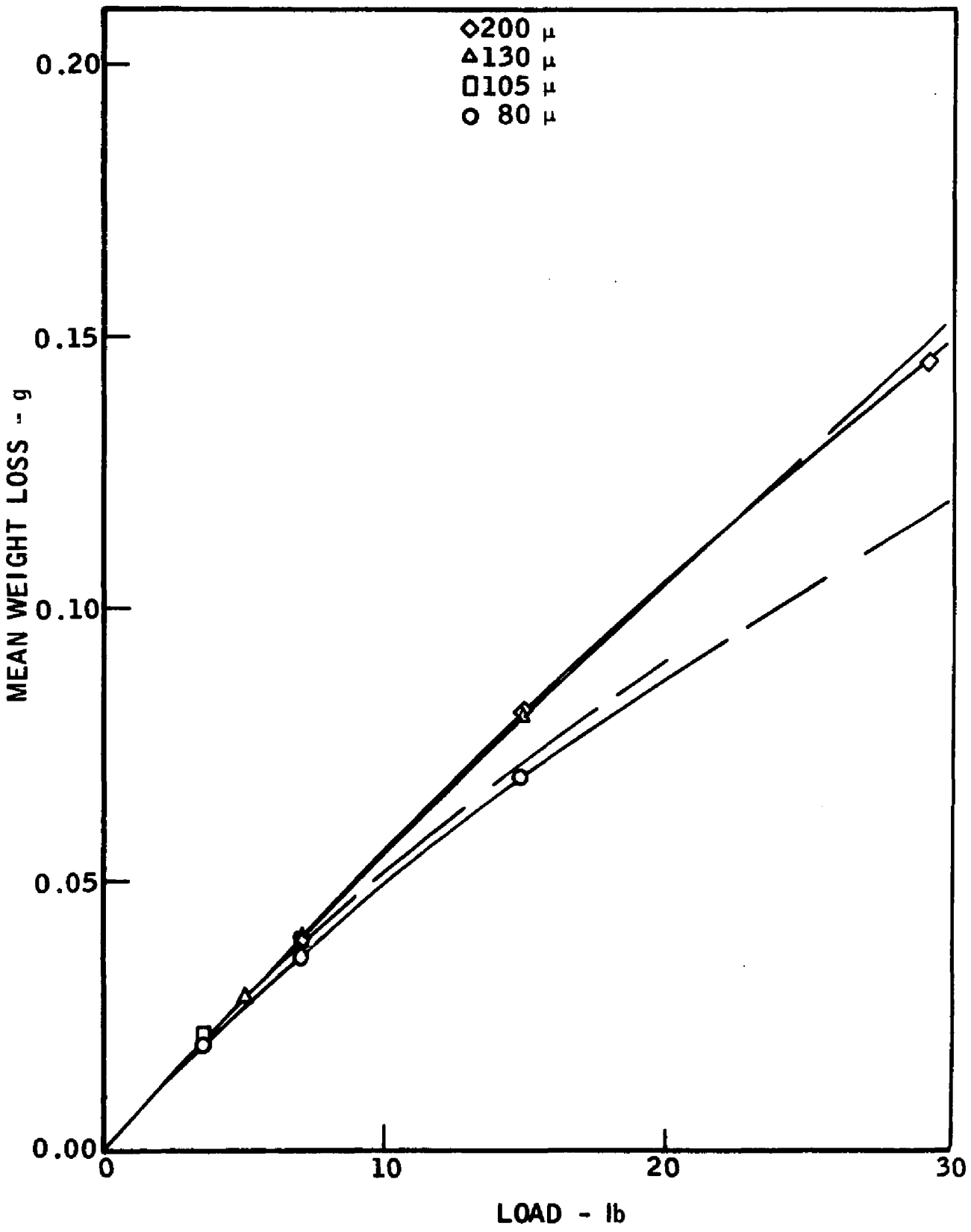

Figure 22 Weight Loss as a Function of Load and Alumina Abrasive Particle Size for Alloy BB

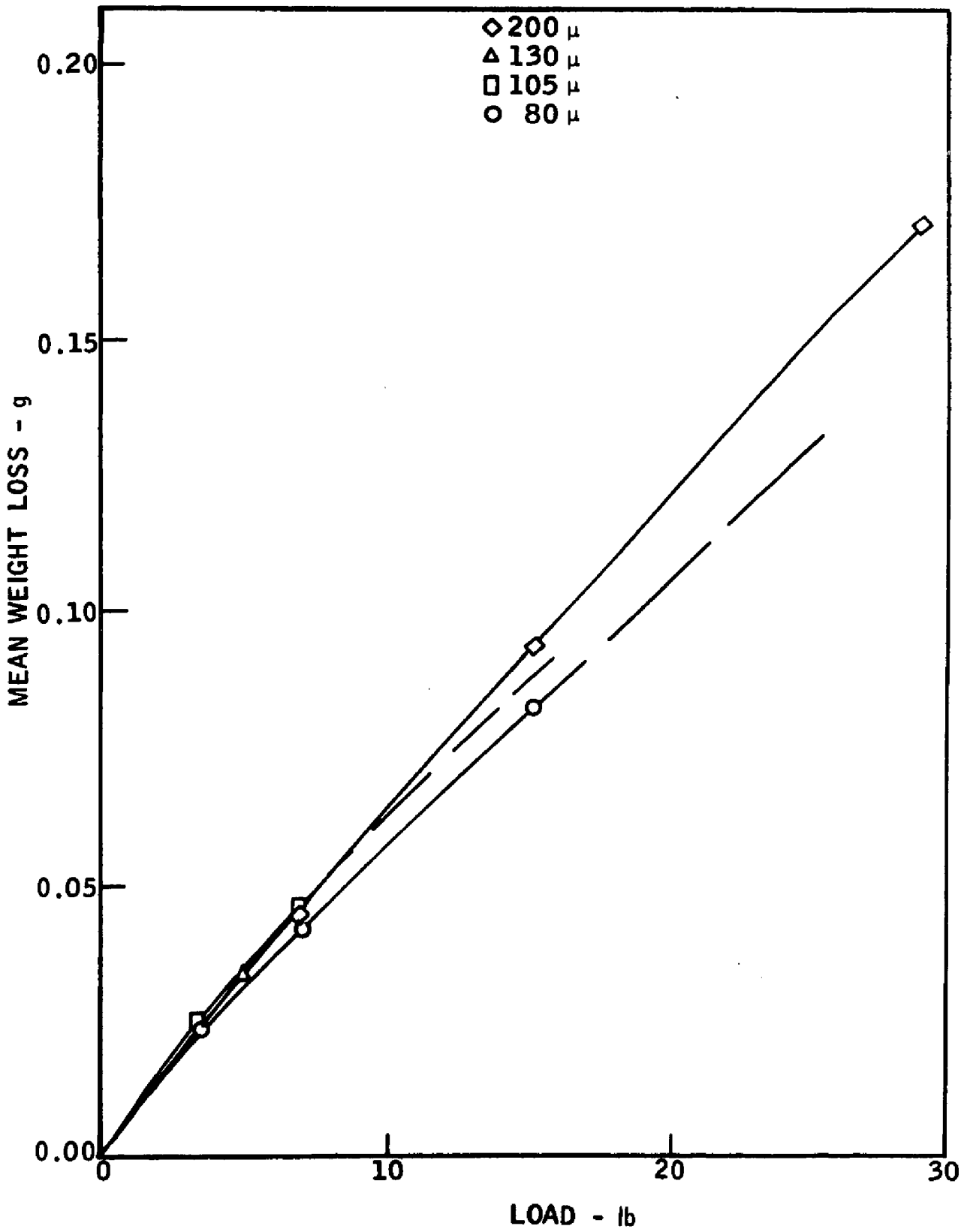

Figure 23 Weight Loss as a Function of Load and Alumina Abrasive Particle Size for Alloy II

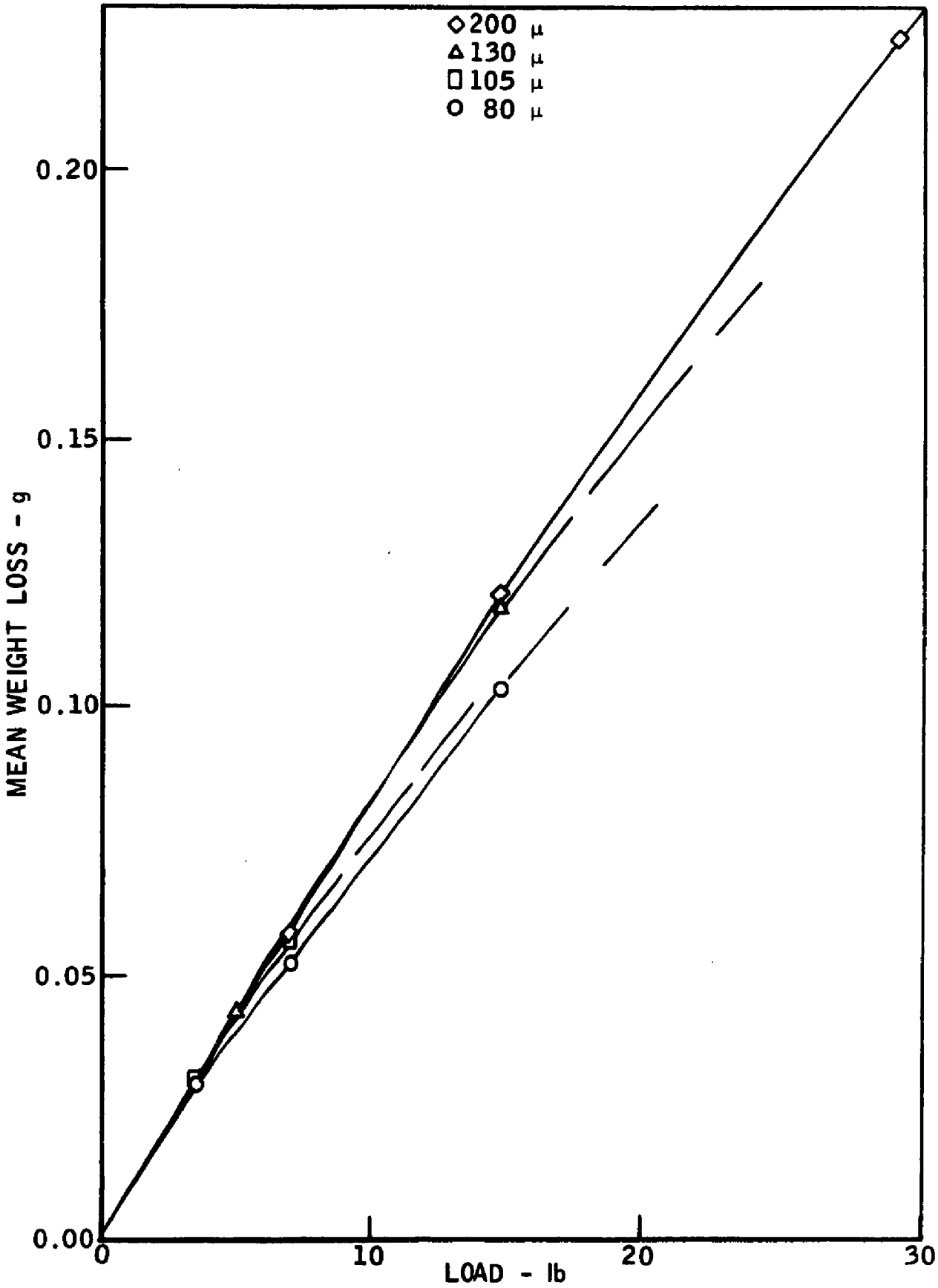

Figure 24 Weight Loss as a Function of Load and Alumina Abrasive Particle Size for Alloy CC

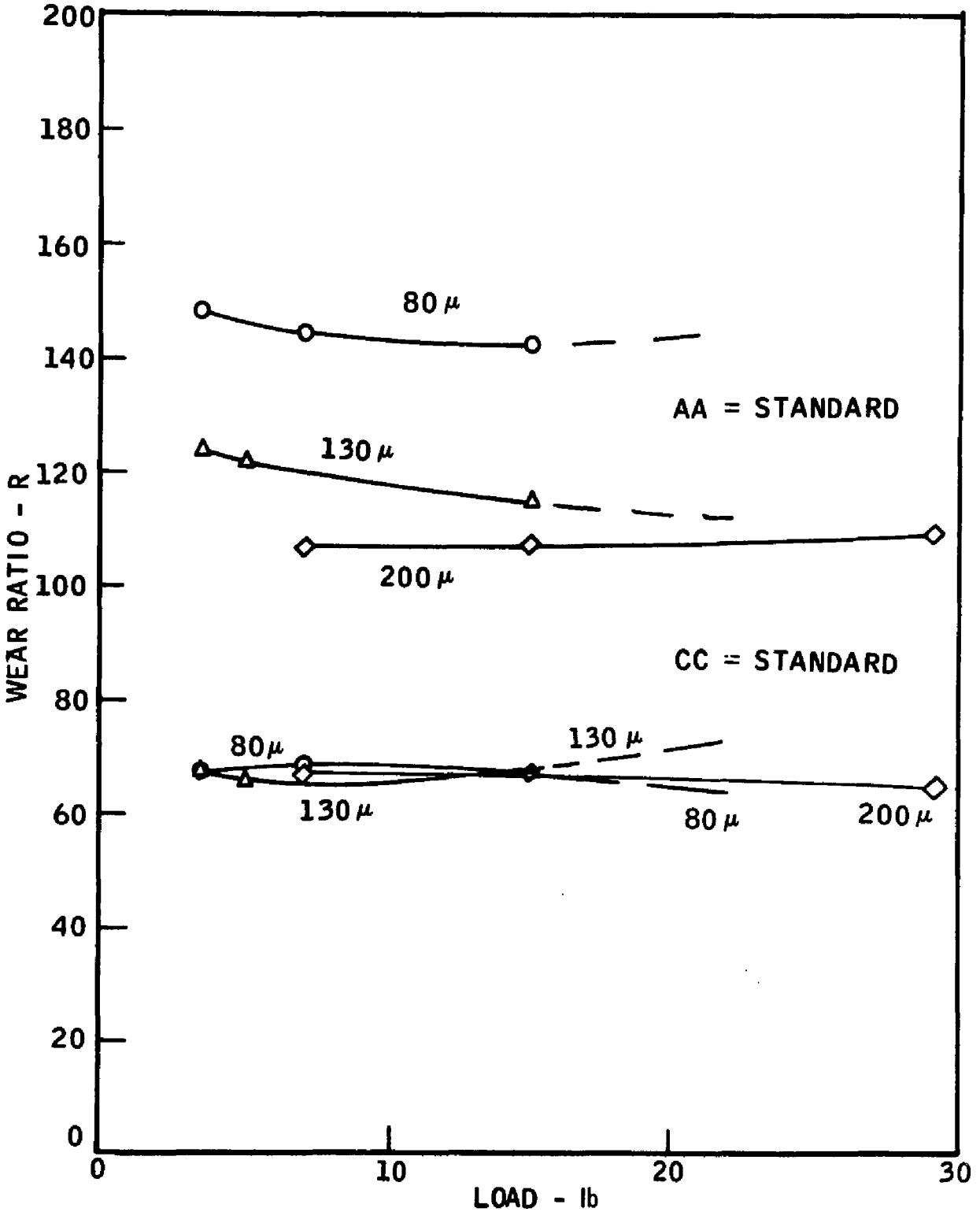

Figure 25 Wear Ratio as a Function of Load and Alumina Abrasive Particle Size for Alloy BB using as Standards Alloys AA and CC

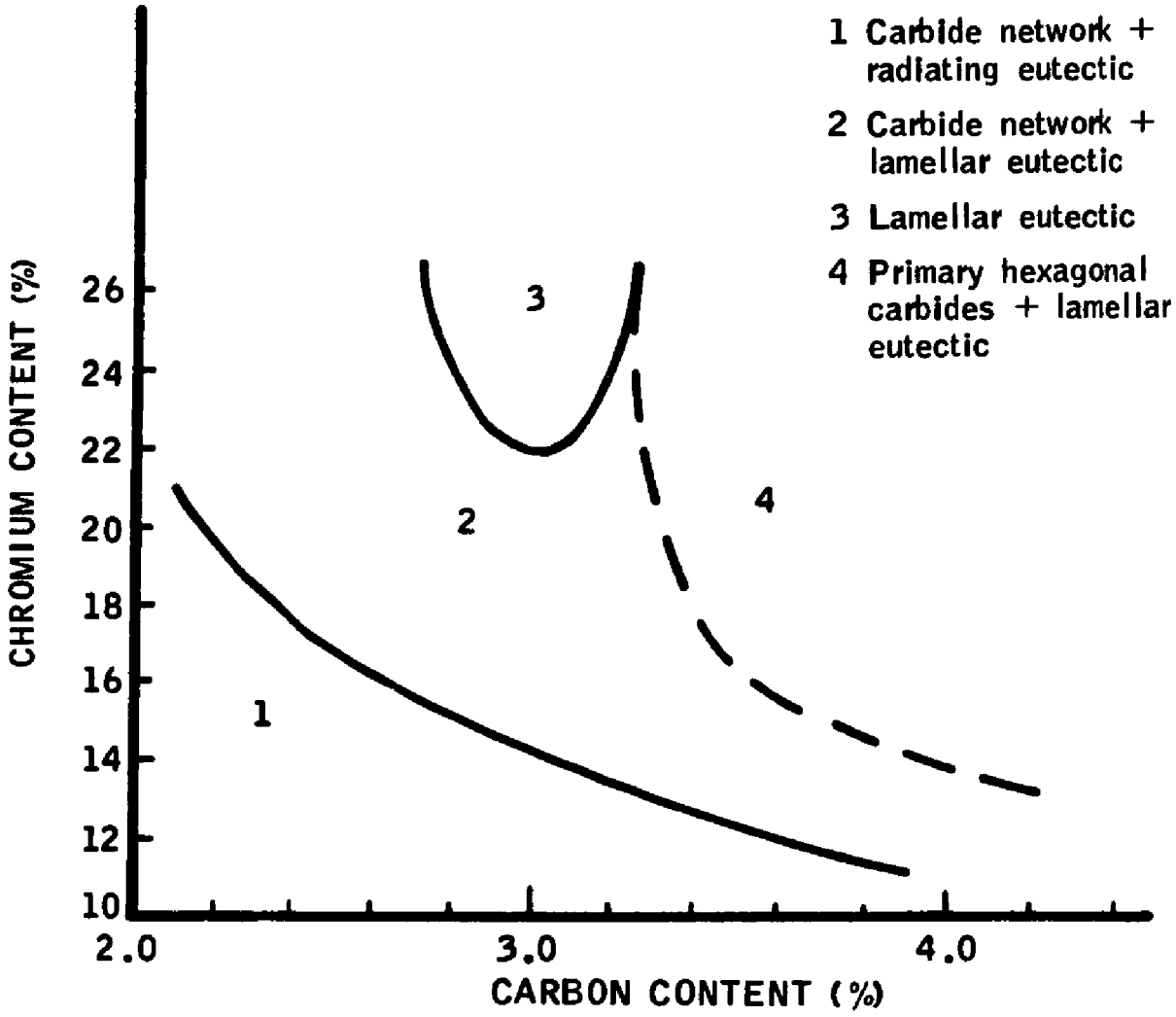

Figure 26 Relation among the Chromium Content, the Amount of Carbon, and the Microstructure (Ref. 37)

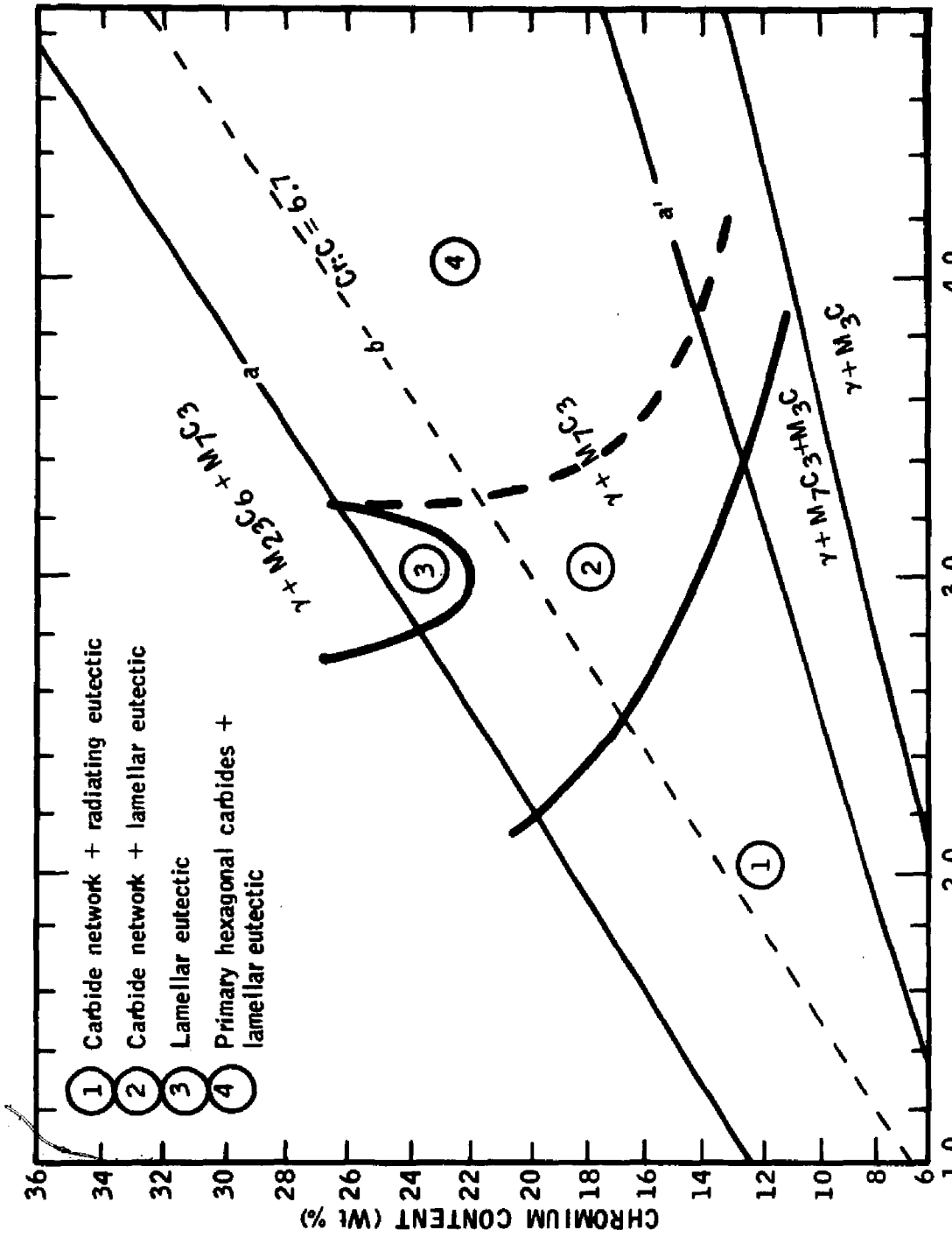

Figure 27 Effect of Chromium and Carbon Content on the Type and Morphology of Carbide

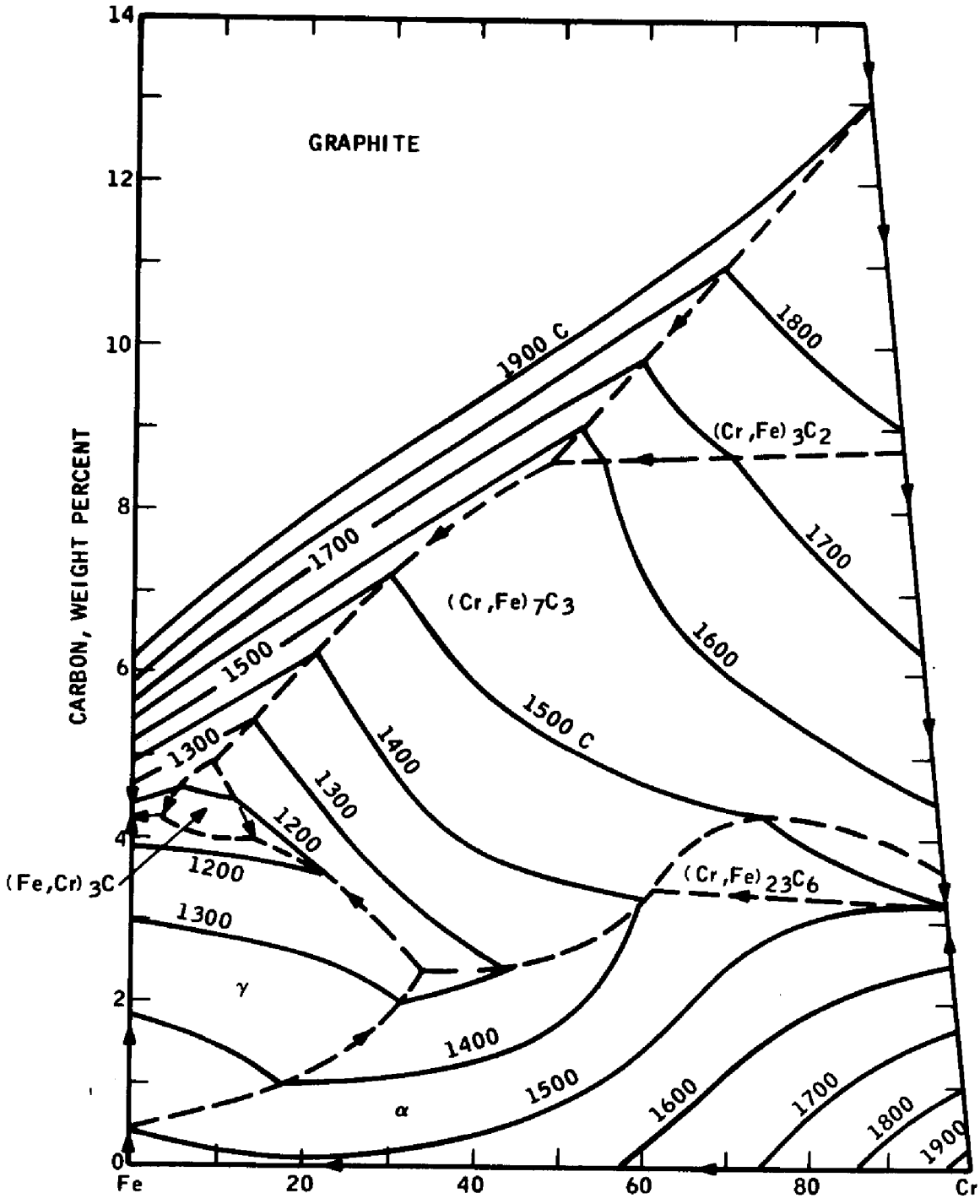

Figure 28 Liquidus Surface of the Fe-C-Cr System (Reference 40)

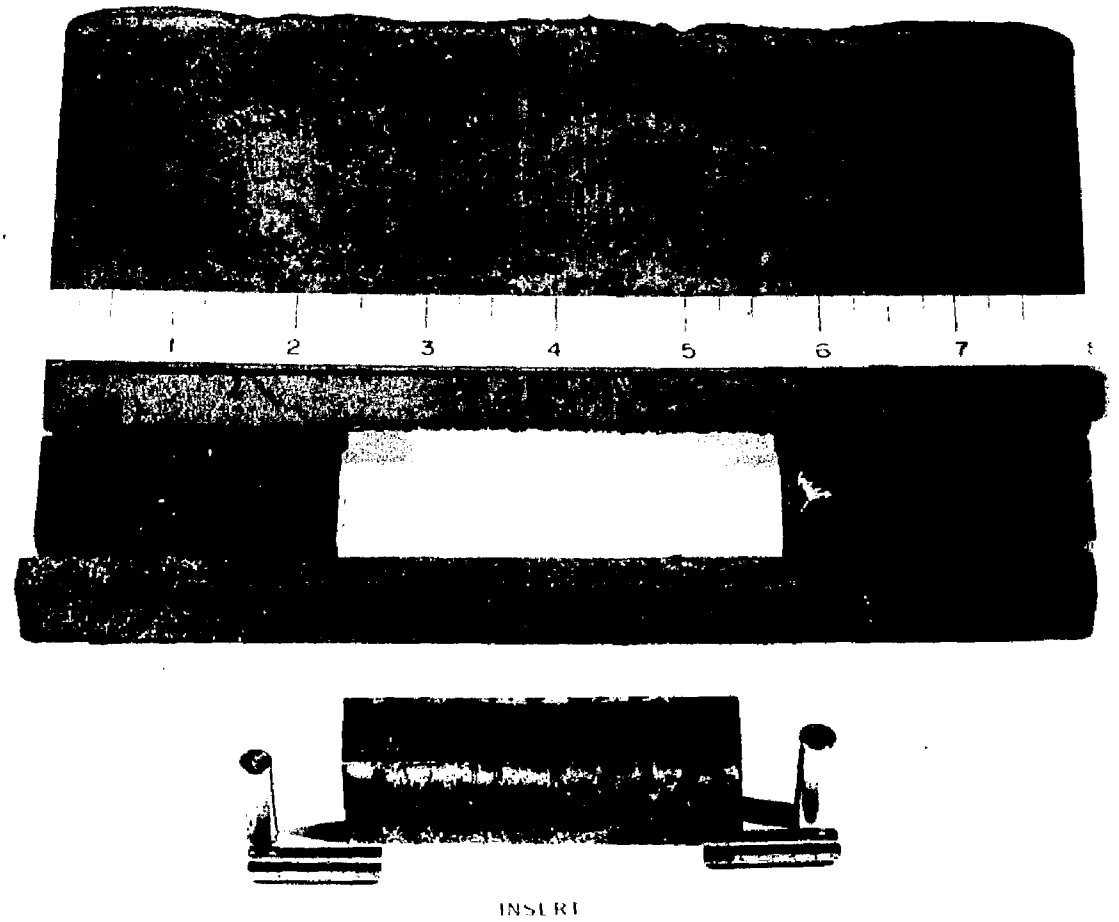

Figure 29 Specimen Positions

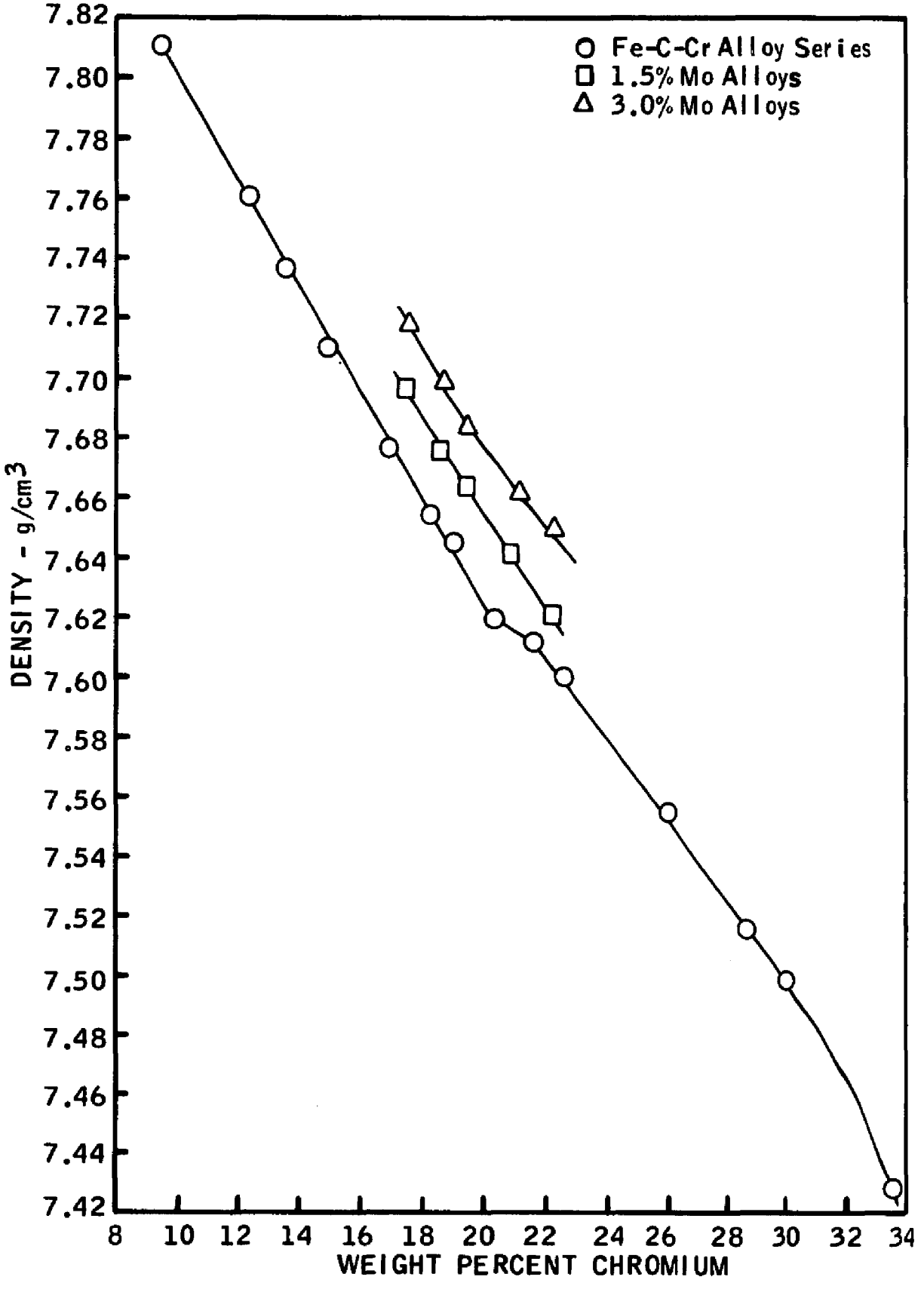

Figure 30 Alloy Density as a Function of Composition in Alloys with a Cr:C of 6.64

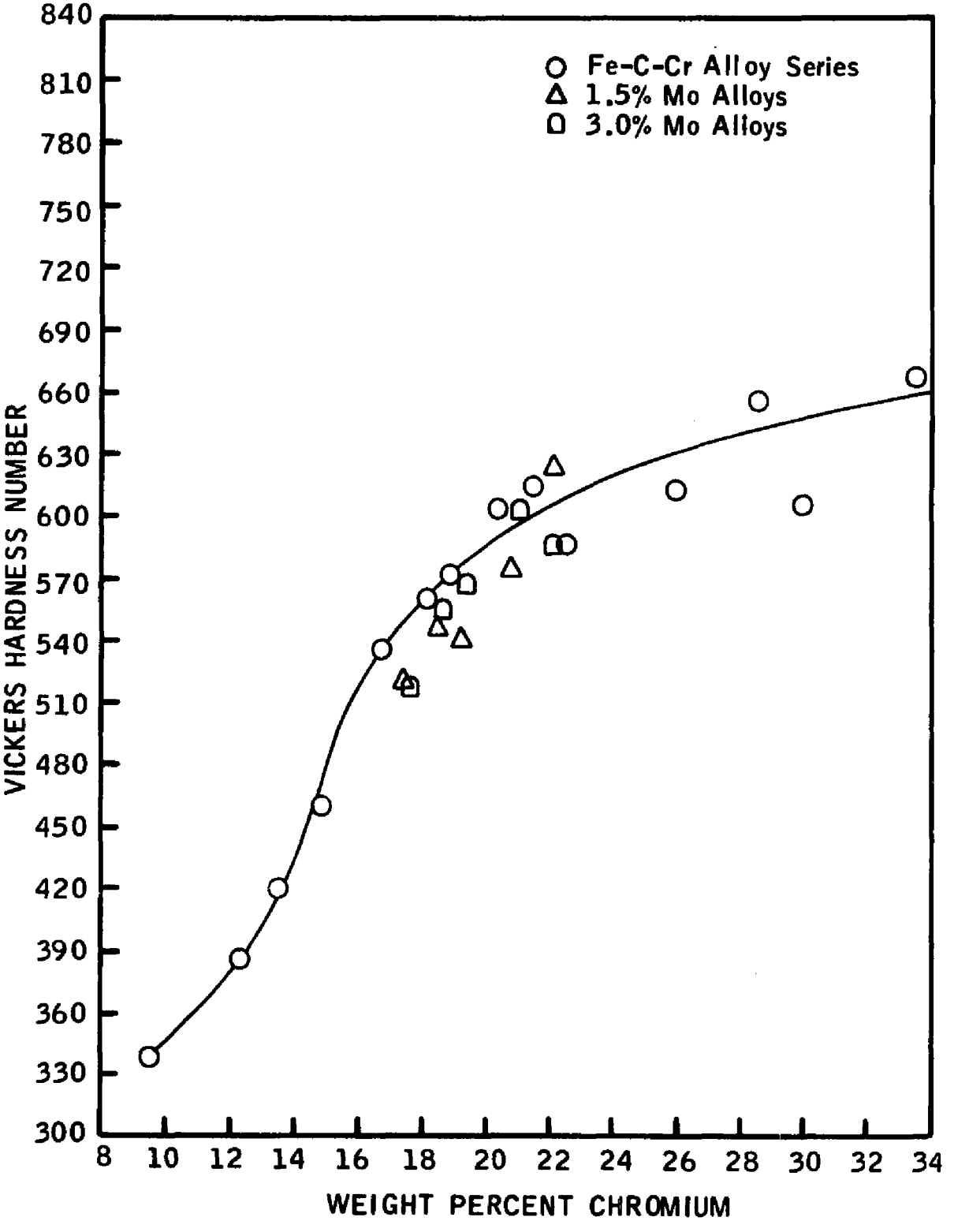

Figure 31 Vickers Hardness Determined under 10 kg Loading as a Function of Composition in the Non-Abraded Alloys with a Cr:C of 6.64

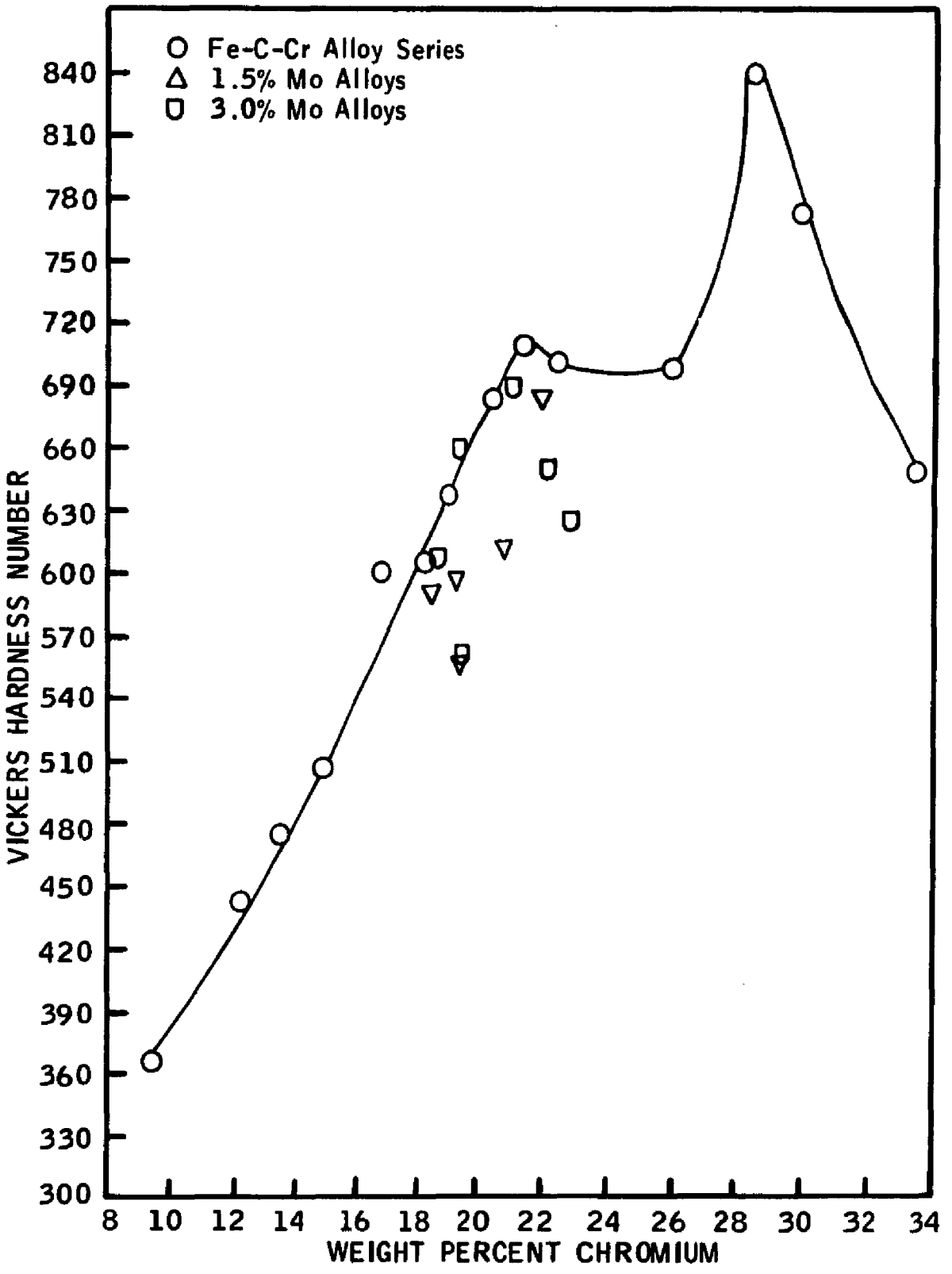

Figure 32 Vickers Hardness Determined under 10 kg Loading as a Function of Composition in the Abraded Alloys with a Cr:C of 6.64

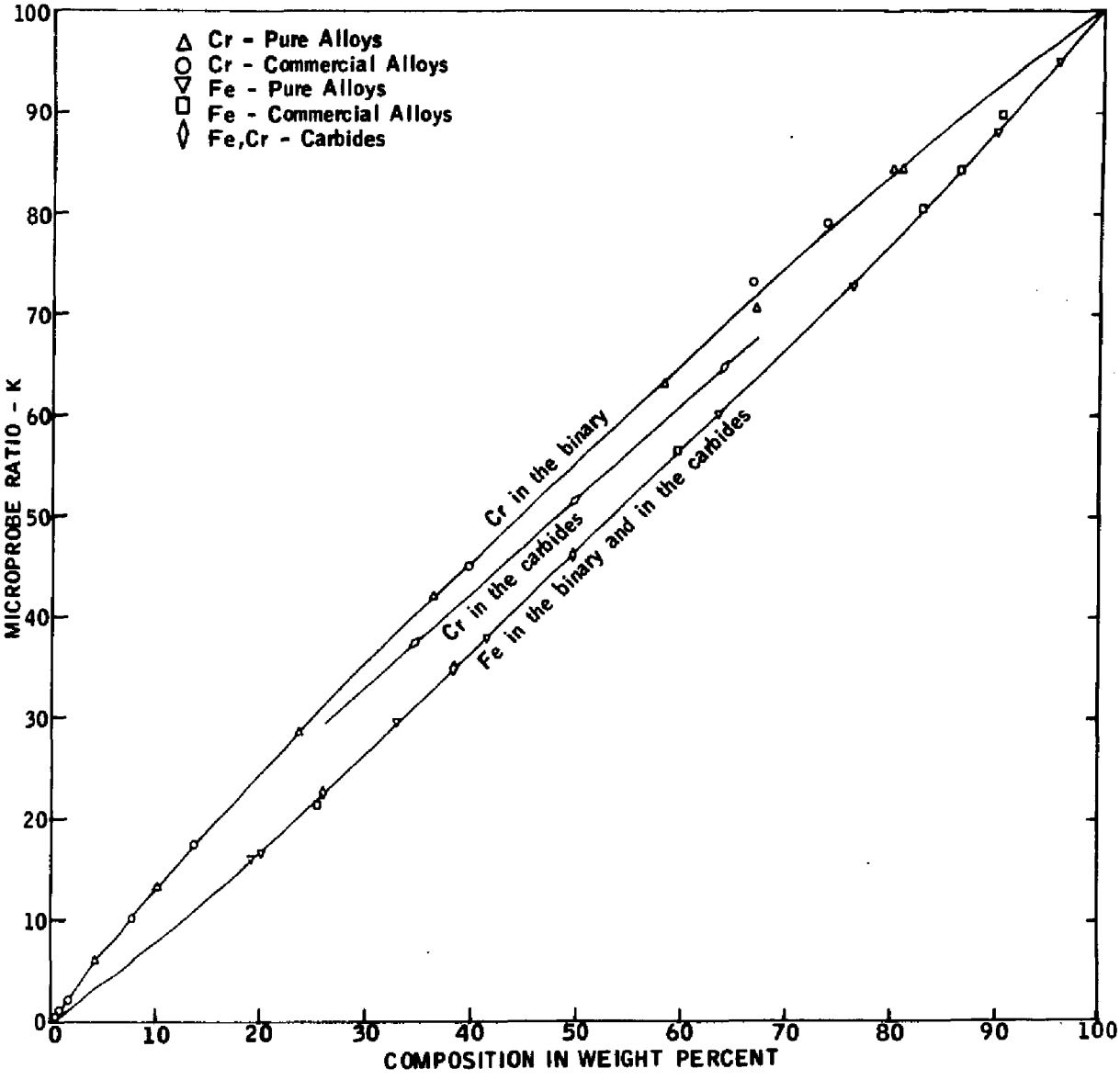

Figure 33 Microprobe Calibration Curves for Fe-Cr Solid Solution Phases and for $(Cr,Fe)_7C_3$ [Plot reduced by 65 percent for reproduction]

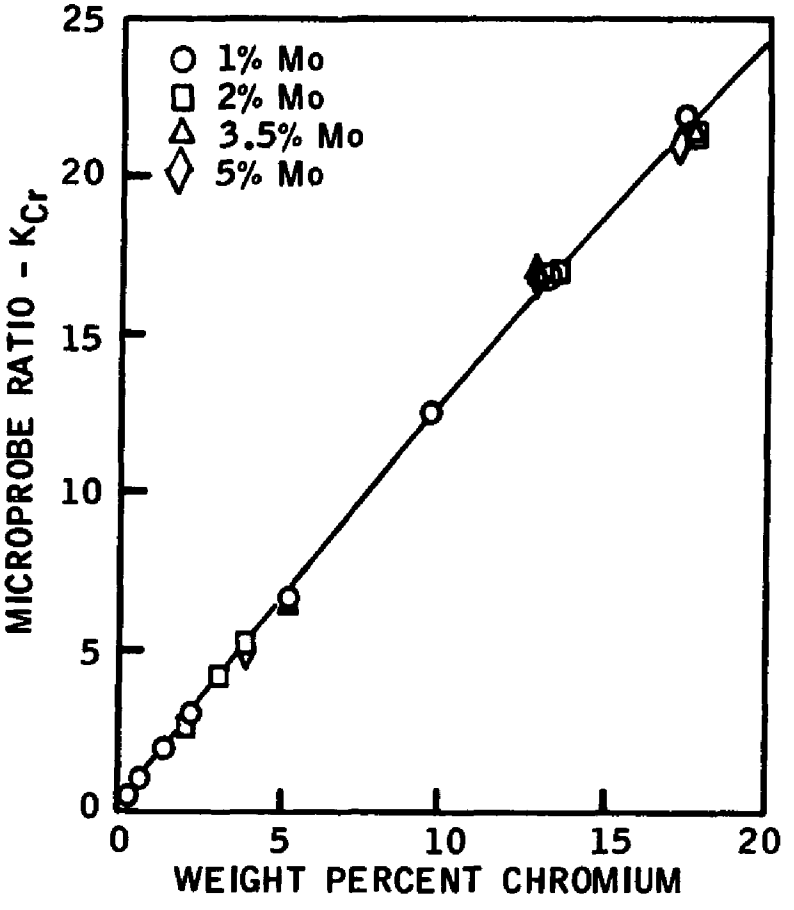

Figure 34 Microprobe Calibration Curve for Cr in Fe-Cr-Mo Alloys with up to 5 Weight Percent Mo

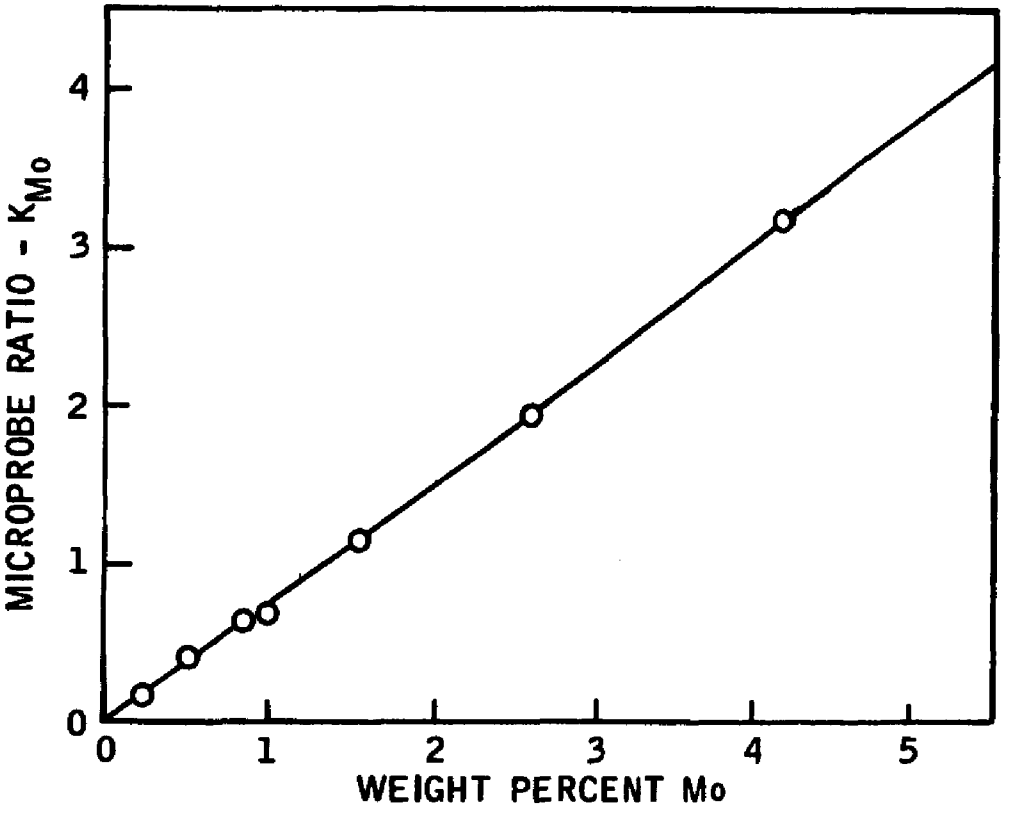

Figure 35 Microprobe Calibration Curve for Mo in Fe-Cr-Mo Alloys with Less than 4 Weight Percent Cr

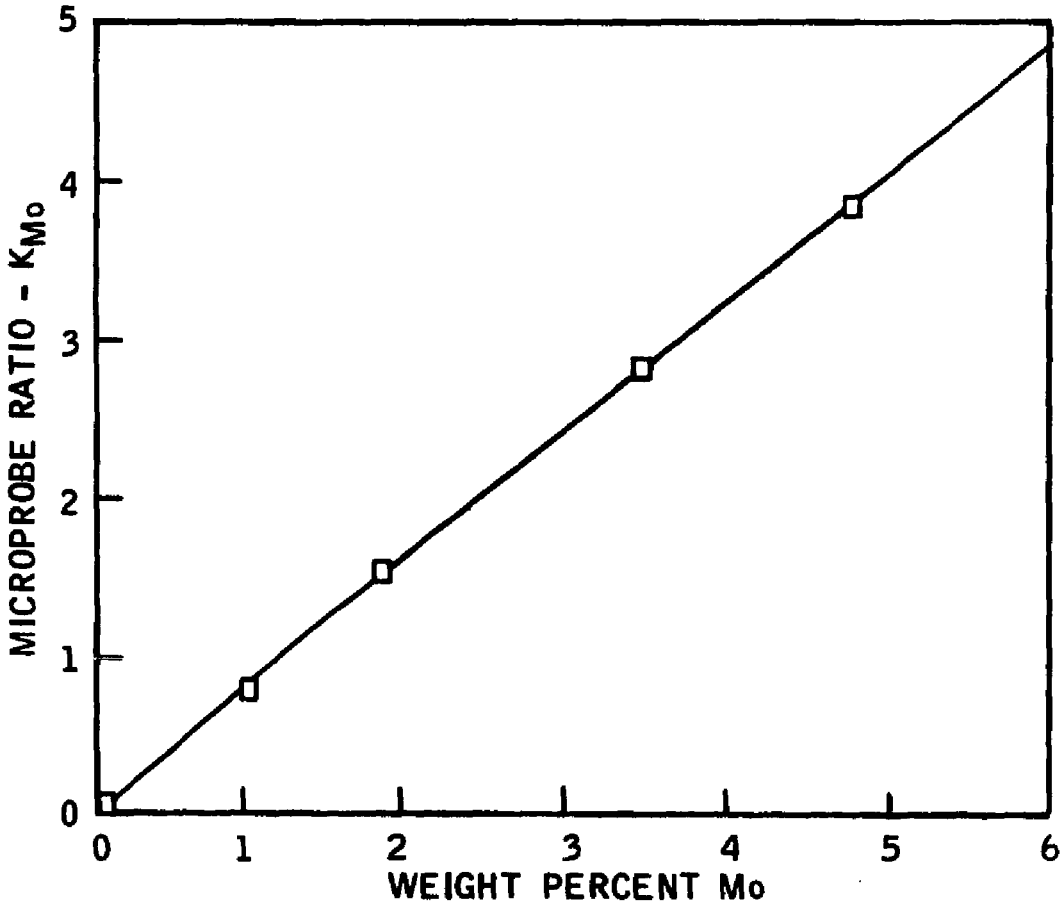

Figure 36 Microprobe Calibration Curve for Mo in Fe-Cr-Mo Alloys with 13 Weight Percent Cr

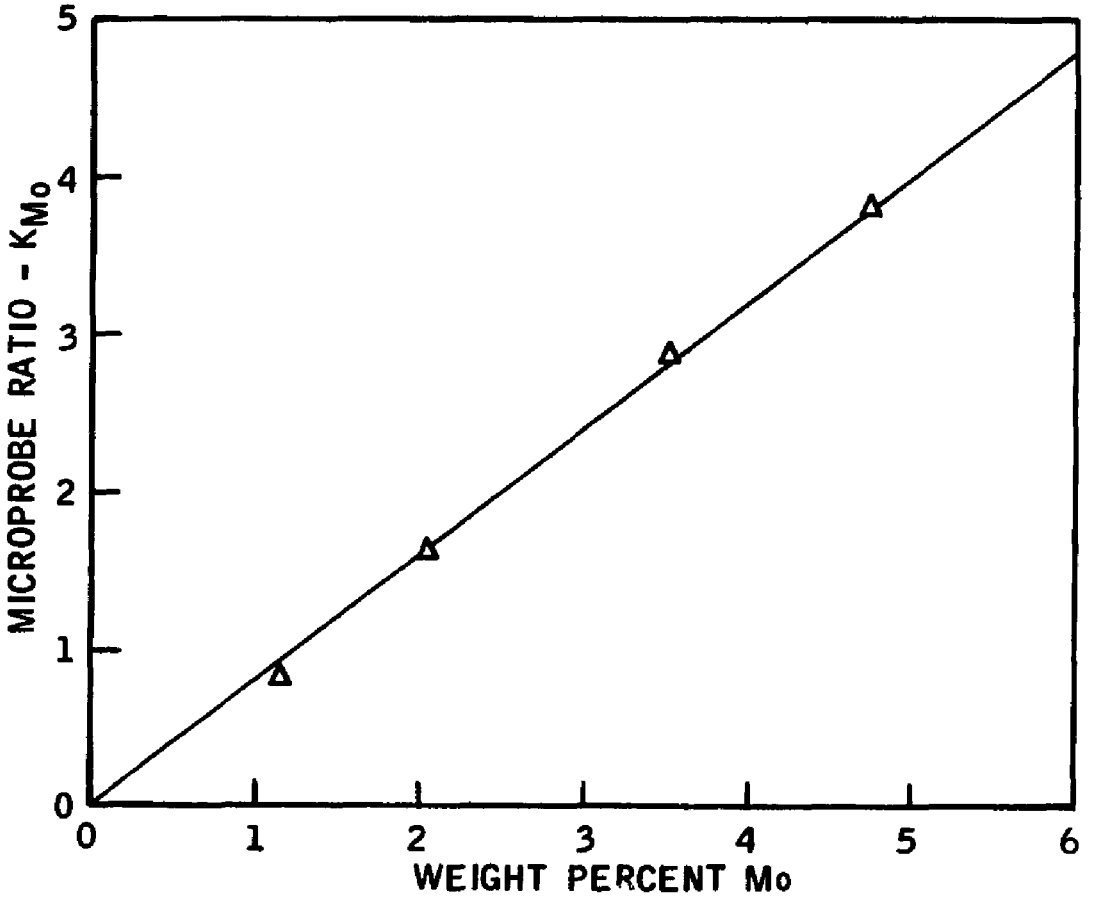

Figure 37 Microprobe Calibration Curve for Mo in Fe-Cr-Mo Alloys with 17.5 Weight Percent Cr

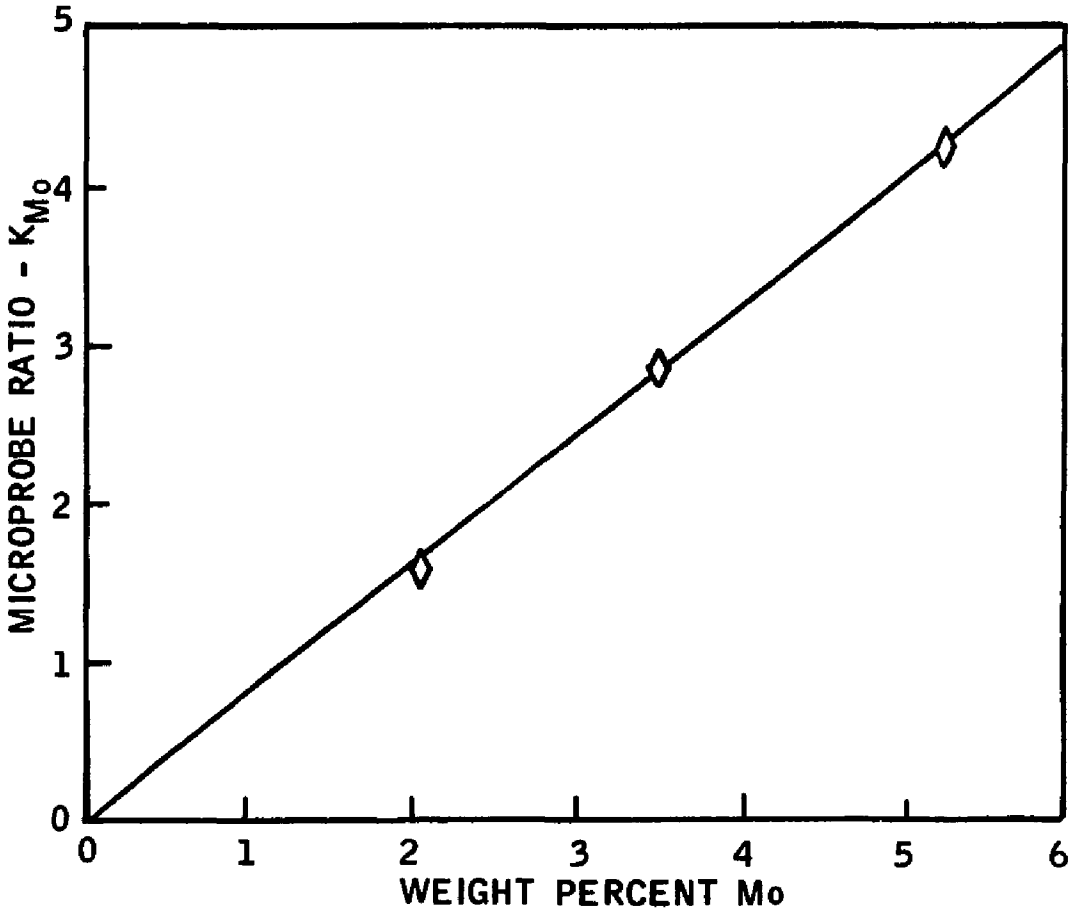

Figure 38 Microprobe Calibration Curve for Mo in Fe-Cr-Mo Alloys with 25 Weight Percent Cr

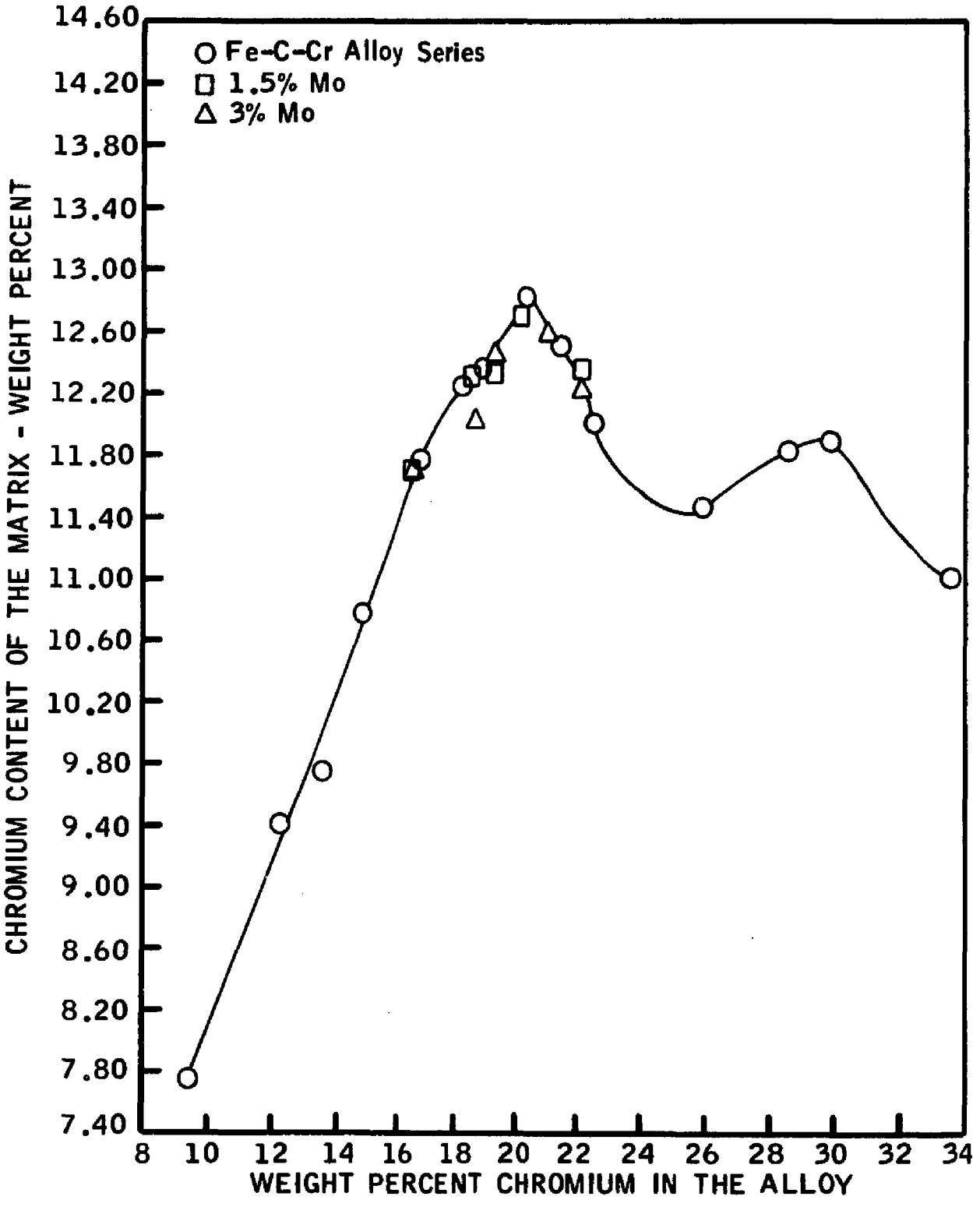

Figure 39 Chromium Content of the Matrix as a Function of Total Chromium in Alloys with a Cr:C of 6.64

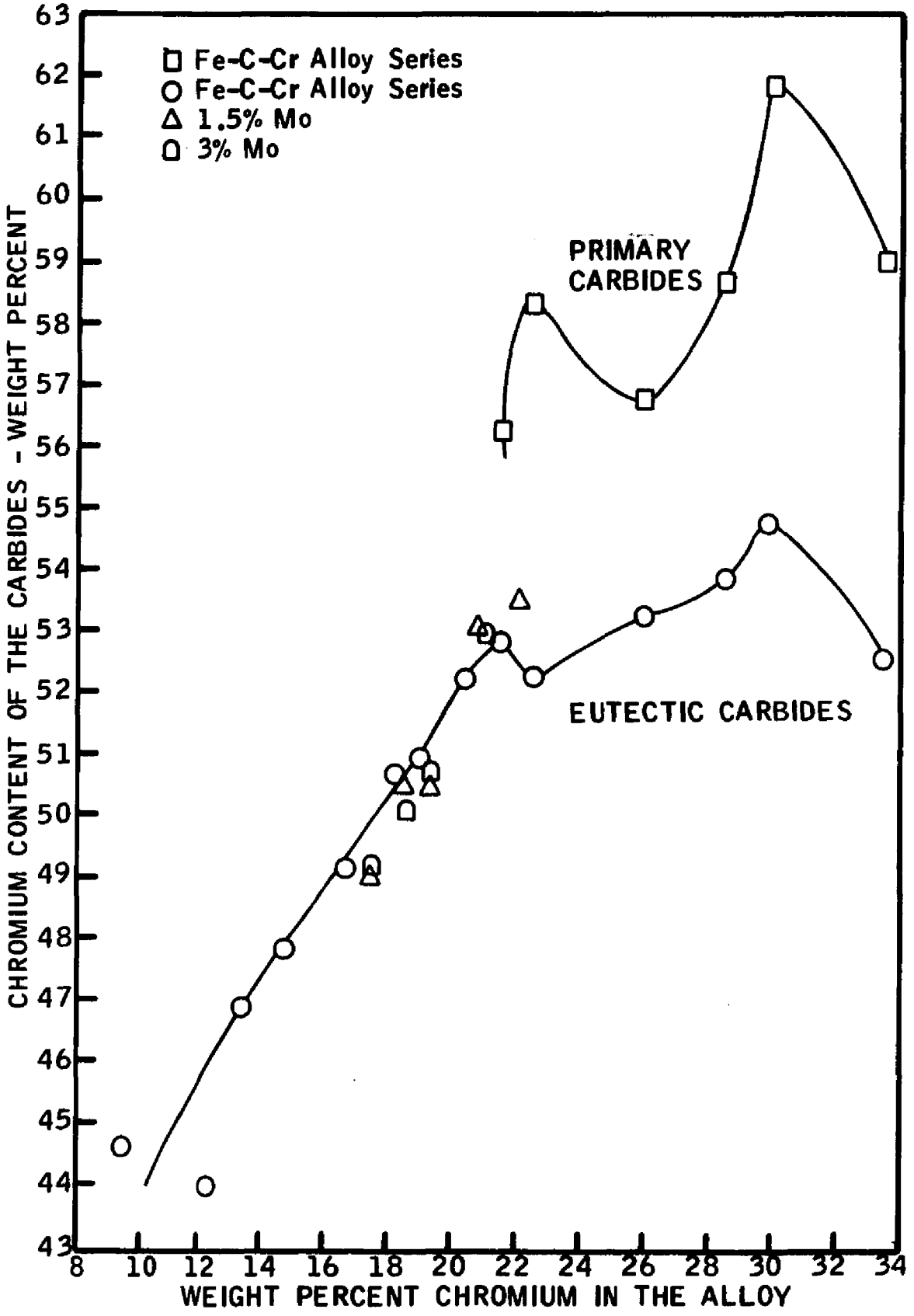

Figure 40 Chromium Content of the Carbides as a Function of Total Chromium in Alloys with a Cr:C of 6.64

(a) X500

(b) X250

(c) X500

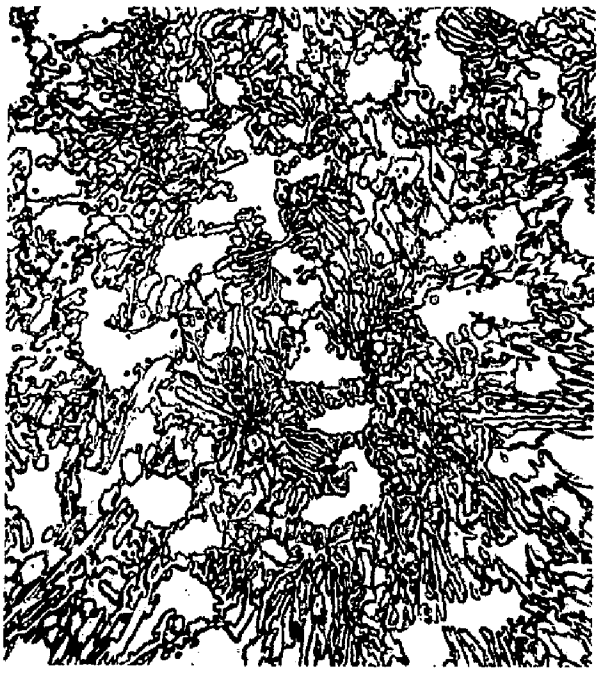

(d) X250

Figure 41 Carbide Morphologies (a and b) Lamellar Eutectic Carbides in Specimens KV and I, Respectively, (c and d) Radiating Eutectic Carbides in Specimens I and IV, Respectively

(e) X500

(f) X250

(g) X500

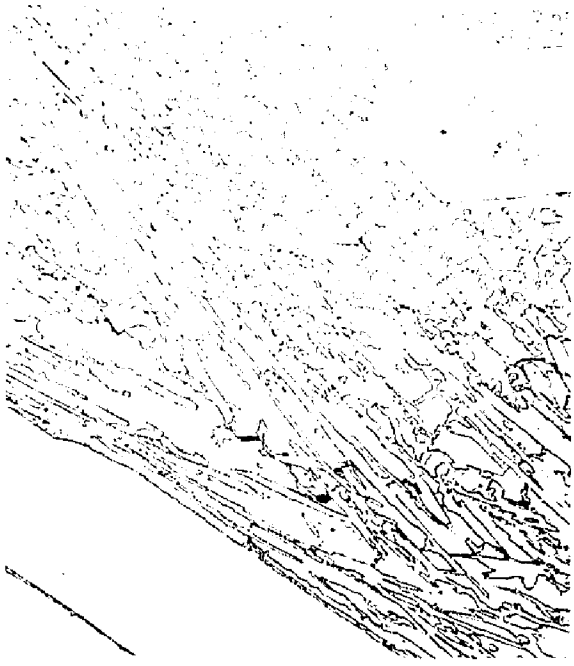

(h) X250

Figure 41 [Continued] (e and f) Eutectic Carbide Rods in Transverse Cross Sections in Specimens N and K, Respectively, (g and h) Primary Carbides in Longitudinal and Transverse Cross Sections in Specimens N and K, Respectively

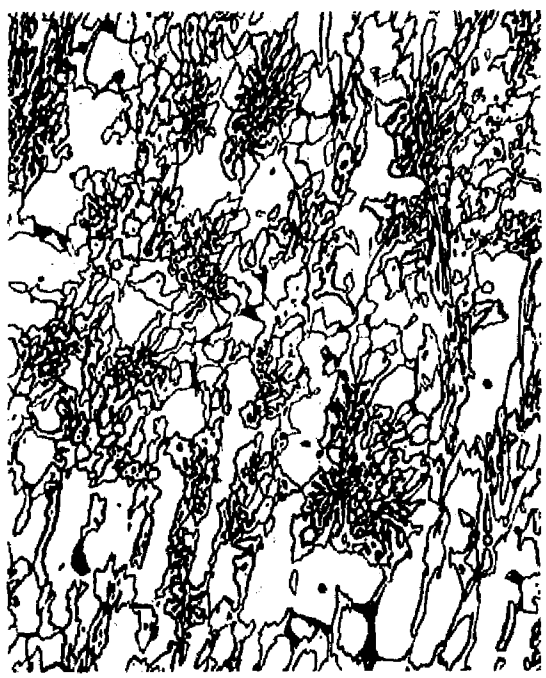

(a) X250

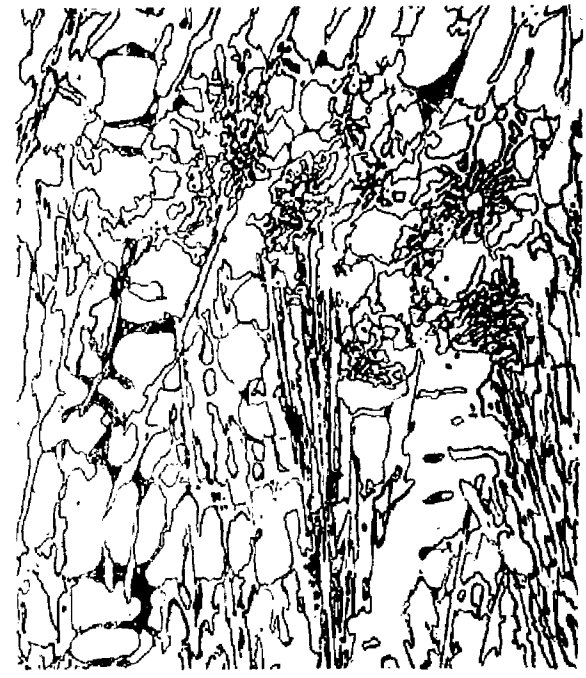

(b) X250

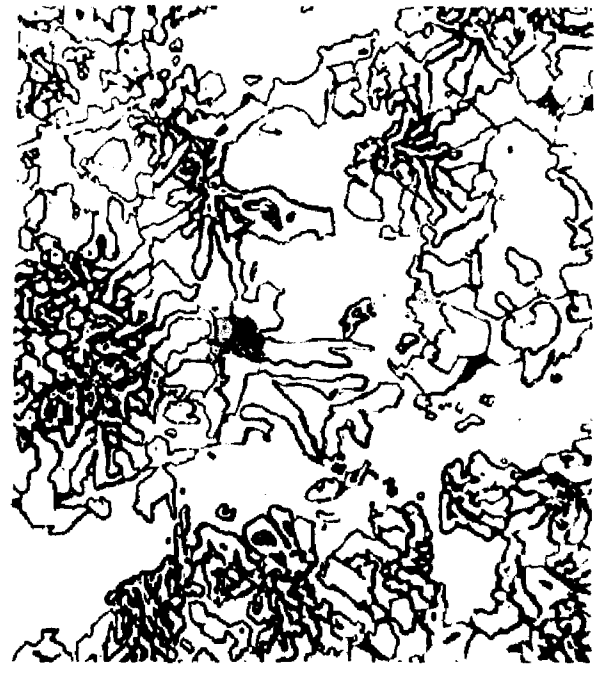

(c) X500

Figure 42 Carbide Morphologies and Structures in Molybdenum Containing Alloys (a) and (c) Radiating and Transverse Cross Section Eutectic Carbides, and Mo_2C Eutectic Carbides in Specimen I2V, (b) Radiating, Lamellar, and Mo_2C Eutectic Carbides in Specimen I2V

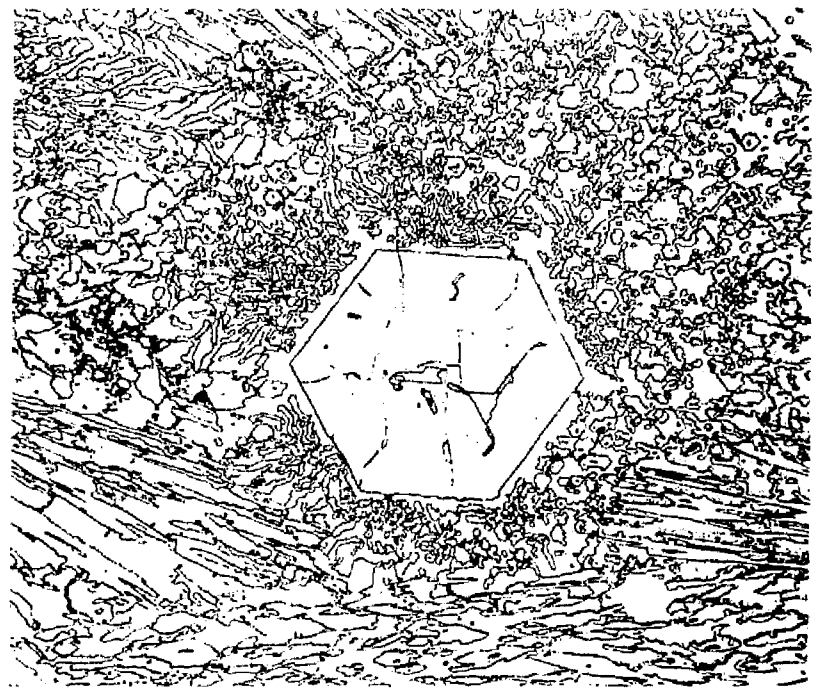

(a) X250

(b) X250

Figure 43 Mixed Carbide Morphologies (a) Lamellar, Radiating, and Transverse Cross Section Eutectic Carbides plus Primary Carbide in Specimen N, (b) Primary Carbides and Transverse Cross Section and Lamellar Eutectic Carbides in Specimen N

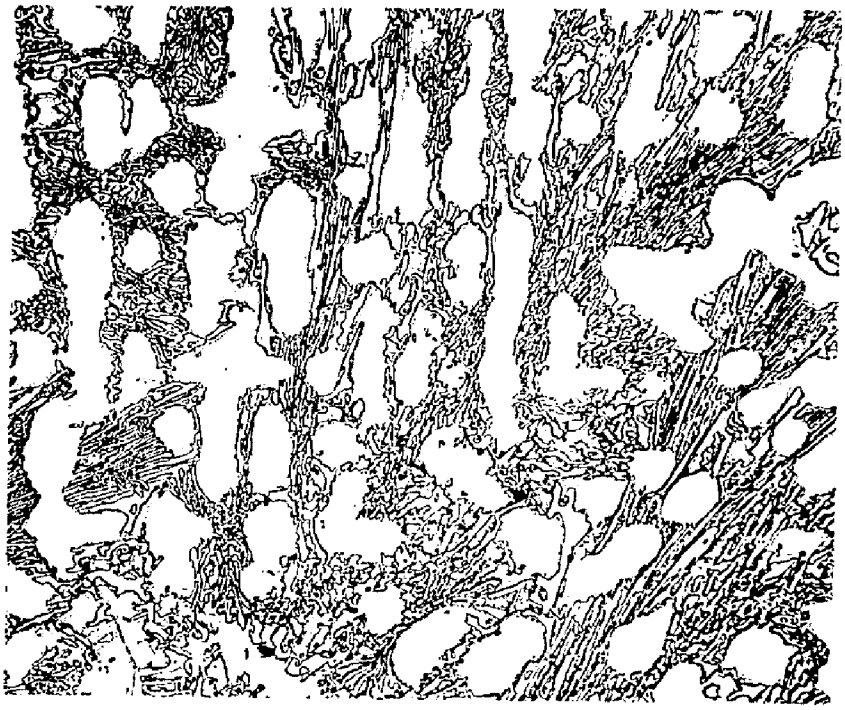

(c) X250

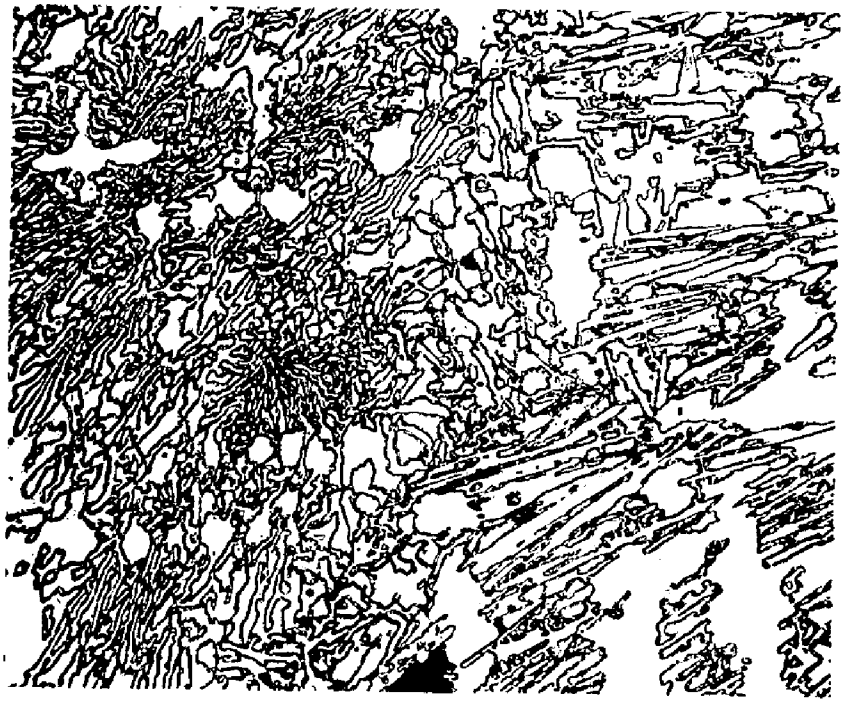

(d) X250

Figure 43 [Continued] (c) Radiating and Lamellar Eutectic Carbides in Specimen F, (d) Radiating, Lamellar and Transverse Cross Section Eutectic Carbides in Specimen I

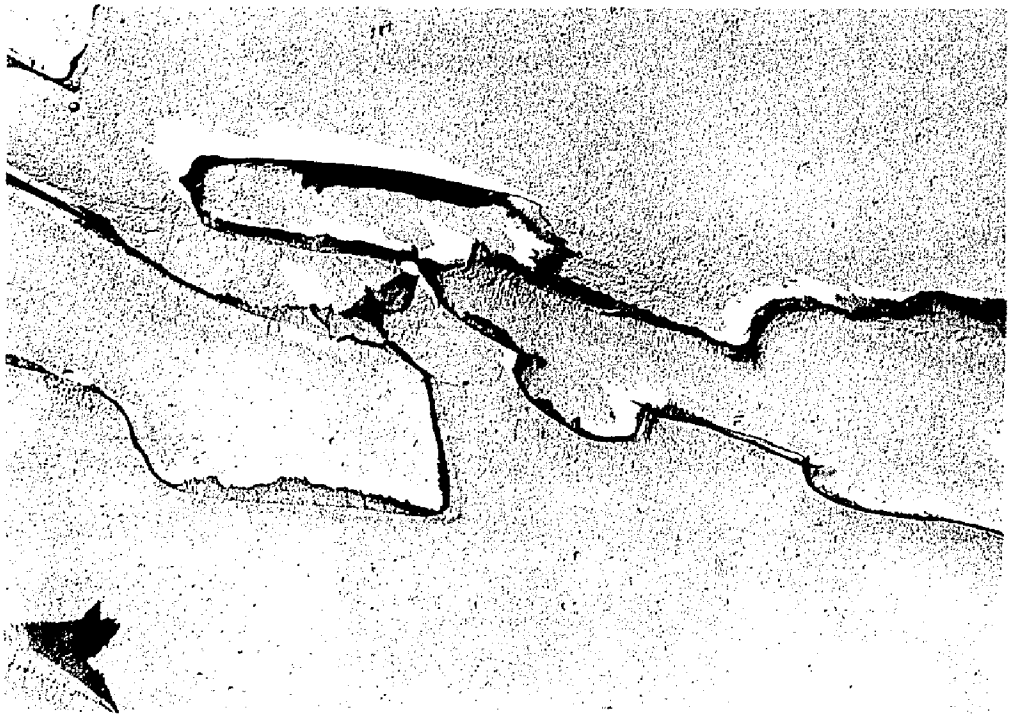

X10,000

Figure 44 Surface Replica of Specimen K1

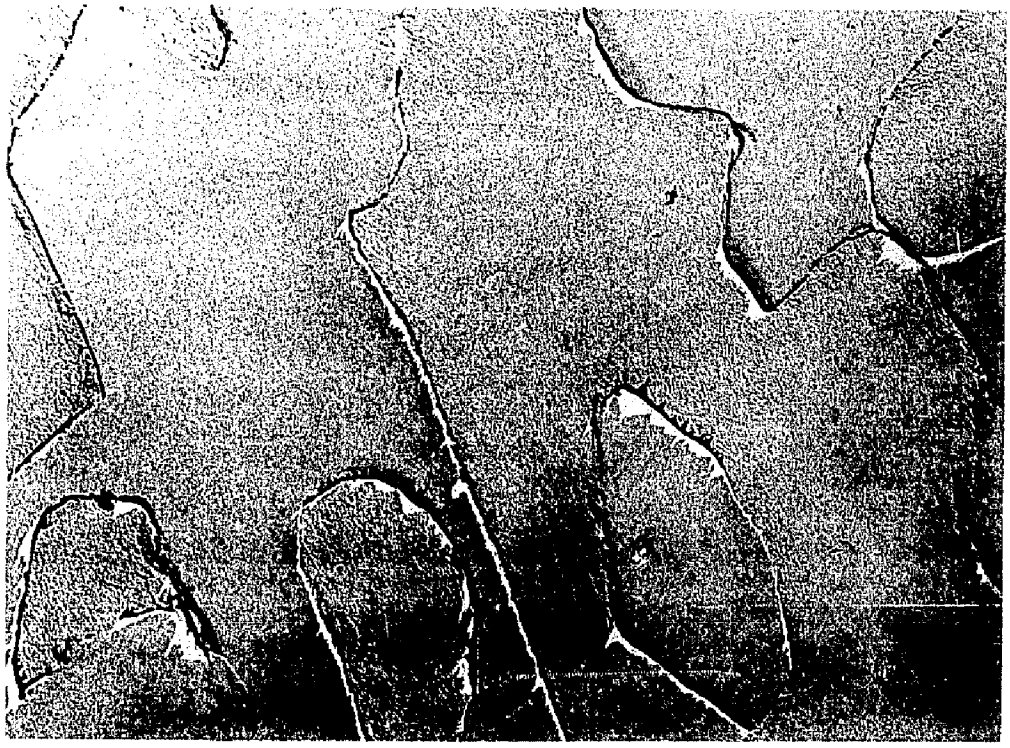

X10,000

Figure 45 Surface Replica of Specimen N

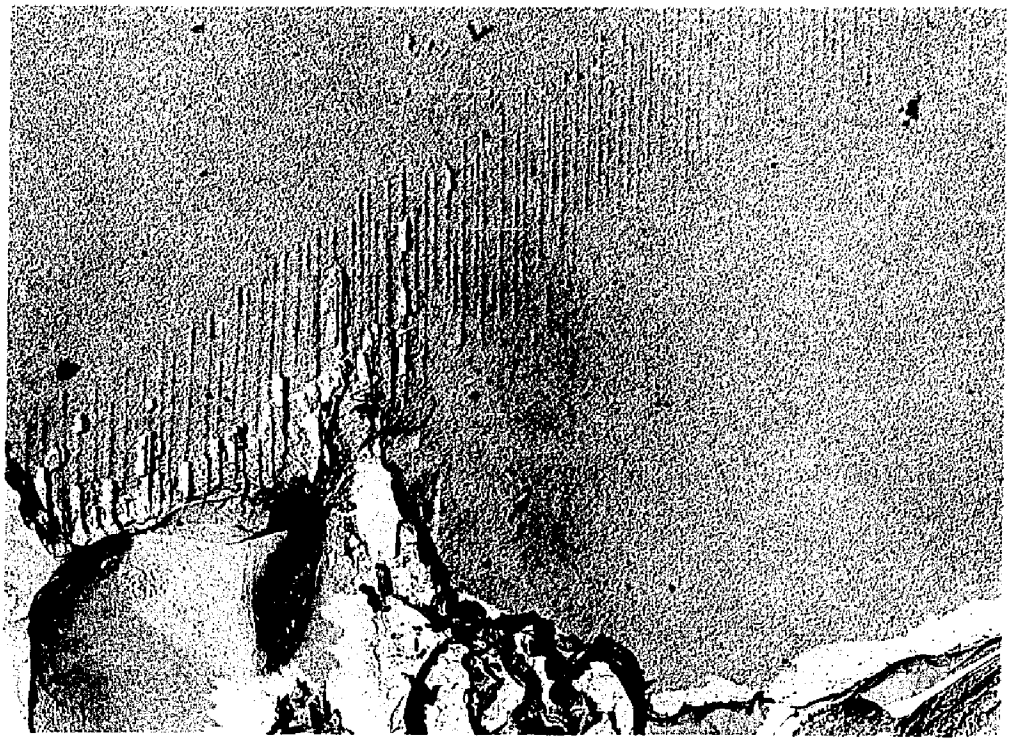

X5000

Figure 46 Surface Replica showing Slip Lines in Specimen C-

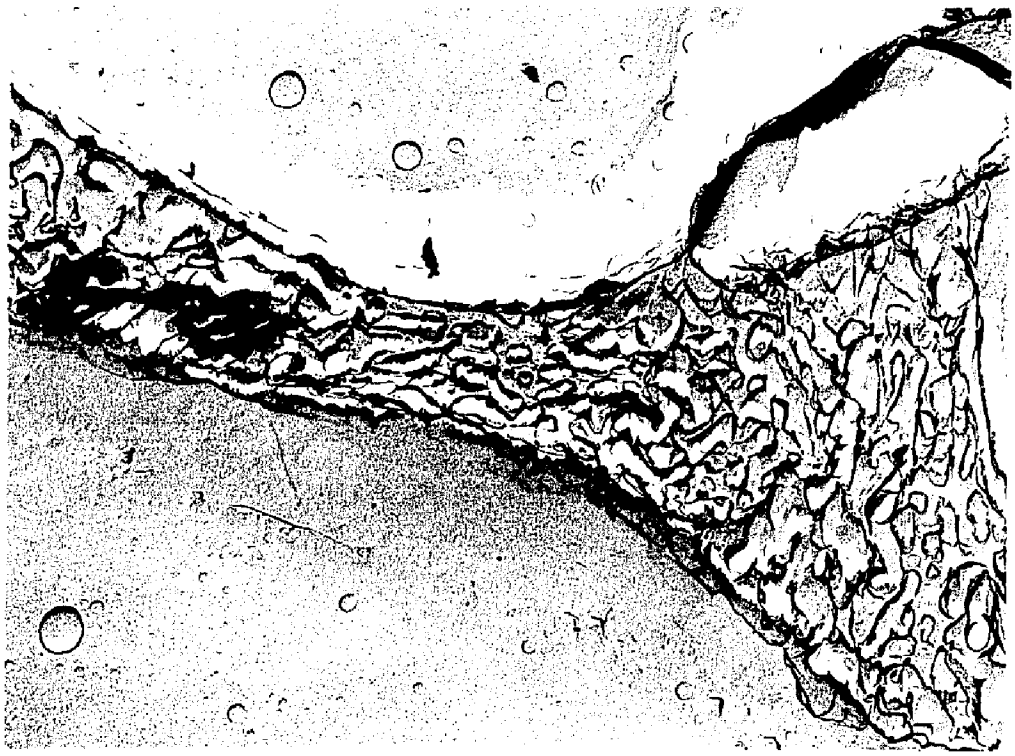

X10,000

Figure 47 Surface Replica showing the Mo_2C Eutectic in Specimen F2

(a) X18,000

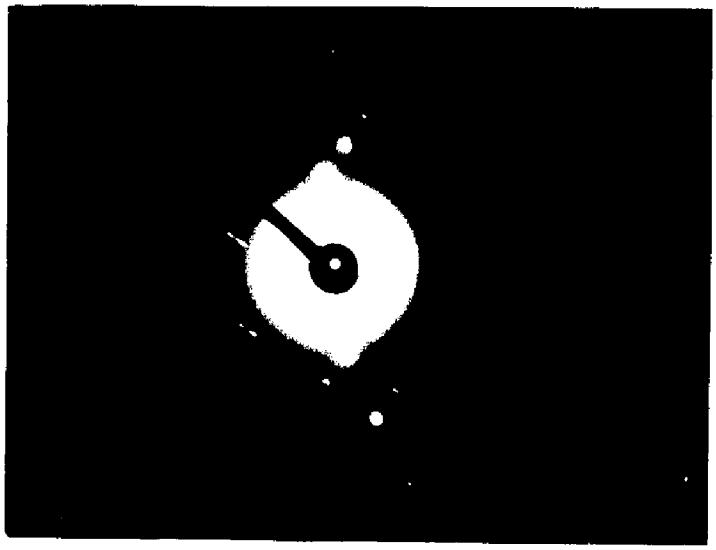

(b)

Figure 48 (a) Particle Extracted from the Surface of Specimen K2, (b) Diffraction Pattern of (a)

(a) X160

(b) X400

(c) X800

(d) X1600

Figure 49 Scanning Electron Images of the Abraded Surface of Specimen B-

(a) X400

(b) X2400

(c) X240

(d) X2400

Figure 50 Scanning Electron Images of the Abraded Surface of Specimen E-

(a) X160

(b) X800

(c) X1600

(d) X2400

Figure 51 Scanning Electron Images of the Abraded Surface of Specimen CV-

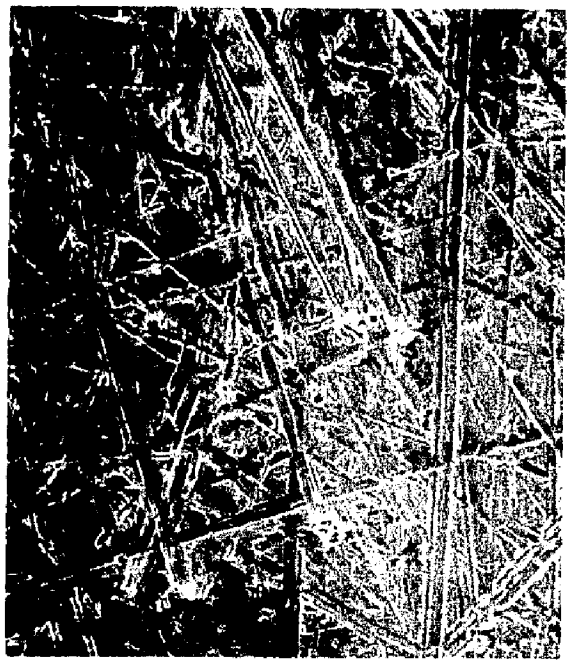

(a) X160

(b) X800

(c) X2400

(d) X4000

Figure 52 Scanning Electron Images of the Abraded Surface of Specimen IV-

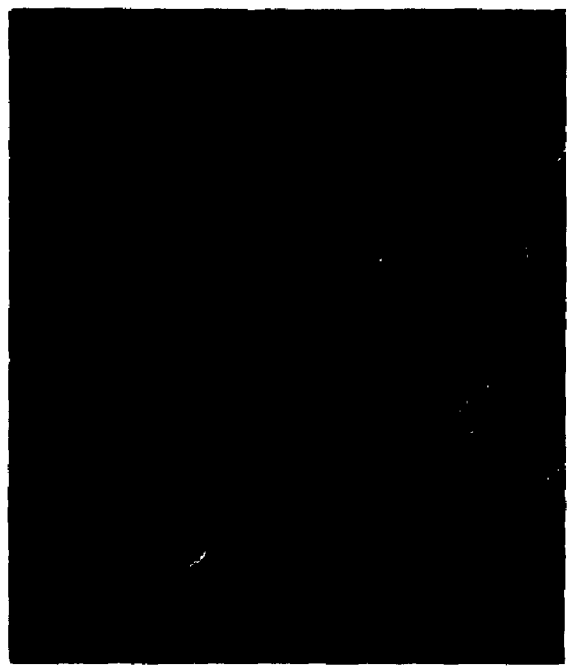

(a) X160

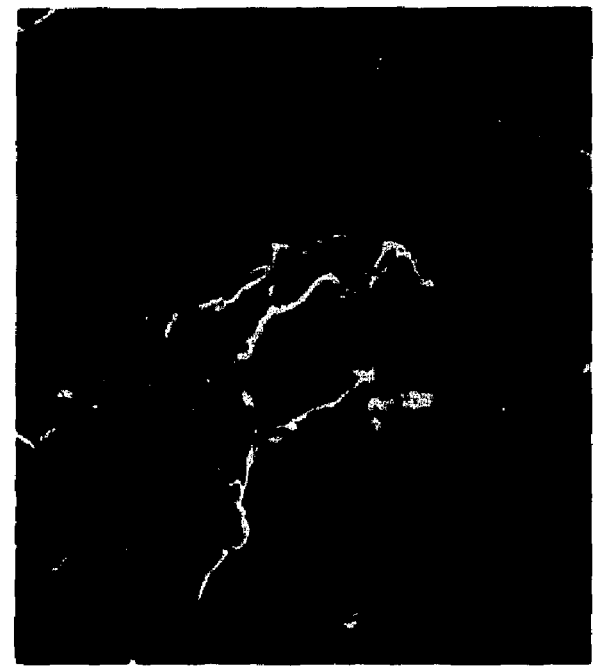

(b) X800

(c) X2400

Figure 53 Scanning Electron Images of the Abraded Surface of Specimen KV-

(a) X400

(b) X1600

(c) X2400

(d) X4000

Figure 54 Scanning Electron Images of the Abraded Surface of Specimen N-

(a) X160

(b) X800

(c) X2400

Figure 55 Scanning Electron Images of the Abraded Surface of Specimen P-

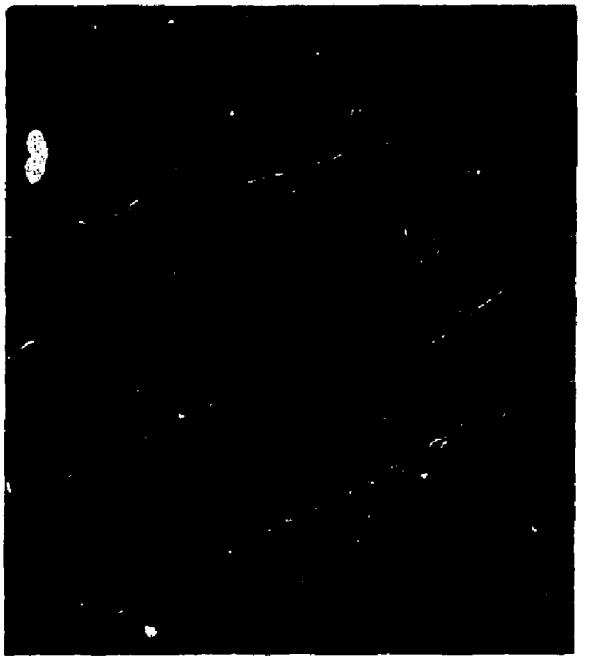

X160

Figure 56 Scanning Electron Image of the Abraded Surface of Specimen H2- after Light Removal of the Matrix

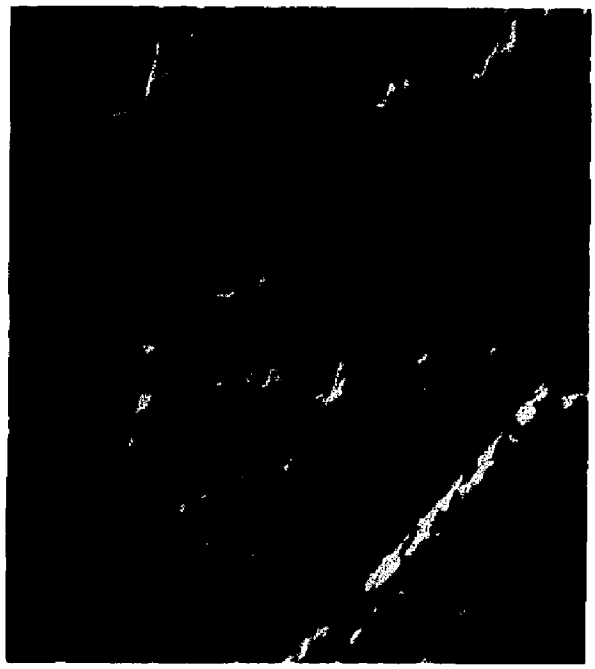

(a) X800

(b) X1600

(c) X800

(d) X2400

Figure 57 Scanning Electron Images of the Abraded Surface of Specimen FV-after Light Removal of the Matrix

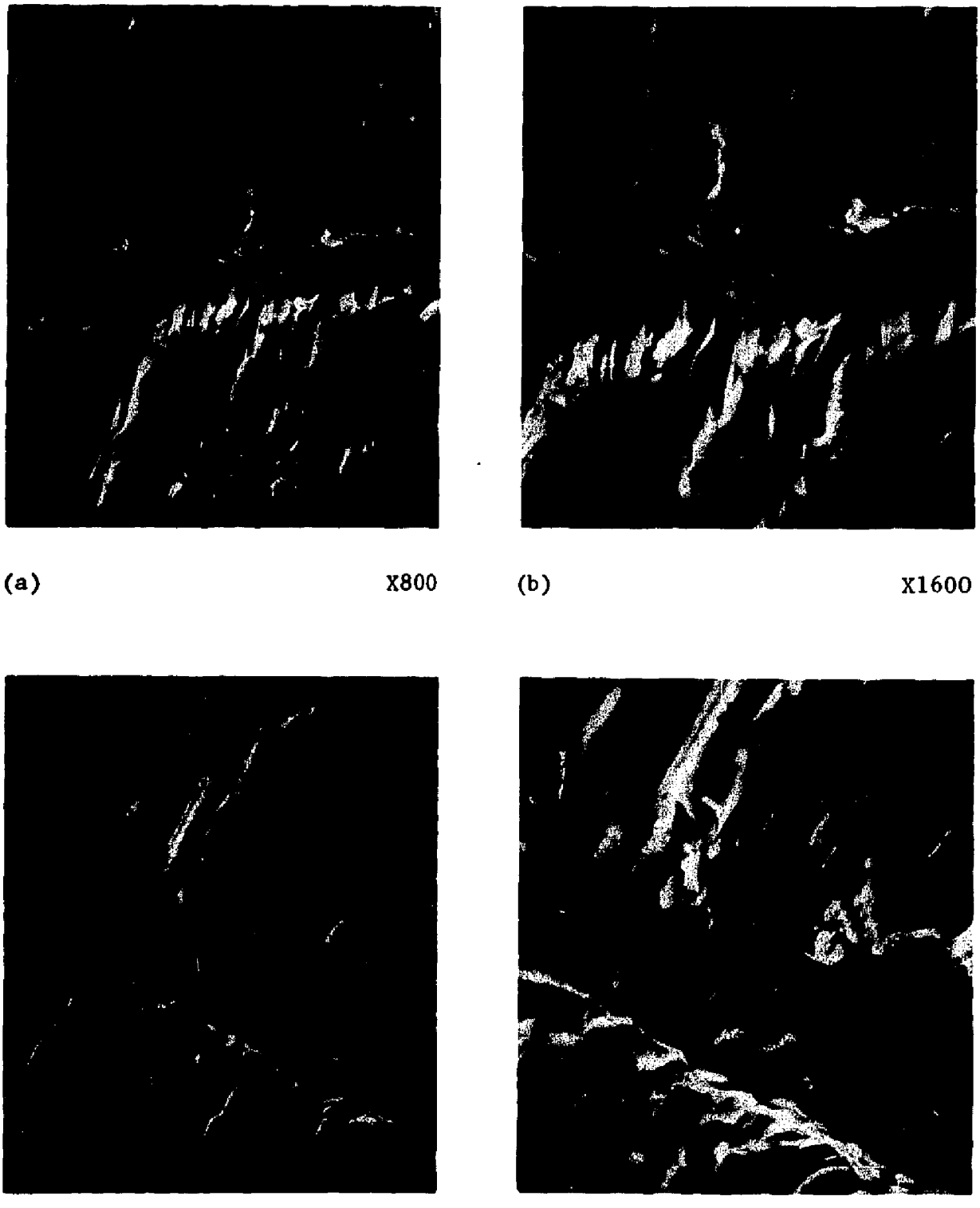

(a) X800 (b) X1600

(c) X800 (d) X1600

Figure 58 Scanning Electron Images of the Abraded Surface of Specimen J-after Light Removal of the Matrix

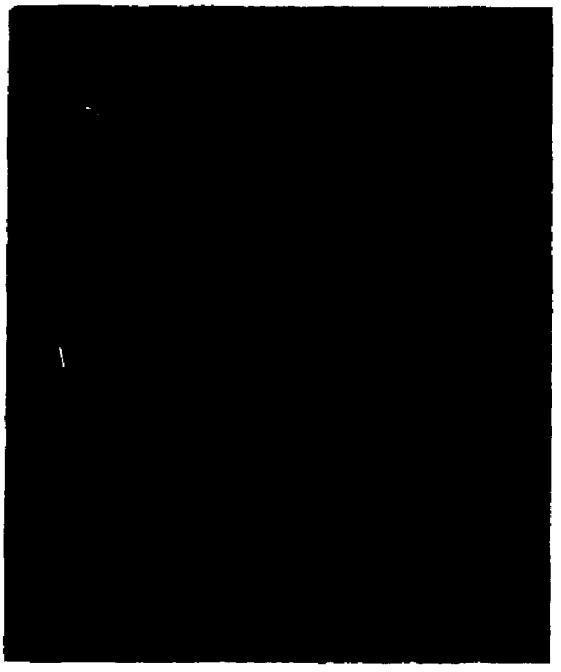

(a) X160

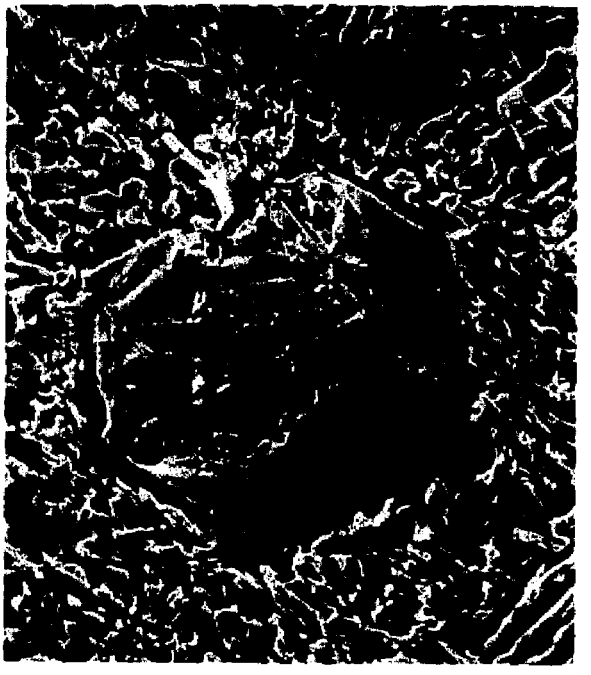

(b) X400

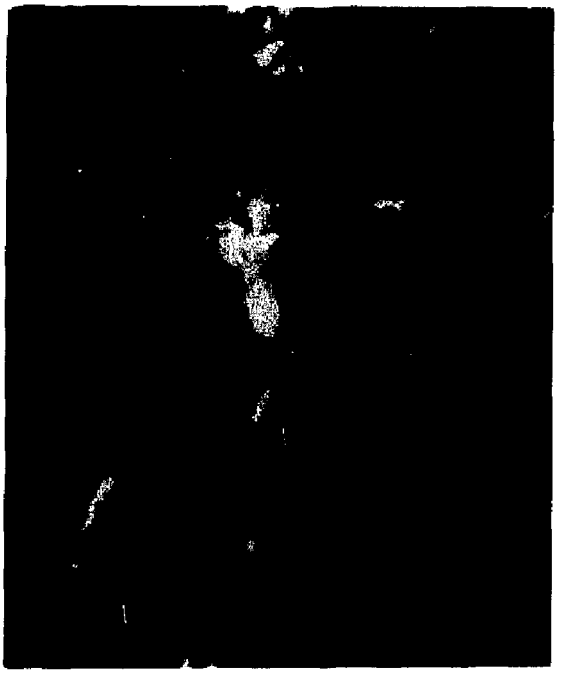

(c) X1600

(d) X160

Figure 59 Scanning Electron Images of the Abraded Surface of Specimen M-after Light Removal of the Matrix

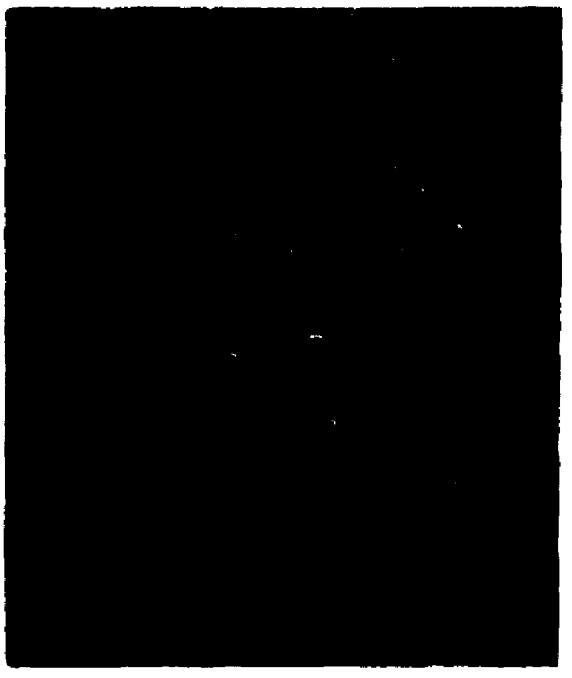

(a) X160

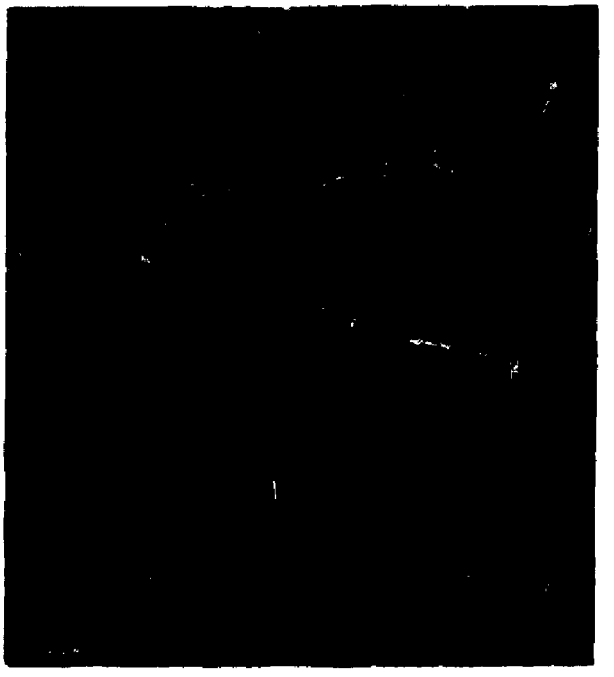

(b) X400

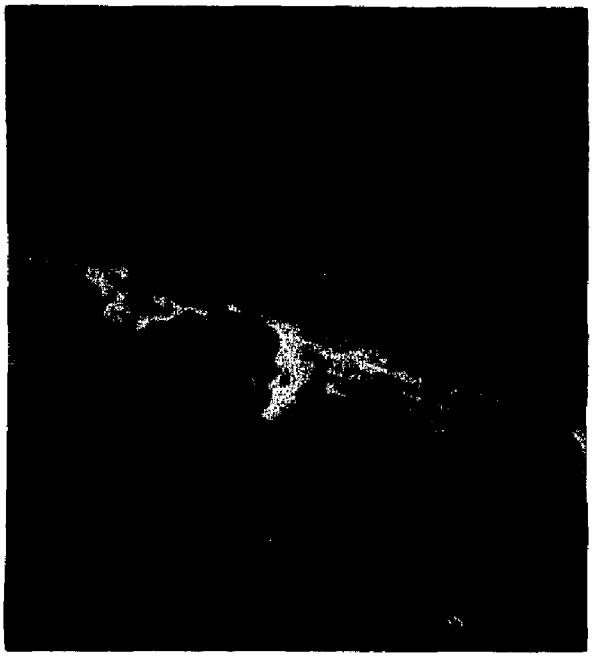

(c) X2400

Figure 60 Scanning Electron Images of the Abraded Surface of Specimen N-after Light Removal of the Matrix

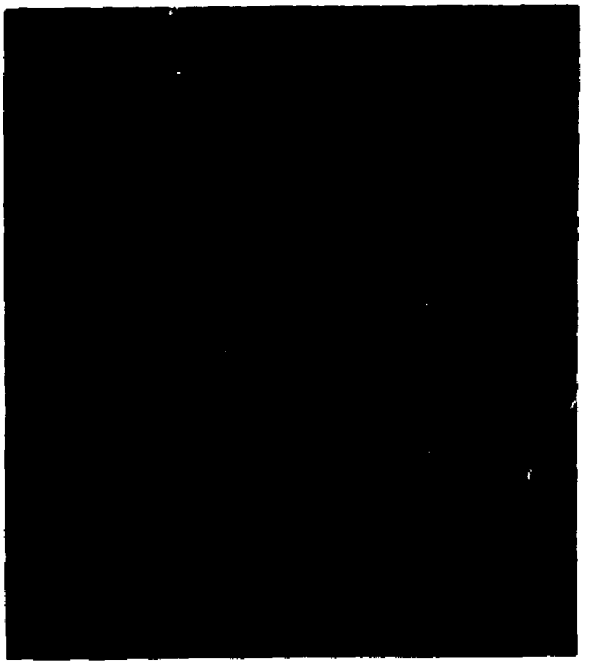

(d) X240

(e) X800

(f) X2400

Figure 60 [Continued]

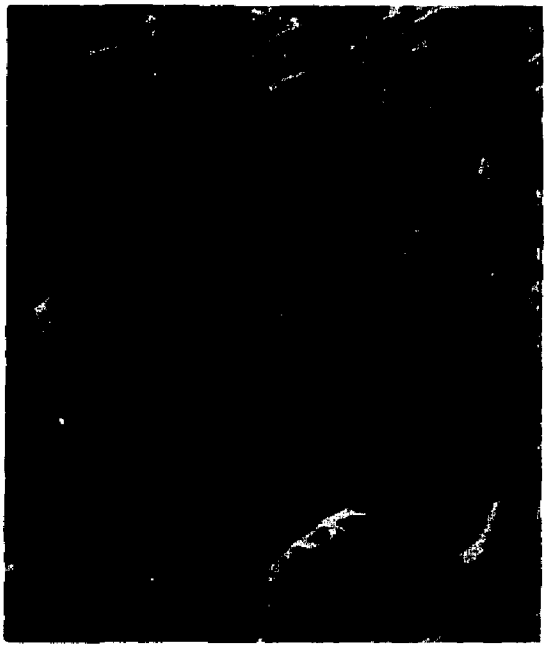

(a) X240

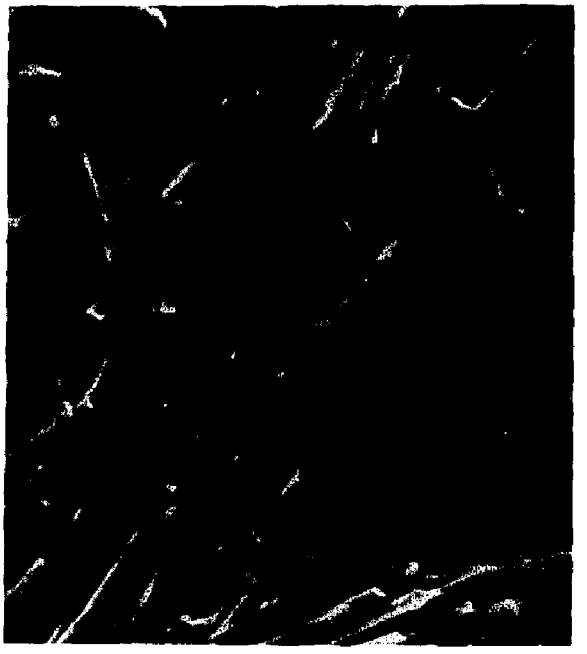

(b) X800

(c) X800

(d) X2400

Figure 61 Scanning Electron Images of Carbide Morphology in Specimen F-

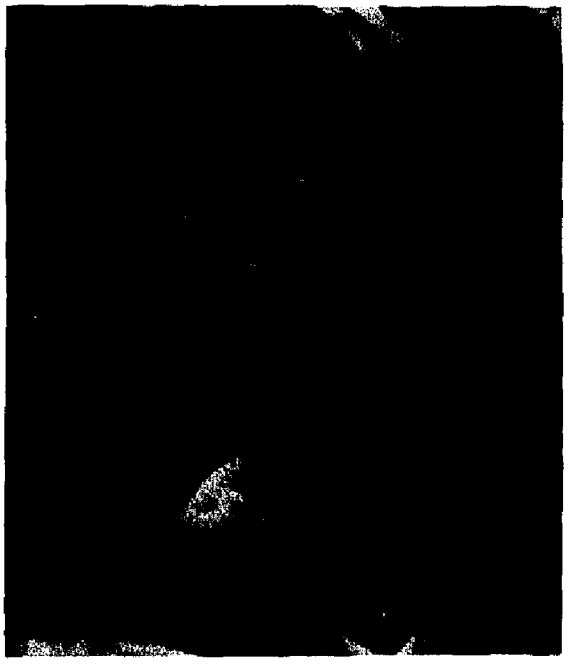

(a) X2400

(b) X4000

(c) X2400

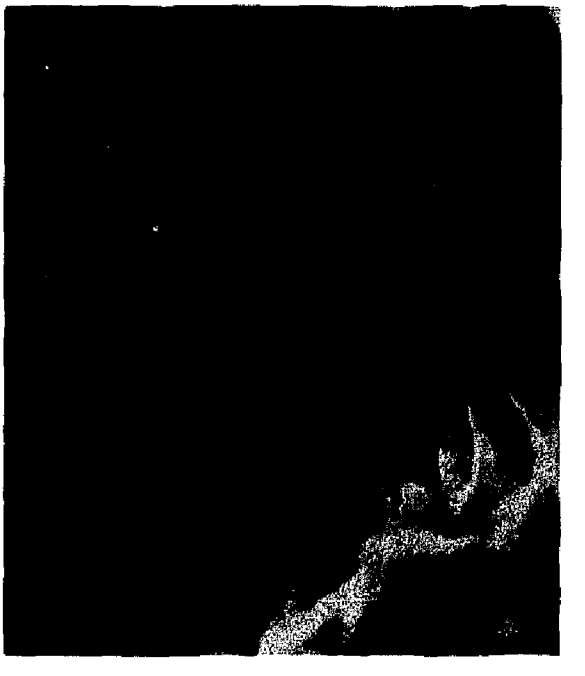

(d) X4000

Figure 62 Scanning Electron Images of Carbide Morphology in Specimen H-

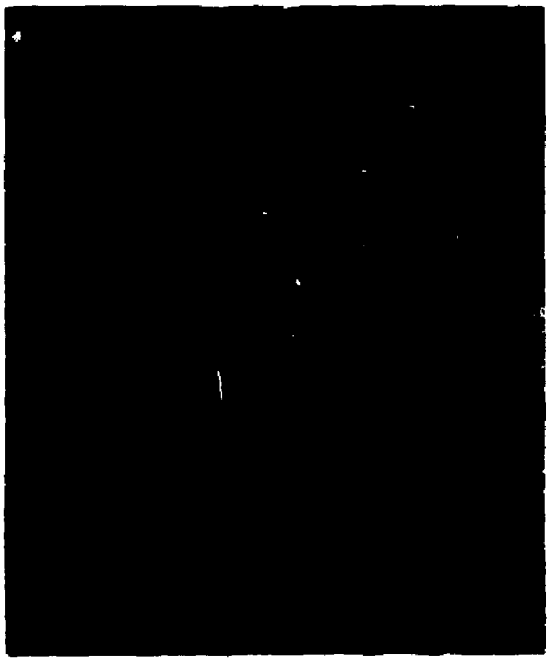

(a)

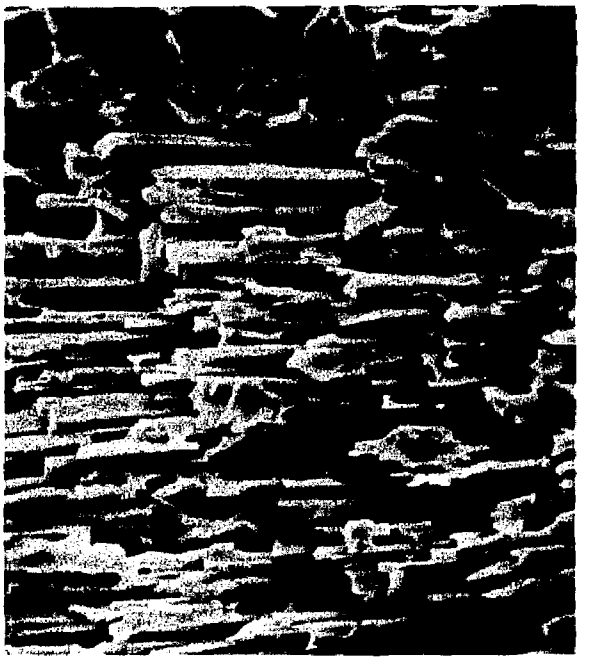

(b)

(c)

Figure 63 Scanning Electron Images of Carbide Morphology (a) and (b) Specimen KV- X160 and X800, Respectively, (c) Specimen BV- X1600

(a) X160

(b) X800

(c) X240

Figure 64 Scanning Electron Images of Carbide Morphology in Specimen O-

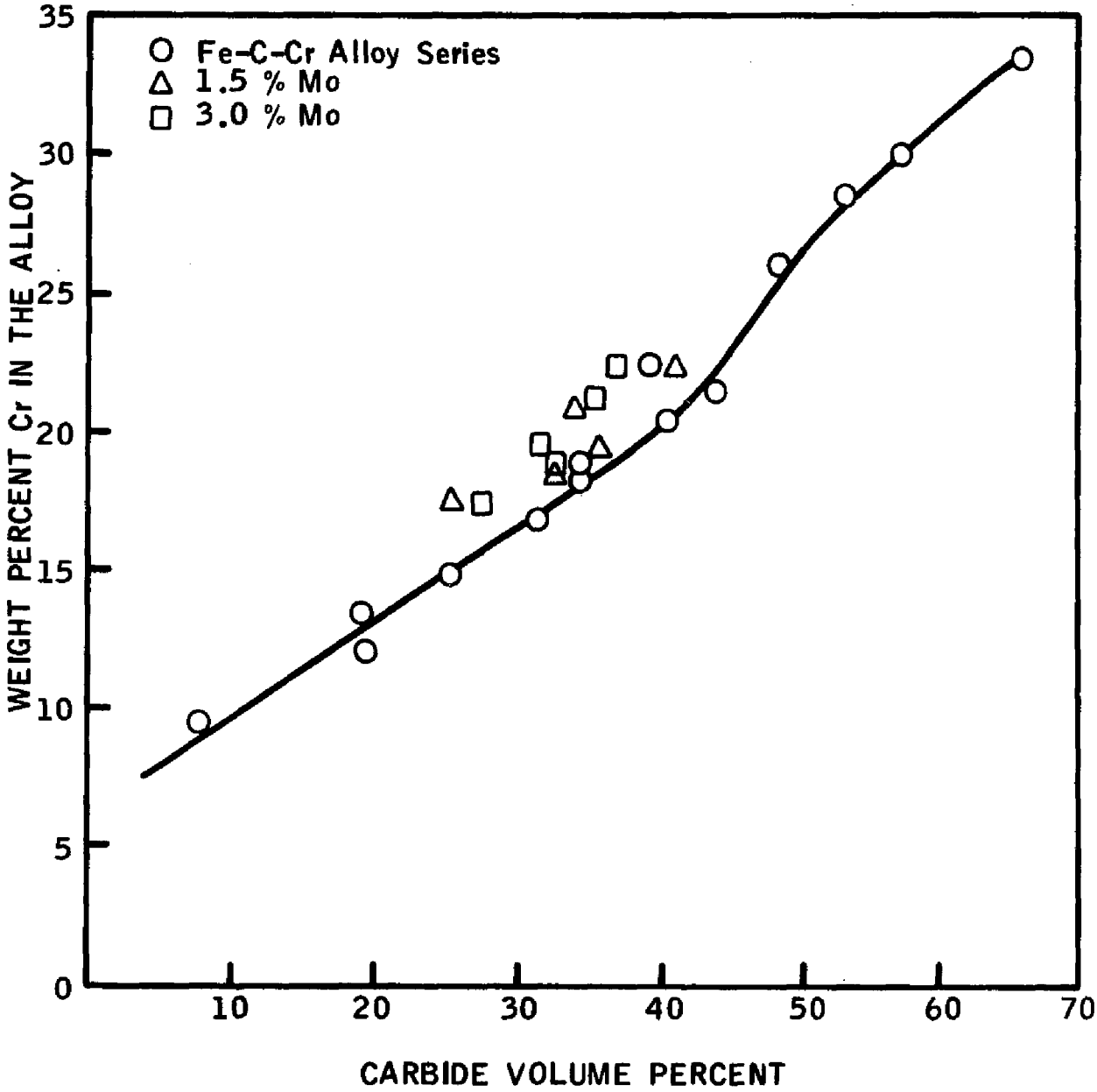

Figure 65 Carbide Volume as a Function of Total Chromium in Alloys with Cr:C of 6.64

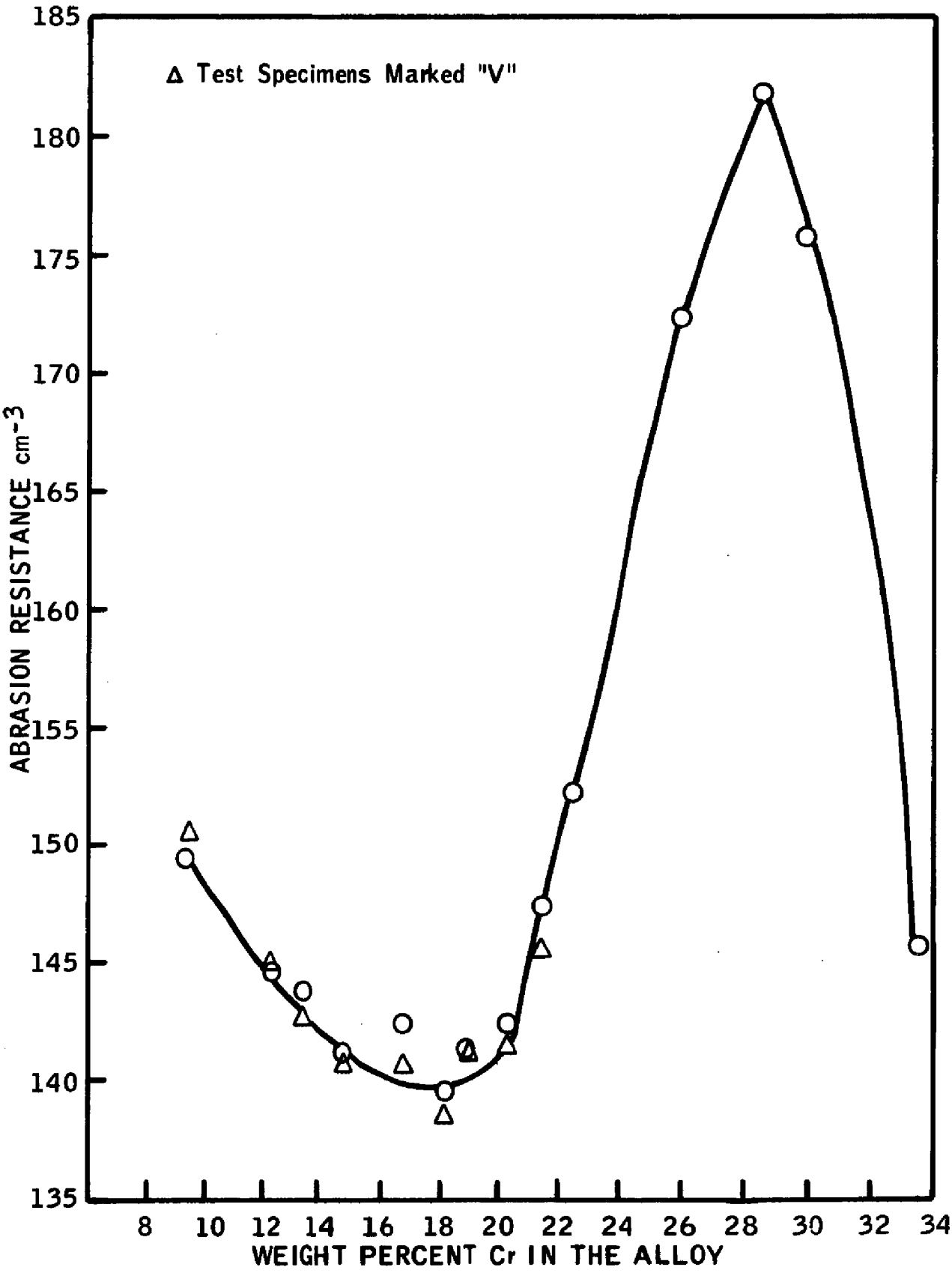

Figure 66 Abrasion Resistance as a Function of Total Cr Content in Alloys with Cr:C of 6.64

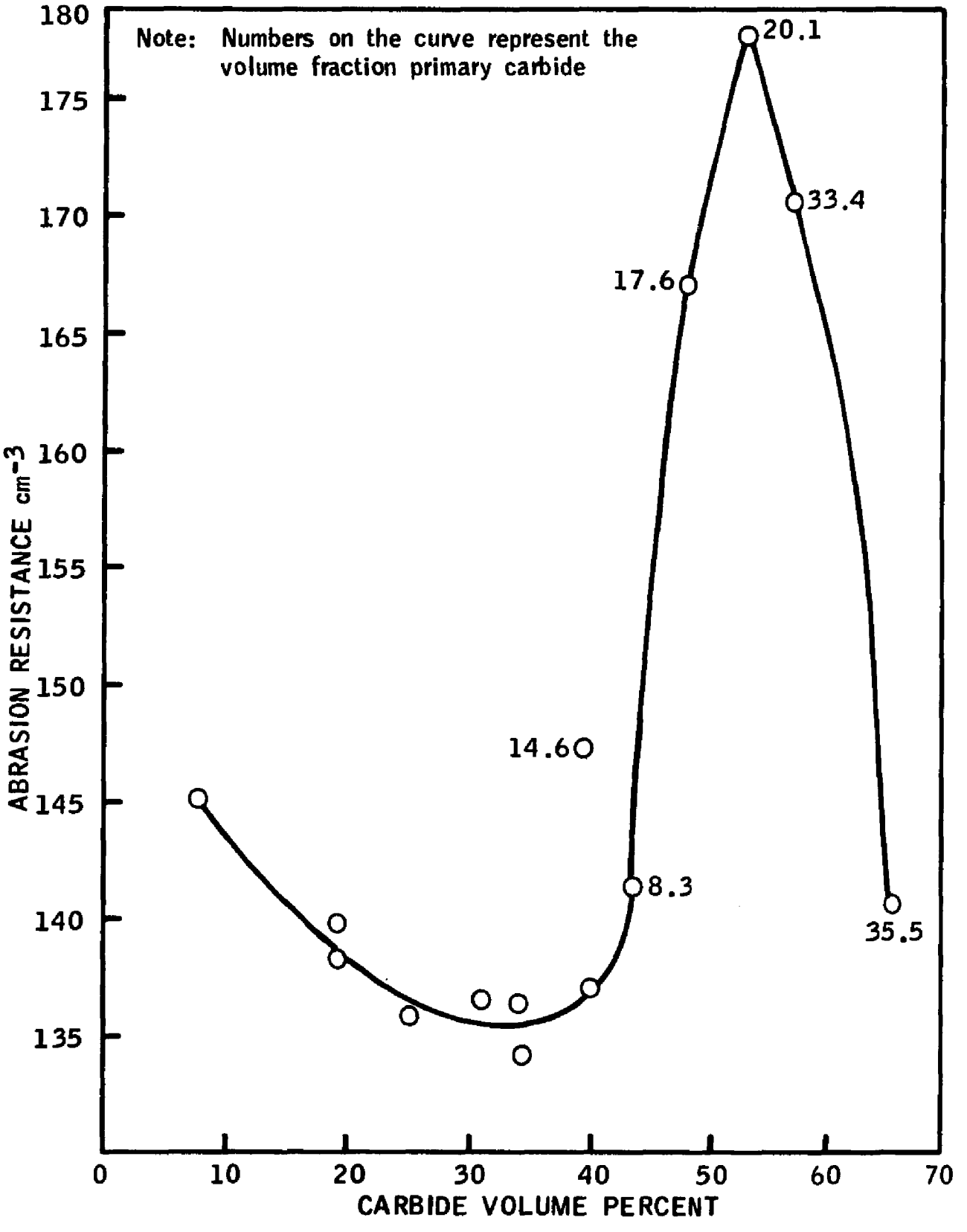

Figure 67 Abrasion Resistance as a Function of Carbide Volume

TABLES

Table 1

Alloys Used to Evaluate the Abrasion Testing Apparatus

Alloy Designation	Type of Alloy	Composition							Heat Treatment	Hardness on* Worn Ball Surface RC	Wear** Ratio
		C	Mn	Si	Cr	Mo	Ni	V			
AA	Martensitic high chromium white iron	3.0	0.68	0.44	19.71	1.39	0.67	--	1750 F/5 hr, Air-cooled; 400 F/4 hr	66.2	90
BB	Cr-Mo Steel	0.88	0.42	0.53	6.61	1.13	--	--	1875 F/3 hr, Air-cooled; 450 F/4 hr	63.0	100
CC	2Si - 1Mo Steel	0.24	0.68	1.90	--	0.92	--	0.086	1700 F/2 hr, 1540 F/1 hr, Water-quenched; 400 F/4+4	44.6	148
FF	Ni - Cr White Iron	3.4	0.5	0.5	2.1	--	4.2	--	As-cast; Tempered 450 F	61.9	108
GG	Pearlitic Cr-Mo Steel	0.8	0.7	0.5	2.1	0.3	--	--	Air-quenched and tempered	40.8	120
II	Austenitic Manganese Steel	1.1	13.0	0.7	--	--	--	--	1900 F; Water-quenched	51.0	136

* Rockwell C hardness on surface of ball after being tested in an ore grinding mill.
** Wear ratio determined after ball mill test using Alloy BB as a standard.

Table 2

Densities of the Alloys used to Evaluate the Abrasion Testing Apparatus

Alloy Designation	Density (g/cc)			
	Sample 1	Sample 2	Sample 3	Average
AA	7.524	7.618	7.608	7.583
BB	7.722	7.800	7.810	7.777
CC	7.792	7.629	7.752	7.724
FF	7.718	7.816	7.781	7.771
GG	7.689	7.818	--	7.753
II	7.78	7.77	7.77	7.77

Table 3

Statistical Results for the Alloys Tested on Different Abrasives of 105 μ Particle Size Under 7 lb Load*

Alloy Designation	Mean Weight Loss - $\bar{X}$ (g)			95% Confidence Limits of the Mean Expressed as a Percentage of the Mean (± %)			n**		
	Alumina	Silicon Carbide	Garnet	Alumina	Silicon Carbide	Garnet	Alumina	Silicon Carbide	Garnet
AA	0.02964	0.0447	0.01182	1.181	1.141	3.130	31	32	>128
BB	0.03792	0.0426	0.03698	1.108	1.197	1.622	28	34	82
CC	0.05568	0.0594	0.05720	1.365	1.515	1.573	42	52	76
FF	0.02946	0.0389	0.01966	0.713	0.900	1.526	13	20	72
GG	0.05233	0.0558	0.05038	1.127	1.667	3.315	18	35	>119
II	0.04588	0.0493	0.04586	0.763	0.791	2.115	16	17	>109

* The silicon carbide and alumina results are based on 9 tests, and those for garnet, on 12 tests.

** n is equal to the number of tests that would be required to locate the true population mean within ± 0.01 $\bar{X}$ of the calculated sample mean $\bar{X}$ with risks of 0.05 for α and 0.05 for β.

Table 4

Statistical Results for the Alloys Tested on 80 μ Particle Size Alumina Under the Given Loads*

Alloy Designation	Mean Weight Loss - $\bar{X}$ (g)			95% Confidence Limits of the Mean Expressed as a Percentage of the Mean (± %)			n**		
	3.5 lb	7 lb	15 lb	3.5 lb	7 lb	15 lb	3.5 lb	7 lb	15 lb
AA	0.01319	0.02465	0.04823	6.520	3.611	0.726	>128	68	6
BB	0.01953	0.03557	0.06876	4.096	2.671	0.509	93	39	4
CC	0.02898	0.05194	0.10296	3.278	1.097	0.680	58	9	5
FF	0.01402	0.02631	0.05154	4.565	0.380	0.931	109	3	7
II	0.02268	0.04170	0.08214	4.630	2.830	0.353	110	43	3

* Data based on four tests for each alloy under each loading condition.

** n is equal to the number of tests that would be required to locate the true population mean within ± $\bar{X}$ of the calculated sample mean $\bar{X}$ with risks of 0.05 for α and 0.05 for β.

Table 5

Statistical Results for the Alloys Tested on 105 μ Particle Size Alumina Under the Given Loads

Alloy Designation	Mean Weight Loss - $\bar{X}$ (g)		95% Confidence Limits of the Mean Expressed as a Percentage of the Mean (± %)		n*	
	3.5 lb**	7 lb***	3.5 lb	7 lb	3.5 lb	7 lb
AA	0.01524	0.02964	10.761	1.181	>128	31
BB	0.02092	0.03792	3.681	1.108	31	28
CC	0.03048	0.05568	0.984	1.365	5	42
FF	0.01597	0.02946	3.507	0.713	28	13
II	0.02465	0.04588	0.162	0.763	3	16

* n is equal to the number of tests that would be required to locate the true population mean within ± 0.01 $\bar{X}$ of the calculated sample mean $\bar{X}$ with risks of 0.05 for α and 0.05 for β.

** Each value based on 3 tests.

*** Each value based on 9 tests.

Table 6

Statistical Results for the Alloys Tested on 130 μ Particle Size Alumina Under the Given Loads

Alloy Designation	Mean Weight Loss - $\bar{X}$ (g)			95% Confidence Limits of the Mean Expressed as a Percentage of the Mean (± %)			n*		
	3.5 lb**	5 lb***	15 lb**	3.5 lb	5 lb	15 lb	3.5 lb	5 lb	15 lb
AA	0.01637	0.02292	0.06942	1.955	1.571	1.095	22	23	9
BB	0.02025	0.02787	0.07970	4.395	3.301	0.477	107	93	4
CC	0.03008	0.04238	0.11809	3.391	4.271	1.431	60	97	13
FF	0.01602	0.02225	0.06646	5.556	3.101	0.527	>119	99	4
II	0.02328	0.03314	0.09376	1.375	4.134	1.056	12	96	8

* n is equal to the number of tests that would be required to locate the true population mean within ± 0.01 $\bar{X}$ of the calculated sample mean $\bar{X}$ with risks of 0.05 for α and 0.05 for β.

** Each value based on 4 tests.

*** Values for Alloys AA, BB, and FF based on 5 tests and for Alloys CC and II on 4 tests.

Table 7

Statistical Results for the Alloys Tested on 200 μ Particle Size Alumina Under the Given Loads*

Alloy Designation	Mean Weight Loss - $\bar{X}$ (g)			95% Confidence Limits of the Mean Expressed as a Percentage of the Mean (± %)			n**		
	7 lb	15 lb	29.2 lb	7 lb	15 lb	9.2 lb	7 lb	15 lb	29.2 lb
AA	0.03613	0.07483	0.13283	0.886	1.483	0.956	7	13	7
BB	0.03858	0.08026	0.14525	1.477	1.184	0.792	15	10	6
CC	0.05752	0.12044	0.22430	1.321	1.079	1.248	12	8	10
FF	0.03407	0.06998	0.12778	2.231	0.357	1.119	28	3	9
II	0.04570	0.09384	0.17054	1.532	1.087	0.708	16	8	6

* Each value is based on 4 tests.

** n is equal to the number of tests that would be required to locate the true population mean within ± 0.01 $\bar{X}$ of the calculated sample mean $\bar{X}$ with risks of 0.05 for α and 0.05 for β.

Table 8

Mean Weight Losses and Ranking of Alloys Tested
on Alumina Abrasive and in the Ball Mill

Alloy Designation	Mean Weight Loss (g)			Ranking*		
	105 μ, 7 lb	80 μ, 15 lb	Ball Mill	105 μ, 7 lb	80 μ, 15 lb	Ball Mill
AA	0.02964	0.04823	404	2	1	1
BB	0.03792	0.06876	445	3	3	2
CC	0.05568	0.10296	634	5	5	5
FF	0.02946	0.05154	486	1	2	3
II	0.04588	0.08214	605	4	4	4

* The alloys are ranked 1 through 5; number 1 is the most abrasive resistant, number 5 is the least.

Table 9

Composition (Cr and C) and Heat-Treating Temperature of "Commercial-Type" Alloys Used in Microprobe Calibration Studies

Specimen No.	Weight Percent		Temperature °C
	Cr	C	
3	0.34	0.36	1300
4	0.35	0.35	1300
5	0.34	0.35	1300
6	0.34	0.34	1300
7	0.74	0.37	1300
10	0.73	0.37	1300
11	1.54	0.36	1300
14	1.51	0.35	1300
19	2.16	0.0045	1300
21	2.27	0.010	1300
24	3.18	0.38	1300
25	3.14	1.03	1200
26	3.99	0.80	1200
27	3.98	1.14	1200
28	5.31	0.97	1200
30	5.36	0.0011	1200
34	7.82	0.97	1200
35	8.64	0.99	1225
39	13.68	0.003	1250
40	13.14	0.005	1250
41	13.60	0.002	1250
42	12.94	0.003	1250
43	13.04	0.003	1250
44	17.35	0.002	1250
45	17.53	0.003	1250
46	17.61	0.004	1250
47	17.58	0.005	1250
48	17.38	0.004	1250
50	25.26	0.002	1250
51	25.25	0.002	1250
52	25.58	0.002	1250
53	39.76	0.008	1250
54	66.70	0.049	1250
54'	73.70	0.049	1250

Table 10

Compositions in Weight Percent of the Alloys Tested in High Stress Abrasion

Alloy Designation	C	Cr	Mn	Si	Mo	Cr/C
B	1.40	9.44	0.39	0.55	--	6.74
C	1.86	12.30	0.40	0.57	--	6.61
D	2.00	13.46	0.41	0.54	--	6.73
E	2.25	14.82	0.41	0.53	--	6.59
F	2.54	16.78	0.40	0.53	--	6.61
G	2.70	18.20	0.41	0.55	--	6.74
H	2.84	18.98	0.40	0.53	--	6.68
I	3.11	20.39	0.39	0.57	--	6.56
J	3.09	22.78	0.41	0.53	--	7.37
K	3.26	21.49	0.39	0.52	--	6.59
L	3.38	22.49	0.42	0.51	--	6.65
M	3.98	25.98	0.42	0.58	--	6.53
N	4.25	28.57	0.41	0.58	--	6.72
O	4.54	29.96	0.42	0.55	--	6.60
P	5.07	33.56	0.42	0.60	--	6.62
F1	2.53	17.42	0.39	0.56	1.41	6.89
F2	2.50	17.48	0.38	0.54	2.88	6.99
G1	2.65	18.46	0.40	0.57	1.42	6.97
G2	2.72	18.63	0.37	0.57	2.86	6.85
H1	2.82	19.34	0.40	0.54	1.42	6.86
H2	2.79	19.38	0.36	0.54	2.92	6.95
I1	3.00	20.80	0.40	0.58	1.44	6.93
I2	3.01	21.03	0.36	0.56	2.97	6.99
J1	3.06	23.14	0.40	0.56	1.44	7.56
J2	3.06	22.96	0.36	0.53	2.96	7.50
K1	3.26	22.10	0.40	0.55	1.42	6.78
K2	3.23	22.16	0.38	0.55	2.90	6.86

Table 11

Densities in g/cc of the Alloys Tested in High Stress Abrasion

Alloy Designation	X*	X-	XV	XV-	Average of X'S Alloy Density
B	7.81100	7.81150	7.81055	7.81045	7.81095
C	7.76135	--	7.76038	7.76005	7.76059
D	7.73646	7.73717	7.73557	--	7.73640
E	7.70849	--	7.71062	7.72233	7.71381
F	--	7.67629	7.67689	--	7.67659
G	7.65649	7.65309	7.65034	7.65699	7.65423
H	7.64205	7.64427	7.64383	7.64801	7.64454
I	7.62063	7.61814	7.62101	7.61818	7.61950
J	--	7.59825	7.60361	7.60077	7.60088
K	7.60791	--	7.61211	7.61352	7.61118
L	7.59856	7.59950	NS**	NS	7.59903
M	7.54482	7.54427	NS	NS	7.54455
N	7.51889	7.51302	NS	NS	7.51596
O	7.49008	--	NS	NS	7.49008
P	7.42966	7.42741	NS	NS	7.42854
F1	7.69929	7.69588	7.69454	7.69834	7.69702
F2	7.71838	7.71760	7.72011	7.71733	7.71836
G1	7.67605	7.67739	7.67427	--	7.67590
G2	7.70315	7.69763	7.69398	7.69889	7.69842
H1	7.66873	7.65866	7.66518	7.66331	7.66398
H2	7.67644	7.68678	--	7.68647	7.68323
I1	7.64156	7.64276	7.63877	7.63823	7.64033
I2	--	7.66032	7.66211	7.66092	7.66112
J1	--	7.62292	7.61769	7.61675	7.61912
J2	7.64450	7.64530	7.64671	7.64753	7.64601
K1	7.62097	--	7.61983	7.61931	7.62004
K2	7.64724	7.64853	7.65043	7.65339	7.64990

* X represents alloy letter

** No specimen was available since these alloys were not tested in the "V" direction

Table 12

High Stress Abrasion Test Results

Alloy Designation	Mean Weight Loss (g)	95% Confidence Limits of the Mean Weight Loss, ±g	Mean Volume Loss $cm^3 \times 10^3$	Abrasion Resistance "AR", cm^{-3}
B	0.05222	0.00035	6.6855	149.58
BV	0.05190	0.00024	6.6445	150.50
C	0.05366	0.00035	6.9144	144.63
CV	0.05353	0.00035	6.8977	144.98
D	0.05378	0.00050	6.9516	143.85
DV	0.05424	0.00040	7.0110	142.63
E	0.05468	0.00066	7.0886	141.07
EV	0.05480	0.00033	7.1041	140.76
F	0.05388	0.00038	7.0187	142.47
FV	0.05453	0.00033	7.1034	140.78
G	0.05480	0.00052	7.1594	139.68
GV	0.05530	0.00031	7.2248	138.41
H	0.05407	0.00028	7.0730	141.38
HV	0.05412	0.00033	7.0796	141.25
I	0.05353	0.00021	7.0254	142.34
IV	0.05380	0.00043	7.0608	141.63
J	0.05422	0.00028	7.1334	140.02
JV	0.05543	0.00047	7.2926	137.13
K	0.05157	0.00035	6.7756	147.59
KV	0.05225	0.00035	6.8649	145.69
L	0.04992	0.00026	6.5693	152.22
M	0.04382	0.00033	5.8082	172.17
N	0.04131	0.00078	5.4963	181.94
O	0.04262	0.00064	5.6902	175.74
P	0.05097	0.00166	6.8614	145.74
F1	0.05307	0.00045	6.8949	145.03
F1V	0.05256	0.00035	6.8286	146.44
F2	0.05139	0.00040	6.6582	150.19
F2V	0.05227	0.00028	6.7722	147.66
G1	0.05272	0.00021	6.8682	145.60
G1V	0.05237	0.00033	6.8227	146.57
G2	0.05168	0.00019	6.7131	148.96
G2V	0.05141	0.00052	6.6780	149.75
H1	0.05118	0.00019	6.6780	149.75
H1V	0.05118	0.00033	6.6780	149.75
H2	0.05126	0.00040	6.6717	149.89
H2V	0.05187	0.00031	6.7511	148.12
I1	0.05111	0.00033	6.6895	149.49
I1V	0.05193	0.00031	6.7968	147.13
I2	0.05028	0.00039	6.5630	152.37
I2V	0.05092	0.00031	6.6465	150.46

Table 12 (Continued)

Alloy Designation	Mean Weight Loss (g)	95% Confidence Limits of the Mean Weight Loss, ±g	Mean Volume Loss $cm^3 \times 10^3$	Abrasion Resistance "AR", cm^{-3}
J1	0.05198	0.00035	6.8203	146.58
J1V	0.05240	0.00033	6.8774	145.40
J2	0.05150	0.00033	6.7355	148.47
J2V	0.05174	0.00033	6.7669	147.78
K1	0.04919	0.00043	6.4553	154.91
K1V	0.05081	0.00050	6.6679	149.97
K2	0.04792	0.00031	6.2641	159.64
K2V	0.04852	0.00073	6.3426	157.66

Table 13

Vickers Hardness Numbers* of Alloys Tested in High Stress Abrasion

Alloy Designation	VHN Non-Abraded	VHN Abraded
B	339	367
C	386	444
D	420	475
E	461	506
F	535	601
G	559	605
H	571	638
I	602	684
J	592	707
K	613	710
L	586	702
M	613	699
N	655	839
O	604	773
P	667	649
F1	520	561
F2	518	565
G1	546	595
G2	552	610
H1	540	596
H2	567	662
I1	574	615
I2	601	693
J1	588	664
J2	612	627
K1	623	689
K2	585	653

* VHN determined under 10-kg loading.

Table 14

Vickers Microhardness, 20-g Load, of Microconstituents in the Alloys Tested in High Stress Abrasion

Alloy Designation	VHN of the Austenite	VHN of the Carbides
B	314 (87)*	1172 (45)
C	353 (82)	1345 (42)
D	371 (80)	1561 (39)
E	371 (80)	1412 (41)
F	371 (80)	1735 (37)
G	390 (78)	1122 (46)
H	362 (81)	1735 (37)
IV	400 (77)	1831 (36)
J	380 (79)	1560 (39)
KV	434 (74)	2054 (34)
L	400 (77)	1831 (36)
M	411 (76)	1937 (35)
N	380 (79)	1831 (36)
O	411 (76)	1937 (35)
P	434 (74)	1937 (35)
G1	362 (81)	1735 (37)
G2	353 (82)	1735 (37)
I1	380 (79)	1937 (35)
I2V	362 (81)	1664 (38)
K1	380 (79)	1937 (35)
K2	390 (78)	1831 (36)

* Numbers in parentheses designate the average lengths of all the identation diagonals in filar units at 800X.

Table 15

Alloy Compositions for Microprobe Calibration Curve of the Fe-Cr System

Specimen No.	Cr	Fe	C	Mn	Si	Mo	Other	K_{Cr}	K_{Fe}
	"Commercial-Type" Alloys								
3	0.34	97.96	0.36	0.83	0.38	0.01		0.499	98.239
7	0.74	97.52	0.37	0.85	0.37	0.02		1.001	98.256
11	1.54	96.74	0.36	0.86	0.37	0.01		2.012	96.844
34	7.82	90.17	0.97	0.43	0.61	-		10.115	89.776
39	13.68	86.23	0.003	-	-	0.08		17.342	84.313
44	17.35	82.63	0.002	-	-	0.01		21.832	80.511
53	39.76	59.64	0.008	-	0.33	-		45.087	56.547
54	66.7	32.38	0.049	0.39	0.48	-		73.140	25.049
54'	73.7	25.38	0.049	0.39	0.48	-		78.905	21.308
	"Pure" Fe-Cr Alloys								
1P	4.38	95.62						6.007	94.956
2P	10.21	89.79						13.141	88.079
3P	23.78	76.22						28.533	72.706
4P	36.40	63.60						41.989	60.160
5P	58.32	41.68						63.068	37.912
6P	66.96	33.04						70.479	29.598
7P	79.81	20.19						84.260	16.571
8P	80.79	19.21						84.316	16.065
	Carbides								
1C	34.81	49.66					4.38W	37.383	46.058
3C	50.09	38.40					0.74W	51.559	34.836
4C	64.23	25.98					0.03W	64.843	22.442

Table 16

Alloys Utilized for the Study of the Effect of Mo on the Microprobe Calibration for Cr in the Fe-Cr Base System

Specimen No.	Cr	Fe	C	Mo	other	K_{Cr}
	Fe-Cr Alloys with Approximately 1 Weight Percent Mo					
6	0.34	97.23	0.34	0.78		0.46381
10	0.73	96.83	0.37	0.76		1.0168
14	1.51	95.99	0.35	0.84		2.0144
21	2.27	95.87	0.01	1.00		2.9984
28	5.31	91.37	0.97	1.15	0.27V	6.7509
35	9.64	87.20	0.99	1.20		12.581
40	13.14	85.81	0.005	1.04		16.801
45	17.53	81.32	0.004	1.14		21.972
	Fe-Cr Alloys with Approximately 2 Weight Percent Mo					
19	2.16	93.83	0.0045	1.53	0.23V	2.6890
25	3.14	90.82	1.03	2.21	1.26V	4.2362
27	3.98	88.88	1.14	2.46	1.12V	5.2559
41	13.60	84.51	0.002	1.88		17.048
46	17.61	80.36	0.004	2.02		21.554
	Fe-Cr Alloys with Approximately 3.5 Weight Percent Mo					
30	5.36	87.25	0.0011	2.96	2.07 Ni, 2.06 Mn	6.7047
42	12.94	83.57	0.003	3.48		16.968
47	17.58	78.89	0.005	3.52		21.468
	Fe-Cr Alloys with Approximately 5 Weight Percent Mo					
26	3.99	89.56	0.80	4.18	1.02V	5.3543
43	13.04	82.18	0.003	4.77		16.834
48	17.38	77.86	0.004	4.75		21.081

Table 17

Alloys Utilized for the Study of the Effect of Cr on the Microprobe Calibration for MO in the Fe-Cr Base System

Specimen No.	Cr	Fe	C	Mo	Other	K_{MO}
	Molybdenum Containing Fe-Cr Alloys with Less than 4 Weight Percent Cr					
4	0.35	97.71	0.35	0.24		0.19254
5	0.34	97.49	0.35	0.51		0.43476
14	1.51	95.99	0.35	0.84		0.62964
21	2.27	95.87	0.01	1.00		0.69198
19	2.16	93.83	0.0045	1.53	0.23V	1.1658
24	3.18	91.93	0.38	2.59	0.39V	1.9575
26	3.99	89.56	0.80	4.18	1.02V	3.1918
	Molybdenum Containing Fe-Cr Alloys with Approximately 13 Weight Percent Cr					
39	13.68	86.23	0.003	0.08		0.068319
40	13.14	85.81	0.005	1.04		0.80119
41	13.60	84.51	0.002	1.88		1.5465
42	12.94	83.57	0.003	3.48		2.8259
43	13.04	82.18	0.003	4.77		3.8507
	Molybdenum Containing Fe-Cr Alloys with Approximately 17.5 Weight Percent Cr					
45	17.53	81.32	0.004	1.14		0.86330
46	17.61	80.36	0.004	2.02		1.6521
47	17.58	78.89	0.005	3.52		2.8942
48	17.38	77.86	0.004	4.75		3.8258
	Molybdenum Containing Fe-Cr Alloys with Approximately 25 Weight Percent Cr					
50	25.26	72.51	0.002	2.05		1.6086
52	25.58	70.76	0.002	3.49		2.8632
51	25.25	69.33	0.002	5.24		4.2792

Table 18

Microprobe Background Counts of Alloys Based on 100 Seconds Counting Time, 1.25×10^{7} Amperes Beam Current, and 20 kv Excitation Voltage

Specimen No.	Weight Percent		Background Counts*		
	Cr	Mo	Cr	Fe	Mo
11	1.54	0.01	1290; 1340	2620	740
14	1.51	0.84	1240; 1300	2680	750
39	13.68	0.08	1400; 1380	2560	720
40	13.14	1.04	1360; 1340	2490	710
41	13.60	1.88	1340; 1340	2510	770
3P	23.78	--	1420; 1400	2460	680
50	25.26	2.05	1350; 1380	2420	700
51	25.25	5.24	1420; 1440	2420	760
52	25.58	3.49	1360; 1360	2480	690
53	39.76	--	1480	2270	--
1C	34.81	--	1490	2230	--
3C	50.09	--	1390	2100	--
4C	64.23	--	1430	1860	--
Pure Cr	100	--	1760	1740	--
Pure Fe	--	--	1260	2760	--
Pure Mo	--	100	--	--	1815

* If more than one number appears per column, then the determinations were made on different occasions.

Table 19

Average Composition of the Matrix and Carbide Phase of the Alloys Tested in High Stress Abrasions

Alloy Designation	Compositions in Weight Percent								
	Matrix			Eutectic Carbide			Primary Carbide		
	Cr	Fe	Mo	Cr	Fe	Mo	Cr	Fe	Mo
B	7.75	89.43		44.60	46.88				
C	9.43	88.23		43.93	47.70				
D	9.75	87.50		46.85	44.20				
E	10.78	87.59		47.80	44.58				
F	11.75	86.63		49.18	43.43				
G	12.25	85.13		50.70	41.69				
H	12.35	85.55		50.93	41.03				
I	12.83	84.63		52.88	39.50				
J	14.25	84.05		56.50	36.63				
K	12.48	85.80		52.80	40.25		56.28	37.50	
L	12.00	86.13		52.23	40.38		58.30	35.20	
M	11.45	85.73		53.25	38.70		56.75	35.15	
N	11.85	87.20		53.85	39.63		58.90	35.25	
O	11.87	85.85		54.75	38.15		61.85	31.70	
P	11.00	88.20		52.50	40.33		59.00	34.70	
F1	11.69	85.88	0.731	49.06	41.30	2.96			
F2	11.69	85.39	1.27	49.14	39.33	4.78			
G1	12.29	84.55	0.731	50.50	40.13	2.55			
G2	12.06	84.00	1.30	50.03	38.60	4.40			
H1	12.35	85.73	0.745	50.45	38.84	1.96			
H2	12.50	84.20	1.21	50.73	38.05	3.99			
I1	12.69	84.48	0.714	53.07	38.50	1.57			
I2	12.59	84.33	1.24	52.98	37.30	3.34			
J1	14.35	82.78	0.663	57.83	35.25	1.55			
J2	14.09	83.70	1.22	55.33	35.09	4.17			
K1	12.35	85.88	0.738	53.51	36.97	1.41	56.23	35.88	1.11
K2	12.21	83.83	1.50	53.43	36.98	2.66	56.13	--	2.19

Table 20

Quantitative Metallography Results of Carbide Morphology

Alloy Design.	Percent of Each Type of Eutectic Carbide Morphology			PC†	Magnification††
	LE*	RE**	XE***		
C	27.72	56.79	15.49		400 x
CV	0	68.08	31.92		400 x
D	11.48	70.73	17.80		400 x
DV	5.42	84.07	10.51		400 x
E	48.13	20.22	31.65		400 x
EV	3.57	67.78	28.65		400 x
F	40.42	44.43	15.16		400 x
FV	4.23	47.91	47.86		400 x
G	45.82	33.80	20.38		400 x
GV	53.58	36.18	10.24		400 x
H	31.71	50.08	18.21		400 x
HV	34.72	45.22	20.05		400 x
I	40.89	43.95	15.16		400 x
IV	31.43	38.40	30.17		400 x
J	52.41	27.41	20.18		400 x
JV	50.54	17.24	32.22		400 x
K	33.22	4.17	62.61	8.30	300 x
KV	49.46	10.72	39.82	8.30	300 x
L	41.54	31.16	27.30	14.60	400 x
M	45.76	22.44	31.79	17.56	300 x
N	52.48	17.06	30.46	20.11	300 x
O	21.24	25.23	53.54	33.41	300 x
P	13.27	24.49	62.24	35.51	300 x
G1	9.80	63.46	26.74		400 x
G1V	0.82	54.58	44.61		400 x
G2	8.62	57.99	33.39		400 x
G2V	0.96	59.16	39.87		400 x
I1	33.44	40.00	26.56		400 x
I1V	6.37	60.34	33.29		400 x
I2	47.98	39.65	12.37		400 x
I2V	12.11	50.00	37.89		400 x
K1	37.03	26.80	36.17	9.26	400 x
K1V	24.47	4.21	71.32	4.66	400 x
K2	68.24	1.86	29.90	11.19	400 x
K2V	2.18	14.00	83.82	9.77	400 x

* LE = Lamellar Eutectic Carbide.
** RE = Radiating Eutectic Carbide.
*** XE = Eutectic Carbide Rod in transverse cross section.
† PC is the absolute percent of primary carbide in the alloy.
†† Magnification at which point counts were performed.

Table 21

Quantitative Metallography Results Obtained from the Quatimet Analysis and from Point Counting*

Alloy Design	Inter	SI	End Count	SEC	Area	SA	AFR	APS	ROC	Shape	SPV	GS	FL	FR	FX	FP
B	3067	110	225	9	34991	130	.0700	155.52	0.29	11.41	.0061	163	--	--	--	0
BV	2805	105	190	9	42066	159	.0841	221.40	0.27	15.00	.0056	178	--	--	--	0
C	4956	114	216	9	85798	208	.1716	397.21	0.17	17.31	.0099	100	4.76	9.75	2.66	0
CV	4232	101	272	9	106748	252	.2135	392.46	0.26	25.22	.0085	118	0	14.54	6.81	0
D	5926	136	259	9	85958	2302	.1719	331.88	0.17	14.51	.0119	84	1.97	12.16	3.06	0
DV	6722	187	297	10	104958	289	.2099	353.39	0.18	15.61	.0134	74	1.14	17.65	2.21	0
E	7035	164	391	18	115372	338	.2307	295.07	0.22	16.40	.0141	71	11.10	4.66	7.30	0
EV	9195	190	444	17	135483	271	.2710	305.14	0.19	14.73	.0184	54	0.967	18.37	7.76	0
F	11409	244	433	12	157786	275	.3156	364.40	0.15	13.83	.0228	43	12.76	14.02	4.78	0
FV	12238	181	715	27	155399	198	.3108	217.34	0.23	12.70	.0245	40	1.31	14.89	14.87	0
G	12673	225	654	23	170821	345	.3416	261.19	0.21	13.48	.0253	39	15.65	11.55	6.96	0
GV	13037	248	571	16	171765	276	.3435	300.81	0.18	13.18	.0261	38	18.40	12.43	3.52	0
H	9359	182	379	10	168667	250	.3373	445.03	0.16	18.02	.0187	53	10.70	16.89	6.14	0
HV	13888	164	635	17	172850	294	.3457	272.20	0.18	12.45	.0278	36	12.00	15.63	6.93	0
I	11990	324	547	20	181045	307	.3621	330.98	0.18	15.10	.0240	41	14.81	15.91	5.49	0
IV	12511	287	624	28	219234	220	.4385	351.34	0.20	17.52	.0250	39	13.78	16.84	13.23	0
J	10130	248	703	15	193810	284	.3876	275.69	0.28	19.13	.0203	49	20.31	10.62	7.82	0
JV	17905	293	1176	37	168610	311	.3372	143.38	0.26	9.42	.0358	27	17.04	5.81	10.86	0
K	13715	258	675	22	204416	256	.4088	302.84	0.20	14.90	.0274	36	10.82	1.36	20.40	8.30
KV	15460	291	512	24	235062	308	.4701	459.11	0.13	15.20	.0309	32	19.15	4.15	15.41	8.30
L	11313	224	684	21	195150	335	.3903	285.10	0.24	17.25	.0226	44	12.13	9.10	7.97	14.60
M	13018	392	596	38	240600	365	.4816	403.69	0.18	18.48	.0260	38	11.88	5.83	8.25	17.56
N	10816	234	738	26	264550	311	.5291	358.47	0.27	24.46	.0216	46	14.58	4.74	8.46	20.11
O	13838	391	780	42	286300	462	.5726	367.05	0.23	20.69	.0277	36	2.95	3.51	7.45	33.41
P	11592	459	1231	99	328850	1013	.6577	267.14	0.42	28.37	.0232	43	1.59	2.93	7.44	35.51
F1	6088	123	262	16	128722	425	.2574	491.31	0.17	21.14	.0122	82	--	--	--	0
F1V	10965	239	698	39	123316	377	.2466	176.67	0.25	11.25	.0219	45	--	--	--	0
F2	10231	302	475	30	145430	361	.2909	306.17	0.19	14.21	.0205	48	--	--	--	0
F2V	11813	184	794	46	126443	374	.2529	159.25	0.27	10.70	.0236	42	--	--	--	0

Table 21 (Continued)

Alloy Design	Inter	SI	End Count	SEC	Area	SA	AFR	APS	ROC	Shape	SPV	GS	FL	FR	FX	FP
G1	10335	298	548	29	167996	381	.3360	306.56	0.21	16.26	.0207	48	3.29	21.32	8.98	0
G1V	10863	282	536	30	158112	359	.3162	294.99	0.20	14.56	.0217	46	0.259	17.26	14.11	0
G2	9948	296	528	25	158622	312	.3172	300.42	0.21	15.95	.0199	50	2.73	18.39	10.59	0
G2V	9918	239	443	18	165887	267	.3318	374.46	0.18	16.73	.0198	50	0.319	19.63	13.23	0
H1	11349	279	573	24	161317	286	.3226	281.53	0.20	14.21	.0227	44	--	--	--	0
H1V	11496	252	575	24	193093	373	.3862	335.81	0.20	16.80	.0230	43	--	--	--	0
H2	11575	391	729	31	156404	417	.3128	214.55	0.25	13.51	.0232	43	--	--	--	0
H2V	11396	278	624	32	160449	332	.3209	257.13	0.22	14.08	.0228	43	--	--	--	0
I1	11590	322	704	41	161973	590	.3239	230.08	0.24	13.98	.0232	43	10.83	12.96	8.60	0
I1V	10843	351	702	45	175177	465	.3504	249.54	0.26	16.16	.0217	46	2.23	21.14	11.66	0
I2	9923	160	457	20	172239	276	.3445	376.89	0.18	17.36	.0198	50	16.53	13.66	4.26	0
I2V	11384	256	404	15	179934	324	.3599	445.38	0.14	15.81	.0228	43	4.36	18.00	13.64	0
J1	13202	217	455	13	211330	275	.4227	464.46	0.14	16.01	.0264	37	--	--	--	0
J1V	13672	365	588	29	206628	407	.4133	351.41	0.17	15.11	.0273	36	--	--	--	0
J2	11617	387	672	19	180639	397	.3613	268.81	0.23	15.55	.0232	43	--	--	--	0
J2V	11443	275	629	23	182776	408	.3656	290.58	0.22	15.97	.0229	43	--	--	--	0
K1	14404	298	698	21	203367	421	.4067	291.36	0.19	14.12	.0288	34	11.63	8.42	11.36	9.26
K1V	10567	313	803	29	206108	507	.4122	256.67	0.30	19.50	.0211	47	8.95	1.54	26.07	4.66
K2	12746	249	540	14	170578	264	.3412	315.89	0.17	13.38	.0255	39	15.65	0.426	6.86	11.19
K2V	10092	280	726	20	198517	332	.3970	273.44	0.29	19.67	.0202	49	0.652	4.19	25.08	9.77

* Inter = Intercept.
SI = Standard deviation of the intercept.
SEC = Standard deviation of the end count.
SA = Standard deviation of the area of carbide.
AFR = Area fraction of carbide.
APS = Average particle size of carbide = (area/end count).
ROC = Radius of curvature = 4 EC/intercept.
Shape = Shape parameter = area/intercept ≃ area/perimeter.
SPV = Shape parameter = (intercept/area)(AFR) = (I/A)(A/500,000) = I/500,000.
GS = 500,000/intercept.
FL = Absolute percentage of lamellar eutectic carbide.
FR = Absolute percentage of radiating eutectic carbide.
FX = Absolute percentage of eutectic carbide rod in transverse cross-section.
FP = Absolute percentage of primary carbide.

Table 22

Interplanar Spacings from the Electron Diffraction Patterns of Particles within the Minor Phase Present in the Molybdenum-Containing Alloys

Interplanar Spacings* of Mo_2C		Interplanar Spacing of Particles**
hk.l	d-Spacing (Å)	d-Spacing (Å)
00.1	4.724	4.63
01.0	2.600	
00.2	2.362	2.35
01.1	2.278	
01.2	1.748	1.75; 1.73; 1.74
11.0	1.501	1.50; 1.50
01.3	1.347	1.35; 1.34
02.0	1.300	
11.2	1.267	1.26
02.1	1.253	
00.4	1.181	
02.2	1.139	1.14
01.4	1.075	1.06
02.3	1.003	0.99; 1.00
12.0	0.983	
12.1	0.962	
00.5	0.945	0.95
11.4	0.928	0.92
12.2	0.907	
01.5	0.888	
02.4	0.874	0.87; 0.88
03.0	0.867	

* Data from reference 43.

** d-spacings from the diffraction of three particles; where more than one number appears per line, d-spacings were calculated from more than one diffraction pattern.

Table 23

Variables used in the Regression Analysis

Variable Number and Description*	Other Variables with Correlation Coefficients Greater than 0.8000 with the Variable Shown in the First Column
1. Abrasion Resistance-the Dependent Variable	22
2. Intercept	8, 9, 15
3. End Count	
4. Area Fraction	13, 17, 19
5. Average Particle Size = Area/End Count	
6. Radius of Curvature	
7. Shape = Area/Intercept	
8. SPV = Intercept/500,000	9, 15
9. GS = Austenite Grain Size = 500,000/Intercept	15, 17
10. SI = Standard Deviation of the Intercept	
11. SEC = Standard Deviation of the End Count	
12. SA = Standard Deviation of the Area	
13. Total % Cr of the Alloy	17, 20
14. Total % Mo of the Alloy	16, 18
15. % Cr in the Matrix	17, 21
16. % Mo in the Matrix	18
17. % Cr in the Eutectic Carbide	20
18. % Mo in the Eutectic Carbide	
19. % Cr in the Primary Carbide	22, 24
20. Vickers Hardness Number	
21. % Eutectic Carbide	
22. % Primary Carbide	
23. % of Lameller Eutectic Carbide	
24. % of Radiating Eutectic Carbide	
25. % of Eutectic Carbide Rod in Transverse Cross-Section	

* The parameters pertain to the carbide phase unless otherwise stated.

Table 24

Regression Analysis Equations

Data Matrix	Regression Equation	Multiple Correlation Coefficient	Standard Error of the Estimate
Hypoeutectic Fe-C-Cr Alloys (1)	$AR(cm^{-3}) = 142.63 - 5.88 \times 10^{-3}$ (End Count) + 3.62×10^{-2} (Volume % Eutectic Carbide Rod in Transverse Cross section) + 1.39×10^{-1} (Shape, pp)* - 6.02×10^{-2} (% Volume of Lamellar Carbide)	0.810	$1.28\ cm^{-3}$
Hypoeutectic Fe-C-Cr and Fe-C-Cr-Mo Alloys (2)	$AR(cm^{-3}) = 148.72 + 2.93$ (% Mo in the Alloy) - 1.32×10^{-1} (Volume % of Eutectic Carbide) - 4.47×10^{-3} (End Count)	0.851	$2.21\ cm^{-3}$
All the data Hypoeutectic and Hypereutectic Fe-C-Cr, and Mo-Containing Alloys (3)	$AR(cm^{-3}) = 132.17 + 1.30$ (Volume % Primary Carbide) + 2.88 (% Mo in the alloy) + 7.53×10^{-1} (Shape, pp) - 2.88×10^{-1} (Volume % Eutectic Carbide Rod in Transverse Cross Section)	0.937	$3.52\ cm^{-3}$

* pp = Dimension expressed in quantimet picture points, 786 pp = 0.200 mm.

APPENDICES

APPENDIX A

DATA AND STATISTICAL RESULTS ON THE EFFECTS OF DIFFERENT ABRASIVES

Table A-1 Weight Losses for the Alloys Tested on 105 Micron Particle Size Alumina Abrasive Under 7lb Loading

Alloy Designation	Weight Loss (g)				Range (g)	Range Expressed as a Percentage of the Mean (%)
	Test 1	Test 2	Test 3	Mean		
AA1*	0.02935	0.02983	0.02968	0.02962	0.00048	1.620
AA2	0.02909	0.02917	0.02956	0.02927	0.00047	1.606
AA3	0.02998	0.02955	0.03052	0.03002	0.00097	3.231
"AA"**				0.02964	0.00143	4.824
BB1	0.03814	0.03722	0.03809	0.03782	0.00092	2.433
BB2	0.03849	0.03735	0.03859	0.03814	0.00124	3.251
BB3	0.03760	0.03740	0.03840	0.03780	0.00100	2.646
"BB"				0.03792	0.00137	3.612
CC1	0.05441	0.05472	0.05653	0.05522	0.00212	3.839
CC2	0.05638	0.05702	0.05675	0.05672	0.00064	1.128
CC3	0.05509	0.05513	0.05510	0.05511	0.00004	0.0726
"CC"				0.05568	0.00261	4.687
FF1	0.02933	0.02914	0.02944	0.02930	0.00030	1.024
FF2	0.02936	0.02964	0.02920	0.02940	0.00044	1.497
FF3	0.03000	0.02940	0.02966	0.02969	0.00060	2.021
"FF"				0.02946	0.00086	2.919
GG1	0.05251	0.05168	0.05201	0.05207	0.00083	1.594
GG2	0.05191	0.05266	0.05321	0.05259	0.00130	2.472
"GG"				0.05233	0.00153	2.923
II1	0.04553	0.04552	0.04601	0.04567	0.00049	1.073
II2	0.04590	0.04587	0.04650	0.04609	0.00063	1.367
II3	0.04519	0.04584	0.04659	0.04587	0.00140	3.052
"II"				0.04588	0.00140	3.051

* The number following the letter for the alloy designation represents the specimen tested for the given alloy.

** Letters in quotation marks include data from all the three specimens of each alloy.

Table A-2 Weight Losses for the Alloys Tested on 105 Micron Particle Size Silicon Carbide Abrasive Under 7lb Loading

Alloy Designation	Weight Loss (g)				Range (g)	Range Expressed as a Percentage of the Mean (%)
	Test 1	Test 2	Test 3	Mean		
AA1*	0.0446	0.0454	0.0439	0.0445	0.0011	2.472
AA2	0.0443	0.0438	0.0444	0.0442	0.0006	1.357
AA3	0.0456	0.0455	0.0453	0.0455	0.0003	0.659
"AA"**				0.0447	0.0018	4.026
BB1	0.0437	0.0424	0.0420	0.0427	0.0017	3.981
BB2	0.0429	0.0433	0.0432	0.0431	0.0004	0.928
BB3	0.0419	0.0421	0.0422	0.0421	0.0003	0.713
"BB"				0.0426	0.0018	4.225
CC1	0.0599	0.0595	0.0583	0.0592	0.0016	2.703
CC2	0.0605	0.0604	0.0604	0.0604	0.0001	0.166
CC3	0.0599	0.0582	0.0573	0.0585	0.0026	4.444
"CC"				0.0594	0.0032	5.387
FF1	0.0393	0.0388	0.0382	0.0388	0.0011	2.835
FF2	0.0387	0.0393	0.0385	0.0388	0.0008	2.062
FF3	0.0394	0.0394	0.0388	0.0392	0.0006	1.531
"FF"				0.0389	0.0012	3.084
GG1	0.0558	0.0554	0.0556	0.0556	0.0004	0.719
GG2	0.0545	0.0564	0.0571	0.0560	0.0026	4.643
"GG"				0.0558	0.0026	4.659
II1	0.0485	0.0488	0.0499	0.0491	0.0014	2.851
II2	0.0492	0.0495	0.0499	0.0495	0.0007	1.414
II3	0.0489	0.0492	0.0498	0.0493	0.0009	1.826
"II"				0.0493	0.0014	2.839

* The number following the letter for the alloy designation represents the specimen tested for the given alloy.

** Letters in quotation marks include data from all the three specimens of each alloy.

Table A-3 Weight Losses for the Alloys Tested on 105 Micron Particle Size Garnet Abrasive Under 7lb Loading

Alloy Designation	Weight Loss (g)					Range (g)	Range Expressed as a Percentage of the Mean (%)
	Test 1	Test 2	Test 3	Test 4	Mean		
AA1*	0.01205	0.01273	0.01249	0.01198	0.01231	0.00075	6.093
AA2	0.01110	0.01168	0.01124	0.01112	0.01129	0.00058	5.137
AA3	0.01167	0.01230	0.01213	0.01135	0.01186	0.00095	8.010
"AA"**					0.01182	0.00163	13.790
BB1	0.03653	0.03720	0.03617	0.03778	0.03692	0.00161	4.361
BB2	0.03758	0.03784	0.03702	0.03865	0.03777	0.00163	4.316
BB3	0.03602	0.03703	0.03491	0.03699	0.03624	0.00212	5.850
"BB"					0.03698	0.00374	10.113
CC1	0.05560	0.05687	0.05528	0.05781	0.05639	0.00253	4.487
CC2	0.05706	0.05791	0.05590	0.06011	0.05775	0.00201	3.480
CC3	0.05675	0.05668	0.05804	0.05840	0.05747	0.00172	2.993
"CC"					0.05720	0.00483	8.444
FF1	0.01995	0.01968	0.01866	0.01984	0.01953	0.00129	6.605
FF2	0.02001	0.01923	0.01917	0.01948	0.01947	0.00084	4.314
FF3	0.02013	0.02011	0.01969	0.02002	0.01999	0.00044	2.201
"FF"					0.01966	0.00147	7.477
GG1	0.05105	0.04751	0.05087	0.05187	0.05033	0.00436	8.663
GG2	0.05097	0.04828	0.04941	0.05307	0.05043	0.00479	9.498
"GG"					0.05038	0.00556	11.036
II1	0.04663	0.04327	0.04478	0.04764	0.04558	0.00437	9.588
II2	0.04708	0.04407	0.04634	0.04716	0.04616	0.00309	6.694
II3	0.04614	0.04406	0.04605	0.04710	0.04584	0.00304	6.632
"II"					0.04586	0.00437	9.529

* The number following the letter for the alloy designation represents the specimen tested for the given alloy.

** Letters in quotation marks include data from all the three specimens of each alloy.

Table A-4 Statistical Analysis for the Data of the Alloys Tested on 105 Micron Particle Size Alumina Abrasive Under 7lb Loading

Alloy Designation	$\bar{X}$ (g)	S(x) (g)	$S(\bar{X})$ (g)	95% Confidence Limits of the Mean ($\pm$ g)	95% Confidence Limits Expressed as a Percentage of the Mean ($\pm$ %)	$\frac{\lvert\bar{X}-m\rvert}{S(x)}$	n*
AA1**	0.02962	0.00025	0.00014	0.00060	2.026		
AA2	0.02927	0.00025	0.00015	0.00065	2.221		
AA3	0.03002	0.00049	0.00028	0.00120	3.997		
"AA"***	0.02964	0.00044	0.00015	0.00035	1.181	0.674	31
BB1	0.03782	0.00052	0.00030	0.00129	3.411		
BB2	0.03814	0.00068	0.00039	0.00168	4.405		
BB3	0.03780	0.00068	0.00040	0.00172	4.550		
"BB"	0.03792	0.00053	0.00018	0.00042	1.108	0.715	28
CC1	0.05522	0.00114	0.00066	0.00284	5.143		
CC2	0.05672	0.00032	0.00019	0.00082	1.446		
CC3	0.05511	0.00002	0.00001	0.00004	0.073		
"CC"	0.05568	0.00098	0.00033	0.00076	1.365	0.568	42
FF1	0.02930	0.00015	0.00009	0.00039	1.331		
FF2	0.02940	0.00022	0.00013	0.00056	1.905		
FF3	0.02969	0.00030	0.00017	0.00073	2.459		
"FF"	0.02946	0.00027	0.00009	0.00021	0.713	1.091	13
GG1	0.05207	0.00042	0.00024	0.00103	1.978		
GG2	0.05259	0.00065	0.00038	0.00164	3.118		
"GG"	0.05233	0.00057	0.00023	0.00059	1.127	0.918	18
II1	0.04567	0.00028	0.00016	0.00069	1.511		
II2	0.04609	0.00036	0.00021	0.00090	1.953		
II3	0.04587	0.00070	0.00040	0.00172	3.750		
"II"	0.04588	0.00045	0.00015	0.00035	0.763	1.020	16

* n is equal to the number of tests that would be required to locate the true population mean within $\pm$ 0.01 $\bar{X}$ of the calculated sample mean $\bar{X}$ with risks of 0.05 for α and 0.05 for β.

** The number following the letter for the alloy designation represents the specimen tested for the given alloy.

*** Letters in quotation marks include data from all the three specimens of each alloy.

Table A-5 Statistical Analysis for the Data of the Alloys Tested on 105 Micron Particle Size Silicon Carbide Abrasive Under 7lb Loading

Alloy Designation	$\bar{X}$ (g)	S(x) (x)	$S(\bar{X})$ (g)	95% Confidence Limits of the Mean ($\pm$ g)	95% Confidence Limits Expressed as a Percentage of the Mean ($\pm$ %)	$\frac{\lvert \bar{X}-m \rvert}{S(x)}$	n*
AA1**	0.0445	0.00056	0.00032	0.00138	3.101		
AA2	0.0442	0.00032	0.00019	0.00082	1.855		
AA3	0.0455	0.00016	0.00009	0.00039	0.857		
"AA"***	0.0447	0.00067	0.00022	0.00051	1.141	0.667	32
BB1	0.0427	0.00089	0.00051	0.00219	5.129		
BB2	0.0431	0.00021	0.00012	0.00052	1.206		
BB3	0.0421	0.00016	0.00009	0.00039	0.926		
"BB"	0.0426	0.00066	0.00022	0.00051	1.197	0.645	34
CC1	0.0592	0.00083	0.00048	0.00207	3.497		
CC2	0.0604	0.00007	0.00004	0.00017	0.281		
CC3	0.0585	0.00132	0.00076	0.00327	5.590		
"CC"	0.0594	0.00116	0.00039	0.00090	1.515	0.512	52
FF1	0.0388	0.00055	0.00032	0.00138	3.557		
FF2	0.0388	0.00042	0.00024	0.00103	2.655		
FF3	0.0392	0.00035	0.00020	0.00086	2.194		
"FF"	0.0389	0.00044	0.00015	0.00035	0.900	0.884	20
GG1	0.0556	0.00020	0.00012	0.00052	0.935		
GG2	0.0560	0.00135	0.00078	0.00336	6.000		
"GG"	0.0558	0.00089	0.00036	0.00093	1.667	0.627	35
II1	0.0491	0.00074	0.00043	0.00185	3.737		
II2	0.0495	0.00035	0.00020	0.00086	1.736		
II3	0.0493	0.00046	0.00026	0.00112	2.272		
"II"	0.0493	0.00051	0.00017	0.00039	0.791	0.967	17

* n is equal to the number of tests that would be required to locate the true population mean within $\pm$ 0.01 $\bar{X}$ of the calculated sample mean $\bar{X}$ with risks of 0.05 for α and 0.05 for β.

** The number following the letter for the alloy designation represents the specimen tested for the given alloy.

*** Letters in quotation marks include data from all the three specimens of each alloy.

Table A-6 Statistical Analysis for the Data of the Alloys Tested on 105 Micron Particle Size Garnet Abrasive Under 71b Loading

Alloy Designation	$\bar{X}$ (g)	S(x) (g)	$S(\bar{x})$ (g)	95% Confidence Limits of the Mean ($\pm$ g)	95% Confidence Limits Expressed as a Percentage of the Mean ($\pm$ %)	$\frac{\lvert\bar{X}-m\rvert}{S(x)}$	n*
AA1**	0.01231	0.00036	0.00018	0.00077	6.255		
AA2	0.01129	0.00027	0.00014	0.00060	5.314		
AA3	0.01186	0.00043	0.00022	0.00095	8.010		
"AA"***	0.01182	0.00055	0.00016	0.00037	3.130	0.233	>128
BB1	0.03692	0.00071	0.00036	0.00155	4.198		
BB2	0.03777	0.00068	0.00034	0.00146	3.866		
BB3	0.03624	0.00100	0.00050	0.00215	5.933		
"BB"	0.03698	0.00091	0.00026	0.00060	1.622	0.406	82
CC1	0.05639	0.00083	0.00042	0.00181	3.210		
CC2	0.05775	0.00178	0.00089	0.00383	6.632		
CC3	0.05747	0.00088	0.00044	0.00189	3.289		
"CC"	0.05720	0.00135	0.00039	0.00090	1.573	0.424	76
FF1	0.01953	0.00059	0.00030	0.00129	6.605		
FF2	0.01947	0.00038	0.00019	0.00082	4.212		
FF3	0.01999	0.00020	0.00010	0.00043	2.151		
"FF"	0.01966	0.00045	0.00013	0.00030	1.526	0.437	72
GG1	0.05033	0.00192	0.00096	0.00413	8.206		
GG2	0.05043	0.00207	0.00104	0.00448	8.884		
"GG"	0.05038	0.00184	0.00065	0.00167	3.315	0.274	>119
II1	0.04558	0.00194	0.00097	0.00417	9.149		
II2	0.04616	0.00144	0.00072	0.00310	6.716		
II3	0.04584	0.00128	0.00064	0.00275	5.999		
"II"	0.04586	0.00145	0.00042	0.00097	2.115	0.316	>109

* n is equal to the number of tests that would be required to locate the true population mean within $\pm$ 0.01 $\bar{X}$ of the calculated sample mean $\bar{X}$ with risks of 0.05 for α and 0.05 for β.

** The number following the letter for the alloy designation represents the specimen tested for the given alloy.

*** Letters in quotation marks include data from all the three specimens of each alloy.

APPENDIX B

DATA AND STATISTICAL RESULTS ON THE EFFECTS OF LOAD AND GRIT SIZE

Table B-1 Weight Losses for the Alloys Tested on 80 Micron Particle Size Alumina Under the Given Loading

Alloy Designation	Weight Loss (g)					Range (g)	Range Expressed as a Percentage of the Mean (%)
	Test 1	Test 2	Test 3	Test 4	Mean		
			3.5 lb				
AA2*	0.01382	0.01348	0.01269	0.01278	0.01319	0.00113	8.567
BB2	0.01988	0.01998	0.01888	0.01939	0.01953	0.00110	5.632
CC2	0.02932	0.02950	0.02815	0.02869	0.02898	0.00135	4.568
FF2	0.01425	0.01446	0.01374	0.01363	0.01402	0.00083	5.920
II2	0.02354	0.02198	0.02240	0.02280	0.02268	0.00156	6.878
			7 lb				
AA1	0.02463	0.02529	0.02394	0.02473	0.02465	0.00135	5.477
BB3	0.03564	0.03610	0.03472	0.03581	0.03557	0.00138	3.880
CC3	0.05244	0.05189	0.05185	0.05157	0.05194	0.00087	1.675
FF3	0.02625	0.02637	0.02628	0.02635	0.02631	0.00012	0.456
II3	0.04160	0.04087	0.04163	0.04268	0.04170	0.00181	4.341
			15 lb				
AA1	0.04851	0.04801	0.04829	0.04812	0.04823	0.00050	1.037
BB3	0.06891	0.06846	0.06896	0.06872	0.06876	0.00050	0.727
CC3	0.10326	0.10272	0.10340	0.10245	0.10296	0.00095	0.923
FF3	0.05156	0.05153	0.05190	0.05118	0.05154	0.00072	1.397
II3	0.08233	0.08224	0.08203	0.08195	0.08214	0.00038	0.463

* The number following the letter for the alloy designation represents the specimen tested for the given alloy.

Table B-2 Weight Losses for the Alloys Tested on 105 Micron Particle Size Alumina Under the Given Loading

Alloy Designation	Weight Loss (g)				Range (g)	Range Expressed as a Percentage of the Mean (%)
	Test 1	Test 2	Test 3	Mean		
			3.5 lb			
AA2*	0.01456	0.01526	0.01589	0.01524	0.00133	8.727
BB2	0.02059	0.02096	0.02120	0.02092	0.00061	2.916
CC2	0.03062	0.03041	0.03042	0.03048	0.00021	0.689
FF2	0.01574	0.01601	0.01617	0.01597	0.00043	2.693
II2	0.02467	0.02463	0.02464	0.02465	0.00004	0.162
			7 lb			
"AA"**				0.02964	0.00143	4.824
"BB"	Detailed Data Under			0.03792	0.00137	3.612
"CC"	these Conditions are			0.05568	0.00261	4.687
"FF"	Given in Table A1			0.02946	0.00086	2.919
"II"				0.04588	0.00140	3.051

* The number following the letter for the alloy designation represent the specimen tested for the given alloy.

** Letters in quotation marks include data from all the three specimens of each alloy.

Table B-3 Weight Losses for the Alloys Tested on 130 Micron Particle Size Alumina Under the Given Loading

Alloy Designation	Weight Loss (g)						Range (g)	Range Expressed as a Percentage of the Mean (%)
	Test 1	Test 2	Test 3	Test 4	Test 5	Mean		
			3.5 lb					
AA2*	0.01623	0.01652	0.01655	0.01617		0.01637	0.00038	2.321
BB2	0.01952	0.02070	0.02070	0.02008		0.02025	0.00118	5.827
CC2	0.02967	0.03102	0.02986	0.02976		0.03008	0.00135	4.488
FF2	0.01684	0.01593	0.01556	0.01574		0.01602	0.00128	7.990
II2	0.02337	0.02335	0.02343	0.02298		0.02328	0.00045	1.933
			5 lb					
AA2	0.02313	0.02243	0.02313	0.02301	0.02290	0.02292	0.00070	3.054
BB2	0.02725	0.02748	0.02743	0.02817	0.02901	0.02787	0.00176	6.315
CC2	0.04009	0.04296	0.04203	0.04356	-------	0.04238	0.00259	6.111
FF2	0.02127	0.02213	0.02244	0.02255	0.02284	0.02225	0.00157	7.056
II2	0.03210	-------	0.03288	0.03411	0.03347	0.03314	0.00201	6.065
			15 lb					
AA1	0.06940	0.06879	0.06955	0.06994		0.06942	0.00115	1.657
BB3	0.07963	0.07942	0.07973	0.08001		0.07970	0.00059	0.740
CC3	0.11781	0.11685	0.11827	0.11941		0.11809	0.00256	2.168
FF3	0.06660	0.06639	0.06619	0.06666		0.06646	0.00047	0.707
II3	0.09358	0.09297	0.09419	0.09431		0.09376	0.00134	1.429

* The number following the letter for the alloy designation represents the specimen tested for the given alloy.

Table B-4 Weight Losses for the Alloys Tested on 200 Micron Particle Size Alumina Under the Given Loading

Alloy Designation	Weight Loss (g)					Range (g)	Range Expressed as a Percentage of the Mean (%)
	Test 1	Test 2	Test 3	Test 4	Mean		
			7 lb				
AA1*	0.03610	0.03593	0.03640	0.03607	0.03613	0.00047	1.301
BB3	0.03837	0.03827	0.03909	0.03858	0.03858	0.00082	2.125
CC3	0.05805	0.05753	0.05762	0.05688	0.05752	0.00117	2.034
FF3	0.03434	0.03427	0.03431	0.03336	0.03407	0.00098	2.876
II3	0.04567	0.04600	0.04605	0.04508	0.04570	0.00097	2.123
			15 lb				
AA3	0.07587	0.07449	0.07472	0.07424	0.07483	0.00163	2.178
BB1	0.08054	0.07934	0.08048	0.08068	0.08026	0.00134	1.670
CC1	0.12082	0.11921	0.12081	0.12093	0.12044	0.00172	1.428
FF1	0.07022	0.06987	0.06990	0.06994	0.06998	0.00035	0.500
II1	0.09408	0.09315	0.09352	0.09460	0.09384	0.00145	1.545
			29.2 lb				
AA3	0.13296	0.13307	0.13169	0.13360	0.13283	0.00191	1.438
BB1	0.14527	0.14625	0.14483	0.14466	0.14525	0.00159	1.095
CC1	0.22244	0.22526	0.22624	0.22325	0.22430	0.00380	1.694
FF1	0.12656	0.12864	0.12797	0.12733	0.12778	0.00208	1.628
II1	0.17012	0.17045	0.17165	0.16994	0.17054	0.00153	0.897

* The number following the letter for the alloy designation represents the specimen tested for the given alloy.

Table B-5 Statistical Analysis for the Data of the Alloys Tested on 80 Micron Particle Size Alumina Under the Given Loading

Alloy Designation	$\bar{X}$ (g)	S(x) (g)	$S(\bar{x})$ (g)	95% Confidence Limits of the Mean ($\pm$ g)	95% Confidence Limits Expressed as a Percentage of the Mean ($\pm$ %)	$\frlvert\bar{X}-m\frrvert$ / S(x)	n*
			3.5 lb				
AA2**	0.01319	0.00055	0.00027	0.00086	6.520	0.240	>128
BB2	0.01953	0.00051	0.00025	0.00080	4.096	0.383	93
CC2	0.02898	0.00060	0.00030	0.00095	3.278	0.483	58
FF2	0.01402	0.00040	0.00020	0.00064	4.565	0.351	109
II2	0.02268	0.00066	0.00033	0.00105	4.630	0.344	110
			7 lb				
AA1	0.02465	0.00055	0.00028	0.00089	3.611	0.448	68
BB3	0.03557	0.00060	0.00030	0.00095	2.671	0.593	39
CC3	0.05194	0.00036	0.00018	0.00057	1.097	1.443	9
FF3	0.02631	0.00006	0.00003	0.00010	0.380	4.385	3
II3	0.04170	0.00074	0.00037	0.00118	2.830	0.564	43
			15 lb				
AA1	0.04823	0.00022	0.00011	0.00035	0.726	2.192	6
BB3	0.06876	0.00023	0.00011	0.00035	0.509	2.990	4
CC3	0.10296	0.00045	0.00022	0.00070	0.680	2.288	5
FF3	0.05154	0.00029	0.00015	0.00048	0.931	1.777	7
II3	0.08214	0.00018	0.00009	0.00029	0.353	4.563	3

* n is equal to the number of tests required in future testing to locate the true population mean within $\pm$ 0.01 $\bar{X}$ of the calculated sample mean $\bar{X}$ with risks of 0.05 for α and 0.05 for β.

** The number following the letter for the alloy designation represents the specimen tested for the given alloy.

Table B-6 Statistical Analysis for the Data of the Alloys Tested on 105 Micron Particle Size Alumina Under the Given Loading

Alloy Designation	$\bar{X}$ (g)	S(x) (g)	S($\bar{X}$) (g)	95% Confidence Limits of the Mean ($\pm$ g)	95% Confidence Limits Expressed as a Percentage of the Mean ($\pm$ %)	$\frac{\lvert\bar{X}-m\rvert}{S(x)}$	n*
			3.5 lb				
AA2**	0.01524	0.00067	0.00038	0.00164	10.761	0.227	>128
BB2	0.02092	0.00031	0.00018	0.00077	3.681	0.675	31
CC2	0.03048	0.00012	0.00007	0.00030	0.984	2.540	5
FF2	0.01597	0.00022	0.00013	0.00056	3.507	0.726	28
II2	0.02465	0.00002	0.00001	0.00004	0.162	12.325	3
			7 lb				
"AA"***	0.02964	0.00044	0.00015	0.00035	1.181	0.674	31
"BB"	0.03792	0.00053	0.00018	0.00042	1.108	0.715	28
"CC"	0.05568	0.00098	0.00033	0.00076	1.365	0.568	42
"FF"	0.02946	0.00027	0.00009	0.00021	0.713	1.091	13
"II"	0.04588	0.00045	0.00015	0.00035	0.763	1.020	16

* n is equal to the number of tests that would be required to locate the true population mean within $\pm$ 0.01 $\bar{X}$ of the calculated sample mean $\bar{X}$ with risks of 0.05 for α and 0.05 for β.

** The number following the letter for the alloy designation represents the specimen tested for the given alloy.

*** Letters in quotation marks include data from all the three specimens of each alloy.

Table B-7 Statistical Analysis for the Data of the Alloys Tested on 130 Micron Particle Size Alumina Under The Given Loading

Alloy Designation	$\bar{X}$ (g)	S(x) (g)	$S(\bar{x})$ (g)	95% Confidence Limits of the Mean ($\pm$ g)	95% Confidence Limits Expressed as a Percentage of the Mean ($\pm$ %)	$\frac{\lvert\bar{X}-m\rvert}{S(x)}$	n*
			3.5 lb				
AA2**	0.01637	0.00020	0.00010	0.00032	1.955	0.819	22
BB2	0.02025	0.00057	0.00028	0.00089	4.395	0.355	107
CC2	0.03008	0.00063	0.00032	0.00102	3.391	0.477	60
FF2	0.01602	0.00057	0.00028	0.00089	5.556	0.281	>119
II2	0.02328	0.00020	0.00010	0.00032	1.375	1.164	12
			5 lb				
AA2	0.02292	0.00029	0.00013	0.00036	1.571	0.790	23
BB2	0.02787	0.00073	0.00033	0.00092	3.301	0.382	93
CC2	0.04238	0.00113	0.00057	0.00181	4.271	0.375	97
FF2	0.02225	0.00060	0.00025	0.00069	3.101	0.371	99
II2	0.03314	0.00086	0.00043	0.00137	4.134	0.385	96
			15 lb				
AA1	0.06942	0.00048	0.00024	0.00076	1.095	1.446	9
BB3	0.07970	0.00025	0.00012	0.00038	0.477	3.188	4
CC3	0.11809	0.00106	0.00053	0.00169	1.431	1.114	13
FF3	0.06646	0.00021	0.00011	0.00035	0.527	3.165	4
II3	0.09376	0.00062	0.00031	0.00099	1.056	1.512	8

* n is equal to the number of tests that would be required to locate the true population mean within $\pm$ 0.01 $\bar{X}$ of the calculated sample mean $\bar{X}$ with risks of 0.05 for α and 0.05 for β.

** The number following the letter for the alloy designation represents the specimen tested for the given alloy.

Table B-8 Statistical Analysis for the Data of the Alloys Tested on 200 Micron Particle Size Alumina Under the Given Loading

Alloy Designation	$\bar{X}$ (g)	S(x) (g)	S($\bar{X}$) (g)	95% Confidence Limits of the Mean (± g)	95% Confidence Limits Expressed as a Percentage of the Mean (± %)	$\frac{\lvert \bar{X}-m \rvert}{S(x)}$	n*
			7 lb				
AA1**	0.03613	0.00020	0.00010	0.00032	0.886	1.807	7
BB3	0.03858	0.00037	0.00018	0.00057	1.477	1.043	15
CC3	0.05752	0.00048	0.00024	0.00076	1.321	1.198	12
FF3	0.03407	0.00047	0.00024	0.00076	2.231	0.725	28
II3	0.04570	0.00045	0.00022	0.00070	1.532	1.016	16
			15 lb				
AA3	0.07483	0.00069	0.00035	0.00111	1.483	1.084	13
BB1	0.08026	0.00062	0.00031	0.00095	1.184	1.295	10
CC1	0.12044	0.00082	0.00041	0.00130	1.079	1.469	8
FF1	0.06998	0.00016	0.00008	0.00025	0.357	4.374	3
II1	0.09384	0.00064	0.00032	0.00102	1.087	1.466	8
			29.2 lb				
AA3	0.13283	0.00081	0.00040	0.00127	0.956	1.640	7
BB1	0.14525	0.00071	0.00036	0.00115	0.792	2.046	6
CC1	0.22430	0.00176	0.00088	0.00280	1.248	1.274	10
FF1	0.12778	0.00091	0.00045	0.00143	1.119	1.404	9
II1	0.17054	0.00077	0.00038	0.00121	0.708	2.215	6

* n is equal to the number of tests that would be required to locate the true population mean within $\pm$ 0.01 $\bar{X}$ of the calculated sample mean $\bar{X}$ with risks of 0.05 for α and 0.05 for β.

** The number following the letter for the alloy designation represents the specimen tested for the given alloy.

APPENDIX C

DATA AND STATISTICAL RESULTS OF THE Fe-C-Cr AND Fe-C-Cr-Mo ALLOYS TESTED IN HIGH STRESS ABRASION

Table C-1

High Stress Abrasion Test Results

Alloy Design	Weight Loss (g)					Mean Wt Loss (g) of Dup Alloy Samples Taken in 1 Direction	Std Deviation (g) of Dup Alloy Samples Taken in 1 Direction	Standard Error of Mean (g) Duplicate Samples
	Test 1	Test 2	Test 3	Test 4	Mean			
B	0.05220	0.05210	0.05280	0.05177	0.05222			
B-	0.05192	0.05234	0.05172	0.05288	0.05222	0.05222	0.00044	0.00015
BV	0.05185	0.05177	0.05205	0.05205	0.05193			
BV-	0.05202	0.05127	0.05206	0.05216	0.05188	0.05190	0.00029	0.00010
C	0.05381	0.05387	0.05312	0.05394	0.05369			
C-	0.05436	0.05360	0.05344	0.05315	0.05364	0.05366	0.00042	0.00015
CV	0.05363	0.05322	0.05425	0.05295	0.05351			
CV-	0.05383	0.05353	0.05307	0.05372	0.05354	0.05353	0.00043	0.00015
D	0.05371	0.05319	0.05408	0.05315	0.05353			
D-	0.05403	0.05356	0.05500	0.05350	0.05402	0.05378	0.00060	0.00021
DV	0.05458	0.05422	0.05493	0.05442	0.05454			
DV-	0.05438	0.05332	0.05392	0.05411	0.05393	0.05424	0.00048	0.00017
E	0.05465	0.05397	0.05402	0.05412	0.05419			
E-	0.05558	0.05462	0.05614	0.05434	0.05517	0.05468	0.00079	0.00028
EV	0.05444	0.05502	0.05435	0.05443	0.05456			
EV-	0.05525	0.05504	0.05533	0.05451	0.05503	0.05480	0.00040	0.00014
F	0.05339	0.05396	0.05429	0.05431	0.05399			
F-	0.05419	0.05311	0.05411	0.05364	0.05376	0.05388	0.00045	0.00016
FV	0.05450	0.05375	0.05485	0.05425	0.05434			
FV-	0.05445	0.05485	0.05499	0.05456	0.05471	0.05453	0.00040	0.00014
G	0.05527	0.05481	0.05479	0.05408	0.05474			
G-	0.05564	0.05381	0.05536	0.05466	0.05487	0.05480	0.00063	0.00022
GV	0.05541	0.05549	0.05540	0.05467	0.05524			
GV-	0.05570	0.05503	0.05569	0.05501	0.05536	0.05530	0.00036	0.00013
H	0.05446	0.05424	0.05420	0.05409	0.05425			
H-	0.05356	0.05353	0.05412	0.05432	0.05388	0.05407	0.00034	0.00012
HV	0.05405	0.05412	0.05368	0.05358	0.05388			
HV-	0.05433	0.05456	0.05470	0.05393	0.05438	0.05412	0.00040	0.00014

Table C-1 (Continued)

Alloy Design	Weight Loss (g)					Mean Wt Loss (g) of Dup Alloy Samples Taken in 1 Direction	Std Deviation (g) of Dup Alloy Samples Taken in 1 Direction	Standard Error of Mean (g) Duplicate Samples
	Test 1	Test 2	Test 3	Test 4	Mean			
I	0.05340	0.05317	0.05401	0.05346	0.05351			
I-	0.05353	0.05337	0.05376	0.05350	0.05354	0.05353	0.00026	0.00009
IV	0.05418	0.05392	0.05389	0.05464	0.05416			
IV-	0.05385	0.05333	0.05355	0.05303	0.05344	0.05380	0.00050	0.00018
J	0.05380	0.05432	0.05408	0.05406	0.05407			
J-	0.05479	0.05432	0.05450	0.05386	0.05437	0.05422	0.00033	0.00012
JV	0.05543	0.05472	0.05618	0.05481	0.05529			
JV-	0.05613	0.05545	0.05572	0.05502	0.05558	0.05543	0.00056	0.00020
K	0.05201	0.05115	0.05187	0.05159	0.05166			
K-	0.05171	0.05160	0.05190	0.05075	0.05149	0.05157	0.00043	0.00015
KV	0.05253	0.05163	0.05216	0.05173	0.05201			
KV-	0.05287	0.05209	0.05253	0.05247	0.05249	0.05225	0.00043	0.00015
L	0.05010	0.05030	0.04986	0.04980	0.05002			
L-	0.05033	0.04960	0.04991	0.04942	0.04982	0.04992	0.00032	0.00011
M	0.04425	0.04337	0.04396	0.04380	0.04385			
M-	0.04448	0.04344	0.04363	0.04362	0.04379	0.04382	0.00039	0.00014
N	0.04217	0.04121	0.04136	0.04039	0.04128			
N-	0.04304	0.04064	0.04137	0.04033	0.04135	0.04131	0.00093	0.00033
O	0.04382	0.04175	0.04293	0.04215	0.04266			
O-	0.04347	0.04206	0.04293	0.04186	0.04258	0.04262	0.00078	0.00027
P	0.05223	0.05354	0.05342	0.04896	0.05206			
P-	0.04961	0.04827	0.05100	0.05066	0.04989	0.05097	0.00199	0.00070
F1	0.05314	0.05316	0.05301	0.05275	0.05302			
F1-	0.05251	0.05284	0.05291	0.05427	0.05313	0.05307	0.00053	0.00019
F1V	0.05289	0.05211	0.05282	0.05265	0.05262			
F1V-	0.05288	0.05229	0.05303	0.05182	0.05251	0.05256	0.00044	0.00015
F2	0.05123	0.05047	0.05160	0.05089	0.05105			
F2-	0.05180	0.05183	0.05146	0.05181	0.05173	0.05139	0.00049	0.00017

Table C-1 (Continued)

Alloy Dsgn	Weight Loss (g)					Mean Wt Loss (g) of Dup Alloy Samples Taken in 1 Direction	Std Deviation (g) of Dup Alloy Samples Taken in 1 Direction	Standard Error of Mean (g) Duplicate Samples
	Test 1	Test 2	Test 3	Test 4	Mean			
F2V	0.05166	0.05246	0.05233	0.05278	0.05231			
F2V-	0.05237	0.05199	0.05244	0.05209	0.05222	0.05227	0.00034	0.00012
G1	0.05298	0.05256	0.05266	0.05295	0.05279			
G1-	0.05297	0.05224	0.05284	0.05254	0.05265	0.05272	0.00026	0.00009
G1V	0.05241	0.05230	0.05263	0.05171	0.05226			
G1V-	0.05272	0.05235	0.05292	0.05194	0.05248	0.05237	0.00040	0.00014
G2	0.05192	0.05167	0.05151	0.05153	0.05166			
G2-	0.05195	0.05130	0.05173	0.05183	0.05170	0.05168	0.00022	0.00008
G2V	0.05190	0.05071	0.05183	0.05237	0.05170			
G2V-	0.05147	0.05148	0.05056	0.05096	0.05112	0.05141	0.00063	0.00022
H1	0.05139	0.05138	0.05121	0.05119	0.05129			
H1-	0.05134	0.05080	0.05125	0.05089	0.05107	0.05118	0.00022	0.00008
H1V	0.05144	0.05053	0.05119	0.05120	0.05109			
H1V-	0.05158	0.05087	0.05170	0.05095	0.05128	0.05118	0.00039	0.00014
H2	0.05165	0.05189	0.05180	0.05123	0.05164			
H2-	0.05082	0.05089	0.05115	0.05067	0.05088	0.05126	0.00047	0.00017
H2V	0.05204	0.05117	0.05164	0.05166	0.05163			
H2V-	0.05212	0.05202	0.05230	0.05202	0.05212	0.05187	0.00036	0.00013
I1	0.05150	0.05103	0.05100	0.05037	0.05098			
I1-	0.05136	0.05081	0.05151	0.05129	0.05124	0.05111	0.00039	0.00014
I1V	0.05179	0.05202	0.05242	0.05165	0.05197			
I1V-	0.05190	0.05248	0.05183	0.05136	0.05189	0.05193	0.00038	0.00013
I2	0.05061	0.05006	0.05058	0.04994	0.05030			
I2-	0.04986	0.04987	0.05116	0.05016	0.05026	0.05028	0.00046	0.00016
I2V	0.05108	0.05167	0.05058	0.05060	0.05098			
I2V-	0.05078	0.05106	0.05067	0.05095	0.05087	0.05092	0.00036	0.00013
J1	0.05133	0.05210	0.05201	0.05253	0.05199			
J1-	0.05236	0.05141	0.05226	0.05182	0.05196	0.05198	0.00043	0.00015

Table C-1 (Continued)

Alloy Design	Weight Loss (g)					Mean Wt Loss (g) of Dup Alloy Samples Taken in 1 Direction	Std Deviation (g) of Dup Alloy Samples Taken in 1 Direction	Standard Error of Mean (g) Duplicate Samples
	Test 1	Test 2	Test 3	Test 4	Mean			
J1V	0.05265	0.05177	0.05270	0.05216	0.05232			
J1V-	0.05301	0.05220	0.05213	0.05254	0.05248	0.05240	0.00040	0.00014
J2	0.05202	0.05177	0.05200	0.05108	0.05172			
J2-	0.05120	0.05119	0.05159	0.05118	0.05129	0.05150	0.00039	0.00014
J2V	0.05175	0.05217	0.05159	0.05096	0.05162			
J2V-	0.05211	0.05150	0.05193	0.05192	0.05187	0.05174	0.00039	0.00014
K1	0.04947	0.04868	0.04983	0.04915	0.04928			
K1-	0.04893	0.04865	0.04993	0.04888	0.04910	0.04919	0.00050	0.00018
K1V	0.05115	0.05108	0.05132	0.05171	0.05130			
K1V-	0.05053	0.05008	0.05057	0.05001	0.05030	0.05081	0.00061	0.00021
K2	0.04814	0.04786	0.04764	0.04733	0.04774			
K2-	0.04864	0.04793	0.04788	0.04797	0.04811	0.04792	0.00038	0.00013
K2V	0.04777	0.04835	0.04798	0.04750	0.04790			
K2V-	0.04913	0.04864	0.04853	0.05029	0.04915	0.04852	0.00088	0.00031

APPENDIX D

MICROPROBE DATA AND RESULTS

Table D-1

Composition of Alloys Utilized in Microprobe Calibration Studies

Specimen No.	Cr	Fe	C	Mn	Si	Mo	Other
3	0.34	97.96	0.36	0.83	0.38	0.01	
4	0.35	97.71	0.35	0.83	0.39	0.24	
5	0.34	97.49	0.35	0.80	0.38	0.51	
6	0.34	97.23	0.34	0.80	0.38	0.78	
7	0.74	97.52	0.37	0.85	0.37	0.02	
10	0.73	96.83	0.37	0.82	0.36	0.76	
11	1.54	96.74	0.36	0.86	0.37	0.01	
14	1.51	95.99	0.35	0.82	0.36	0.84	
19	2.16	93.83	0.0045	2.10	0.031	1.53	0.23 V
21	2.27	95.87	0.010	0.42	0.38	1.00	
24	3.18	91.93	0.38	0.59	0.91	2.59	0.39 V
25	3.14	90.82	1.03	0.59	0.95	2.21	1.26 V
26	3.99	89.56	0.80	0.25	0.12	4.18	1.02 V
27	3.98	88.88	1.14	0.38	2.04	2.46	1.12 V
28	5.31	91.37	0.97	0.64	0.29	1.15	0.27 V
30	5.36	87.25	0.0011	2.06	0.041	2.96	2.07 Ni
34	7.82	90.17	0.97	0.43	0.61		
35	8.64	87.20	0.99	0.31	0.66	1.20	
39	13.68	86.23	0.003			0.08	
40	13.14	85.81	0.005			1.04	
41	13.60	84.51	0.002			1.88	
42	12.94	83.57	0.003			3.48	
43	13.04	82.18	0.003			4.77	
44	17.35	82.63	0.002			0.01	
45	17.53	81.32	0.003			1.14	
46	17.61	80.36	0.004			2.02	
47	17.58	78.89	0.005			3.52	
48	17.38	77.86	0.004			4.75	
50	25.26	72.51	0.002		0.019	2.05	0.13 Ni
51	25.25	69.33	0.002		0.019	5.24	0.13 Ni
52	25.58	70.76	0.002		0.019	3.49	0.13 Ni
53	39.76	59.64	0.008		0.33		
54	66.70	32.38	0.049	0.39	0.48		
54'	73.70	25.38	0.049	0.39	0.48		
Pure Fe-Cr Alloys							
1P	4.38	95.62					
2P	10.21	89.79					
3P	23.78	76.22					
4P	36.40	63.60					
5P	58.32	41.68					
6P	66.96	33.04					
7P	79.81	20.19					
8P	80.79	19.21					
Carbides							
1C	34.81	49.66					
3C	50.09	38.40					
4C	64.23	25.98					

Table D-2

Microprobe Ratios, K's, and Compositions in Weight Percent of Phases in the High-Stress Abrasion Tested Alloys*

Alloy Design	Matrix (Austenite)						Eutectic Carbide						Primary Carbide**					
	K_{Cr} x 10^{-2}	%Cr	K_{Fe} x 10^{-2}	%Fe	K_{Mo} x 10^{-2}	%Mo	K_{Cr} x 10^{-2}	%Cr	K_{Fe} x 10^{-2}	%Fe	K_{Mo} x 10^{-2}	%Mo	K_{Cr} x 10^{-2}	%Cr	K_{Fe} x 10^{-2}	%Fe	K_{Mo} x 10^{-2}	%Mo
B	0.10416	7.90	0.87548	89.25			0.47273	45.60	0.41879	45.60								
BV	0.10080	7.60	0.87970	89.60			0.45469	43.40	0.44646	48.15								
C	0.12167	9.75	0.86301	88.20			0.44105	42.10	0.46246	49.75								
CV	0.11830	9.10	0.86266	88.25			0.47578	45.75	0.42004	45.65								
D	0.12630	9.75	0.84670	86.70			0.48831	46.85	0.39982	43.60								
DV	0.12574	9.75	0.86398	88.30			0.48613	46.85	0.41337	44.90								
E	0.13977	10.85	0.84797	87.30			0.49939	48.25	0.40513	44.15								
EV	0.13701	10.70	0.85971	87.87			0.49092	47.35	0.41350	45.00								
F	0.15241	11.90	0.84083	86.25			0.52525	51.00	0.38423	42.10								
FV	0.14816	11.60	0.84846	87.00			0.49178	47.35	0.41169	44.75								
G	0.15562	12.25	0.81845	84.35			0.52055	50.65	0.37676	41.37								
GV	0.15522	12.25	0.84043	85.90			0.52226	50.75	0.38407	42.00								
H	0.15703	12.35	0.81982	84.35			0.53240	51.25	0.35819	39.40								
HV	0.15572	12.35	0.84631	86.75			0.52052	50.60	0.39070	42.65								
I	0.16232	12.75	0.81997	84.50			0.54960	53.75	0.35003	38.75								
IV	0.16328	12.90	0.82111	84.75			0.53693	52.00	0.36598	40.25								
J	0.17928	14.25	0.80519	83.30			0.57833	56.75	0.32055	35.75								
JV	0.17969	14.25	0.82404	84.80			0.57393	56.25	0.33789	37.50								
K	0.16185	12.25	0.82991	85.25			0.56067	54.75	0.34627	38.35			0.57562	56.40	0.33306	37.15		
KV	0.15511	12.20	0.84207	86.35			0.52338	50.85	0.38481	42.15			0.57263	56.15	0.34171	37.85		
L	0.15263	12.00	0.83898	86.13			0.55178	52.23	0.36595	40.38			0.59147	58.30	0.31470	35.20		
M	0.14722	11.45	0.83412	85.73			0.54664	53.25	0.34994	38.70			0.57862	56.75	0.31443	35.15		
N	0.15195	11.85	0.85176	87.20			0.55172	53.85	0.35811	39.63			0.59828	58.90	0.31529	35.25		
O	0.15077	11.87	0.83641	85.85			0.56024	54.75	0.34346	38.15			0.60396	61.85	0.30432	31.70		
P	0.14143	11.00	0.86235	88.20			0.53898	52.50	0.36641	40.33			0.60061	59.00	0.30728	34.70		
F1	0.14999	11.70	0.84799	86.90	0.00579	0.712	0.50885	49.40	0.37833	41.50	0.02190	2.694						
	0.14899	11.65					0.50885	49.35										
F1V	0.14938	11.70	0.82468	84.85	0.00609	0.749	0.50354	48.75	0.37367	41.10	0.02618	3.220						
	0.14928	11.70					0.50351	48.75										
F2	0.15154	11.80	0.82715	85.15	0.01050	1.292	0.50295	51.40	0.35755	39.35	0.04321	5.315						
	0.15075	11.85					0.47808	46.05										
F2V	0.14916	11.70	0.83170	85.62	0.01020	1.255	0.51131	49.60	0.35674	39.30	0.03456	4.251						
	0.14716	11.40					0.51041	49.50										
G1	0.15562	12.25	0.82815	85.25	0.00606	0.745	0.52967	51.50	0.36412	40.15	0.01853	2.279						
	0.15532	12.25					0.52370	50.85										
G1V	0.15637	12.35	0.81320	83.85	0.00583	0.717	0.52149	50.63	0.36270	40.10	0.02291	2.818						
	0.15460	12.30					0.50674	49.00										

* Each value was calculated from the average of five determinations in each phase. For the molybdenum-containing specimens (alloys designated by letter and number), an additional determination for Cr is also reported.

** Whenever values are not reported for the primary carbides, the alloys are hypoeutectic.

Table D-2 (Continued)

Microprobe Ratios, K's, and Compositions in Weight Percent of Phases in the High-Stress Abrasion Tested Alloys*

Alloy Design	Matrix (Austenite)						Eutectic Carbide						Primary Carbide**					
	K_{Cr} x 10^{-2}	%Cr	K_{Fe} x 10^{-2}	%Fe	K_{Mo} x 10^{-2}	%Mo	K_{Cr} x 10^{-2}	%Cr	K_{Fe} x 10^{-2}	%Fe	K_{Mo} x 10^{-2}	%Mo	K_{Cr} x 10^{-2}	%Cr	K_{Fe} x 10^{-2}	%Fe	K_{Mo} x 10^{-2}	%Mo
G2	0.15512	12.20	0.81883	84.35	0.01038	1.276	0.51629	50.15	0.35219	38.90	0.03614	4.445						
	0.15064	11.85					0.51270	49.80										
G2V	0.15659	12.00	0.81062	83.65	0.01081	1.330	0.52379	50.90	0.34543	38.30	0.03533	4.346						
	0.15652	12.20					0.50856	49.25										
H1	0.15708	12.30	0.81889	84.25	0.00620	0.763	0.49052	47.30	0.34638	38.38	0.02010	2.010						
	0.15735	12.35					0.53569	52.15										
H1V	0.15820	12.50	0.82205	87.20	0.00591	0.727	0.53414	52.10	0.35643	39.30	0.01554	1.911						
	0.15542	12.25					0.51752	50.25										
H2	0.16172	12.40	0.80877	83.60	0.01012	1.245	0.53134	51.65	0.33870	37.60	0.03422	4.209						
	0.15722	12.30					0.52714	51.25										
H2V	0.15877	12.50	0.82192	84.80	0.00959	1.180	0.52289	50.75	0.34762	38.50	0.03073	3.780						
	0.15311	12.80					0.50889	49.25										
I1	0.16540	13.00	0.81985	84.30	0.00552	0.679	0.54775	53.50	0.34609	38.30	0.01438	1.769						
	0.15828	12.50					0.54112	52.50										
I1V	0.16101	12.35	0.82191	84.65	0.00608	0.748	0.54768	53.50	0.34938	38.70	0.01122	1.380						
	0.16308	12.90					0.54052	52.76										
I2	0.16182	12.40	0.81985	84.30	0.01191	2.349	0.54414	53.25	0.34027	37.75	0.02905	3.575						
	0.16027	12.60					0.53627	52.25										
I2V	0.16332	12.85	0.81955	84.35	0.01006	1.237	0.54404	53.10	0.33126	36.85	0.02526	3.107						
	0.15911	12.50					0.54421	53.30										
J1	0.18008	14.30	0.80160	83.35	0.00557	0.685	0.57353	58.90	0.32058	35.75	0.01602	1.970						
	0.18261	14.50					0.57806	56.75										
J1V	0.18088	14.30	0.79415	82.20	0.00520	0.640	0.59961	59.00	0.30764	34.75	0.00909	1.120						
	0.18164	14.30					0.57740	56.65										
J2	0.17703	14.10	0.80575	83.25	0.00965	1.190	0.55094	53.75	0.31065	34.80	0.03093	3.804						
	0.17917	14.15					0.57163	56.00										
J2V	0.17481	13.85	0.81724	84.15	0.01020	1.255	0.56526	56.25	0.31694	35.38	0.04969	6.110						
	0.17879	14.25					0.54692	55.30										
K1	0.15966	12.60	0.82840	85.15	0.00609	0.749	0.55055	53.75	0.33922	35.24	0.01179	1.450	0.57289	56.20	0.32034	36.10	0.0093	1.140
	0.15490	12.15					0.55308	54.00					0.57452	56.35				
K1V	0.15487	12.50	0.84345	86.60	0.00595	0.726	0.55875	54.60	0.34980	38.70	0.01118	1.375	0.57250	56.10	0.31883	35.65	0.00881	1.084
	0.15513	12.15					0.52881	51.38					0.57327	56.25				
K2	0.15726	12.35	0.81799	84.20	0.01170	1.440	0.54774	53.60	0.33294	37.10	0.02580	3.173	0.57423	56.25			0.01780	2.189
	0.15753	12.20					0.54692	53.30										
K2V	0.15372	12.10	0.80979	83.45	0.01276	1.569	0.54805	53.60	0.32686	36.85	0.02445	3.074	0.57153	56.00			0.01780	2.189
	0.15479	12.20					0.54447	53.20										

* Each value was calculated from the average of five determinations in each phase. For the molybdenum-containing specimens (alloys designated by letter and number), an additional determination for Cr is also reported.

** Whenever values are not reported for the primary carbides, the alloys are hypoeutectic.

APPENDIX E

QUANTITATIVE METALLOGRAPHY PARAMETERS

Abrasion, as investigated in the present research, can be considered a surface phenomenon. Thus the quantitative characterization of the microstructures studied can be simplified by considering them two-dimensional.

Smith and Guttman[44] show, that for a two dimensional structure the projected width (of a plane figure) is equal to twice the perimeter divided by π. As mentioned in an earlier section, the intercept value obtained from the quantimet is the projected length of the carbide; it is seen that the perimeter of the carbide particles is equal to the (intercept)(π)/2. A useful shape parameter which can indicate the "roundness" of a carbide particle is the ratio of the carbide area to the perimeter. Because we are interested in relative quantities for the different carbide structures, the perimeter can be substituted with the value of the intercept. A shape parameter called "shape" in this work was calculated from the quantimet data as the ratio of the total picture points for the area of the carbides to the total picture points for the intercept of the carbides.

The average curvature $\left(\frac{1}{R}\right)$ of the carbide particles was calculated by the area tangent count devised by Rhines[45]. By this method the curvature is calculated from the ratio of the number of tangents formed by sweeping test lines over the sample, to the intercept. In the present case the value taken for the number of tangents was twice the end count. As described earlier, the quantimet scans the sample with a set of parallel lines; therefore each particle resulting in

one end count should have formed an average of two tangents with the scanning line. The radius of curvature ROC was calculated as (4)(end count)/intercept.

Other parameters calculated from the quantimet data were (1) the average particle size, APS, equal to the total area of carbide divided by the end count, (2) the area fraction of carbide, AFR, equal to the number of picture points making up the carbide divided by the total number of picture points (500,000) in the scan, and (3) the austenite grain size calculated from the total number of picture points used in scanning (500,000) divided by the intercept.